Appendix 1
Terminology

Event tree analysis is an inductive analysis that depicts the sequence of occurrences that shows the logical sequence of the occurrence of events in, or states of, a system following an initiating event.

A *failure mode* is a way that failure can occur, described by the means by which element or component failures must occur to cause loss of the sub-system or system function.

Fault tree analysis is a systems engineering method for representing the logical combinations of various component states and possible causes that can result in a specific system state (called the top event).

A *fragility curve* is a function that defines the probability of failure, conditioned on some appropriately defined intensity such as an applied load, a velocity, flood elevation, or other parameter.

A *hazard* is a threat, which may result from either an external cause (e.g. earthquake, flood, or human agency) or an internal vulnerability, with the potential to initiate a failure mode. It is a source of potential harm or a situation with a potential to cause loss.

The *performance* of a system or component is its ability to meet functional requirements. The performance of an item was described by various elements, such as flood protection, reliability, capability, efficiency, and maintainability. The design and operation of the system affects this performance.

A *system* is an entity comprising an interacting collection of discrete elements and commonly defined using deterministic models. The word *deterministic* implies that the system is identifiable and not uncertain in its architecture. The definition of the system is based on analyzing its functional and/or performance requirements. A description of a system may be a combination of functional and physical elements. A system was divided into subsystems that interact. Additional details in the definition of the system lead to a description of the physical elements, components, and various aspects of the system. Methods to address uncertainty in systems architecture are available and was employed as provided by Ayyub and Klir (1996).

Reliability is the ability of a system or a component to fulfill its design functions under designated operating and/or environmental conditions for a specified time period. This ability is commonly measured using probabilities. Reliability is, therefore, the probability that the failure event, however defined, does not occur.

Consequences are damages or losses from some failure event. Each failure of a system has some consequence(s). A failure could cause economic damage, environmental damage, injury or loss of human life, or other possible events. Consequences need to be quantified in terms of failure-consequence severities using relative or absolute measures for various consequence types to facilitate risk analysis.

Risk is the potential of losses for a system resulting from an uncertain exposure to a hazard or as a result of an uncertain event. Risk should be based on identified risk events or event scenarios. Risk is a multi-dimensional quantity that includes event-occurrence probability, event-occurrence consequences, consequence significance, and the exposed population; however, it is commonly measured as a pair of the probability of occurrence of an event, and the outcomes or consequences associated with the event's occurrence. Another common representation of risk is in the form of a curve depicting specified losses and the probability of exceeding those losses.

Probability is a measure of the likelihood, chance, odds, or degree of belief that a particular outcome will occur. A conditional probability is the probability of event occurrence based on the assumption that another event (or multiple events) has occurred.

Safety was defined as the judgment of risk tolerance (or acceptability in the case of decision making) for the system. Safety is a relative term since the decision of risk acceptance may vary depending on the individual or the group of people making the judgment.

Risk analysis is the technical and scientific process to breakdown risk into its underlying components. Risk analysis provides the processes for identifying hazards, event-probability assessment, and consequence assessment. The risk analysis process answers three basic questions: (1) What can go wrong? (2) What is the likelihood that it will go wrong? (3) What are the consequences if it does go wrong? Also, risk analysis can include the impact of making any changes to a system to control risks.

Risk Assessment an examining of the tradeoffs that must take in any effort directed toward risk mitigation or risk reduction.

Risk communication was defined as an interactive process of exchange of information and opinion among stakeholders such as individuals, groups, and institutions. It often involves multiple messages about the nature of risk or expressing concerns, opinions, or reactions to risk managers or to legal and institutional arrangements for risk management. Risk communication greatly affects risk acceptance and defines the acceptance criteria for safety.

A *scenario* is a unique combination of circumstances that lead to an outcome of interest. Thus there may be loading scenarios, failure scenarios or downstream flooding scenarios.

Appendix 2
New Orleans East Basin

NOE – Background

The New Orleans East hurricane protection system was designed as part of the Lake Pontchartrain, LA and Vicinity Hurricane Protection Project. The New Orleans East (NOE) portion of the project protects 45,000 acres of urban, industrial, commercial, and ecological lands. As designed, the levees were generally constructed with a 10-foot crown width with side slopes of 1 on 3. The height of the levees varies but was in the range of 12 – 19 feet depending upon location and design characteristics. There are also floodwall segments along the line of protection that consists of sheet-pile walls or concrete I-walls constructed on the top of sheet-pile. The line of protection was designed to provide protection from the Standard Project Hurricane (approximately a fast moving Category 3 storm). As designed, there is a total of approximately 206,000 linear feet of levees and floodwalls, 8 pump stations, 3 U.S. Fish and Wildlife Service (USFWS) pump stations, a multitude of culverts through/over the levee/ floodwall, and multiple gate closures for road and rail crossings. The NOE basin is essentially broken into two major sections, as shown in Figure 2-1. The west side of the basin is primarily residential and the east side is essentially a wetlands area. These two areas are separated by a small levee. The west side of the basin is further divided into residential and industrial areas. The area along the Gulf Intercoastal WaterWay (GIWW) and Inner Harbor Navigation Channel (IHNC) is primarily industrial while the remainder of the western portion is residential in nature.

NOE – Design Memorandums

For the purposes of the IPET risk assessment, each basin must be broken into "reaches" that are defined by a combination of physical characteristics, major elevation changes, and potential consequences. Many of the basic reaches were defined initially by when individual design memorandums (DM) were completed and then constructed since different stretches of the levee/floodwall were raised at different times throughout the life of the structure. There are a total of 7 levee/floodwall major stretches separated by different DM's within NOE. These 7 are defined below and illustrated in Figure 2-1.

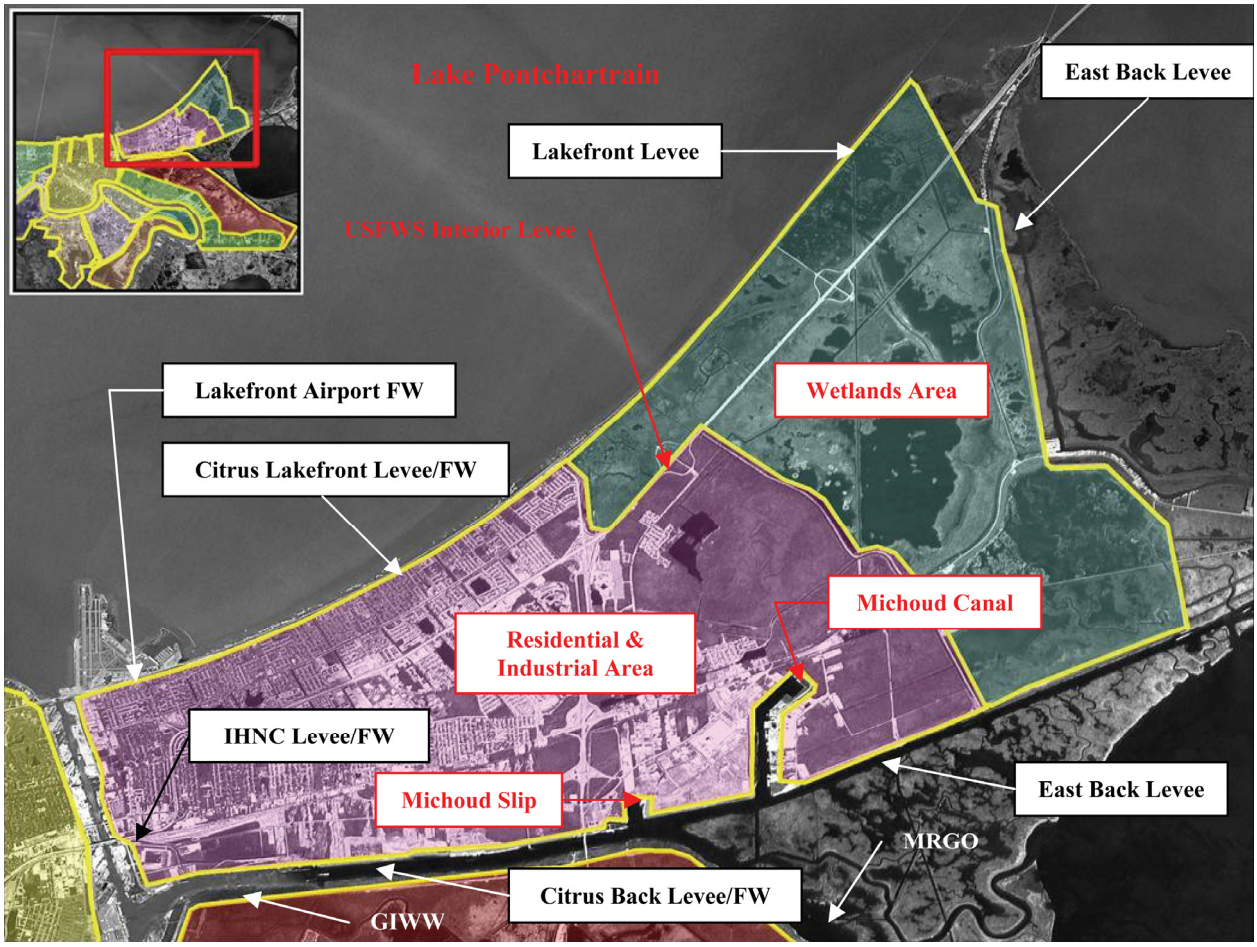

Figure 2-1. New Orleans East Basin – Major Stretches by DM

Lakefront Airport Floodwall
Beginning Point: Northwest corner of basin below Ted Hickey Bridge
Ending Point: End of floodwall just south of Hayne Blvd closure gate

Citrus Lakefront Levee/Floodwall
Beginning Point: Begin transition levee just south of Hayne Blvd closure
Ending Point: Levee height transition at Paris Road and USFWS levee

Lakefront Levee
Beginning Point: Levee transition at Paris Road and USFWS interior levee
Ending Point: South Point at northeast end of Basin

East Levee
Beginning Point: South Point at northeast corner of Basin
Ending Point: GIWW at southeast corner of Basin

East Back Levee
Beginning Point: GIWW at southeast corner of Basin
Ending Point: Northeast end of Michoud Canal floodwall

Citrus Back Levee/Floodwall
Beginning Point: Northeast end of Michoud Canal floodwall
Ending Point: Southwest corner of basin at IHNC

IHNC East Levee/Floodwall
Beginning Point: Southwest corner of basin at IHNC
Ending Point: Northwest corner of basin under Ted Hickey Bridge

NOE – Layout of Reaches for Risk Model by Physical Feature

Within these major stretches defined by the DM's there are reaches, which are defined by physical changes in the protection system, i.e. switching from floodwall to levee, etc…, or by changes in geotechnical parameters. Within each reach, there are specific "key points" whose reliability needs to be determined in order to calculate the effect on the overall reach being evaluated. An example of a "key point" would be a closure gate at a road or rail line crossing along a floodwall. IPET engineers reviewed existing plans, damage survey reports, and conducted field verification inspections to ensure each basin was accurately defined within the system. As a part of the field verification inspections, GPS coordinates were obtained and stationing from DM's and "as-built" plans was verified. For each Basin, this information was transformed into a spread sheet and then a system map for each Basin, as shown in Figure 2-2. Finally, digital photographs with incorporated notes were developed to compliment the spread sheets and system map for further clarification. This collection of information was then categorized to get a clear picture of how the basin should be defined for risk assessment purposes. A summary of the reach and point definitions for NOE is provided in Figure 2-2 with a brief supporting narrative on each reach. Basin definition starts at the northwest corner of the basin where the floodwall along the IHNC intersects the floodwall along the Lakefront Airport (NOE1). This occurs at Sta. 4+02 B/L, which is equal to the DM stationing of 10+13 W/L. The end of the physical definition of the NOE basin occurs at the same point since it is self enclosed.

The details of each reach and key point is detailed in the spread sheet for individual basins in the Risk and Reliability Appendix. The NOE is summarized by reach as follows:

Reach NOE1 (Lakefront Airport DM). This reach is defined by 2,326 linear feet of floodwall at the Lakefront Airport. It is located at the northwest end of the Basin. There are two key points (NOE1a and NOE1b) within this reach, both closure gates, located near the end of this reach. The reach ends just after the second closure gate for Hayne Boulevard. There was significant scour from overtopping along this section of I-wall, as shown in Figure 2-3, but the wall performed well with no noticeable deformation.

Reach NOE2 (Citrus Lakefront DM). This reach is defined by a short 97' transition levee between the end of the Lakefront Airport floodwall and the beginning of the Stars and Stripes Floodwall. There are no key points within this reach.

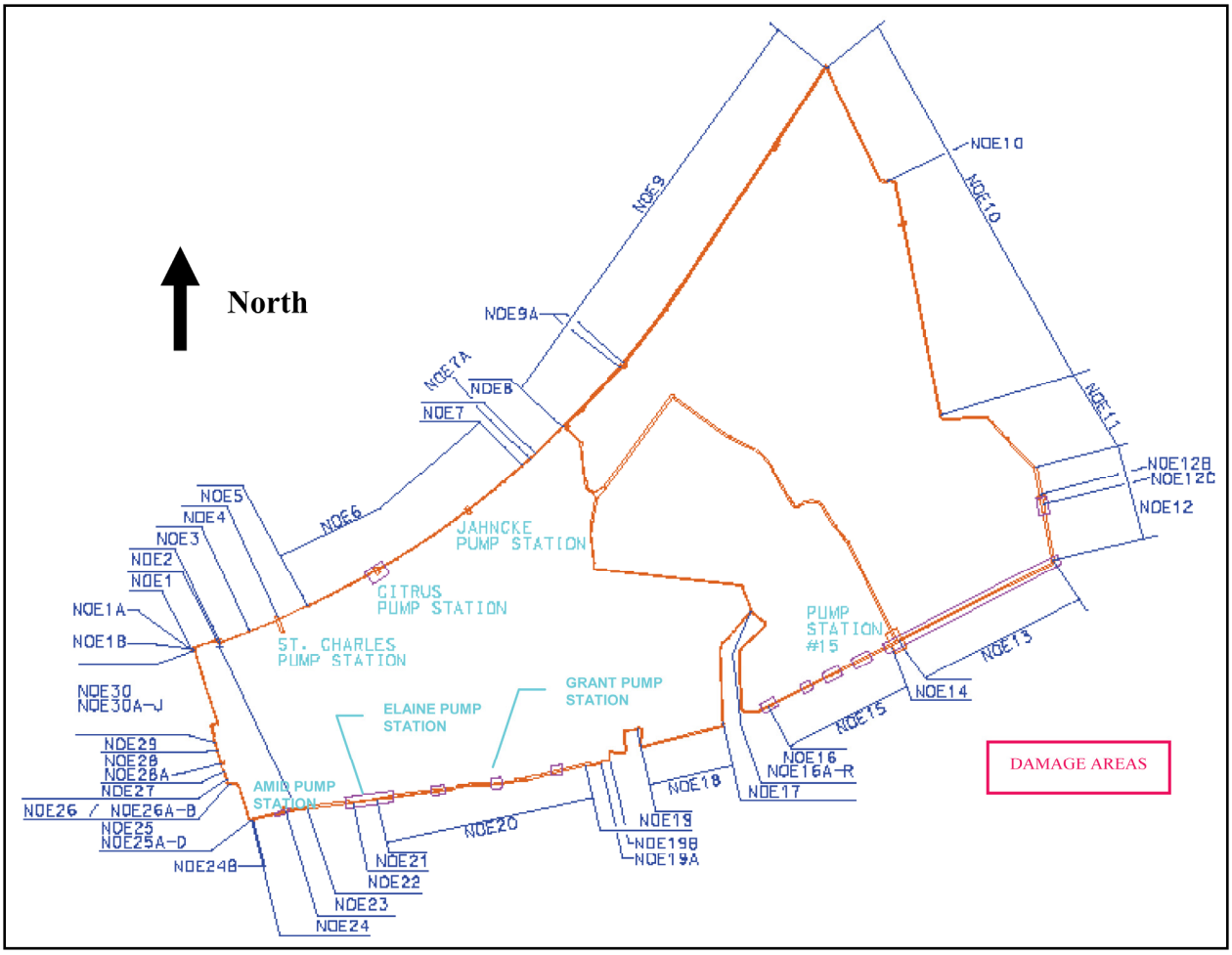

Figure 2-2. New Orleans East Basin – Reaches Defined

Reach NOE3 (Citrus Lakefront DM). This reach is defined by 2,325 linear feet of floodwall. There are two basic types of floodwall along this reach each consisting of about ½ the length of this reach. The first type is a short concrete capped I-wall with levee high on both sides and the second is a taller I-wall section where the protected side has a concrete sidewalk adjacent to a road.

Reach NOE4 (Citrus Lakefront DM). This reach is defined by 2,330 linear feet of the Stars and Stripes Levee. A small concrete I-wall for the discharge pipes at the St. Charles Pump Station is located near the end of this reach.

Reach NOE5 (Citrus Lakefront DM). This reach is defined by 2,270 linear feet of the Stars and Stripes floodwall. There are no key points within this reach.

Figure 2-3. Scour Behind Lakefront Airport FW from Overtopping

Reach NOE6 (Citrus Lakefront DM). This reach is defined by a 19,112 linear feet segment of levee. It begins at the end of the Stars and Stripes floodwall and ends at the west side of the Lincoln Beach floodwall. There are two "key" points within this segment: two small floodwall sections embedded within the levee for the discharge pipes of the Citrus and Jahncke Pump Stations. There was some minor scouring and overtopping of this levee at various locations, as indicated in Figure 2-4, but no failures.

Reach NOE7 (Citrus Lakefront DM). This reach is defined by a 1,474 linear feet segment of floodwall near Lincoln Beach. There is one "key point" located in the flood wall, which is a closure gate, shown as NOE7a.

Reach NOE8 (Citrus Lakefront DM). This reach of levee, 2,724 linear feet, ends the Citrus Lakefront section at the intersection of Paris Road, the interior local levee, and the west side of the Lakefront Levee. There are no key points within this reach, although the levee height is considerably different as it proceeds to the Lakefront Levee section, as shown in Figure 2-5.

Reach NOE9 (Lakefront Levee DM). This reach covers 33,165 feet of levee along Lake Pontchartrain from Paris Road to South Point, which is the extreme northeast corner of the Basin. There is 368' long I-wall around the Exxon/Mobil pipeline crossing that is the only "key point" within the reach, depicted at NOE9a in Figure 2-2.

Reach NOE10 (East Levee DM). This reach is defined by a 27,665 linear feet segment of levee from South Point to where Highway 90 crosses the levee. There are several "key points" within this stretch including 4 culverts through the levee (3 gravity structures and 1 USFWS pump station) and 1 gated closure at Highway 11. For clarity, these are not illustrated in Figure 2-2. Reference the spread sheet in the appendix for further details regarding their location and description.

Reach NOE11 (East Levee DM). This levee is 8,942' long and goes from Highway 11 and serves as a transition section where the design changes. There are no "key points" located within this reach.

Reach NOE12 (East Levee DM). The final reach of levee along the East section is 7,190' long and extends to the GIWW. There are 4 key points along the levee (3 culverts thru the levee and a gated closure at the railroad crossing). The railroad closure structure, shown as NOE12c in Figure 2-2, experienced severe damage during Katrina from overtopping. An aerial view of that damage is shown in Figure 2-6.

Reach NOE13 (East Back Levee DM). This section of levee, measuring 22,257 linear feet, was heavily damaged during Katrina from overtopping. It begins at the east end where it ties into the East Levee and continues to the east end of the floodwall around the Orleans Parish Pump Station #15. There are no key points within this reach. Much of this levee was destroyed, as shown in Figure B7, and is in the process of being rebuilt.

Figure 2-4. Minor Scour from Overtopping at Jahncke Pump Station

Figure 2-5. Begin Lakefront Levee at Citrus Lakefront and Paris Road (Lakefront Levee @ El. 19.0 +/- and Citrus Lakefront Levee @ 13.5+/-)

Figure 2-6. Aerial View of Damage at RR Closure Along East Levee (Point NOE12c on System Map)

Figure 2-7. Failure of Levee by Overtopping East of PS #15 (East Back Levee)

Reach NOE14 (East Back DM). This reach is defined by the floodwall around Pump Station #15. There are two types of walls within this reach, sheet pile walls at the edges and concrete I-walls around the discharge pipes. The total length of wall is 493 feet. Portions of the transition sheet pile sections were heavily damaged during Katrina from overtopping, as shown in Figure 2-8. There are no key points within this short reach.

Reach NOE15 (East Back DM). This 10,120 ft section of levee extends from the east end of the Orleans Parish #15 floodwall to the start of the floodwall on the east side of the Michoud Canal at the GIWW. There is one key point within this reach for a utility pipe crossing.

Reach NOE16 (East Back DM). This reach consists of the east floodwall around the Michoud Canal. It is approximately 10,757 feet long. It starts at the GIWW and continues along the Michoud Canal where it joins with the Citrus Back floodwall. There are 18 key points along this reach for gated closures at industry and road crossings. However, from site inspections, it appears as if 5 of these gates are placed in the permanently closed position. As shown in Figure 2-9, the transition sheet pile floodwall at the beginning of this reach failed during Katrina.

Figure 2-8. Floodwall Failure Near Orleans Pump Station #15

Figure 2-9. Floodwall Failure at East End of Michoud Canal FW

Reach NOE17 (Citrus Back DM). The beginning of the Citrus Back stretch starts with this reach at the northwest end of the Michoud Canal and ends at the southwest side of the Michoud Canal at the GIWW. This reach consists of 9,318 feet of floodwall with no key points within this reach.

Reach NOE18 (Citrus Back DM). This reach represents the 7,905' segment of levee between the Michoud Canal and Michoud Slip. There are no key points within this reach of levee.

Reach NOE19 (Citrus Back DM). The reach represents the 6,155 ft of floodwall around the Michoud Slip. There are 2 gates closures and 2 ramps within this reach.

Reach NOE20 (Citrus Back DM). This reach contains 15,940 ft of levee between the west end of the Michoud Slip and the east end of the combination floodwall for the bulk loading facility. There are three key points within this reach for culverts crossing the levee, including the discharge pipes for Grant Pump Station, as reference in Figure 2-2.

Reach NOE21 (Citrus Back DM). This reach is defined by the 1,820 ft combination floodwall built for the bulk loading facility and Elaine Pump Station, whose relative location is shown on the system map in Figure 2-2. This wall was heavily damaged during Katrina, as shown in Figure 2-10, and is currently being repaired.

Figure 2-10. Floodwall Failure at Bulk Loading Facility/Elaine PS

Reach NOE22 (Citrus Back DM). This reach is for the levee (3,453 ft long) between the floodwalls at the bulk loading facility/Elaine PS (east side) and Amid PS (west side). There are no key points within this reach.

Reach NOE23 (Citrus Back DM). This reach is the 1,587 ft section of floodwall located just east of the Amid Pump Station. This wall did suffer minor overtopping, but no major damage. There are no key points within this reach.

Reach NOE24 (Citrus Back DM). The final reach of this DM is 2,348 feet of levee extending from the end of the floodwall just east of the Amid Pump Station to its tie in with the Inner Harbor Navigation Canal (IHNC) east levee. There are two key points located within this reach including the discharge pipes over the levee at Amid PS and the railroad closure gate structure just east of the tie in with the IHNC levee. This structure was overtopped and sustained serious erosion problems, but no major structural damage, as indicated by the eroded areas in Figure 2-11.

Figure 2-11. Erosion Damage Around RR Closure (Citrus Back Levee)

Reach NOE25 (IHNC DM). This reach is 3,803 ft long and consists of levee. There are 4 closure gates within this reach each of which suffered erosion damage from overtopping during Katrina. Structural damage was minimal to these closure structures. The very end of this reach suffered a major washout area where the levee serves as a ramp just near the I-10 overpass. A photograph of this washout damage is shown in Figure 2-12.

Figure 2-12. Major Washout Area from Overtopping Near I-10 Overpass (Citrus Back Levee)

Reach NOE26 (IHNC DM). This short reach of floodwall (537 ft) starts near the end of the washout area and extends just under the I-10 overpass. This section is considered a reach because it faces several different directions and contains two key points, both closure gates.

Reach NOE27 (IHNC DM). This reach consists of a short transition levee (526 ft) between floodwalls. There are no key points within this short reach.

Reach NOE28 (IHNC DM). This section of floodwall (1,876 ft) starts between the I-10 and Highway 90 overpasses and ends where it serves as the foundation for the Dupuy Storage Facility (see Figure 2-12). There is one key point in this section which is the old Highway 90 overpass location. It does not appear as if remedial repairs were made this transition section when the overpass was relocated.

Reach NOE29 (IHNC DM). This short section of floodwall (643 ft) serves as the Dupuy Storage Building foundation, as shown in Figure 2-13. This section was deemed an individual reach because overtopping issues along this short reach may not be of major concern with the building.

Figure 2-13. Floodwall Serves as Building Foundation (Dupuy Storage Facility – IHNC East)

Reach NOE30 (IHNC DM). The last reach of the basin consists of 8,168 ft of floodwall. There are several key points within this reach including the Dwyer PS discharge pipes and several closure gates. Portions of this wall were overtopped as indicated by the erosion behind the floodwall adjacent to closure gate E-13 and shown in Figure 2-14. This erosion, which measures approximately 8' wide by 2.5' deep, did not cause major structural problems with the wall at this location.

In summary, the NOE basin is divided into 30 reaches for the purposes of the risk analysis. There are a total of 14 floodwall reaches (49,749 linear feet) and 16 levee reaches (167,577 linear feet). Thus, the basin is roughly 23% floodwall and 77% levee for evaluation purposes. Approximately 6,700 feet of levee, primarily the East Back Levee section, was damaged or destroyed from overtopping during Katrina. An additional 24,600 feet of floodwall was damaged to some extent from overtopping. This was spread out across different sections of the Basin. Some of the damage to the floodwalls will only require that landside fill be placed back where scouring took some of the resisting, passive wedge away. Other shorter sections of wall are being totally rebuilt as a result of the overtopping causing their failure.

Figure 2-14. Erosion Behind Floodwall Adjacent to Gate E-13 (IHNC East)

NOE – Elevations Along the Defined Reaches

One of the critical inputs to completing the risk assessment for the hurricane protection system is a clear understanding of the elevations along each basin both pre-Katrina and as a result of any fixes from Task Force Guardian. There are different ways this can be addressed when conducting the risk assessment, but in order to get the best information, Risk team engineers developed "average" lengths of elevations to the nearest ½ foot increment. A variety of survey information was required to develop this information for NOE. Four different sources of data were required to obtain the best estimate of levee/floodwall elevations at the time of Katrina. A September 2005 LIDAR survey was used to establish elevations for most non-failed sections of

levees. For the Citrus Back Levee, September 2000 Plan and Profile sheets were provided by TFG. For levee sections that had major failures (East Back Levee), October 2001 survey data was available and provided by TFG. Finally, LIDAR survey data is collected by aerial means and it did not pick up the top of floodwalls. In November 2005, a field survey was done using NAVD88 datum to determine top of floodwall elevations at the various locations along NOE.

The survey information for NOE was collected and categorized along each reach. The elevations vary considerably, but were developed where "average" ½ foot elevation changes occurred and then stations were matched to these locations. This information is provided in the NOE spread sheet. In summary, the weighted average of levee/floodwall height coupled with the range is provided in Table 2-1.

Table 2-1
Elevation Information by Reach for NOE Basin

Reach	DM	Weighted Average Elevation	Maximum Elevation in Reach	Minimum Elevation in Reach	Source
NOE1	Lakefront Airport	11.6	11.7	11.6	Nov05 Survey
NOE2	Citrus Lakefront	13.0	13.0	13.0	Sep05 LIDAR
NOE3	Citrus Lakefront	need data	need data	need data	???
NOE4	Citrus Lakefront	13.2	13.5	11.5	Sep05 LIDAR
NOE5	Citrus Lakefront	14.3	14.6	14.1	Nov05 Survey
NOE6	Citrus Lakefront	13.0	13.5	12.0	Sep05 LIDAR
NOE7	Citrus Lakefront	12.5	12.7	12.2	Nov05 Survey
NOE8	Citrus Lakefront	12.9	13.0	12.5	Sep05 LIDAR
NOE9	Lakefront Levee	18.4	20.0	18.0	Sep05 LIDAR
NOE10	East Levee	15.1	15.5	12.5	Sep05 LIDAR
NOE11	East Levee	16.8	17.5	16.5	Sep05 LIDAR
NOE12	East Levee	17.8	19.0	13.5	Sep05 LIDAR
NOE13	East Back Levee	15.5	16.5	15.0	Oct01 Survey
NOE14	East Back Levee	19.9	22.2	17.5	Nov05 Survey
NOE15	East Back Levee	16.8	17.0	16.5	Oct01 Survey
NOE16	East Back Floodwall	17.9	18.0	17.5	Nov05 Survey
NOE17	Citrus Back Floodwall	20.7	21.0	20.5	Nov05 Survey
NOE18	Citrus Back Levee	17.4	17.5	17.0	Nov05 Survey
NOE19	Citrus Back Floodwall	17.2	17.1	17.8	Nov05 Survey
NOE20	Citrus Back Levee	14.6	15.0	14.0	Sep00 Plan & Profile
NOE21	Citrus Back Floodwall	need data	need data	need data	???
NOE22	Citrus Back Levee	14.0	14.0	14.0	Sep00 Plan & Profile
NOE23	Citrus Back Floodwall	14.5	15.1	14.4	Nov05 Survey
NOE24	Citrus Back Levee	13.6	14.0	13.0	Nov05 Survey
NOE25	IHNC East	12.0	12.5	11.5	Nov05 Survey
NOE26	IHNC East	12.5	12.5	12.5	Nov05 Survey
NOE27	IHNC East	12.5	12.5	12.5	Nov05 Survey
NOE28	IHNC East	13.2	13.5	12.0	Nov05 Survey
NOE29	IHNC East	13.5	13.5	13.5	Nov05 Survey
NOE30	IHNCE East	12.4	13.0	11.5	Nov05 Survey

Appendix 3
Jefferson Basin

Jefferson West Bank Area

The West Bank Basin is composed of four sub-basins that are designed as three projects. These are 1) Cataouatche, 2) Westwego to Harvey Canal, and 3) Harvey Canal to Algiers Canal.

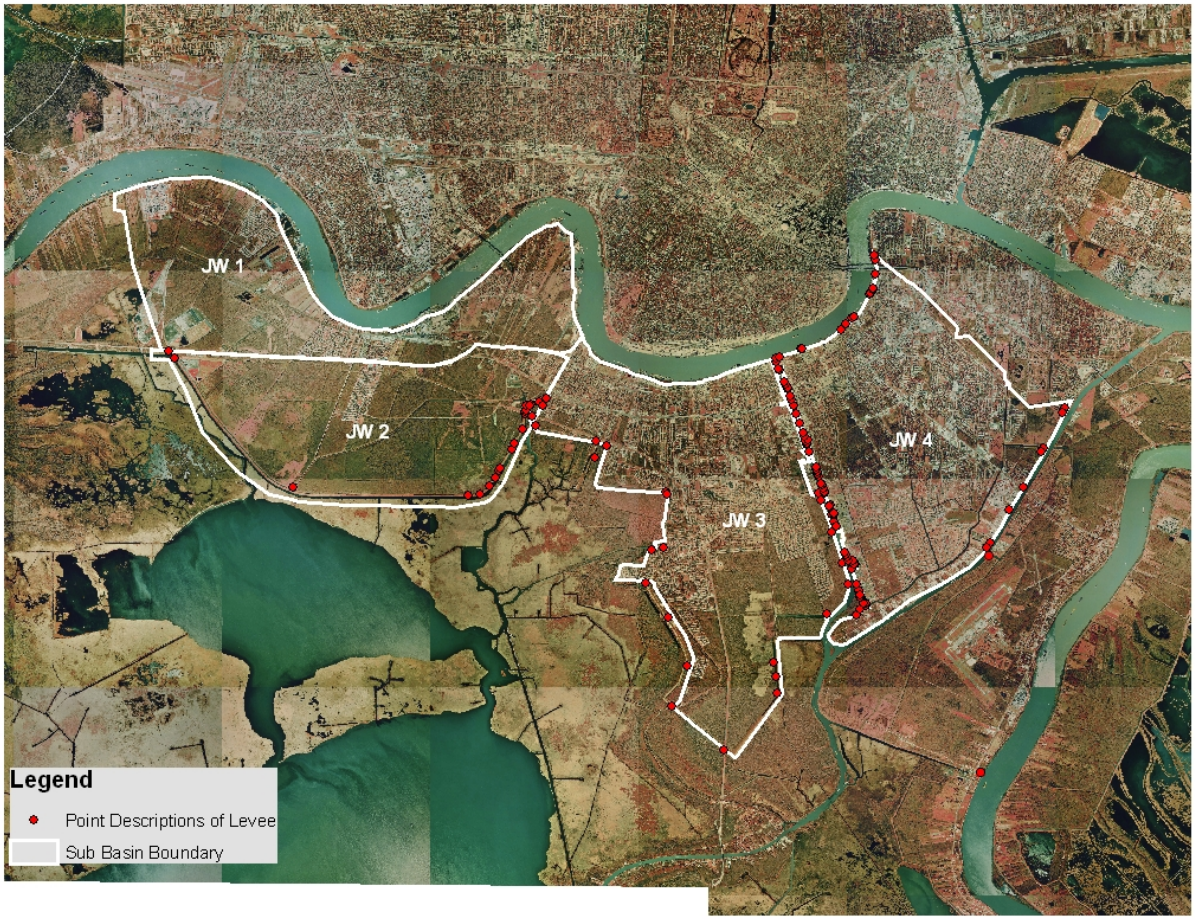

Cataouatche – JW1 and JW2

This area is located in Jefferson Parish and is generally bounded by the Mississippi River and its alluvial ridge to the north and the Lake Cataouatche levee to the west, south and east. The topography is flat with ground elevations ranging from +7.5 feet NGVD on the alluvial ridges along the Mississippi River to -5 feet NGVD in the interior of the area. Approximately 40 percent of the area is below sea level. The surface area is 22.6 square miles. The area is protected by 25.4 miles of levees, natural ridges and floodwalls.

Segment 1 extends from the main line Mississippi River levee (MRL) at the Jefferson Parrish boundary southward to the Texas and Pacific railroad tracks. There are no levees or dikes in this area. The natural contour of the area provides the protection, but this segment is listed since it is possible storm surges to flank the Segment 2 levee reach and cause flooding.

Segment 2 is the proposed levee that follows the crushed stone roadway southward from the Texas and Pacific railroad tracks (that becomes an asphalt roadway which is used by the land fill operators in the area) to US 90.

Segment 3 is a short, small dike built parallel Hwy 90. Hwy 90 is a 4-lane road with a raised median in the center. The median provides the higher level of protection. The road rises as a low relief ramp at the beginning of Segment 4.

Segment 4 is an earthen levee extending southward from Hwy 90 to the Cataouatche Pumping Station. The discharge lines of the first pumping station pass over the levee. The discharge lines of the second pump station (immediately adjacent to the first station) pass through a sheetpile wall.

Levee begins at Hwy 90

Typical Levee in this area

Pump station near Hwy 90 with pipe crossing over Levee

Segment 5 is an all clay levee that extends eastward from the Cataouatche Pumping Station to the I-Wall in the Segnette State Park.

Cataouatche Pump Station

Sheetpile wall transition to concrete capped I-wall at the Segnette State Park

Segment 6 is a concrete I-Wall atop a clay levee. The controlling grade listed for this area is the preconstruction levee grade. The area will have 2 vehicular gates.

Concrete capped I-wall at the Segnette State Park

Swing in the Concrete capped I-wall at the Segnette State Park where Wall ends at the Segnette Pump Station

Segment 7 is completed floodwalls that lie between the Segnette Pump Station and the Old Westwego Pump Station.

Segnette Pump Station

Segment 8 extends from the floodwall at the head of Company Canal (closest line of flood protection to the Mississippi River) to the MRL. The natural contour of the area provides the protection.

Segment 9 is the West Jefferson Levee District Mississippi River levee. This all clay levee closes the north end of the sun-basin and extends from Westwego to the St. Charles Parish line.

Segment 10 is the interior drainage separator which begins at the end of Segment 3. It proceeds along US 90 to the east until it intersects the Texas and Pacific railroad tracks just north of the Westbank Expressway. It then continues to the east along the Railroad until it intersects Segment 8 and then turns north to the MRL. JW1 is to the north of the Segment 10 interior levee and JW2 is to the south.

There are a total of 5 vehicular floodgates (double swing) and 2 pedestrian (single swing) floodgates in the protection system. The sill elevations of these floodgates are at or above the current controlling elevation so these gates are not a factor in draining the area.

There are 4 pumping stations that drain the protected area.

Westwego to Harvey Canal – JW3

This area is located in Jefferson Parish and is generally bounded by the Mississippi River and its alluvial ridges on the north, the Harvey Canal on the east and marshes/wetlands on the south and west. The topography is flat with ground elevations ranging from +7.5 feet NGVD on the alluvial ridges along the Mississippi River to –4 feet NGVD in the interior of the area. Approximately 40 percent of the area is below sea level. The surface area is 21.4 square Miles. The area is protected by 27.5 miles of levees and floodwalls.

Segment 1 is a floodwall stretching between the Old and New Westwego Pumping Stations and connects the Cataouatche sub-basin to Westwego to Harvey Canal sub-basin. The segregation of these two sub-basins is not very pronounced. The general contour tie to the Mississippi River levee is described in Segment 8 the JW1 Cataouatche sub-basin.

Segment 2 is the Westwego Levee that is a geosynthetic reinforced, clay levee running parallel to Mayronne Canal between the New Westwego Pumping Station and Dugues Canal-Westwego Seaplane Airport. A 400’ canal closure is currently under construction at the head of the Dugues Canal.

Segment 3 runs between Dugues Canal and the New Westminster Pump Station and the North-South Levee. This levee is all clay.

Segment 4 is the Westminster Levee, which parallels the Grand Cross Canal, stretches between New Westminster Pumping Station and Orleans Village Pumping Station (out of service). This clay levee is geosynthetically reinforced.

Segment 5 is the Orleans Village levee which is all clay and paralleling Glasco Canal, between Orleans Village Pumping Station (out of service) and Oak Cove Pumping Station. Along this reach is the Ames and Mount Kennedy Pumping Stations connected by floodwall.

Segment 6 consists of the Oak Cove and Hwy 45 clay levees running between Oak Cove Pumping Station and the Hwy 45 crossing. Also found along this length are areas of T-Wall, I-Wall, and one vehicular floodgate at Hwy 45.

Sheet pile transition at the LA Hwy 45

Double Swing gate at the LA Hwy 45 closure in the V-Line levee

Segment 7 is the V-Line Levee which is an I-Wall between LA Hwy 45 and Hwy 3134.

V-line levee continues south of LA Hwy 45 closure

Segment 8 stretches from the V-Line Levee floodwall to the Old Estelle Pumping Station and is an all clay levee with one main road crossing.

Segment 9 is an all clay levee running parallel along the North bank of the Old Estelle pumping Station Outfall Canal. It runs to the Harvey Canal.

Segment 10 is the West bank Harvey Canal Levee. It consists of a clay levee running from the mouth of the Harvey Canal to the LaPalco bridge. Along this segment is the New Estelle Pumping Station, a floodwall at the Bridgeline pipeline, and three areas of sheetpile closure required because of unstable earthen levee sections.

New Estelle Pump Station

LaPalco Bridge Overpass Construction of sector gate is underway

Segment 11 stretches from LaPalco bridge to the Harvey Lock, paralleling the Harvey Canal. This floodwall includes the Harvey and Cousins Pumping Stations, a vehicular gate and ties the Westwego and Harvey Canal sub-basin back into the Mississippi River Main Line levee.

Industrial area along Harvey Canal

US 90 Bridge over Harvey Canal near Harvey Lock Harvey Canal

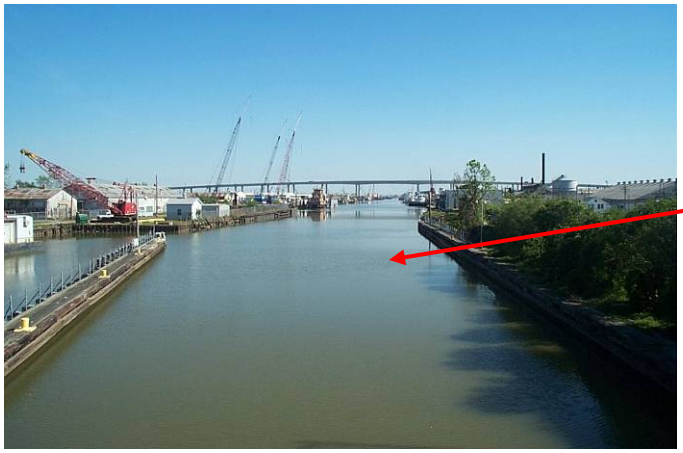

Looking south down Harvey Canal from Hwy 45 Bridge near Harvey Lock

Harvey Lock

Harvey Lock exit toward MS River

MS River Levee at exit of Harvey Canal

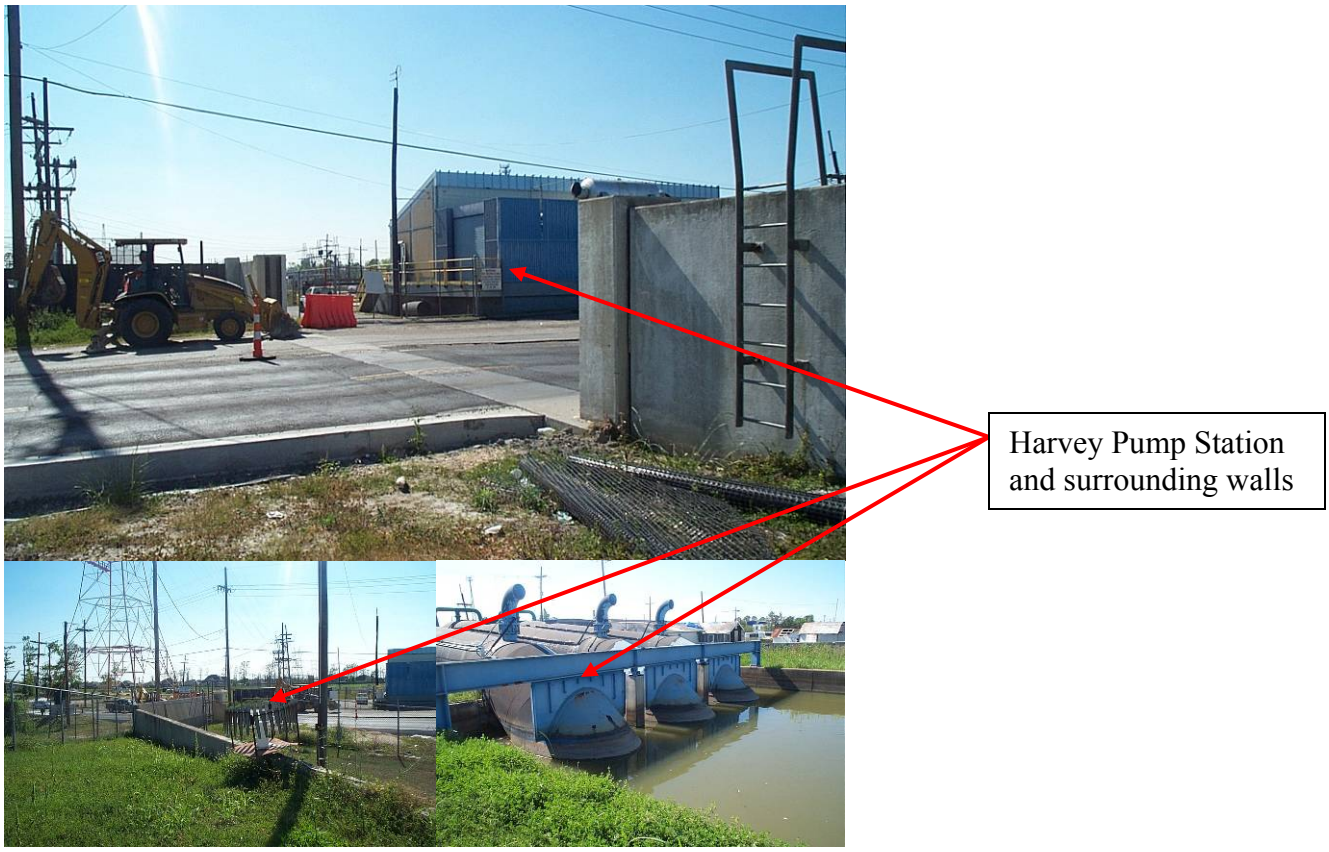

Segment 12 is the West Jefferson Levee District Mississippi River levee. It encloses the north side of the sub-basin between Westwego and Harvey Canal and is an all clay levee.

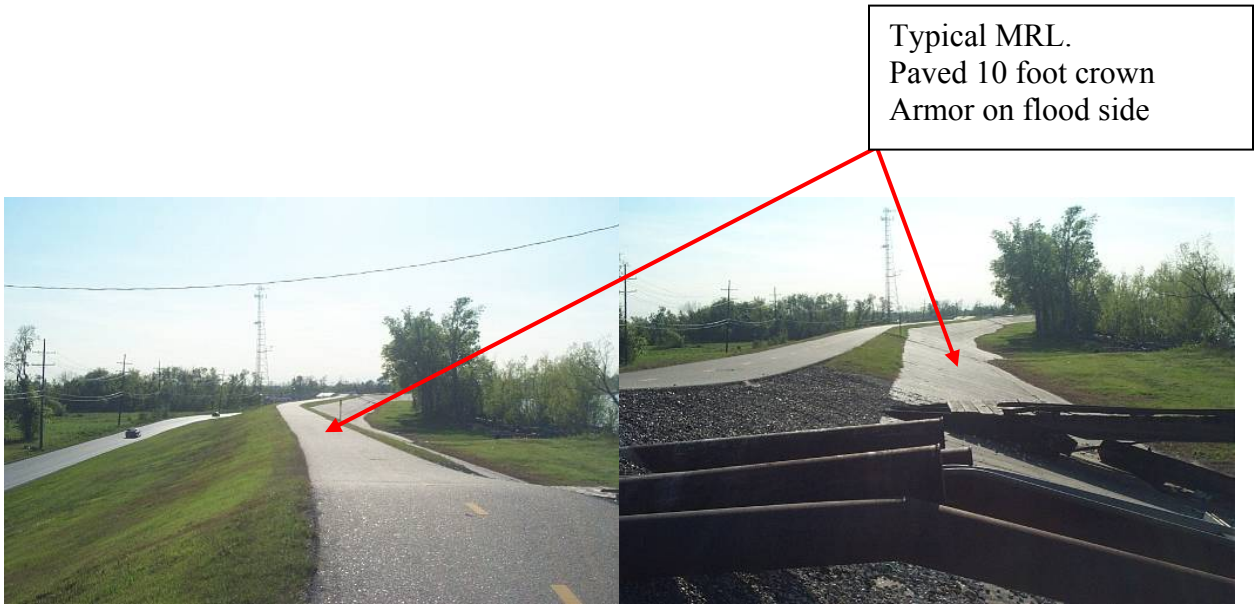

MRL in vicinity of Northrup-Grumman Plant

Typical closure gate (vehicle and pedestrian) along MRL

There are 10 pedestrian floodgates (swing) and two roadway floodgates (one swing and one miter).

There are 11 pumping stations that drain the protected area. The location of the pumping stations

Harvey Canal to Algiers Canal - JW4

This area is located in Jefferson and Plaquemines Parish and is generally bounded by the Mississippi River on the north, the Jefferson, Plaquemines & Orleans Parish lines on the east, the Algiers Canal on the south, and the Harvey Canal on the west. The topography is flat with ground elevations ranging from +15 feet NGVD on the alluvial ridges along the Mississippi

River to -5 feet NGVD in the interior of the area. Approximately 40 percent of the area is below sea level. The surface area is 18.8 square miles. The area is protected by 21.3 miles of levees and floodwalls.

Segment 1 extends from the Harvey Canal Lock at the Mississippi River down the East bank of the Harvey Canal to the Hero Pumping Station where the pumping station discharge lines pass through a T-Wall. This clay levee is a local levee in a heavily industrialized area.

Segment 2 extends from the South end of the Hero Pumping Station around the bend where it ties into the Algiers Canal levee. The clay levee is also a local levee in a heavily industrialized area.

Segment 3 picks up where segment 2 ended and continues along the West bank of the Algiers Canal. The clay levee is interrupted by floodwall segments that cross over the Belle Chasse tunnel and in front of Planters Pumping Station. It ends at the tie-in of the local levee separating Plaquemines and Orleans Parishes. A railroad track crosses over the top of the existing levee. A future floodgate is planned for the area.

Segment 4 is an all clay levee that runs along the length of the Orleans Parish line between Algiers Canal and the Mississippi River levee at the Greater New Orleans Bridge.

Segment 5 is the West Jefferson Levee District Mississippi River Levee stretching between the Harvey Canal and the Orleans Parish line beneath the Greater New Orleans Bridge. This levee consists of all clay levees with short reaches of concrete I-Wall atop clay levees with railroad and vehicular gates.

There are no floodgates, control structures, or drainage structures in the protection system.

There are 2 pumping stations that drain the protected area.

Appendix 4
St. Charles Basin

The St. Charles hurricane protection system (HPS), shown in Figure 4-1 below, was designed as part of the Lake Pontchartrain, LA and Vicinity Hurricane Protection Project. The St. Charles (SC) HPS protects 17.2 square miles of urban, industrial, commercial, and ecological lands that is essentially a low density residential community with a small business district along U.S. Highway 61. The St. Charles Basin is generally bounded on the north by the St. Charles HPS, on the south by the Mississippi River Levee (MRL) and on the west by the Bonnet Carre guide levee. As designed, the HPS levees were generally constructed with a 10-foot crown width with side slopes of 1V on 3H for both the flood side and protected side. Topography is flat with ground elevations ranging from +12 feet NGVD on the alluvial ridges along the Mississippi River to –2 feet NGVD near the locally maintained levee south of Lake Pontchartrain. Approximately 25 percent of the developed area is below sea level. The design elevation of the HPS levees varies from 13 feet on the west to 12 feet on the east. There are also floodwall segments along the line of protection that consists of sheet-pile walls or concrete capped sheetpile walls constructed on the top of the levee. The line of protection was designed to provide protection from the Standard Project Hurricane (approximately a fast moving Category 3 storm). As designed, there is a total of approximately 9.5 miles of earthen levees, 1 mile of floodwall, 1 pump station, and 5 drainage structures, 3 swing gate closures for road and rail crossings, and one open gap for a rail crossing. The MRL is generally designed to elevation 26 feet with a 10 foot crown and a 1 V on 3 H slope on the land side and a 1 V on 4 H on the flood side. Similarly, the Bonnet Carre guide levee is generally designed to elevation **XX** feet with a 10 foot crown and a 1 V on 3 H slope on the land side and a 1 V on 4 H on the flood side.

The SC Basin is a mix of industrial and residential areas. The area between the HPS and Lake Pontchartrain is essentially a wetlands area. There are two sub-basins in the polder as shown in Figure 4-1.

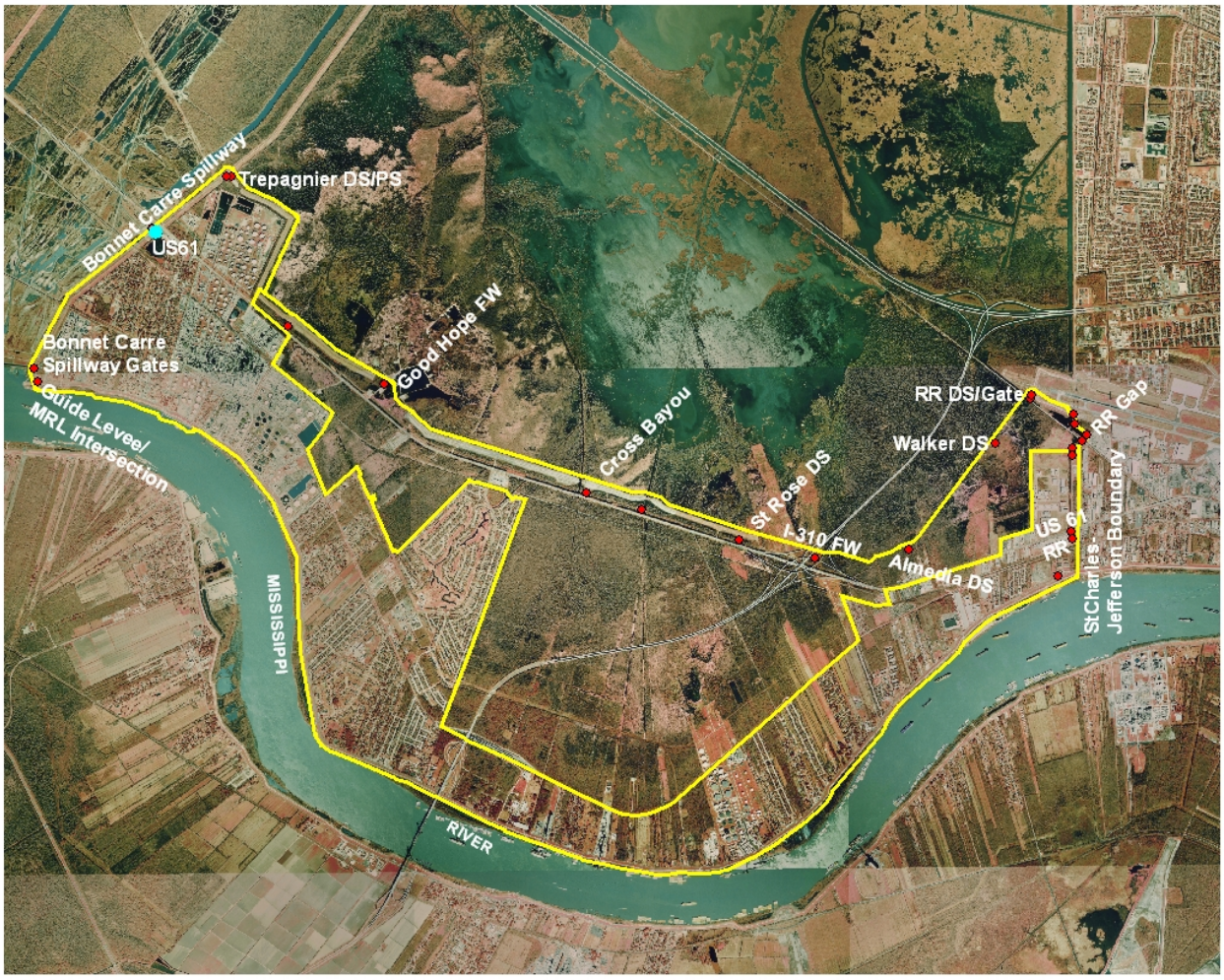

Figure 4-1. St. Charles Basin with sub-basins and annotations for significant features.

The St. Charles HPS is made up of Reach SC1 – SC4 which begins at the Bonnet Carre Guide levee and extends eastward to the St. Charles – Jefferson Parrish border.

Reach SC1 is approximately 17000 ft long earthen levee (with a Geotextile blanket) and contains (1) the Bayou Trepagnier Pump Station and Drainage Structure, with a transition sheetpile wall, (2) a pipeline crossing and (3) the Good Hope floodwall. It was designed to a net grade of 13 ft MSL.

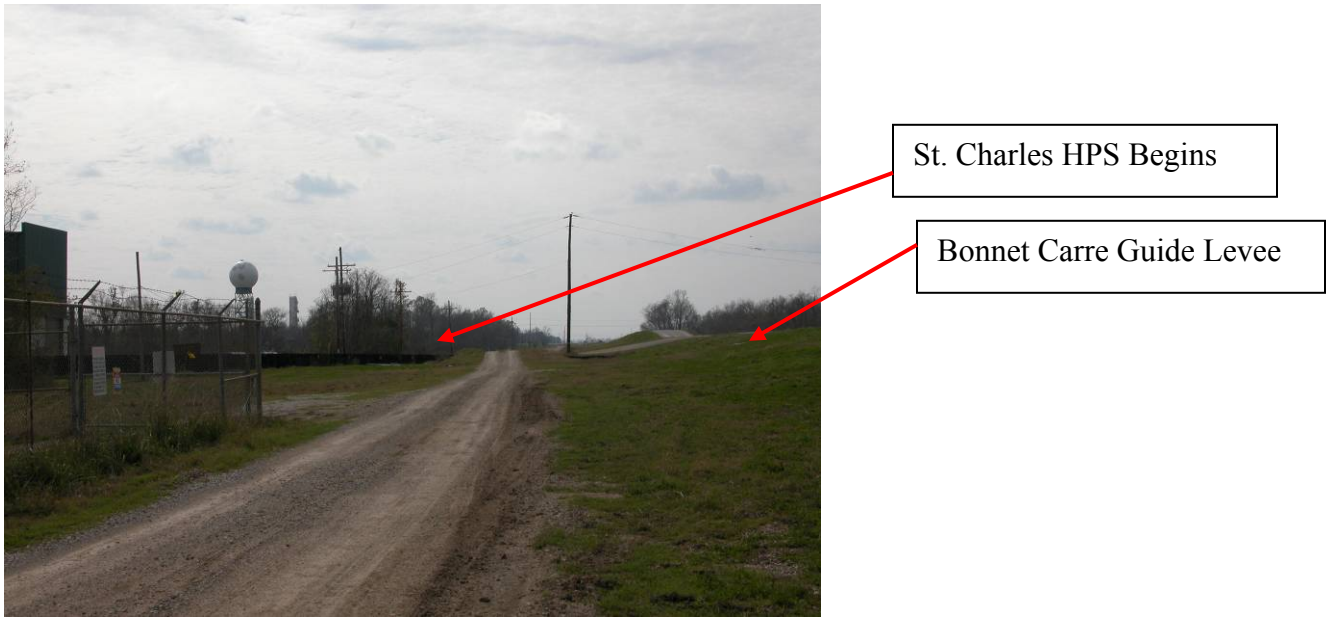

Intersection of St. Charles HPS and the Bonnet Carre Guide Levee

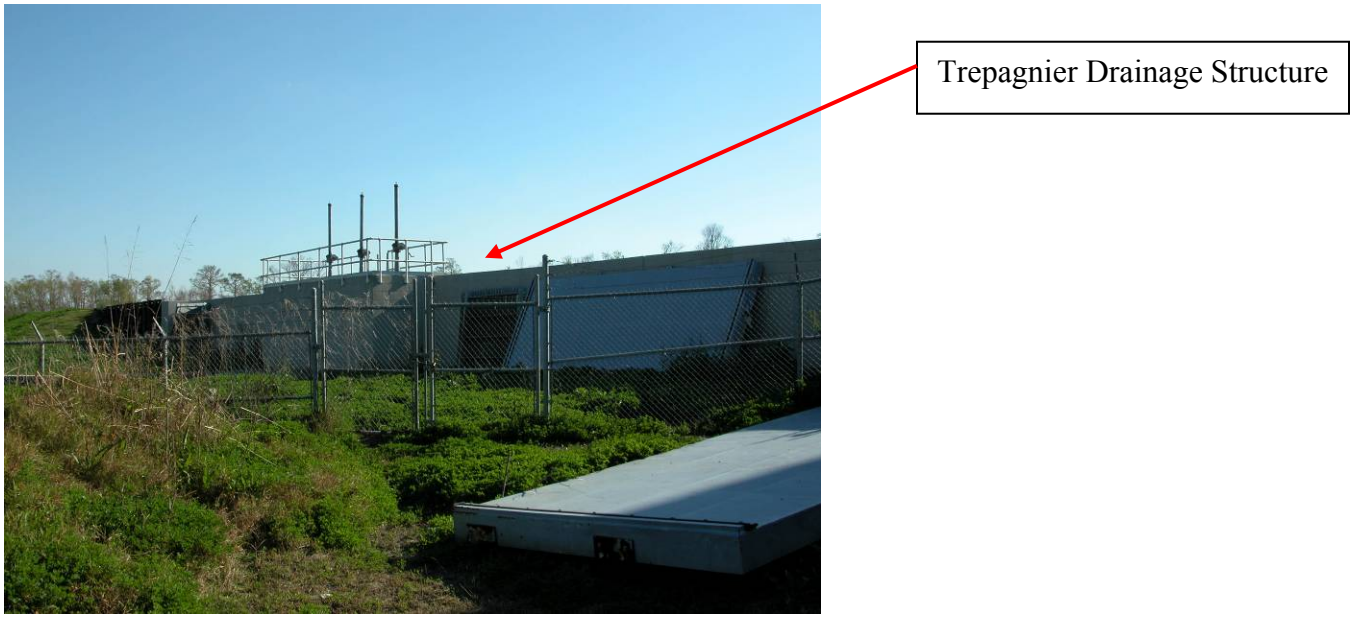

Trepagnier DS and Pump Station

Pipeline crossing (ramp)

Closure Gate for Industrial plant

Reach SC2 is approximately 12000 ft long earthen levee (with a Geotextile blanket) and contains (1) the Cross Bayou Drainage structure and the Gulf South Pipeline crossing. It is designed to an elevation of 12.5 ft. There is a 500 ft transistion from 12.5 ft to 12 ft where SC3 begins.

Cross Bayou Drainage Structure

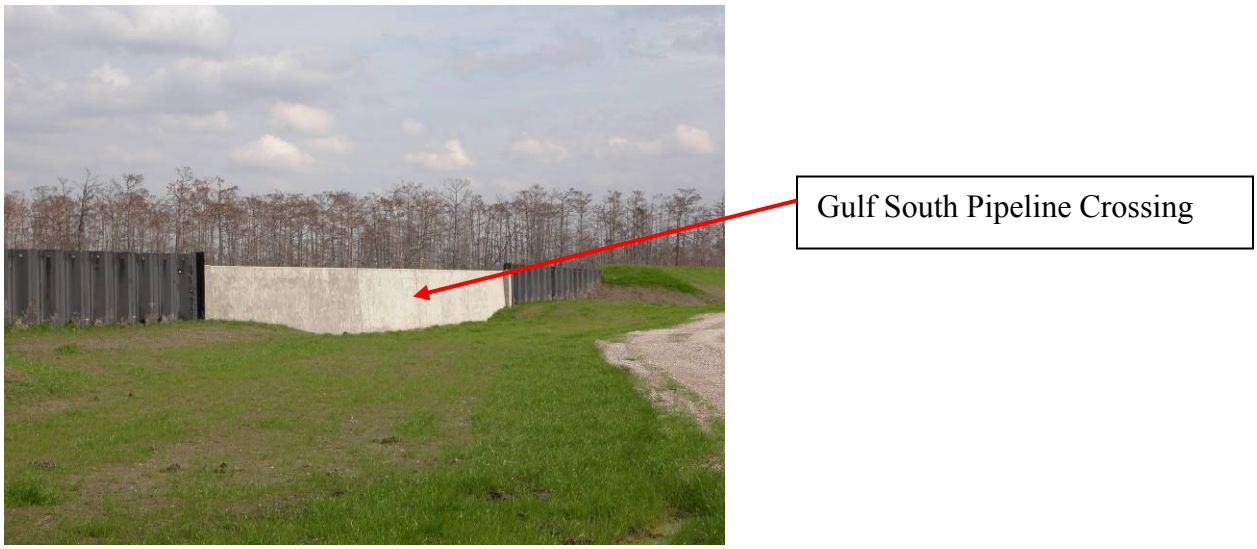

Gulf South Pipeline Crossing

Reach SC3 is approximately 24000 ft long earthen levee (with a Geotextile blanket) and contains (1) The St.Rose, Almedia, and Walker Drainage structures, (2) the I310 Floodwall with one access gate, and (3) the Railroad crossing near the airport runway extention. The RR crossing closure gate was not in place during Hurricane Katrina, but has since been completed. It was closed by sandbags for Katrina.

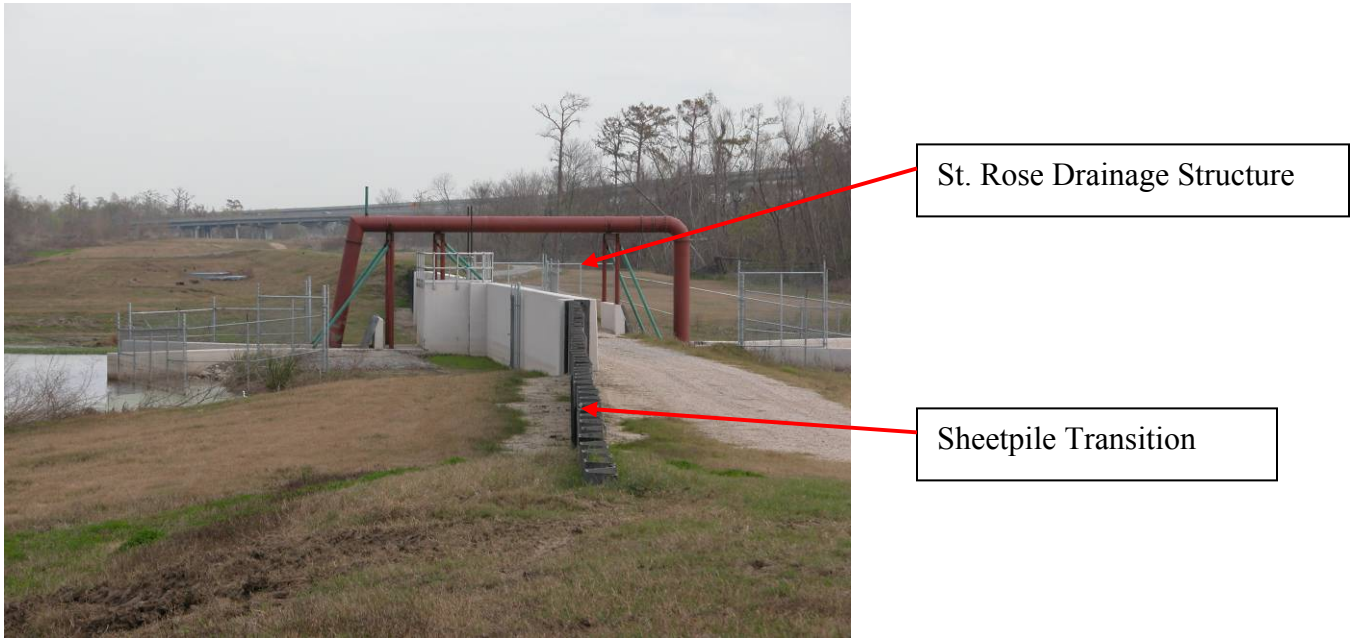

St. Rose Drainage Structure

I 310 Floodwall with 24 ft closure gate

Alemedia Drainage Structure

Walker Drainage Structure with sheetpile transition

Walker Drainage Structure

Railway Gated Crossing at Airport Levee (not constructed during Katrina)

HPS joins Airport Levee just north of the Railway Gated Crossing

Railway Gated Crossing at Airport Levee
(not constructed during Katrina)

Reach SC4 is approximately 8,048 ft long earthen levee with most of it having an embedded sheetpile wall in its crown. It is designed to an elevation of ?? ft. It extends from where the HPS intersects the airport runway extension levee to the St. Charles – Jefferson Parish boundary, then proceeds southward to US 61, and on to the Railroad crossing. Significant features are (1) an abrupt 3 ft drop in elevation at one 90 deg turn in the wall, (2) the 24 ft. gap at the Railroad crossing, (3) the US 61 crossing has no closure gate, and (4) the HPS ends at the Railroad crossing, with the remainder of the Parrish boundary line at the same elevation as the RR until it intersects the MRL. The RR crossing gap was sandbagged during Katrina.

Floodwall as it turns east by the Airport runway extension

Corner of sheetpile floodwall as it turns south by the Airport runway extension (3 ft drop in elevation)

Floodwall as it turns south just north of the Railroad crossing

Railroad crossing has no closure gate. During Katrina it was sandbagged.

St. Charles – Jefferson Parish Boundary Levee ends North of US 61 Highway – Gap at this crossing

St. Charles – Jefferson Levee at North side of US 61

St. Charles – Jefferson Parish Boundary Levee South of US 61 Highway – No closure at this crossing

Short Transition Section of HPS from South of US 61 toward Railroad

St. Charles – Jefferson Levee at South side of US 61

The basin protection then continues westward as the **MRL** at a design elevation of 26 ft. The MRL is an earthen levee with a 10 ft crown. No major structure or pipeline passes through the MRL.

Mississippi River Levee at the St Charles - Jefferson boundary at Hwy 48

Top of Mississippi River Levee at the St. Charles - Jefferson boundary

At the east extend of the basin, the MRL intersects the Bonnet Carre guide levee which continues the protect northward on the west side of the Basin until it reached the HPS. This stretch contains (1) the intersection with the spillway and US 61.

Mississippi River Levee intersection with Bonnet Carre Guide Levee

Bonnet Carre Spillway intersection with Guide Levee

Bonnet Carre Guide Levee Looking North from the Spillway gates

Appendix 5
Plaquemines Basin

Background

The Plaquemines Basin is made up of 11 sub-basins as shown in Figure 5-1. It is generally composed of the Plaquemines Parrish along the east and west banks of the Mississippi River south of Mile 82. Both the west and east bank protection includes the Mississippi River levees as a part of each sub-basin. There are 134 miles of MRL and floodwall, 53 miles of hurricane protection, 12 miles of floodwall, 19 pump stations, a 110 foot small boat lock, and a marine floodgate. The damage consisted of 20 miles of MRL and HPS levee, 9.4 miles of floodwall, and 5 pump stations.

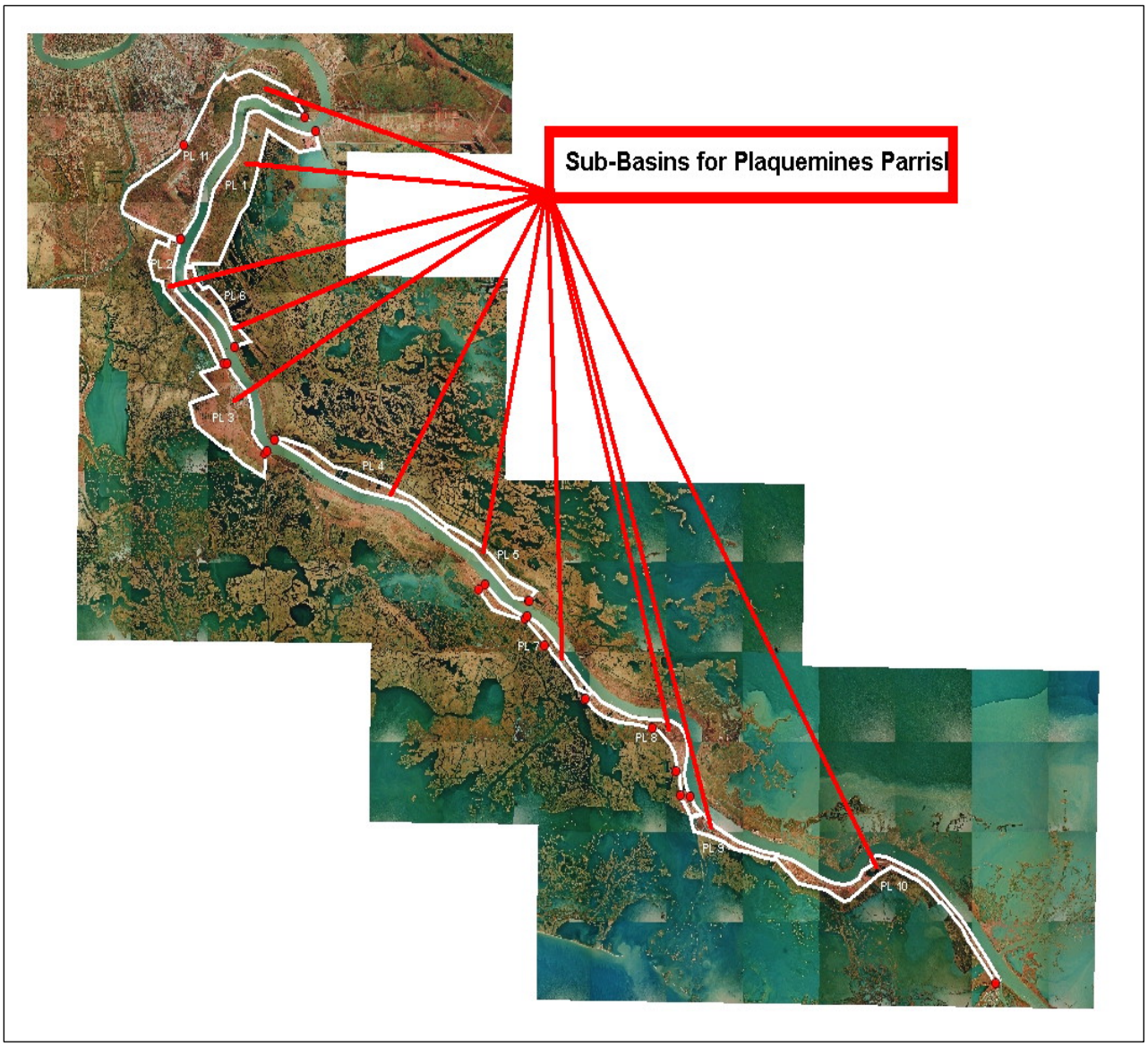

Figure 5-1. Plaquemines Parrish with levee protection footprint and sub-basins (PL1 – PL11)

PL 11

PL 11 begins along the west back of the MRT, Shown in Figure 5-2, is generally bounded on the east by the Mississippi River, the Intercoastal Waterway on the west, the Plaquemines-Orleans Parrish boundary on the north, and the Hero Canal on the south.

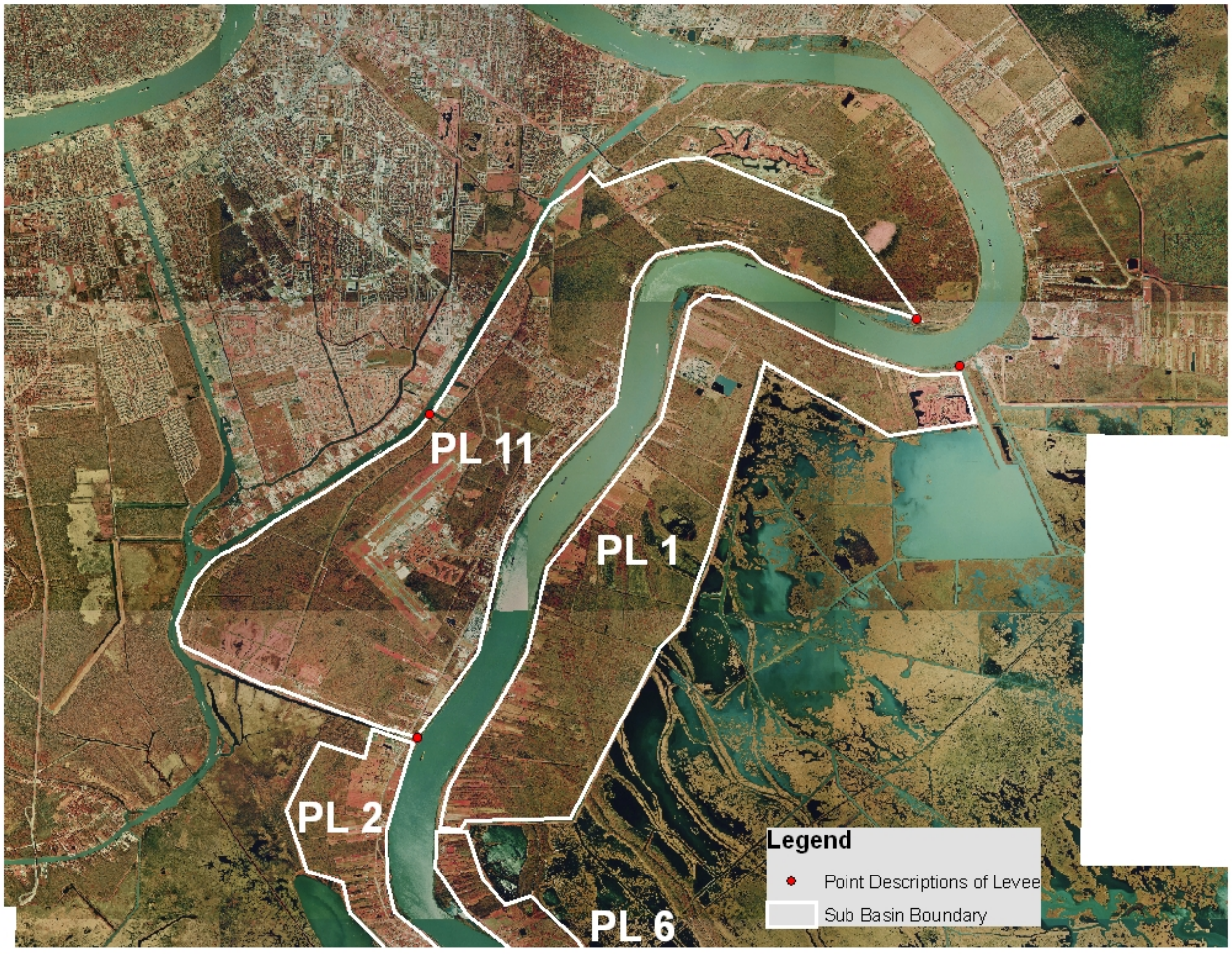

Figure 5-2. PL 11 Sub-Basins and PL 1 with Reach Beginning and Ending Points (Red Dots)

The Federal levee begins at the MRL inside the U.S. Coast Guard station.

Back levee continues inside U.S. Coast Guard Station

Back levee crossed by roadway inside U.S. Coast Guard Station. Roadway is 2 feet lover than levee. No closure structure

Back levee continues outside U.S. Coast Guard toward GIWW Station

Drainage structure under Back Levee outside U.S. Coast Guard station. Screw gat closure on culvert

Back Levee intersects Hwy 406 looking toward the GIWW and General De Gaulle Bride overpass

Back Levee intersects Hwy 406. No closure at Hwy

Back Levee passed under General De Gaulle onramp from Hwy 406. Buckling of concrete slab on levee under ramp

The interior Orleans-Plaquemines Parrish levee ends at the GIWW. The Federal Back levee along the GIWW the proceeds south and passes under the General De Gaulle Highway bridge overpass.

Going south along the GIWW to the Belle Chase Pump Station.

Sub-basin continues south along the GIWW to the Highway 23 and Railroad Bridge Crossing and Tunnel under GIWW.

Highway 23 Bridge over GIWW and Levee

Railroad Bridge

Highway 23 Bridge

Highway 23 Tunnel under the GIWW

Pipe crossing over the GIWW levee

A point of Levee Erosion along the GIWW, however most is in good condition.

Typical levee section. Numerous gates across levee to contain cattle.

Typical levee section along the GIWW

Plaquemines Pump Stations 1 and 2

PL 11 Back levee intersects Hwy 23 north of Jesuit Bend

The MRL then forms the remaining section of PL 11 as it goes north along the river to the point where it intersects the Plaquemines Parish interior levee inside the US Coast Guard station.

Numerous pipes cross over the MRL in this area.

The crown of the levee is generally 10 feet wide, with most paved and some stretches gravel.

A number of off-load facilities are located along this portion of the MRL similar to this grain loading facility.

There were a few cases of erosion along the MRL

More typical condition along this section of the MRL, with concrete paved or stone crown and concrete armored floodside.

PL 2

PL 2 begins at this point and continues south toward the Alliance Refinery as a non-Federal Levee. Figure 5-3 shows the sub-basins PL2, PL3 and PL 6.

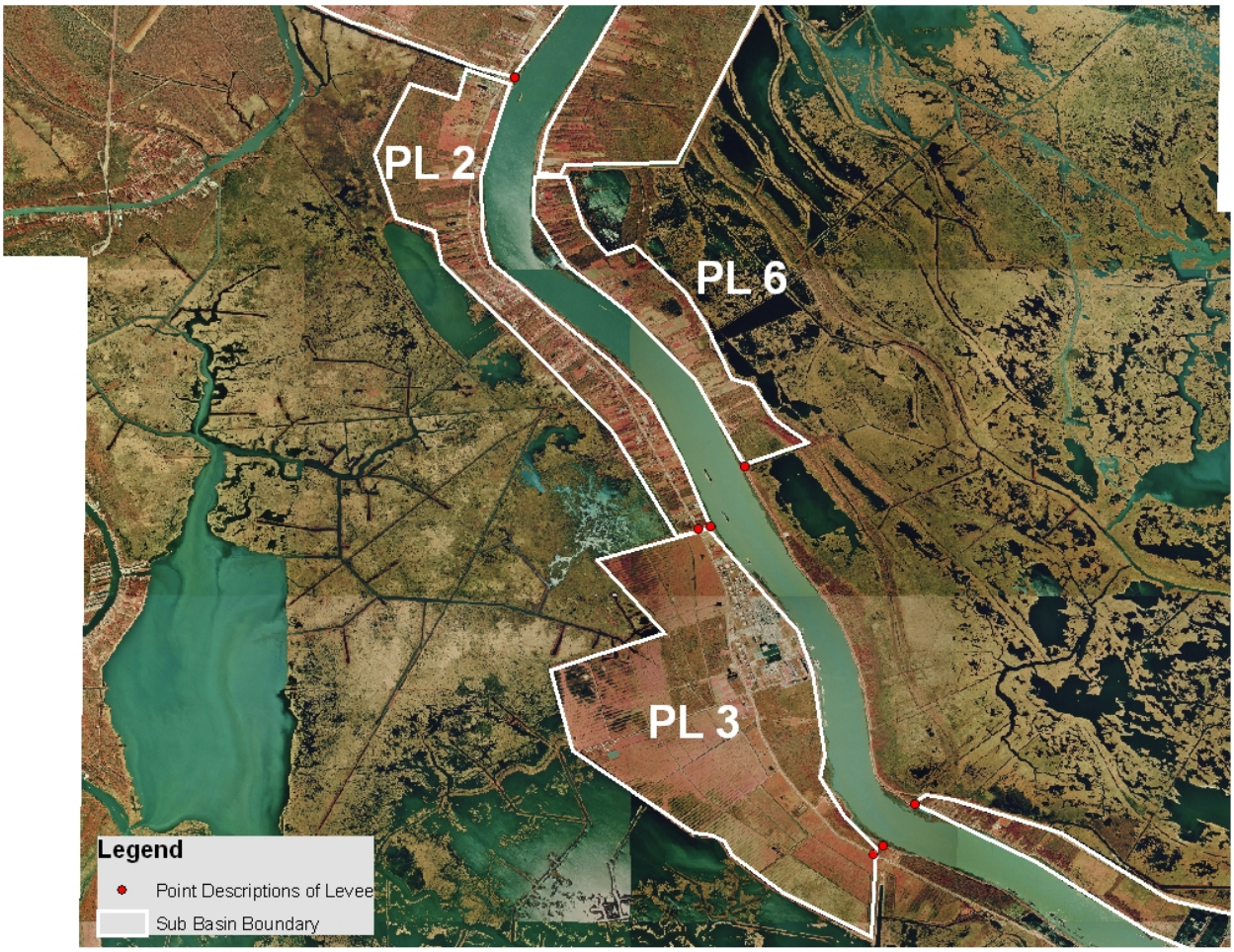

Figure 5-3. Location of Sub-basins PL 2, PL 3, and PL 6

Ollie Pump Station

The condition of the non-Federal levee varies. The crown is generally in better condition if cows are present on the levee.

The PL 2 back levee comes to an end back at Hwy 23 just north of the Alliance Refinery. It then is completed by the MRL as it goes north along the river.

PL 3

PL 3 then begins at this point, just north of the Alliance Refinery, as a non-Federal levee and proceeds southward to Myrtle Grove, where it intersects Hwy 23. Levee conditions are generally poorer than the PL 2 back levee, with large overgrowth being common. Many places are impassable by 4 WD vehicles.

The condition of the non-Federal levee also varies. The crown is generally poor condition, with much impassable by motorized vehicle.

Continuing southward, the along the MRT the sub basin enclosed by the Citrus Lands Back Levee will not be included. There was an extensive breach in this levee and continues to be difficult to keep repaired. Below is the initial repair.

Citrus Lands Back Levee repairs to breach.

The Back Levee crosses Hwy 23 and connects to the MRL. The Sub Basin enclosure then goes north as the MRL.

The Back Levee intersects the MRL after it crosses Hwy 23.

As the MRL proceeds north, numerous locations of erosion occurred due to overtopping. Some have been repaired and some not extensive enough to require repair. Debris is located on the levee top and slopes.

Also the MRL has numerous locations where the concrete armor was eroded and was replaced with stone.
More cases of erosion.

PL 4, 5, 7, 8, 9 and 10

These sub-basins are on the west bank, south of St. Jude. These sub-basins are in a project named New Orleans to Venice (NOV), Hurricane Protection Project.

NOV

The Mississippi River Levees also serve as the Hurricane protection system south of St. Jude and is part of the New Orleans to Venice, LA Hurricane Protection Project. On the East Bank, the project extends 16 miles from Phoenix down to Bohemia. On the West Bank it extends 37 miles from St. Jude to Venice.

Figure 5-4a and 5-4b give a comparison the NOV project definitions and the Sub-basin PL 4, 5, 7, 8, 9, and 10 locations.

West Bank Back Levees

St. Jude to City Price. The St. Jude to City Price reach includes 3 miles of enlarged back levees from St. Jude to City Price (between approximate river miles 47.1 and 43.9 Above Head of Passes (AHP). This levee was constructed to elevation 7.0 feet NGVD as a Non-Federal levee. The non-Federal levee was later incorporated into the Federal project at 12.5 ft NGVD). The NOV project area includes approximately 15,600 acres of land including 4,300 acres in Reach A; 3,800 acres in Reach B-1; 2,300 acres in Reach B-2; 4,500 acres in Reach C and 700 acres in the St. Jude to City Price area.

Reach A includes 13 miles of enlarged back levees from City Price to Tropical Bend and two 54" flap-gated culverts (between approximate river miles 43.9 and 30.7 AHP). It consists of approximately 12.8 miles of levee system with a net elevation of 12.5-14.5 feet and includes floodwalls at the Hayes Canal and Gainard Woods Pump Stations. The levee enlargement consisted of a marsh side embankment with a wave berm. The base of the levee incorporated geotextile fabric with a sand blanket and a clay cap at least 2 feet thick. The embankment was constructed of uncompacted clay, though a sand core may have been substituted in places. The main levee cross section is 1V on 3H.

Reach B-1 includes 12 miles of enlarged back levees with a net elevation of 15 ft. from Tropical Bend to Fort Jackson (between approximate river miles 30.7 and 20.5 AHP) and a marine floodgate at Empire. The main levee cross section is 1V on 4H. The Flood Side (FS) and Protected Side (PS) berms generally vary from 1V on 15-20H and from 1V on 12-20H respectively. The reach also includes a flood gate at Empire and floodwalls at the Bayou Grand Laird (I- and T-wall) and Sunrise Pump Stations. The Empire Floodgate is in the Empire to Gulf Waterway and consists of a reinforced concrete U-shaped gate bay with a steel gage hinged at the bottom, guide walls and fenders, inverted T-wall reinforce concrete floodwalls extending about 150 feet on each side of the structure, access road and breakwater.

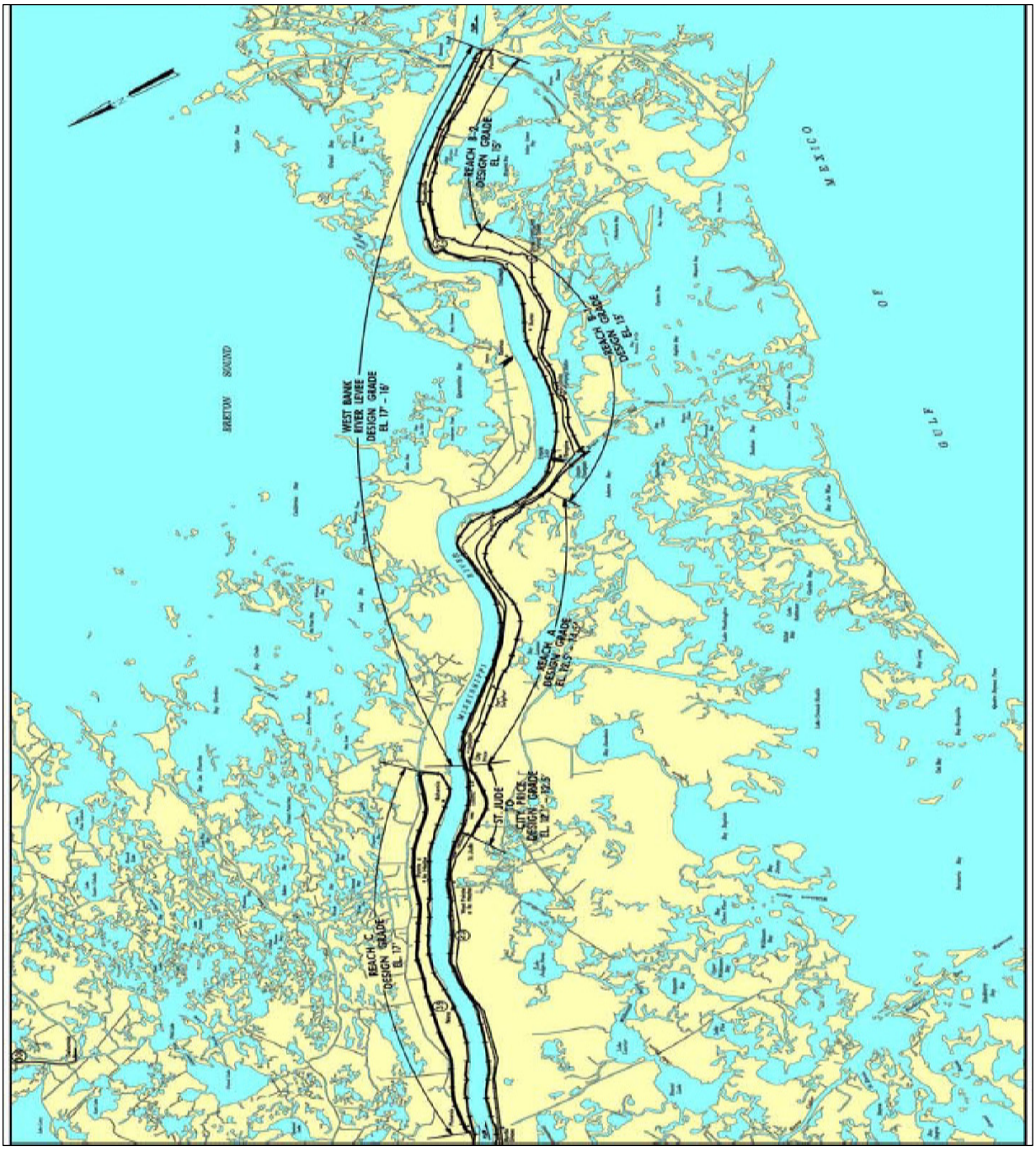

Figure 5-4a. New Orleans to Venice, LA Hurricane Protection Project

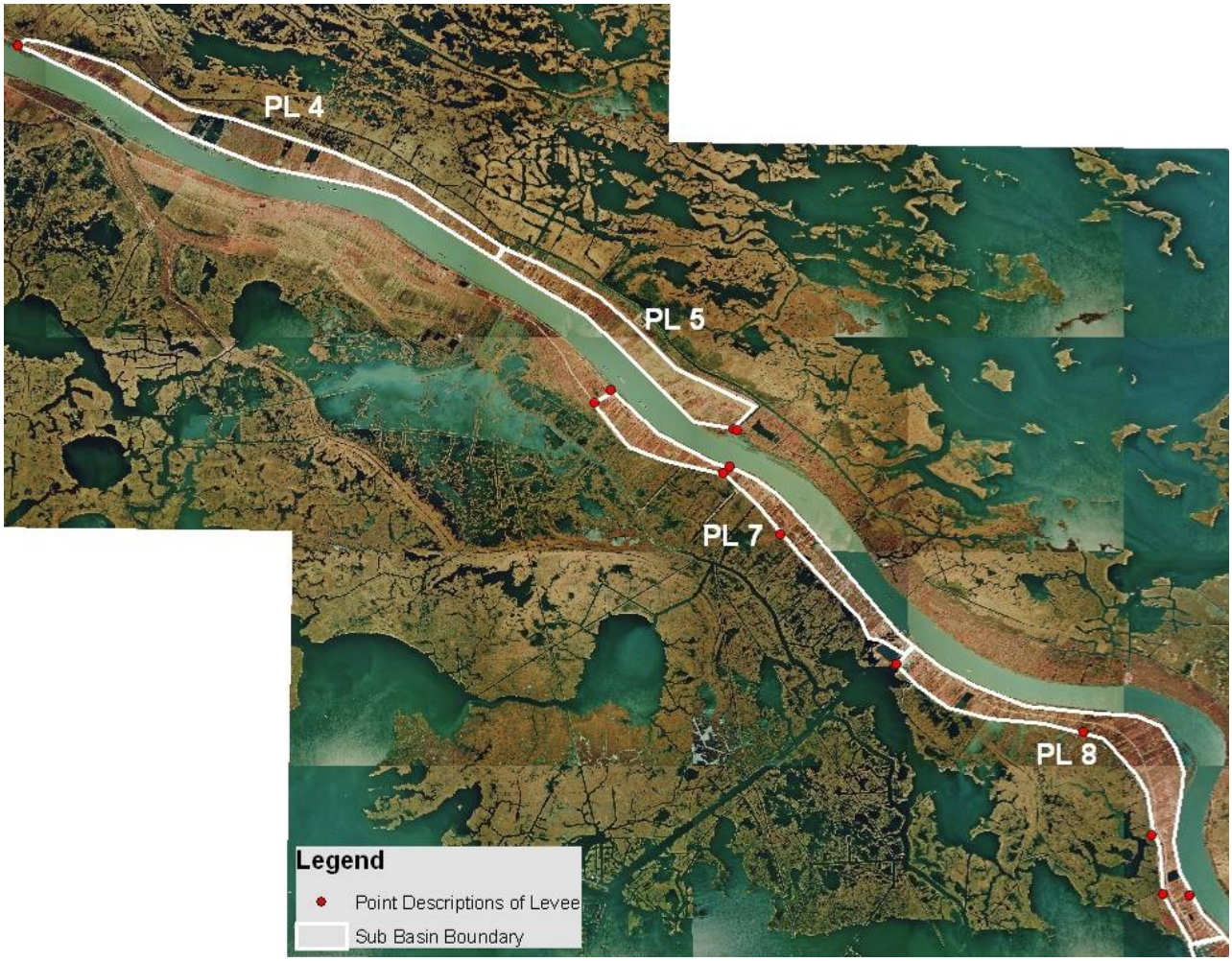

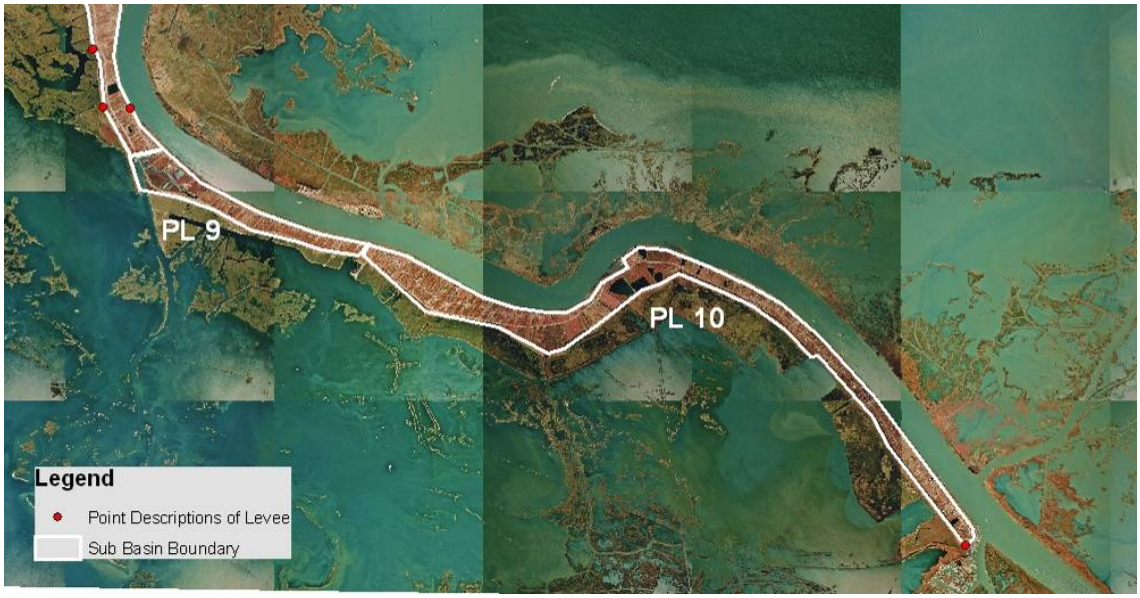

Figure 5-4b. Sub-basins PL 4, 5, 7, 8, 9, and 10

Reach B-2 includes 9 miles of enlarged back levees with a net elevation of 15 ft. from Fort Jackson to Venice between approximate river miles 20.5 and 10.4 AHP and includes floodwalls at the Venice Pump Station. The levee consists of a sand core with hydraulic clay fill. The levee construction occurred in three stages or lifts. The main levee cross section is 1V on 4H with the Flood Side (FS) and Protected Side (PS) berms generally varying from 1V on 15-74H FS and from 1V on 29-71H PS.

West Bank River Levee

The West Bank River Levee (WBRL) includes 34 miles of West Bank Mississippi River levees built to a net design elevation of 16 to 17 ft, from City Price to Venice (between Mississippi river miles 44 to 10 AHP) (Note: the lock at Empire is a State of Louisiana facility).

PL 7

Sub-basin PL 7 begins near City Price at Diamond Pump Station and continues past Hayes Pump Station and on southward near Homeplace as shown in Figure 5-4.

PL 8

Sub-basin PL 8 begins at this location and proceeds on to near Empire Lock.

PL 9

Sub-basin PL 9 begins near Empire Lock and proceeds on to near Sunrise Pump Stations.

PL 10

Sub-basin PL 10 begins at Sunrise Pump Stations and proceeds on to near Venice.

East Bank

PL 4 and PL 5

The back levee begins at Phoenix and proceeds southward to Bohemia. The separation between PL 4 and PL 5 occurs near Pointe a La Hache. Reach C of the NOV and the East Bank of the MRL enclose these Sub-basins. Reach C consists of approximately 16 miles of enlarged back levees with a net elevation of 17 feet . The back levee has a sand core with clay blanket. It was enlarged with hauled fill and raised from approximately 14 feet elevation to the 17 foot design level. It includes floodwalls (I-type sheet piling) at the pump stations near Bellevue and Pointe a La Hache. Construction of the levee to date has included three of the designed four lifts. It lays between approximate river miles 59.3 and 44.3 AHP and 10 flap-gated culverts.

The NOV was damaged by Hurricane Katrina when it made landfall near Buras-Triumph, which is on Reach B-1. The storm produced storm surge levels that exceed the level of the constructed protection. Numerous breaches occurred along the back levees on both the east and west bank sides of the NOV project. Levees were overtopped and breached, resulting in extensive erosion and scour, along both the back levees and the Mississippi River levees (as enlarged for hurricane protection). In addition there was damage to the floodgate at Empire and to the floodwalls along the MRL and back levees.

PL 1 and PL 6

The final two sub basins (PL 1 and PL 6) are on the eat bank of the river across from PL 11 (Figures 5-2 and 5-3). The non-Federal back levee begins near the Plaquemines-St. Benard Parrish boundary and continues south, ending south of Belair. The protection level is at elevation 6 feet. These sub-basins are closed by the MRL as it proceeds north along the river to the Parrish boundary.

Appendix 6
St. Bernard Basin

The St. Bernard (STB) basin is defined by the protection system along the GIWW to the north, MRGO to the east, Caernarvon Canal to the south, and the Mississippi River and Inner Harbor Navigation Canal (IHNC) to the west. Like New Orleans East, it is essentially separated into two distinct areas, a residential/commercial area on the south side of the basin and a marshlands area on the north side. These two sections are separated by a non-federal, interior local levee that runs across the basin from the northwest to the southeast. This area, along with other pertinent information relative to the IPET assessment, is depicted in Figure 6-1.

The levee and floodwall system surrounding the STB basin consists of approximately 157,800 linear feet of varying levels of protection. This provides protection for an area of approximately 81 square miles for the entire basin. The residential area makes up approximately 27 square miles of the basin. In addition, there are two water control sector gate structures along the MRGO at Bayou Bienvenue and Bayou Dupre. There are a total of 9 pump stations within the basin, primarily along the interior local levee, one of these is located along the Caernarvon Canal. These major structures are also depicted in Figure 6-1.

Like the other basins, the St. Bernard basin (STB) was constructed during different times and modified at various places since the last Design Memorandums. For the purposes of IPET and coupled with varying versions of the most recently completed Design Memorandums (DM), the STB basin is separated into three major stretches. These are as follows:

North Side of IHNC Lock thru Caernarvon Canal. This stretch of the STB basin represents the exterior hurricane protection system and begins at the tie-in to the north side of the IHNC Lock, continues northeast along the GIWW, turns and follows the MRGO to the southeast, then goes west back towards the tie-in to the Mississippi River levee.

Mississippi River Levee (MRL). This section is the flood protection system along the Mississippi River system that contains a combination of floodwalls and levees. For numbering purposes, the MRL reaches begin at the tie-in with the Caernarvon Canal and runs northwest along the Mississippi River until it ties back in with the south side of the IHNC Lock.

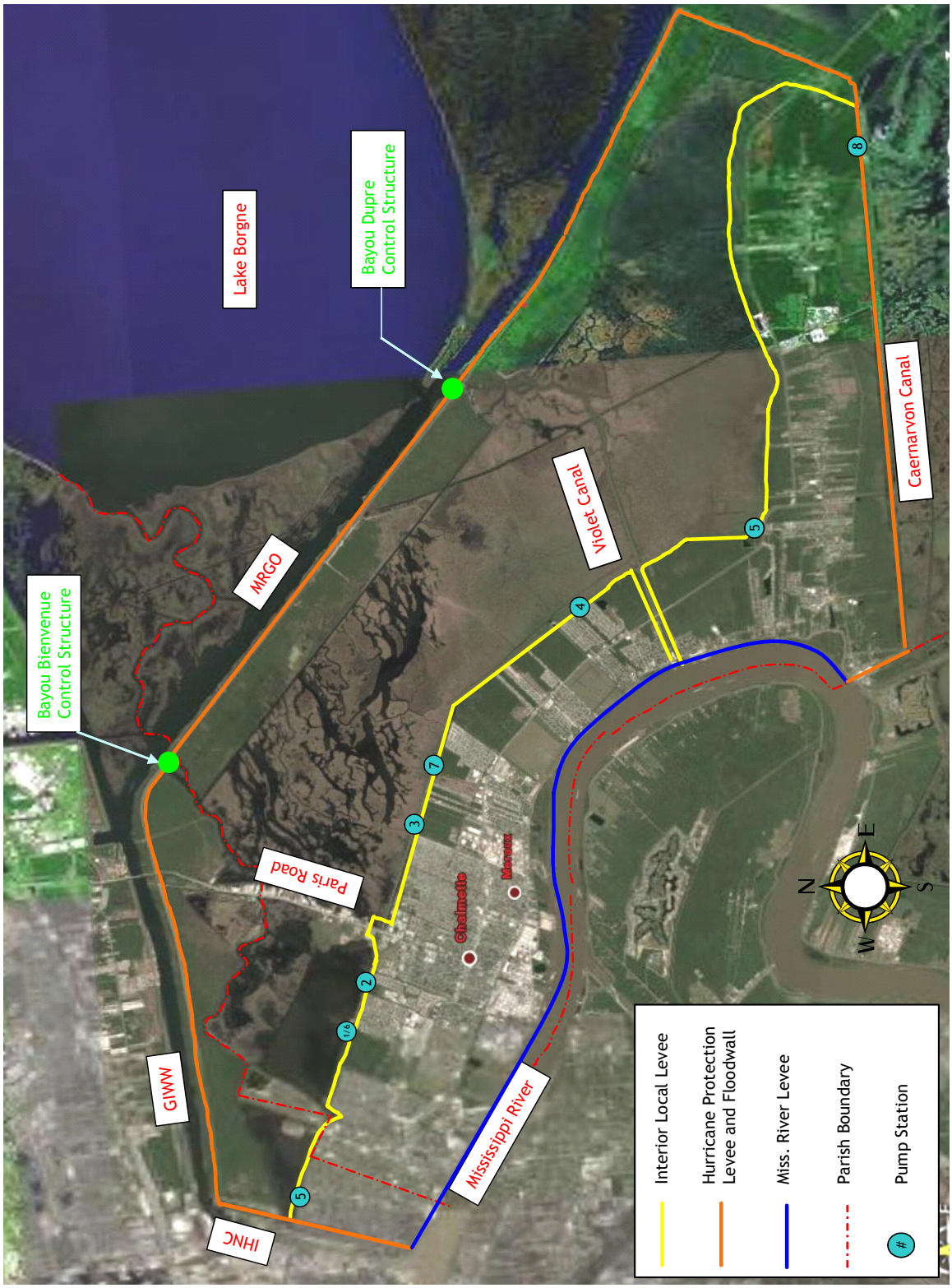

Figure 6-1. St. Bernard Basin

Interior Local Levee (ILL). This section of levee and floodwall separates the residential and marshland areas of the STB basin. The ILL is actually owned by the state of Louisiana and maintained by the LaDOT and Lake Borgne Basin Levee District. USACE was provided a one-time waiver from policy and was tasked with repairing the damage to this levee following Katrina. The ILL basically splits the basin in two and begins along the IHNC and heads generally in a southeast direction along the middle of the basin. The ILL "wraps" around the Violet Canal and goes generally east before turning south and tying back into the exterior levee protection system along the Caernarvon Canal.

STB Basin – Layout of Reaches for Risk Model by Physical Feature (Pre-Katrina)

Within these major stretches of the STB basin there are shorter reaches, which are defined by physical changes in the protection system, i.e., switching from floodwall to levee, etc, or by significant changes in geotechnical parameters. Within each reach, there are specific "key points" whose reliability needs to be determined in order to calculate the effect on the overall reach being evaluated. An example of a "key point" would be a closure gate at a road or rail line crossing along a floodwall. Task 10 engineers reviewed existing plans, damage survey reports, and conducted field verification inspections to ensure each basin was accurately defined within the system. As a part of the field verification inspections, GPS coordinates were obtained and stationing from DM's and "as-built" plans was verified. For each basin, this information was transformed into a spread sheet and then a system map for each basin, as shown in Figure 6-2. Finally, digital photographs with incorporated notes were developed to compliment the spread sheets and system map for further clarification. This collection of information was then categorized to get a clear picture of how the basin should be defined for risk assessment purposes. A summary of the reach and point definitions for STB is shown in Figure 6-2a with a brief supporting narrative on each reach. The layout shown in Figure 6-2b and the narrative that goes along with this figure relates to the pre-Katrina condition. Task Force Guardian (TFG) is making several improvements to the levee/floodwall system which changes the risk for various reaches. These changes by reach are detailed in the next section.

Task 10 basin reach definitions for STB start at the tie-in to the north side of the IHNC Lock. The numbering system for reach definitions continues along the exterior protection system along the GIWW, MRGO, Caernarvon Canal, and then up through the Mississippi River levee system to where it ties back into the south side of the IHNC Lock. Finally, the interior local levee reaches numbers begin at the IHNC and extend until it ends at the Caernarvon Canal. Please refer to Figures 6-1, 6-2a, and 6-2b for further clarification. The STB basin is summarized by the reaches as follows:

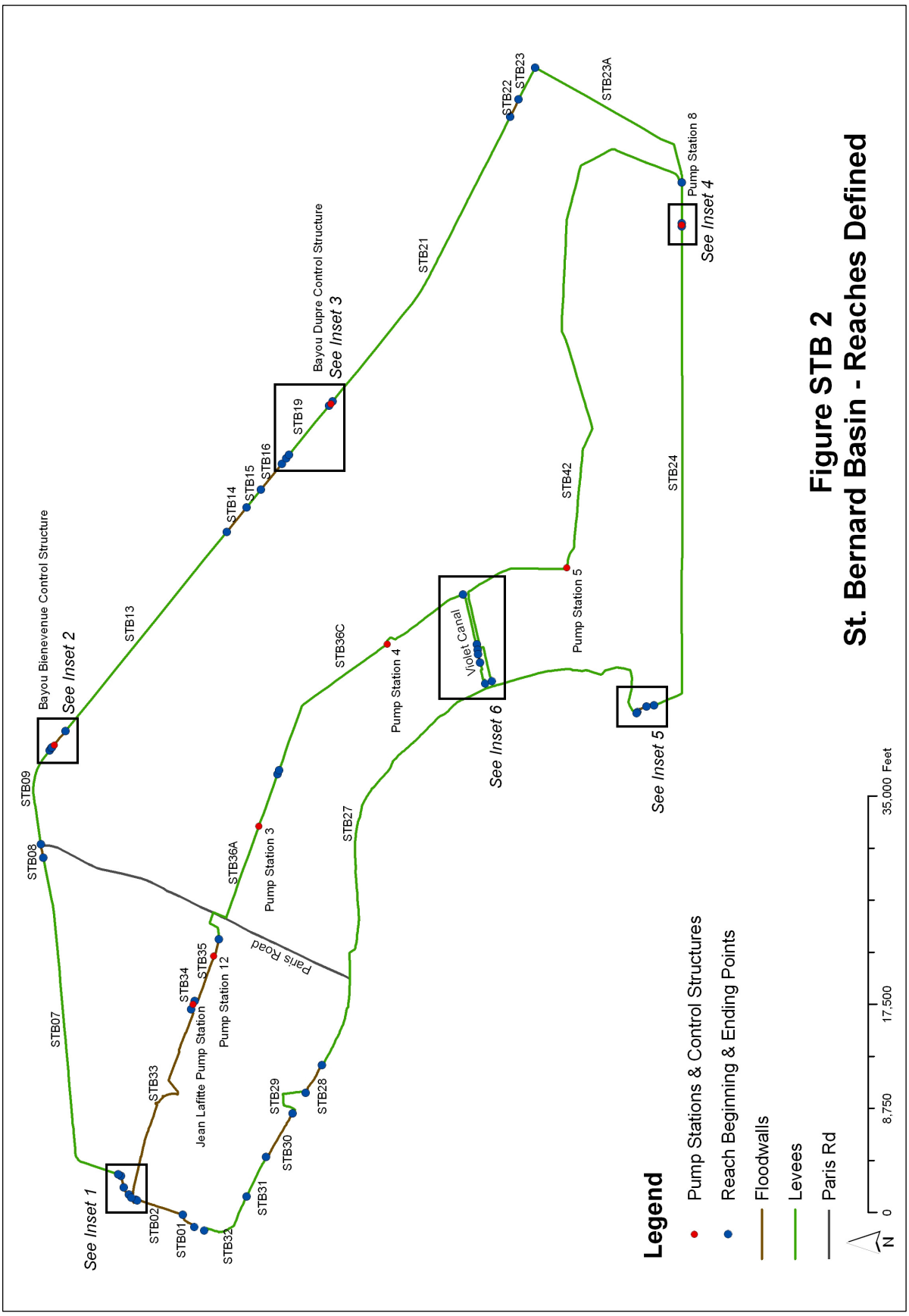

Figure 6-2a. St. Bernard Basin – Reaches Defined

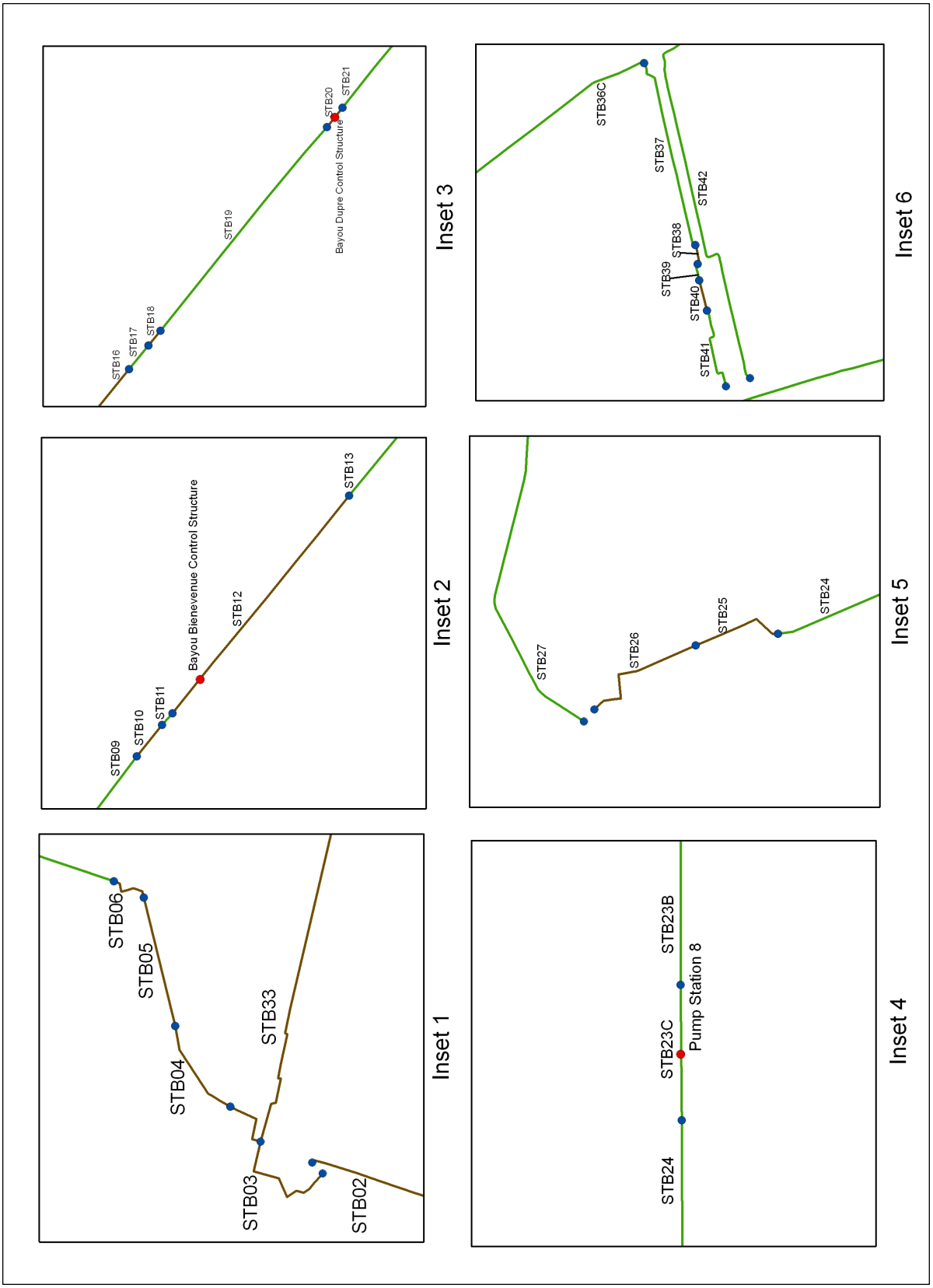

Figure 6-2b. St. Bernard Basin Reaches – Insets 1-6

Reach STB1 (INHC to Caernarvon). This reach is defined by 1,427 linear feet of concrete capped I-wall that ties into the northeast side of the INHC Lock and generally follows the IHNC north, see Figure 6-3, which shows the beginning of the reach where it ties into the northeast lock wall of the IHNC. There is one key point (stb1a) at the beginning of this reach where the natural ground line transitions between the lock wall and I-wall, as shown in Figure 6-4. The reach ends at the south end of the I-wall failure that occurred in the Lower 9th Ward. Other sections of this reach were overtopped during Katrina, but did not fail, in particular near the Claiborne Bridge, as shown in Figure 6-4. The approximate weighted average top of wall elevation for this reach was 13.0 (NAVD88) prior to Katrina.

Figure 6-3. I-wall Section Tying into IHNC Lock Wall (Standing on top of lock wall and looking away from IHNC)

Figure 6-4. Section of Reach STB1 Overtopped During Katrina (Location is just north of Claiborne Avenue Bridge)

Reach STB2 (IHNC to Caernarvon). This reach *was* defined by a 4,038' stretch of I-wall between the Claiborne Avenue Bridge and the railroad bridge near Florida Avenue. There were two separate breaches of this I-wall during Katrina. The southern section of I-wall that failed in the Lower 9th Ward area of St. Bernard during Hurricane Katrina is shown in Figure 6-5. Figure 6-6 shows the authorized design section for this wall, but note the actual elevations for the top of wall were closer to 13.0 when referencing NAVD88 (2004.65) datum. The northern section of I-wall that failed was near the blue railroad bridge close to Florida Avenue. This breach is depicted in Figure 6-7. There were no "key points" within this entire reach. Refer to changes being made by Task Force Guardian (TFG) in the post-Katrina narrative.

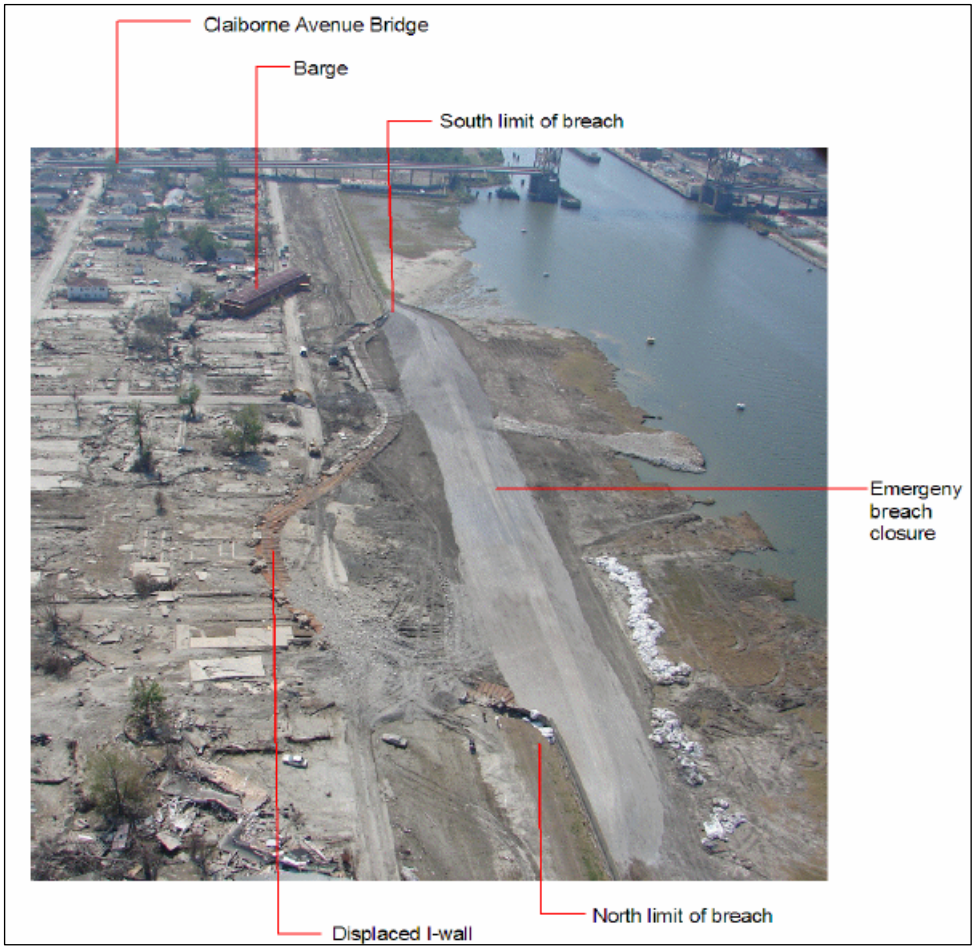

Figure 6-5. Failed I-wall Section of Lower 9th Ward (Reach STB2) (Looking south along IHNC)

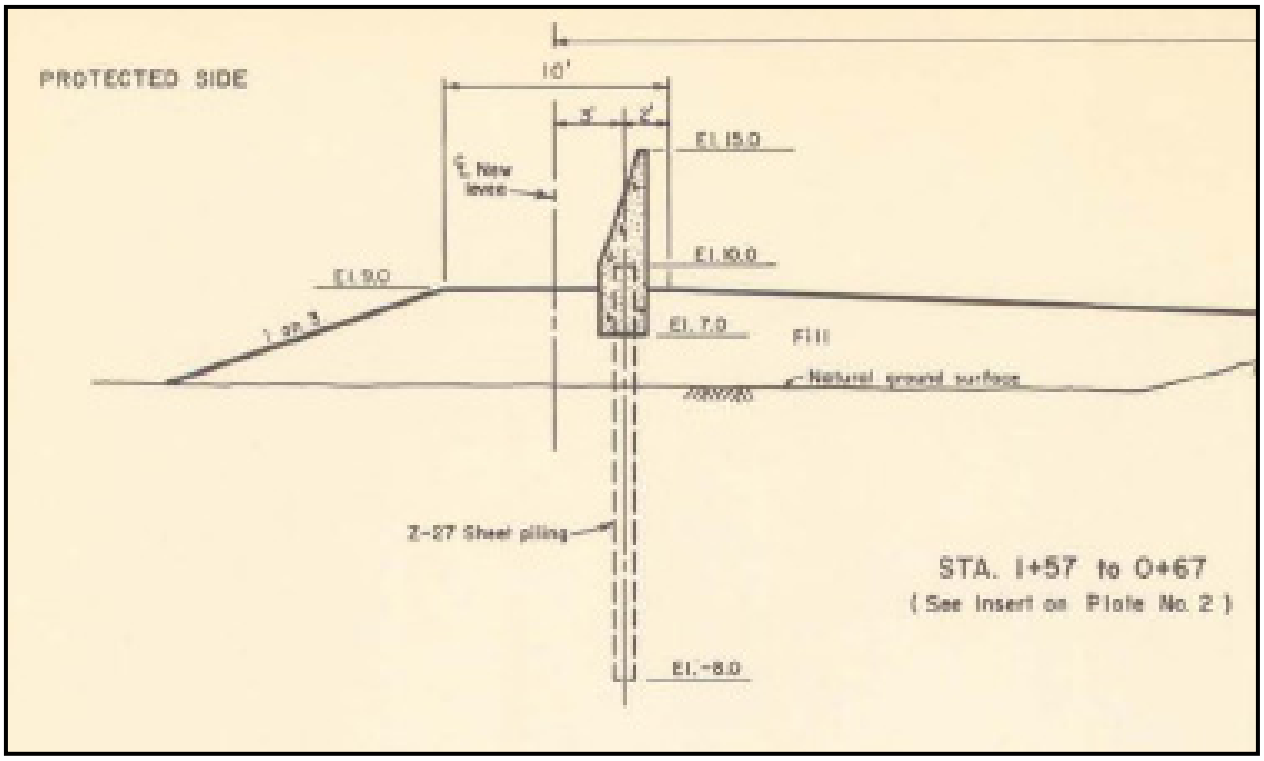

Figure 6-6. Pre-Katrina I-wall Design Section for Reach STB2 (Depicts authorized elevations, not actual elevations)

Figure 6-7. North I-wall Failure within Lower 9th Ward (Reach STB2) (Note: pipes on right side of photo are associated with Pump Station #5)

Reach STB3 (INHC to Caernarvon). This reach is defined by an existing t-wall that is located adjacent to the Surekote Road ramp over the floodwall. The reach is approximately 807 feet in length. There are multiple key points within this reach including the closure gate E-1, as shown in Figure 6-8. Closure gate S-1 at Harbor Road and Florida Avenue and railroad closure gate E-2 are also key points within this reach. The approximate weighted average height of this wall prior to Katrina was elevation 12.5 (NAVD88).

Figure 6-8. Existing T-wall Near Florida Ave. Bridge (Reach STB3) (Looking from protected side towards IHNC)

Reach STB4 (INHC to Caernarvon). This reach is defined by 726 linear feet of I-wall that ties into the levee along the GIWW. There are no key points in this reach. This reach ends where the I-wall ties into the levee. This section of I-wall was overtopped during Katrina, but suffered no major damage. It had an approximate weighted average top of wall elevation of 13.3 (NAVD88) prior to Katrina.

Reach STB5 (INHC to Caernarvon). This reach is defined by 890 linear of levee between the end of the IHNC I-wall and the floodwalls surrounding closure gates S-2 and S-3 near the Southern Scrap Building. There are no key points within this reach. This levee is depicted in Figure 6-9. There was no significant damage to this section from Katrina. It had an approximate weighted average elevation of 13.1 (NAVD88) prior to Katrina.

Figure 6-9. Beginning of Reach STB5 at End of I-wall (Note TFG improvements to Reach STB4 in foreground)

Reach STB6 (IHNC to Caernarvon). This reach is defined by a combination of I-walls and t-walls surrounding closure gates S-2 and S-3. The total length of the reach is 340 feet with t-walls located around the gate closures. These walls were overtopped during Katrina but did not fail. The approximate weighted average top elevation of this reach was 13.0 (NAVD88) prior to Katrina. Reference improvements to the scour protection being made by TFG in the post-Katrina reach description. The gates themselves serve as the two "key points" within this reach, stb6a and stb6b, respectively.

Reach STB7 (IHNC to Caernarvon). This reach is defined by 25,722 feet of levee. There is one pipe crossing located within this reach but it does not represent a significant departure from the levee section and can be ignored for the purposes of this assessment. There was no significant damage to this section of levee from Katrina. The approximate top of levee varied along this reach between 13.5 to 16.5 (NAVD88), but had a weighted average elevation of 15.1 (NAVD88) prior to Katrina.

Reach STB8 (IHNC to Caernarvon). This reach is defined by a 1,016 feet stretch of concrete capped I-walls and t-walls just west of the Paris Road overpass along the GIWW. It is often referred to as the Paris Road floodwall. There is one key point (stb8a), a gate closure, within this floodwall reach. This structure was overtopped during Katrina, but only suffered scour damage. See Figure 6-10 for a photograph depicting this wall during repairs following Katrina. The approximate weighted average top of wall elevation for this reach was 12.4 (NAVD88) prior to Katrina.

Figure 6-10. Paris Road Floodwall (Reach STB8) (Looking east from the west end of the floodwall)

STB9 (IHNC to Caernarvon). This reach is defined by 7,260 linear feet of levee. It goes between the Paris Road floodwall and the floodwalls just prior to reaching the Bayou Bienvenue control structure. There are no key points within this reach. There was some overtopping in this reach during Katrina, but no major damage to the levee. The approximate weighted average for this reach was elevation 17.9 (NAVD88) prior to Katrina.

STB10 (IHNC to Caernarvon). This section is defined by a relatively short 229 feet stretch of flood wall located just northwest of the Bayou Bienvenue Control Structure. It consists of a 61 feet section of I-wall at elevation 17.0 (NAVD88), a 107 feet stretch of t-wall at elevation 15.5 (NAVD88), and another 61 feet of I-wall at elevation 17.0 (NAVD88). The weighted average top of wall across the entire reach is 16.3 (NAVD88). During original construction, this short section of wall was to serve as an access point for an industry that was to be located near the Bayou Bienvenue Control Structure. However, the industry went out of business and it has never been utilized and the flood gate remains permanently closed. This section of wall was overtopped during Katrina as evidenced in Figures 6-11 and 6-12. Since the gate remains permanently closed, there are no "key points" within this reach.

STB11 (IHNC to Caernarvon). This reach is defined by a short section of levee between the floodwall described in reach STB10 and the beginning of the floodwall leading to Bayou Bienvenue Control Structure. The levee section is only 96 feet long and received some damage during Katrina at the transitions to adjoining I-wall sections, as shown in Figure 6-12. The levee had an average weighted elevation of 16.0 (NAVD88) prior to Katrina. There are no "key points" within this short reach.

Figure 6-11. Floodwall Northwest Bienvenue Structure (Reach STB10) (Looking southeast toward Bayou Bienvenue just after Katrina)

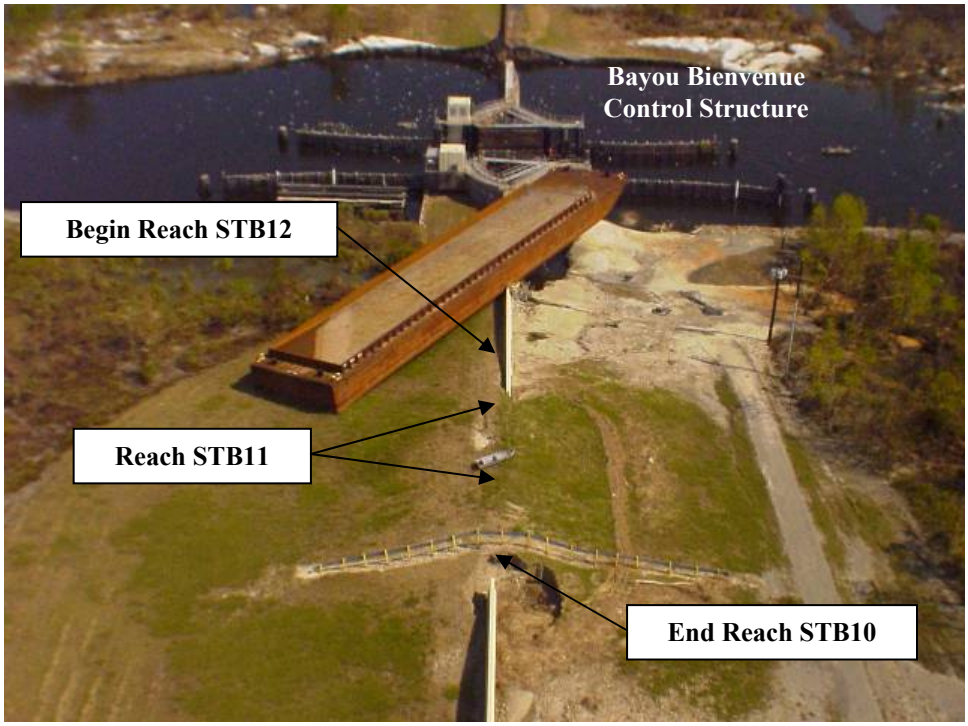

Figure 6-12. Short Levee Section Between Floodwalls (Reach STB11)

Reach STB12 (IHNC to Caernarvon). This reach is defined by the Bayou Bienvenue Control Structure and surrounding floodwalls on either side of it. Prior to Katrina, this reach was made up of 77 feet of concrete capped I-wall at elevation 17.0 (NAVD88), 187 feet of t-wall surrounding the control structure itself at elevation 15.0 (NAVD88), and then 1,208 feet of uncapped, sheet pile I-wall at elevation 18.5 (NGVD). As shown in Figures 6-12, 6-13, and 6-14, the surrounding floodwalls received heavy damage and the uncapped I-wall section failed during Katrina. The sector gate closure itself serves as the only "key point" (stb12a) within this reach.

Figure 6-13. Failed Uncapped I-wall Section on Southeast Side of Bayou Bienvenue Control Structure (Looking southeast along the MR-GO)

Figure 6-14. Picture of Failed Bienvenue I-wall from Protected Side

Reach STB13 (IHNC to Caernarvon). This reach is defined by a 19,858 linear feet stretch of levee. Prior to Katrina, it began at the end of the uncapped sheet pile I-wall on the southeast side of the Bayou Bienvenue Control Structure and continued up to the beginning of an embedded, uncapped I-wall section along the MR-GO. This section of levee was overtopped during Katrina and was heavily damaged. It had an approximate weighted average top elevation of 17.5 (NGVD) based upon a 1998 survey. There was one section of embedded uncapped, sheet pile I-wall in about the middle of this reach, but the top of the wall essentially was at the top of the levee. Due to this fact, this section of I-wall will not be included separately in the analysis and is included as part of the overall reach characteristics.

Reach STB14 (IHNC to Caernarvon). This reach was defined by a 2,427 feet section of uncapped I-wall embedded within the levee. The sheet pile I-wall was installed in 1992 as part of USACE repairs along the MR-GO. This section of wall was heavily damaged during Katrina, as evidenced in Figure 6-15. The weighted average top elevation of the uncapped I-wall was 18.5 (NGVD) prior to Katrina and it had a free standing height of approximately 3.5 feet. As shown in the photo, there are pipe crossings along this reach, but they extend over the levee and do not represent a major change in design or performance parameters, therefore, they are ignored in the risk assessment for this purpose.

Figure 6-15. Failed I-wall Along MR-GO

Reach STB15 (IHNC to Caernarvon). This reach consists of a 1,745 linear feet stretch of levee between uncapped sheet pile I-wall reaches. This section was overtopped and heavily damaged during Katrina. The weighted average height of this levee section was approximately 16.4 (NGVD) prior to Katrina based upon a detailed 1998 survey. There are no "key points" within this reach.

Reach STB16 (IHNC to Caernarvon). This reach consisted of a 2,560 feet stretch of uncapped sheet pile I-wall that was installed in 1992 as part of USACE repairs along the MR-GO. This section also was overtopped and heavily damaged during Katrina. The weighted average top of uncapped I-wall along this reach was elevation 18.5 (NGVD) prior to Katrina. It had an approximate free standing height of 3.5 feet. There are no "key points" within this reach.

Reach STB17 (IHNC to Caernarvon). This reach consists of 566 feet on levee between uncapped, sheet pile I-wall reaches. The approximate weighted average top of levee elevation was 16.5 (NGVD) prior to Katrina based upon a detailed 1998 survey. This section of levee was overtopped during Katrina and heavily damaged. There are no "key points" within this reach.

Reach STB18 (IHNC to Caernarvon). This reach consists of 359 feet of uncapped, sheet pile I-wall installed in 1992 as part of USACE repairs along the MR-GO. The wall had an approximate top elevation of 18.5 (NGVD) with a free standing height of roughly 3.5 feet. It was overtopped and heavily damaged during Katrina. There are no "key points" within this reach.

Reach STB19 (IHNC to Caernarvon). This stretch of levee runs from the end of the uncapped I-wall in Reach STB18 to the northwest transition wall leading to the Bayou Dupre Control Structure. It is approximately 4,994 linear feet and there are no "key points" within this length. It had an approximate weighted average top elevation of 18.7 (NGVD) prior to Katrina. This reach was heavily damaged during Katrina.

Reach STB20 (IHNC to Caernarvon). This reach includes the Bayou Dupree Control Structure and the adjoining transition flood walls. Prior to Katrina, the reach started with 92 linear feet of precast concrete sheet pile wall on the northwest side of the gate structure, 69 feet of t-wall on the northwest side of the gate closure, 134 feet across the closure structure, 69 feet of t-wall on the southeast side of the closure structure, and then 92 feet of precast concrete sheet pile wall on the southeast side of the closure structure. While the concrete sheet pile walls were designed at a higher elevation, settlement across this area left all walls roughly at elevation 15.2 (NAVD88) prior to Katrina. As shown in Figure 6-16, the northwest precast concrete sheet pile I-wall failed during Katrina. The only "key point" in this reach is the closure structure itself.

Reach STB21 (IHNC to Caernarvon). This reach starts with the levee tie-in to the southeast side of the Bayou Dupre Control Structure adjoining floodwall. The approximate length of this reach is 25,562 linear feet and it has no "key points" within the reach. Prior to Katrina, it had a weighted average top elevation of 19.1 (NGVD). The reach was heavily damaged during Katrina from overtopping.

Reach STB22 (IHNC to Caernarvon). This reach was defined by a 1,401 feet section of uncapped, sheet pile I-wall that was installed during 1992 USACE repairs along the MR-GO. The wall had a top elevation of 19.0 (NGVD) prior to Katrina and a free standing height of approximately 4.0 feet. There were no "key points" within this reach. There was scour damage in this area as a result of Katrina.

Figure 6-16. Damage at Bayou Dupre Control Structure (Note failed section of precast concrete pile wall)

Reach STB23a (IHNC to Caernarvon). This reach is defined by the remaining levee along the MR-GO between the end of Reach STB22 and where it turns away from along the Caernarvon Canal. The weighted average top of levee elevation for this reach was approximately 19.5 (NGVD) prior to Katrina. There are no "key points" within this reach. Sections of this reach did receive damage during Katrina.

Reach STB23b (IHNC to Caernarvon). This reach consists of 5,709 feet of levee that begins at the MR-GO and continues to the intersection point with the interior local levee. Although the levee along the Caernarvon Canal continues a new reach had to be defined because the potential for varying consequences due to the presence of the interior local levee. This area of levee received minor damage during Katrina. There are two basic areas along this reach where repairs will be different. The weighted average top elevation of this reach was approximately 17.0 (NAVD88) prior to Katrina. There is one "key point" within this reach (stb23bd) which is the Bayou Road closure gate.

Reach STB23c (IHNC to Caernarvon). This section of levee is 2,692 feet long and goes from the interior local levee to the beginning of the east side floodwall surrounding Pump Station #8. There was minimal scour damage along this stretch during Katrina. It had an approximate weighted average top elevation of 16.0 (NAVD88) prior to Katrina. There are no "key points" within this reach.

Reach STB23d (IHNC to Caernarvon). This reach consists of 231 feet of flood wall around the discharge pipes for Pump Station #8. There are roughly 45 feet of I-walls on both sides of the middle t-wall for the discharge pipes. The t-wall length is approximately 141 feet long. The

top of the I-walls are elevation 17.0 (NAVD88) and the t-wall is at 16.5 (NAVD88). The weighted average top of wall elevation is 16.7 (NAVD88). This wall was not damaged or overtopped during Katrina. There are no "key points" within this reach. For a view of this reach, please refer to Figure 6-17.

Figure 6-17. Floodwalls Surrounding Pump Station #8 Pipes (Viewed Looking West Along Caernarvon Canal)

Reach STB24 (IHNC to Caernarvon). This reach is defined by 36,610 linear feet of levee along the Caernarvon Canal. It starts on the east side at the where it ties into the west end of the Pump Station #8 floodwall and continues until it ties into a sheet pile wall near the Caernarvon Freshwater Diversion Structure. This section received little or no damage during Katrina. There are several utility crossing along this reach, but none significant enough to warrant as a "key point". The approximate weighted average top elevation of the levee is 15.4 (NAVD88) across this reach.

Reach STB25 (IHNC to Caernarvon). This reach consists of 693 linear feet of uncapped, sheet pile I-wall near the Caernarvon Freshwater Diversion Structure. There are no "key points" within this reach. It received little or no damage from Katrina. The reach has a weighted average top elevation of 12.8 (NAVD88) taken with a physical survey following Katrina. See Figure 6-18 for a photograph of this reach.

Figure 6-18. Uncapped Sheet Pile I-wall Near Caernarvon Canal (Building on left side is on flood side)

Reach STB26 (IHNC to Caernarvon). This reach consists of concrete capped I-walls that extend from the end of the sheet pile wall in Reach STB25 to the where the Caernarvon section ties into the Mississippi River levee. This section of wall is 1,104 feet long with a weighted average elevation of 13.0 (NAVD88). It was not damaged during Katrina. There are two "key" points within this reach and both are closure gates, one for a rail line and the other for Highway 39. The location where the floodwall ties into the higher Mississippi River levee is shown in Figure 6-19.

Reach STB27 (Mississippi River Levee). This reach is the most southern section of levee within the STB basin, as reflected as the higher ground area of Figure 6-19. Refer to Figure 6-2 for reference to the reach location relative to the entire polder. The reach consists of 49,877 linear feet of levee and it ends at the southern end of the concrete capped I-wall near the Battlefield site along the Mississippi River. It has a weighted average top elevation of 20.1 (NAVD88).

Reach STB28 (Mississippi River Levee). This reach consists of 2,724 feet of concrete capped I-wall near the Battlefield site. There is one key point with this reach and it is a small access closure gate. A typical stretch of this wall along with the access closure gate is shown in Figure 6-20. The weighted average elevation of the top of the wall for this reach is 17.6 (NAVD88). This reach was not damaged during Katrina.

Figure 6-19. Caernarvon Canal Floodwall Tie-in to Higher MRL (Gate is for Highway 39 closure)

Figure 6-20. Concrete Capped I-wall Along Miss. River Near Battlefield (Access closure gate is key point within this reach)

Reach STB29 (Mississippi River Levee). This reach consists of 3.729 feet of levee along the Mississippi River in and around the Rodriguez Canal. There are four key points within this reach, all gated closures near the Rodriguez Canal. The reach ends where the levee ties into a floodwall near the Domino Sugar Plant. The weighted average top elevation of the levee along this reach is 20,9 (NAVD88). This reach was not damaged during Katrina.

Reach STB30 (Mississippi River Levee). This reach is defined by 5,180 linear feet of concrete capped I-wall that begins near the Domino Sugar Plant. There are three key points within this reach, all of them closure gates. One is located at the Domino Plant, one at the Port Ship Service Dock, and the last one at Mehle Avenue. The weighted average elevation of the top of the wall along this reach is 18.0(NAVD88). This reach was not damaged during Katrina. One of the closure areas and typical I-wall along this stretch is shown in Figure 6-21.

Figure 6-21. Concrete Capped I-wall Near Domino Sugar Plant (Closure represents key point within this reach)

Reach STB31 (Mississippi River Levee). This reach consists of 2,345 feet of levee that is primarily covered with paved slopes and roads. It begins near the Jackson Barracks and ends at the warehouse and dock area near Flood Street. The weighted average elevation along this stretch of levee is 19.0 (NAVD88). There are no key points within this reach, although there are some pipe crossings noted, but not considered significant enough to effect the overall reliability of the reach. This reach was not damaged during Katrina. The end of this reach (viewed from the Reach STB30 side) is shown in Figure 6-22.

Figure 6-22. End Reach STB31 Where Levee Ties into Dock Facility (Viewed from Reach STB30 side)

Reach STB32 (Mississippi River Levee). This reach consists of 4,870 linear feet of levee along the Mississippi River and southeast side of the Inner Harbor Navigation Canal. It begins at the warehouse/dock facilities on the levee near Flood Street and ends at the southeast side of the Inner Harbor Navigation Canal Lock. The weighted average elevation of the top of this levee is 20.9 (NAVD88). There are no key points within this reach. This reach was not damaged during Katrina.

Reach STB33 (Interior Local Levee). This reach consists of approximately 15,455 linear feet of uncapped sheet pile I-wall. The reach starts at the north side of the Interior Local Levee near Pump Station #5, as shown in Figure 6-23. There are two key points within this reach. The first is a railroad closure near the East Bank Wastewater Treatment Plant and the second is a timber closure across a road. An aerial view of the location where the interior local levee sheet pile wall ties into the concrete capped I-wall along the IHNC is shown in Figure 6-23. A close-up view of the start of the interior local levee is shown in Figure 6-24. This location is referenced in Figure 6-23. This reach had a weighted average top of wall elevation of 13.5 (NAVD88) prior to Katrina. Most of this reach was not damaged during Katrina. There was a 4,500 feet stretch of uncapped I-wall and levee near the parish line along this reach that was damaged and in need of repair. The general area where the parish line crosses the interior local levee is shown in Figure 6-1.

Reach STB34 (Interior Local Levee). This reach consists of 685 feet of concrete floodwall surrounding the Jean LaFitte Pump Station. The weighted average top elevation of this reach is 14.0 (NAVD88) taken from a 1999 LaDOT physical survey of the ILL. There was no significant damage during Katrina. There are no key points within this reach.

Figure 6-23. Area Showing Beginning of Interior Local Levee @ IHNC

Figure 6-24. Close-up of Beginning of Interior Local Levee

Reach STB35 (Interior Local Levee). This reach consists of 5,055 linear feet of uncapped sheet pile I-wall within the levee. The weighted average top elevation of this reach is 13.3 (NAVD88) taken from a 1999 LaDOT physical survey of the ILL. There are a couple of pipe crossings along this reach, but no key points for the risk assessment. There was overtopping along this reach during Katrina, but no major damage. The end of the reach where the I-wall ties into an adjoining levee (beginning of Reach STB36) is shown in Figure 6-25.

Figure 6-25. End of Reach STB35 @ Beginning of Reach STB36 (Interior Local Levee near Paris Road)

Reach STB36a (Interior Local Levee). This reach is defined by 15,105 linear feet of levee between floodwalls. The reach begins approximately 2,400 feet west of Paris Road (see Figure 6-25) and ends where the levee ties into the west end of the sheet pile I-wall leading to Pump Station #7 (Bayou Ducros Pump Station). There are two basic sections within this reach, the first is the short section west of Paris Road that had a weighted average elevation of 11.6 (NAVD88) prior to Katrina. From Paris Road east, the weighted average elevation of this reach was 8.4 (NAVD88) prior to Katrina. The main reason this reach is sub-divided is because of the work being carried out by TFG is only being done east of Paris Road with respect to raising the levee. The weighted average top of levee for this reach was 8.9 (NAVD88) prior to Katrina. There was significant overtopping damage to the section of levee east of Paris Road during Katrina. There are no key points within this reach.

Reach STB36b (Interior Local Levee). This reach consists of 350 linear feet of floodwall surrounding Pump Station #7, also referred to at the Bayou Ducros Pump Station. The reach has 140 feet of uncapped sheetpile I-wall west of the discharge pipes, 70 feet of concrete t-wall around the discharge pipes, and 140 feet of uncapped sheetpile I-wall east of the discharge pipes. The weighted average elevation for the top of the 280 feet of uncapped sheet pile I-wall is 9.0

(NAVD88). The weighted average top elevation of the concrete t-wall is 12.5 (NAVD88). The overall weighted average top of wall elevation for the entire reach is 9.7 (NAVD88). A photograph of the 3.5 feet difference in wall height where the sheet pile ties into the adjoining concrete t-wall at the discharge pipes is shown in Figure 6-26.

Figure 6-26. T-wall and I-wall offset at Pump Station #7 Along ILL (Note: wall offset is approximately 3 ½ feet)

Reach STB36c (Interior Local Levee). This reach consists of 20,870 linear feet of levee that begins at the east end of Pump Station #7 I-wall and then ends where the levee adjoins the Violet Canal. This reach of levee had a weighted average top elevation of 9.1 (NAVD88). There are no key points within this reach. This reach of levee was overtopped and damaged during Katrina.

Reach STB37 (Interior Local Levee). This reach is defined by 3,888 linear feet of levee along the north side of the Violet Canal. The weighted average top of levee elevation along this reach was 8.1 (NAVD88) prior to Katrina. There are no key points within this reach. This reach was overtopped and damaged during Katrina.

Reach STB38 (Interior Local Levee). The floodwall for the Soap Factory along the Violet Canal defines this reach. It is 432 linear feet. The weighted average elevation of the top of the wall was 7.0 (NAVD88) prior to Katrina. This section of wall was overtopped during Katrina, but the wall was not heavily damaged. There are no key points within this reach. See Figure 6-27 for a view of this reach along the Violet Canal.

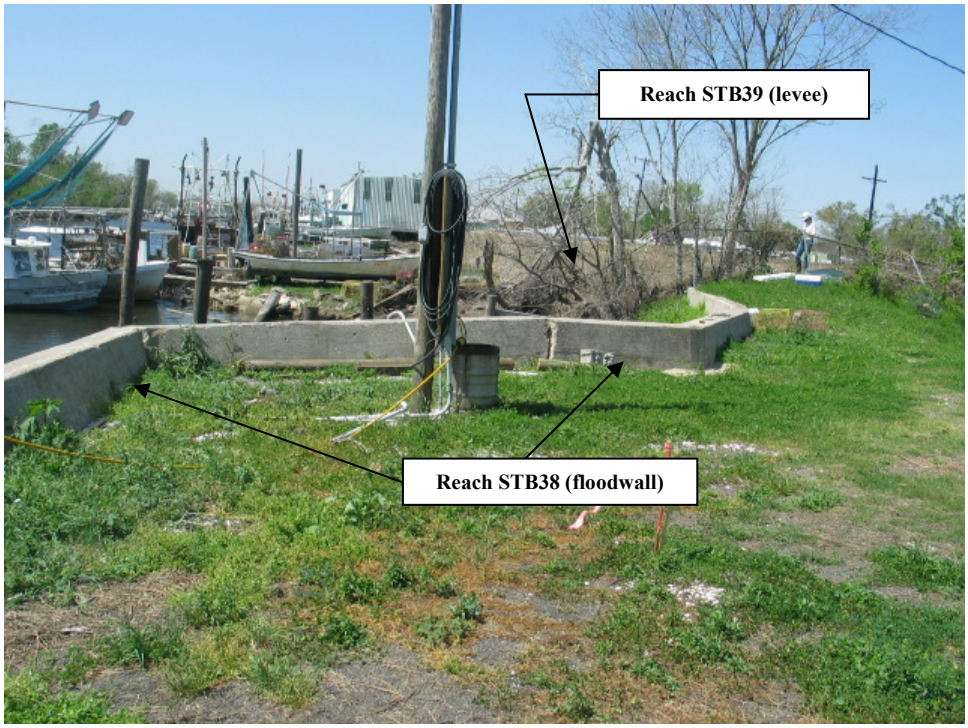

Figure 6-27. Floodwall Along the North Side of Violet Canal (This is Reach STB38 for the Risk Model, Violet Canal is to the left)

Reach STB39 (Interior Local Levee). This stretch of levee runs between the end of the concrete floodwall for the Soap Factory and ties into the series of building on top of the levee along the north side of the Violet Canal. This section can be seen in the background of Figure 6-27. This levee is approximately 510 feet long and had a weighted average top elevation of 8.5 (NAVD88) prior to Katrina. The reach was overtopped and damaged during Katrina.

Reach STB40 (Interior Local Levee). Prior to Katrina, this reach was defined by a short concrete floodwall surrounding a shrimp factory along the Violet Canal. This floodwall was 155 linear feet and had a weighted average top elevation of 7.5 (NAVD88). There are no key points within this reach. The reach was damaged during Katrina.

Reach STB41 (Interior Local Levee). This reach is defined by 2,201 linear feet of levee along the Violet Canal and it ends where it ties into Highway 46. The weighted average top elevation of this reach was 8.7 (NAVD88). There are no key points within this reach. This reach was overtopped and damaged during Katrina.

Reach STB42 (Interior Local Levee). This reach starts on the south side of the Violet Canal at Highway 46 and continues to the tie-in to the exterior levee along the Caernarvon Canal. While there are a few ramp and pipe crossings within this 55,227 ft reach, none are considered key points. The weighted average elevation of the top of the levee along this reach was 7.7 (NAVD88). This reach was overtopped and damaged during Katrina.

STB Basin – Layout of Reaches for Risk Model by Physical Feature (Post Katrina Changes by Task Force Guardian)

Reach STB1 (INHC to Caernarvon). Although this section of wall did not fail during Katrina improvements are being made to this reach to improve its performance for stability and overtopping. A physical survey of this section of wall taken in November 2005 shows an average elevation of 13.0 (NAVD88) across this reach. The wall was designed with a free standing height of 6 feet (see Figure 6-6 with a top of wall elevation of 15.0 and top of levee elevation of at 9.0). TFG is restoring the top of levee to 9.0 feet, thus reducing the free standing height to approximately 4.0 feet. In addition, a scour protection slab is being placed on the protected side. This is generally 6 to 8 feet wide from the base of the wall at the top of the levee on the protected side.

Reach STB2 (INHC to Caernarvon). This section of I-wall failed during Katrina (see Figure 6-5 for reference). The top of the I-wall was approximately at elevation 13.0 (NAVD88 2004.65) prior to Katrina. This wall is being replaced by a t-wall to the authorized elevation of 15.0. In addition, scour protection is being provided on the protected side in the form of an 8" concrete slab that is 8' wide. See Figure 6-28 for a photograph showing the new t-wall under construction and Figure 6-29 for the design section being installed.

Figure 6-28. New T-wall Being Constructed Along IHNC (Reach STB2) (Looking north along the IHNC)

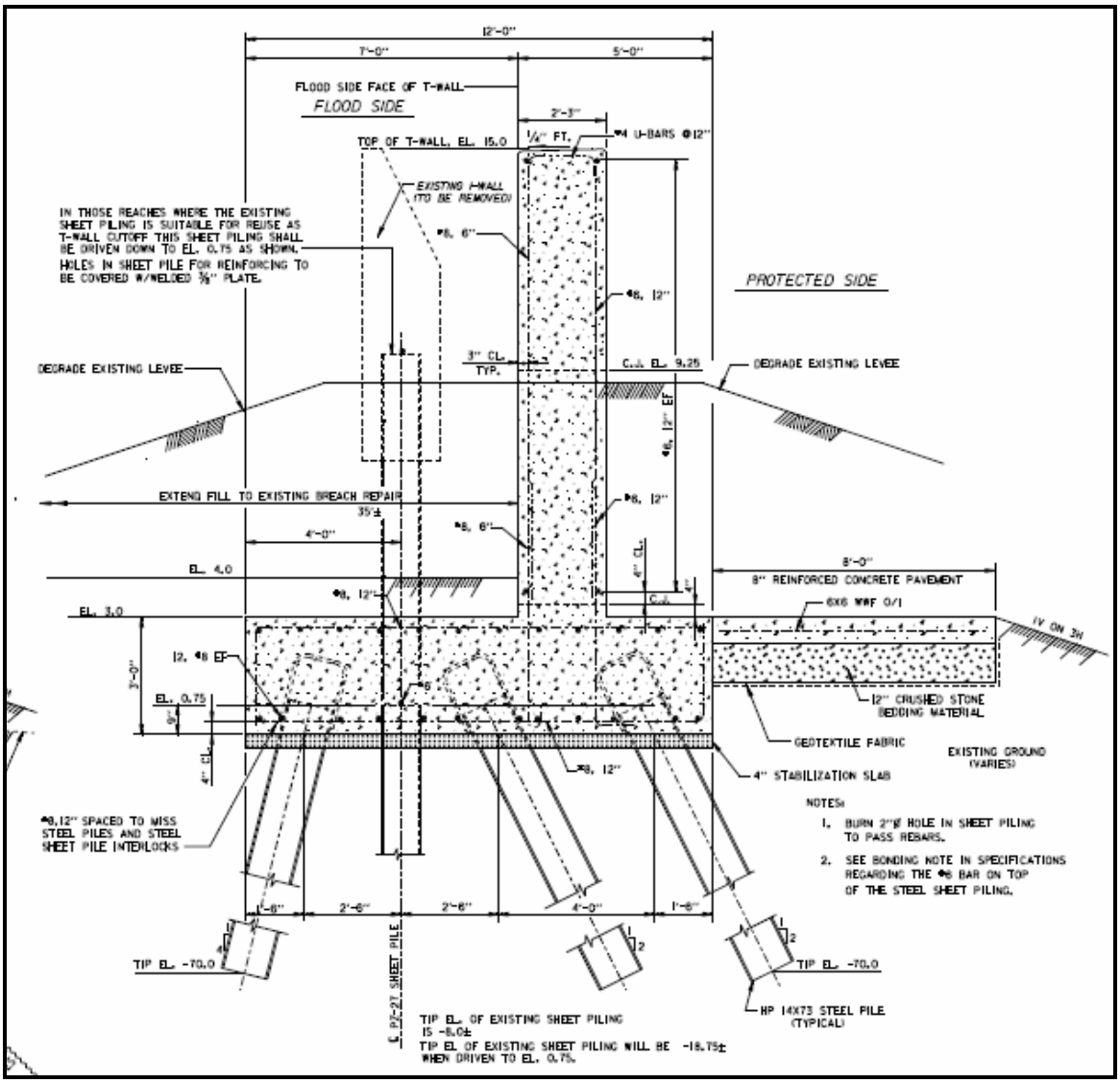

Figure 6-29. New T-wall Design Section (Reach STB2) (Pre-Katrina I-wall shown in picture for reference with authorized elevation of 15.0 feet)

Reach STB3 (IHNC to Caernarvon). The major change to this reach will be that scour protection is being provided on the protected side by means of a concrete slab that is 6 to 8 feet wide extending from the face of the wall on top of the levee.

Reach STB4 (IHNC to Caernarvon). Improvements to this reach include reducing the free standing height of the I-wall and providing scour protection. The approximate weighted average for the top of this wall is elevation 13.3 (NAVD88). The original free standing height design varied, but generally was in the 5.5 feet range with a top of levee elevation at 9.0. TFG will provide a stability berm to elevation 9.0 on the protected side. Therefore, the free standing height will be reduced to approximately 4.3 feet with the increased stability berm. In addition, a scour protection pad, as shown in Figure 6-30, is being installed on the top of the protected side levee.

Figure 6-30. New Scour Protection Pad (Typical) (Photo taken at end of Reach STB4 looking back toward IHNC)

Reach STB5 (INHC to Caernarvon). There are no improvements being made to this reach under TFG.

Reach STB6 (IHNC to Caernarvon). Scour protection is being provided on the protected side of all these walls and around the tie-in to the levee under TFG. Figure 6-31 depicts the recently completed scour protection pad construction.

Reach STB7 (IHNC to Caernarvon). There are no improvements being made to this reach under TFG.

Reach STB8 (IHNC to Caernarvon). The floodwall around Paris Road has a couple of modifications being made to it by TFG. First, the free-standing height of the wall is being returned to the as designed condition. Any location where the free-standing height of wall was greater than designed is being reduced back to a height of 6 feet. Secondly, scour protection is being added around this wall similar to other sections. The pad extends 10 feet away from the vertical face of the protected side. The repairs that have been made are shown in Figure 6-32.

Reach STB9 (IHNC to Caernarvon). There are no improvements being made to this reach under TFG.

Figure 6-31. New Scour Protection Around Reach STB6

Figure 6-32. TFG Repairs to Paris Road Floodwall

Reach STB10 (IHNC to Caernarvon). A scour protection pad has been added around the transition areas with the adjoining levee sections as well as the protected side of this wall by TFG as shown in Figure 6-33. There were no other changes to this reach.

Figure 6-33. New Scour Protection Around Reach STB10 (Viewed from Bienvenue Control Structure side looking northwest)

Reach STB11 (IHNC to Caernarvon). This short section of levee has been topped with heavy riprap between the two floodwall sections as part repairs made by TFG following Katrina. This will be a significant improvement in scour protection for this section since there is no exposed earthen levee and the transition areas have been topped a combination of concrete scour pads and heavy riprap.

Reach STB12 (IHNC to Caernarvon). As shown in Figures 6-11 through 6-13, this area suffered significant damage during Katrina. Two major repair efforts have been undertaken for this set of walls as part of TFG. The first is heavy riprap has been placed around the northwest I-wall/t-wall sections leading to the control gated structure. A photograph of this repair is shown in Figure 6-34 and is also typical of the riprap that has been placed on top of Reach STB 11 as part of the repair effort. The second major repair is a sheet pile diaphragm wall that has been installed to replace the failed uncapped I-wall section. This diaphragm wall is being constructed to an elevation of 18.5 (NGVD). The basic design section for this sheet pile diaphragm wall is shown in Figure 6-35. Note that this sheet pile diaphragm repair is the same one as being used for the northwest walls leading to the Bayou Dupree Control Structure (Reach STB 20) and the section shown is actually from the Bayou Dupre drawing set.

Figure 6-34. Riprap Placement Around Northwest Floodwall Adjoining Bayou Bienvenue Control Structure (Looking southeast alogn MR-GO)

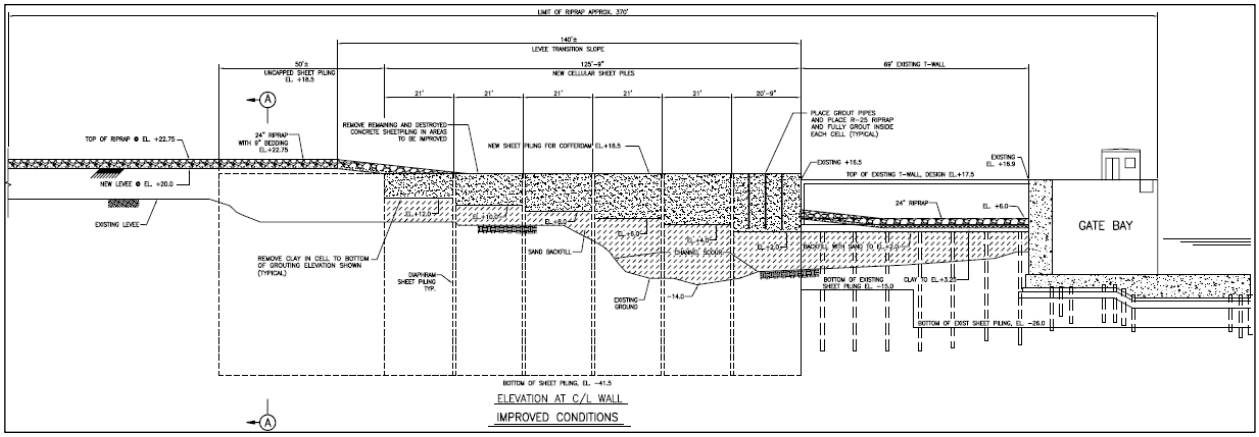

Figure 6-35. New Sheet Pile Diaphragm Wall Replacing Failed Uncapped I-wall at Bayou Bienvenue Control Structure (Note: this is same repair being done for northwest wall at Bayou Dupree)

Reach STB13 (IHNC to Caernarvon). This reach is being rebuilt to a constructed elevation of 20.0 (NGVD) with a final design grade of 17.5 (NGVD). This will allow for 2.5 feet of long-term settlement. There are three locations, each 300 feet long, within this reach where the levee will only be rebuilt to elevation 17.5 (NGVD). These are all at utility pipe crossings. As was noted in the pre-Katrina section, this reach failed and had an approximate weighted average top elevation of 17.5 (NGVD). Therefore, the reach will be 2.5 feet higher initially until it begins to settle over time.

Reach STB14 (IHNC to Caernarvon). The uncapped I-wall that defined this section pre-Katrina is being removed by TFG and the entire stretch is being replaced with a rebuilt levee to a constructed elevation of 20.0 (NGVD) with a final design grade of 17.5 (NGVD), thus, allowing for 2.5 feet of long-term settlement. There are two exceptions to this description within this reach. There are two separate 300-ft stretches where the levee will only be rebuilt to elevation 17.5 (NGVD) because of utility pipe crossings. See Figure 6-36 for reference of these areas along this stretch.

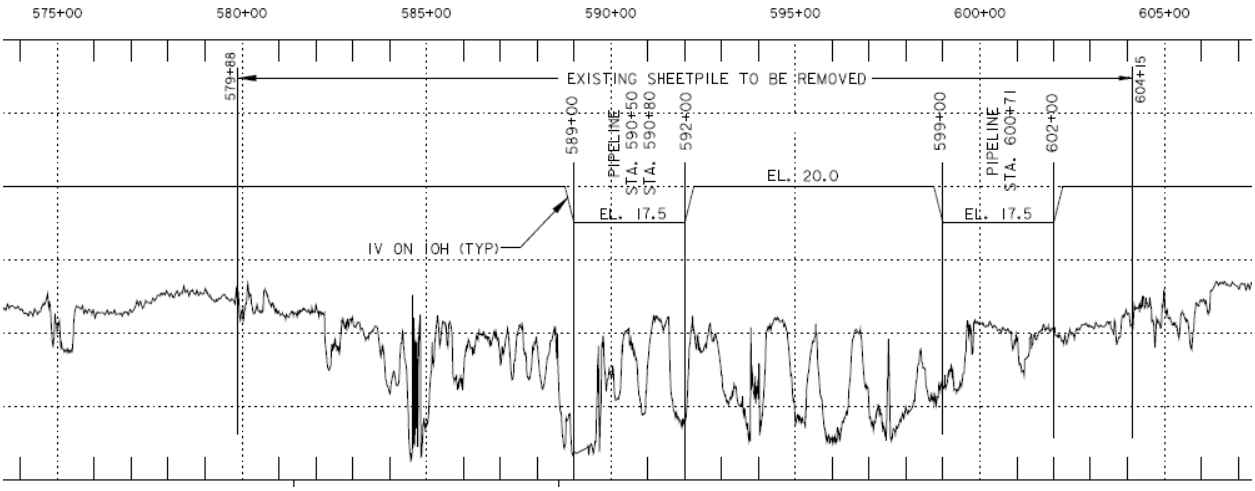

Figure 6-36. Profile of Rebuilt Levee Along MR-GO (Reach STB14) (Note: jagged line represents elevation of levee following Katrina)

Reach STB15 (IHNC to Caernarvon). This section of levee, which had an approximate weighted average top elevation of 16.4 (NGVD) prior to Katrina, is being replaced with a new levee between the two control structures being constructed to elevation 20.0 (NGVD) to allow for 2.5 feet of long-term settlement. Final design grade is elevation 17.5 (NGVD). Thus, the new levee section will be 3.6 feet higher than the pre-Katrina elevation for this levee initially and then 0.9 feet higher assuming a final design grade after settlement occurs.

Reach STB16 (IHNC to Caernarvon). The uncapped I-wall that defined this section pre-Katrina is being removed by TFG and the entire stretch is being replaced with a rebuilt levee to a constructed elevation of 20.0 (NGVD) with a final design grade of 17.5 (NGVD), thus, allowing for 2.5 feet of long-term settlement.

Reach STB17 (IHNC to Caernarvon). This reach of levee is being replaced with a new levee to a constructed elevation of 20.0 (NGVD) with a final grade elevation of 17.5 (NGVD). This will allow for 2.5 feet of long-term settlement. This means the new levee will be 3.5 feet higher than pre-Katrina at the time of construction and its final design elevation should be approximately 1.0 foot higher.

Reach STB18 (IHNC to Caernarvon). The uncapped I-wall that defined this section pre-Katrina is being removed by TFG and the entire stretch is being replaced with a rebuilt levee to a constructed elevation of 20.0 (NGVD) with a final design grade of 17.5 (NGVD), thus, allowing for 2.5 feet of long-term settlement.

Reach STB19 (IHNC to Caernarvon). This reach of levee is being replaced with a new levee to a constructed elevation of 20.0 (NADV88) with a final grade elevation of 17.5 (NAVD88). This will allow for 2.5 feet of long-term settlement. This means the new levee will be 1.3 feet higher than pre-Katrina at the time of construction and its final design elevation will actually be lower than the pre-Katrina weighted average elevation.

Reach STB20 (IHNC to Caernarvon). There are several changes to this structure that are being made by TFG. First the northwest precast concrete sheet pile wall that failed during Katrina is being replaced with a diaphragm sheet pile cell wall (similar to the one shown in Figure 6-35 for Bayou Bienvenue). This diaphragm cell wall will be built to elevation 18.5 (NAVD88). In addition, the adjoining t-walls on both side will remain, but the surrounding earthen sections will be covered with heavy riprap for scour protection. Finally, the southeast precast concrete sheet pile wall will remain, but now has an earthen berm placed on both the sides of the wall and then covered with heavy riprap, as shown in Figure 6-37.

Figure 6-37. Repairs to Southeast Adjoining Walls at Bayou Dupre (Viewed from southeast side looking northwest along the MR-GO)

Reach STB21 (IHNC to Caernarvon). This reach of levee is being replaced with a new levee to a constructed elevation of 20.0 (NGVD) with a final grade elevation of 17.5 (NGVD). This will allow for 2.5 feet of long-term settlement. This means the new levee will be 0.9 feet higher than pre-Katrina at the time of construction and its final design elevation will actually be lower than the pre-Katrina weighted average elevation across this reach if it settles to the design elevation.

Reach STB22 (IHNC to Caernarvon). The uncapped I-wall that defined this section pre-Katrina is being removed by TFG and the entire stretch is being replaced with a rebuilt levee to a constructed elevation of 20.0 (NGVD) with a final design grade of 17.5 (NGVD), thus, allowing for 2.5 feet of long-term settlement. Therefore, the levee will be 1.0 feet higher when constructed, but will be lower if settlement occurs to the design grade.

Reach STB23a (IHNC to Caernarvon). This section of levee is also being rebuilt by TFG to a constructed elevation of 20.0 (NGVD) with a final design grade of 17.5 (NGVD). Therefore, the "new" levee will be slightly higher (0.5 feet) than pre-Katrina when constructed, but lower if it settles to design grade.

Reach STB23b (IHNC to Caernarvon). There are small changes being made to this reach under TFG. The first 1,400 feet or so of this levee is being topped to an elevation of 19.0 (NAVD88). The remainder will only have minimal scour repairs where necessary, thus, overall the reach will not vary greatly from pre-Katrina conditions.

Reach STB23c (IHNC to Caernarvon). There are no major changes planned for this section of levee under TFG. There will be some minor scour repairs to areas that were damaged during Katrina.

Reach STB23d (IHNC to Caernarvon). There are no improvements planned for this reach under TFG.

Reach STB24 (IHNC to Caernarvon). There are no improvements planned for this reach under TFG.

Reach STB25 (IHNC to Caernarvon). Scour protection is being provided along this reach under TFG even though it wasn't overtopped or damaged during Katrina. A photograph of this protection (same general location as pre-Katrina condition shown in Figure 6-18) is shown in Figure 6-38.

Reach STB26 (IHNC to Caernarvon). The only significant repair to this reach undertaken by TFG is to provide a scour protection pad similar to the one shown for Reach STB25 (see Figure 6-38). In addition, any spots that had an I-wall "stick-up" height that was greater than designed then those spots have been modified to reduce free standing height to design levels.

Reaches STB27 through STB33 (Mississippi River Levee). There are no improvements to any of these reaches planned under TFG.

Reach STB33 (Interior Local Levee). Most of this 15,455 feet stretch of levee did not require any modifications by TFG. However, a 4500 ft section of uncapped sheet pile I-wall embedded within the levee is being repaired because of Katrina damage. This repair essentially consists of replacing the damaged wall and levee that was washed away to its pre-Katrina condition. Therefore, for the purposes of the IPET assessment it can be assumed that no improvements to this reach are being made compared to the pre-Katrina condition. A photo-graph of the construction being carried out to repair the damaged section along this reach is shown in Figure 6-39.

Figure 6-38. Scour Repairs to Caernarvon Sheet Pile I-wall Area (Note: compare to pre-Katrina condition shown in Figure 6-18)

Figure 6-39. Repairs to ILL Along Reach STB33 Near Parish Border (Note: This section is being returned to pre-Katrina conditions)

Reach STB34 (Interior Local Levee). There are no improvements to this reach planned under TFG.

Reach STB35 (Interior Local Levee). There are no improvements to this reach planned under TFG.

Reach STB36a (Interior Local Levee). TFG is repairing Katrina damages and raising the levee east of Paris Road within this reach. Prior to Katrina, the weighted average top elevation east of Paris Road was 8.4 (NAVD88) based upon a 1999 LaDOT physical survey. TFG was granted approval on a one-time basis to raise this portion of the levee to elevation 10 (NAVD88 2004.65).

Reach STB36b (Interior Local Levee). There are no major improvements to this reach being planned by TFG.

Reach STB36c (Interior Local Levee). This reach of levee is being rebuilt and raised to elevation 10 (NAVD88 2004.65) under TFG. The pre-Katrina weighted average top of levee elevation across this reach was 9.1 (NAVD88).

Reach STB37 (Interior Local Levee). This reach is being rebuilt and raised to elevation 10 (NAVD88 2004.65) under TFG. The pre-Katrina weighted average top of levee elevation across this reach was 8.1 (NAVD88).

Reach STB38 (Interior Local Levee). There are no improvements planned to this section of wall under TFG.

Reach STB39 (Interior Local Levee). This 510 feet reach of levee is being rebuilt by TFG and raised to elevation 10 (NAVD88 2004.65). Prior to Katrina, the weighted average top elevation of this reach was 8.5 (NAVD88) based upon a 1999 LaDOT physical survey. Figure 6-40 shows the levee being rebuilt by TFG.

Reach STB40 (Interior Local Levee). This reach along the Violet Canal is being repaired by TFG. The section is being reinforced with gabion baskets in front of the building facilities, as shown in Figure 6-41. The new top elevation of this reach will be 10 (NAVD88 2004.65) compared to elevation 7.5 (NAVD88) prior to Katrina.

Reach STB41 (Interior Local Levee). This reach of levee is being rebuilt and raised to elevation 10 (NAVD88 2004.65) by TFG. Prior to Katrina, the weighted average elevation was 8.7 (NAVD88).

Reach STB42 (Interior Local Levee). This reach of levee is also being rebuilt and raised to elevation 10 (NAVD88 2004.65) by TFG. Prior to Katrina, the weighted average elevation was 7.7 (NAVD88).

Figure 6-40. Repairs and Levee Raising to Reach STB39 Along Violet Canal (Viewed looking west from end of Reach STB38)

Figure 6-41. Gabion Basket Repairs to Reach STB40 (Viewed from west side of reach)

TABLE STB 1 - Summary of I-wall Changes from Pre-Katrina to Post Katrina

		Pre-Katrina Information				Post-Katrina Task Force Guardian Improvements				
Reach	Location Description	Primary Type of Protection	Weighted Elevation	Datum Source	Free Standing Height (ft)	Primary Type of Protection	Weighted Elevation	Datum Source	Free Standing Height (ft)	Added Scour Protection
STB1	IHNC to Claiborne Bridge	Concrete I-wall	13.0	NAVD88	6.0				4.0	Yes
STB2	Failed Wall Along IHNC	Concrete I-wall	13.0	NAVD88	6.0	Concrete T-wall	15.0			Yes
STB3	Near Florida Ave Bridge	Concrete T-wall	12.5	NAVD88	6.0					Yes
STB4	Floodwall Ties into GIWW Levee	Concrete I-wall	13.3	NAVD88	5.5				4.3	Yes
STB6	Floodwall Around S-2 and S-3	Concrete I-wall	13.0	NAVD88	6.0					Yes
STB8	Paris Road Floodwall	Concrete I-wall	12.4	NAVD88	6.7				6.0	Yes
STB10	Unused Gate Near B. Bienvenue	Concrete I-wall	16.3	NAVD88	4.9					Yes
STB12	West i-wall of B. Bienvenue	Concrete I-wall	17.0	NAVD88	4.0					Yes
STB12	East i-wall of B. Bienvenue	Sheetpile I-wall	18.5	NAVD88	???	Diaphram Wall	18.5		n/a	Yes
Numerous	MR-GO Sheet Pile Modifications Between Control Structures	Sheetpile I-wall	18.5	NGVD	3.5	Rebuilt Levee	17.5	NAVD88	n/a	n/a
STB20	West Concrete Sheetpile Wall @ Bayou Dupre	Conc Sheetpile	15.2	NAVD88	12.0	Diaphram Wall	18.5		n/a	Yes
STB20	East i-wall of B. Bienvenue	Conc Sheetpile	15.2	NAVD88	7.5		15.2		1.0	Yes
STB22	MR-GO Sheet Pile Mods Between Bayou Dupre and Caernarvon	Sheetpile I-wall	19.0	NGVD	3.5	Rebuilt Levee	20.0	NAVD88	n/a	n/a
STB23d	Floodwalls Around Pump Station #8	Concrete I-wall	16.7	NAVD88	6.0					
STB25	Caernarvon Sheet Pile Wall	Sheetpile I-wall	12.8	NAVD88	5.5					Yes
STB26	Caernarvon Sheet Pile Wall	Concrete I-wall	13.0	NAVD88	6.0					Yes
STB33	Interior Local Levee from IHNC to Pump Station #6	Sheetpile I-wall	13.5	NAVD88	???					
STB34	Floodwalls Around Jean Lafitte Pump Station	Sheetpile I-wall	14.0	NAVD88	???					
STB35	Floodwall Between Jean Lafitte PS to Paris Road	Sheetpile I-wall	13.3	NAVD88	???					
STB36b	Floodwall Around Pump Station #7 (Bayou Ducros)	Sheetpile I-wall	9.7	NAVD88	3.5					
STB38	Floodwall for Soap Factory Along Violet Canal	Conc I-wall	7.0	NAVD88	???					
STB40	Floodwall for Shrimp Factory Along Violet Canal	Conc I-wall	7.5	NAVD88	???					

Appendix 7
Orleans Basin

Orleans East Bank

Insert description

Orleans West Bank

The Orleans Parrish West Bank Basin is composed of two sub-basins (Figure 7-1). These are located on either side of the upper end of the Algiers. OW1, on the west side of Algiers Canal, was designed as part of the Algiers Canal to Hero Canal Project.

OW2, on the east side of the Algiers Canal, was designed as part of the Harvey Canal to Algiers Project.

Figure 7-1. Orleans Parish West Bank Basin

OW1

Orleans West Bank – OW1 (Algiers Canal to Hero Canal Project)

Sub-basin OW1, as shown above, is located on the west bank of the Mississippi River in Orleans Parish and is generally bounded by a portion of the Algiers Canal, the Mississippi River and the Orleans-Plaquemines Parish line. Topography is flat with ground elevations ranging from +5 feet NGVD on the alluvial ridges along the Mississippi River to –7 feet NGVD in the interior of the area. Approximately 40 percent of the area is below sea level. The surface area is 4.7 square miles. The sub-basin area is protected by 15.0 miles of levees and floodwalls. There are no floodgates, drainage structures or control structures in the protection system. There is one pumping station that drains the protected area (NOS&WB Pumping Station #11 at location 29.90962 -89.978)

Segment 1 is a low, all earth (clay) non-Federal levee separating Orleans Parish from Jefferson Parish. It extends from the main line Mississippi River levee (MRL) inside the US Coast Guard Station to the Algiers Canal levee with an elevation 3 – 4 ft NVGD.

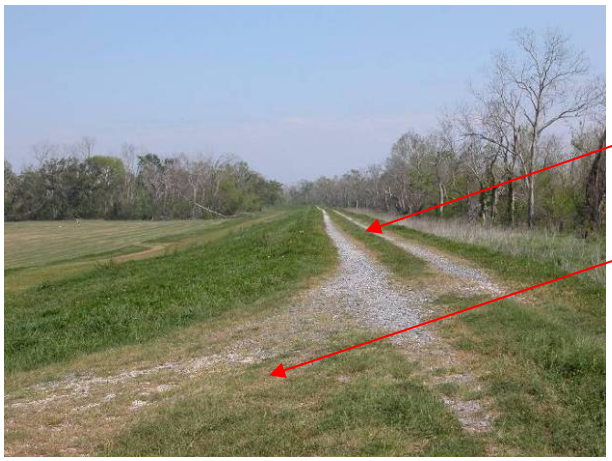

Mississippi River Levee Crown

MRL and back levee intersection inside the U.S. Coast Guard Station

Mississippi River Levee

MRL and back levee intersection inside the U.S. Coast Guard Station

Back levee begins U.S. Coast Guard Station

Back levee continues inside U.S. Coast Guard Station

Back levee crossed by roadway inside U.S. Coast Guard Station. Roadway is 2 feet lover than levee. No closure structure

Back levee continues outside U.S. Coast Guard toward GIWW Station. Crown is rutted.

Drainage structure under Back Levee outside U.S. Coast Guard station. Screw gat closure on culvert.

Back Levee intersects Hwy 406 looking toward the GIWW and General De Gaulle Bride overpass.

Back Levee intersects Hwy 406. No closure at Hwy

Back Levee passed under General De Gaulle onramp from Hwy 406. Buckling of concrete slab on levee under ramp.

Segment 2 is the East bank of the Algiers Canal levee that extends between the local interior levee (Segment 1) and the Algiers Lock. This 9.5 ft NVGD clay levee is interrupted by a floodwall segment that crosses in front of NOS&WB Pumping Station #11.

Abandoned pipe crossing through the Algiers Canal

Typical Algiers Canal levee. No armor.

Segment 3 is the Orleans West Levee District Mississippi River levee. This levee segment closes the North and East side of the sub-basin. It extends from the GIWW and Mississippi River intersection to where it intersects the interior levee (Segment 1) inside the U.S. Coast Guard Station. The MRL is an all clay levee with crushed stone surfacing on the 10' wide crown at elevation 22 ft NVGD.

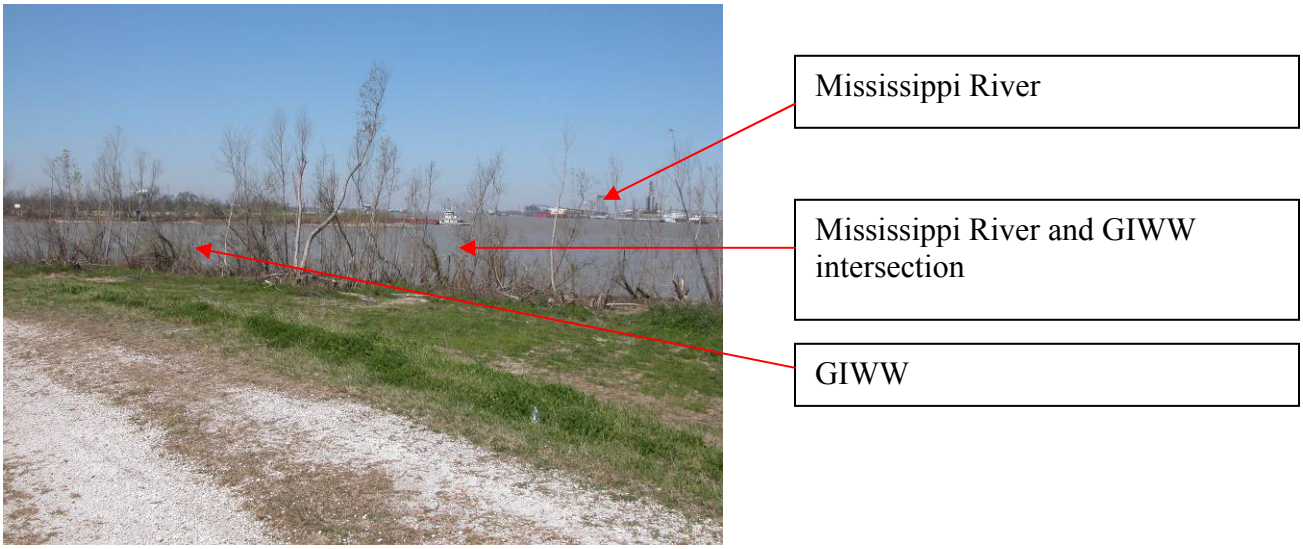

Pipe crossing along MRL just east of GIWW and MRL intersection

Barge still sitting on foot of MRL

Typical MRL
10 FT crown of grass and stone

Concrete armor on River side of MRL

OW2

Orleans West Bank – OW2 (Harvey Canal to Algiers Canal)

Sub-basin OW2, as shown in Figure 7-1 above, is located on the west bank of the Mississippi River in Orleans Parish. It is generally bounded by the Mississippi River,

the Algiers Canal, and the Orleans-Jefferson-Plaquemines Parish boundary. The topography is flat with ground elevations ranging from +10 feet NGVD on the alluvial ridges along the Mississippi River to –5 feet NGVD in the interior of the area. Approximately 25 percent of the area is below sea level. The surface area is 6.3 square miles and the population is approximately 57,000. The sub-basin is protected by 12.6 miles of levees and floodwalls.

Segment 1 is a clay, non-Federal levee that begins at the Greater New Orleans Bridge (US 90) crossing of the Mississippi River Levee and runs along the Orleans-Jefferson Parish line to the Algiers Canal levee, near the NOS&WB Pump Station #13. This interior levee is approximately 4 miles long and is at elevation 3-4 ft NGCD.

Segment 2 is the West bank of the Algiers Canal levee (GIWW) that extends between the local interior levee and the Algiers Lock. This clay levee is interrupted by a floodwall segment that crosses in front of N.O.S. &W.B .Pumping Station #13. It is 1.8 miles long at elevation 9.5 ft NGVD.

Segment 3 is the Orleans West Levee District Mississippi River Levee extending from the Algiers Canal Lock west to the Orleans Parish Line (beneath the Greater New Orleans Bridge, US 90), completing the sub-basin. This MRL is a predominately all clay levee with small reaches of short concrete I-Walls atop the clay levee base. It is 6.8 miles long at elevation 22-23.5 ft NGVD. There are no floodgates, drainage culverts or control structures in the protection system. There is one pumping station that drains the protected area (N.O.S. &W.B .Pumping Station #13 at location 29.8959, -89.9978).

Appendix 8
Hazard Analysis

Hazard Analysis and Initiating Events

Several methods are available to quantify hurricane hazard, typically in the context of wind-related risk. These methods are classified into three main types: historic (HI), joint-probability (JP), and Monte Carlo simulation (MC) methods.

Historic Methods

Historic (HI) methods quantify the hazard based on the rate at which the effect of interest, L, (e.g., L = wind speed or surge or loss) has occurred in the historical record. These methods are fundamentally nonparametric, i.e. they do not assume a specific analytic form for the recurrence rate of the hurricanes or their effects. One problem with purely nonparametric historic approaches is the "granularity" of the results that reflects the small number of significant events in the historical record and the sensitivity of the results to unusual occurrences ("outliers") during the observation period. To reduce these effects, some HI approaches include smoothing procedures. For example, the empirical simulation technique (EST) of Sheffner et al. (1996) "smears" the influential historical hurricanes by replacing them with a sweep of hypothetical events with somewhat different characteristics, typically with different landfall locations. Other smoothing methods fit a specific distribution to the hurricane effects L_i calculated from the historic events. An example of the latter type is the 1987 version of the National Hurricane Center Risk Analysis Program HURISK (Neumann 1987). The EST method has been extensively used by the USACE and FEMA to identify design events with return periods, up to 100 years. Confidence intervals on the results are usually obtained through bootstrapping (resampling) techniques.

Joint Probability (JP) Methods

Joint probability (JP) methods make a parametric representation of hurricanes, typically based on their characteristics $\underline{\Theta}$ at landfall and the filling rate after landfall. For example, $\underline{\Theta}$ might include the location and velocity vector, the central pressure deficit, the radius to maximum winds and possibly a few other parameters at landfall. The historic record is used to

estimate the recurrence rate $\lambda(\underline{\Theta})$. The effects of interest, $L(\underline{\Theta})$, are then calculated for a suitable set of $\underline{\Theta}$ values and, by combining $\lambda(\underline{\Theta})$ and $L(\underline{\Theta})$, the recurrence rate $\lambda(L)$ is obtained.

The values of $\underline{\Theta}$ for which $L(\underline{\Theta})$ is calculated may form a regular (factorial) discretization of a critical region in parameter space. Alternatively, Monte Carlo (MC) simulation or importance sampling may be used to generate a set of values $\{\underline{\Theta}_i\}$ from that region. Factorial discretization and importance sampling are generally preferred when interest is in the tail distribution of L, whereas straight MC simulation is more efficient for short return periods. The MC and importance sampling versions of the JP method may be seen as procedures that replace the actual historical catalog with a much larger synthetic catalog. The JP approach with MC simulation is perhaps the most frequently used method for hurricane wind hazard; see for example Russell (1971), Batts et al. (1980), Georgiou et al. (1983), and Vickery and Twisdale (1995a). If the number of events $\underline{\Theta}_i$ is too large to evaluate the responses L_i with high accuracy, coarser analysis procedures may be used to rank the events or to interpolate the results for a subset of events.

Monte Carlo Simulation Methods

Monte Carlo (MC) simulation methods use a stochastic representation of the origin and temporal evolution of hurricanes in the general region of interest, in this case the North Atlantic region. The random trajectory and parameter evolution are typically represented through Markov processes of suitable order, discrete in time but continuous in state. The state-transition parameters vary spatially and are estimated from the historical record. A large number of hurricane events are simulated using this random dynamic model. The sample is trimmed to retain only the events that are significant to the region and the effects of interest and the retained events are treated like the historical sample in the HI methods. As in the JP method, when the number of retained events is too large to evaluate the responses L_i with high accuracy, it is necessary to use parsimonious high-accuracy runs in combination with less accurate methods. The MC simulation method was first proposed by Vickery et al. (2000). More recent studies that use MC simulation are Huang et al. (2001) and Powell et al. (2005).

Choice of a Method

The attractiveness of a method depends in general on the amount of data and computational resources available as well as the objective of the analysis. Regarding the latter, it matters whether (1) interest is in frequent or rare events, (2) the objective is to identify design events with given return periods (return-period analysis) or find the rate at which certain consequences are exceeded (risk analysis), and (3), in the case risk analysis, whether the losses occur in a small geographical region that may be considered uniformly impacted by any given hurricane or over an extended region where spatial homogeneity of the hurricane loads cannot be assumed. For flood hazard, return-period analysis is generally easier than risk analysis because hurricane severity may be ranked using surrogate quantities (such as a rough estimate of maximum surge) that are much easier to calculate than the flooding conditions themselves.

Since medium to long return periods are of interest, historical methods are discarded. Both JP and MC methods can handle such return periods. MC approaches face the problem of sorting out the potentially damaging events from large suites of simulated hurricane scenarios. This is not a trivial problem for the geographically extended and differently vulnerable system we are considering. For these reasons, the joint probability approach has been selected. This approach is further described in the following sections.

To implement a JP method for hurricane hazard, it is convenient to describe hurricanes at landfall through the parameter vector $\underline{\Theta} = [\Delta P, R_{\max}, X, \theta, V, B]$, where

- ΔP (mb) = central pressure deficit at landfall
- $R_{\max}$ (km) = radius to maximum winds at landfall
- X (km) = longitudinal landfall location relative to downtown New Orleans (positive if east of New Orleans)
- θ (degrees) = direction of storm motion at landfall, ($\theta = 0$ for tracks pointing north, increasing clockwise)
- V (m/s) = storm translation speed at landfall

B = Holland's radial pressure profile parameter at landfall (Holland 1980)

While the variation of these parameters before and after landfall is also of interest, the primary characterization of hurricanes in the risk studies is in terms of their properties at landfall. Hence the main tasks of hazard quantification are the estimation of the recurrence rate $\lambda(\underline{\Theta})$ and the evaluation of the environmental loads $L(\underline{\Theta})$ over a suitable range of $\underline{\Theta}$ values.

Hurricane Recurrence at Landfall

The recurrence law for $\underline{\Theta}$ may be written as

$$\lambda(\underline{\Theta}) = \lambda_o f(\underline{\Theta}) \tag{8-1}$$

where $\lambda(\underline{\Theta})$ is the rate density function for $\underline{\Theta}$, meaning that $\lambda(\underline{\Theta})dV$ is the rate of hurricanes with parameters in an infinitesimal volume dV around $\underline{\Theta}$, λ_o is the total occurrence rate in a suitable region of parameter space, and $f(\underline{\Theta})$ is the joint PDF of $\underline{\Theta}$ inside that region.

Information used to estimate λ_o and $f(\underline{\Theta})$ includes historical data sets (mainly NOAA's HURDAT data for λ_o, ΔP, X, θ and V and data on $R_{\max}$ from Ho et al. 1987) as well as published distribution results. The HURDAT data set (Jarvinen et al. 1984, and recent updates) has been used to extract values of (ΔP, X, θ, V) at landfall over the stretch of coastline between longitudes 85W and 95W. For recurrence analysis, we have considered only storms of hurricane strength at landfall (defined as those having measured or estimated $\Delta P \geq 25$ mb) since 1890. Earlier events have been neglected because prior to 1890 the historical record is incomplete and less accurate. The HURDAT data set has been used also to analyze pre-landfall conditions.

Information on the structure and parameterization of $f(\underline{\Theta})$ is provided in various references, including Holland (1980), Ho et al. (1987), Vickery and Twisdale (1995a,b), Chouinard et al. (1997), Vickery et al. (2000), Huang et al. (2001), Willoughby and Rahn (2004), and Powell et al. (2005). For the coastal area of interest here, the main findings of these studies are:

The distribution of ΔP may be assumed to be either lognormal or Weibull. The Weibull distribution tends to give better fits to the data when all tropical storms are included, whereas the lognormal model is more appropriate when only hurricanes are considered; see Vickery and Twisdale (1995a). Using the lognormal model and a locally weighted maximum-likelihood procedure, Chouinard et al. (1997) found that along the Louisiana Coast the standard deviation of ΔP is almost constant at 21 mb, whereas the mean value of ΔP increases eastward from about 32 mb near the Texas border to about 38 mb near the Mississippi border. This trend is attributed to the sea temperature anomaly of the Loop Current.

Depending on coastal location, the distribution of θ is generally found to be normal or a mixture of two normal distributions, one for easterly storms and the other for westerly storms (Vickery and Twisdale 1995a; Huang et al. 2001).

Vickery et al. (2000) found that V may be taken to be lognormally distributed, with mean value about 6 m/s and standard deviation about 2.5 m/s. V has a mild dependence on θ, increasing as θ increases (Vickery and Twisdale 1995a).

$R_{\max}$ decreases with increasing hurricane pressure deficit ΔP and its conditional distribution given ΔP may be taken to be lognormal (Vickery and Twisdale 1995a; Powell et al. 2005). Using data from Ho et al. (1987), Vickery et al. (2000) fitted several linear and quadratic models to $\ln R_{\max}$ against ΔP and latitude. A simple one, with coefficient of determination $R^2 = 0.28$, is $\ln R_{\max} = 2.636 - 0.00005086\Delta P^2 + 0.03949 Lat$. Willoughby and Rahn (2004) obtained qualitatively similar results when regressing $\ln R_{\max}$ against latitude and maximum wind speed. Their logarithmic standard deviation is 0.66.

B varies with $R_{\max}$ and possibly ΔP or maximum wind speed $V_{\max}$ and latitude (Holland 1980, Vickery et al. 2000, Willoughby and Rahn 2004, Powell et al. 2005). For storms of hurricane strength, Vickery et al. fitted several relations using data from different flight height ranges. Their recommended mean value relation is $B = 1.38 + 0.00184\Delta P - 0.00309 R\text{max}$.. Willoughby and Rahn (2004) studied the dependence of B on $R_{\max}$, $V_{\max}$, and latitude, finding that the distribution of B is nearly symmetrical and somewhat flatter and shorter-tailed than a normal distribution (in part because their estimation algorithm searches for optimal values between 0.5 and 2.5). Although Willoughby and Rahn estimate a linear dependence of B on $ln\, R_{\max}$, the slope coefficient is only marginally significant. The regression residual has standard deviation 0.36. The data analyzed by Powell et al. (2005) is a subset of that of Willoughby and Rahn. The Powell et al. subset uses selection criteria (high winds, low-level flights, and geographical location) that are relevant also to the present study. Powell et al. find that a good fit for ($B|\, R_{\max}$, Lat) is given by a truncated normal distribution with mean value 1.881 – 0.0109Lat –0.00557 $R_{\max}$, standard deviation 0.286 (before truncation), and range between 0.8 and 2.2.

The above observations have been used in the modeling of $\lambda(\underline{\Theta})$. However, dependencies, distribution types and parameter values have been sometimes modified based on further data analyses. Two data sets are used: a broad longitude (BL) data set, which includes HURDAT data at landfall for all hurricanes at ($\Delta P \geq 25$ mb) since 1890 that made landfall between longitudes 85W and 95W. The narrow longitude (NL) data set is the subset with landfall locations between 87.5W and 92.5W. The BL and NL data sets include 62 and 32 events, respectively.

Location X and recurrence rate λ_o. Within both latitude ranges, landfall is approximately uniformly distributed (the uniform distribution easily passes various statistical tests). Using the BL data sets one obtains $\lambda_o = 5.7 \times 10^{-4}$ per longitude-km per year, with a coefficient of variation of 0.18.

Approach angle θ. The distribution of θ for both longitude ranges is very nearly normal (tests of normality pass with P around 0.5 with no evidence of bimodality). For the BL data set, which is preferred for statistical accuracy, the normal distribution fit is shown in Figure 8-1.

Central pressure deficit ΔP. For $\Delta P > 34$ mb, which is the range of interest in the current study, the BL and NL data are fitted well by nearly identical shifted lognormal distributions, with shift parameter 18 mb, i.e. $(\Delta P - 18)$ has lognormal distribution for $\Delta P > 34$ mb. The four largest values of ΔP in the data set are associated with hurricanes Camilla, Katrina, Carmen, and Betsy. All four hurricanes occurred inside the narrow longitude range. The slightly more conservative fit obtained from the NL data set, is shown in Figure 8-2. The local trend in the mean value of ΔP observed by Chouinard et al. (1997) is small and statistically not significant; hence it is ignored.

Translational speed V. The often-used lognormal model is not well supported by our data. Better fits are obtained with a Weibull distribution model. The Weibull fit to the NL data is shown in Figure 8-3.

R_{max}. For $R_{\max}$ we use the model in Eq. 9 of Vickery et al. (2000), which for Lat = 30N gives

$$\ln(R_{\max}) = 3.962 - 0.00567\Delta P + \varepsilon_R \tag{8-2}$$

where ε_R is a normal variable with zero mean and standard deviation 0.313.

Holland's *B*. For B Powell et al.'s (2005) model is used, which for Lat = 30N gives

$$B = 1.554 - 0.00557 R_{\max} + \varepsilon_B \tag{8-3}$$

where ε_B is a normal variable with zero mean and standard deviation 0.286.

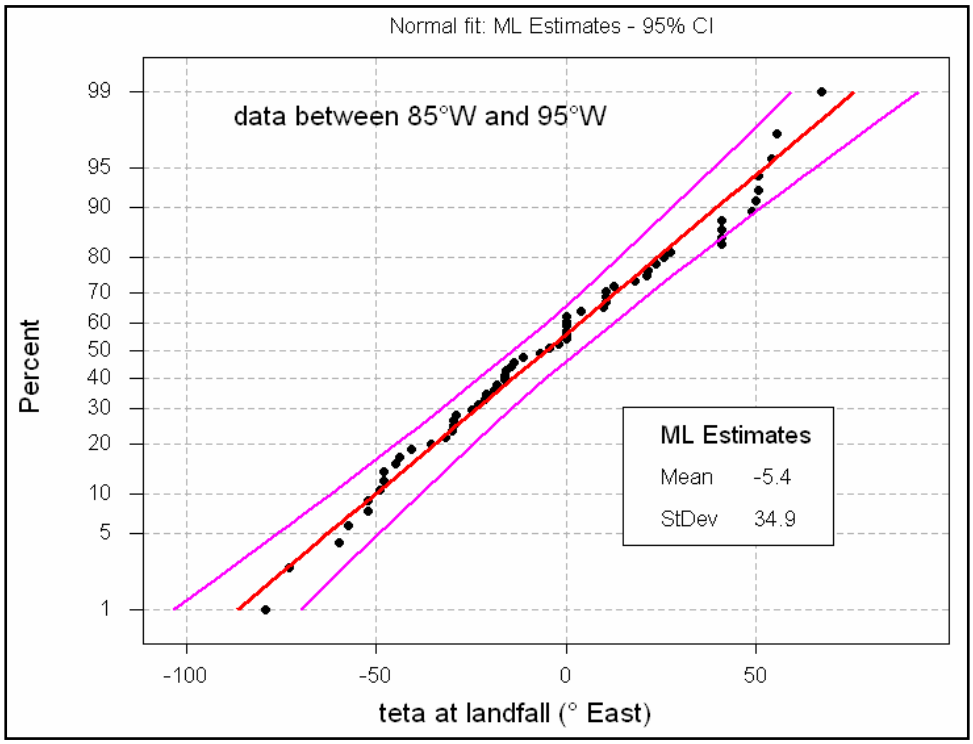

Figure 8-1. Normal distribution Fit for the Approach Angle θ

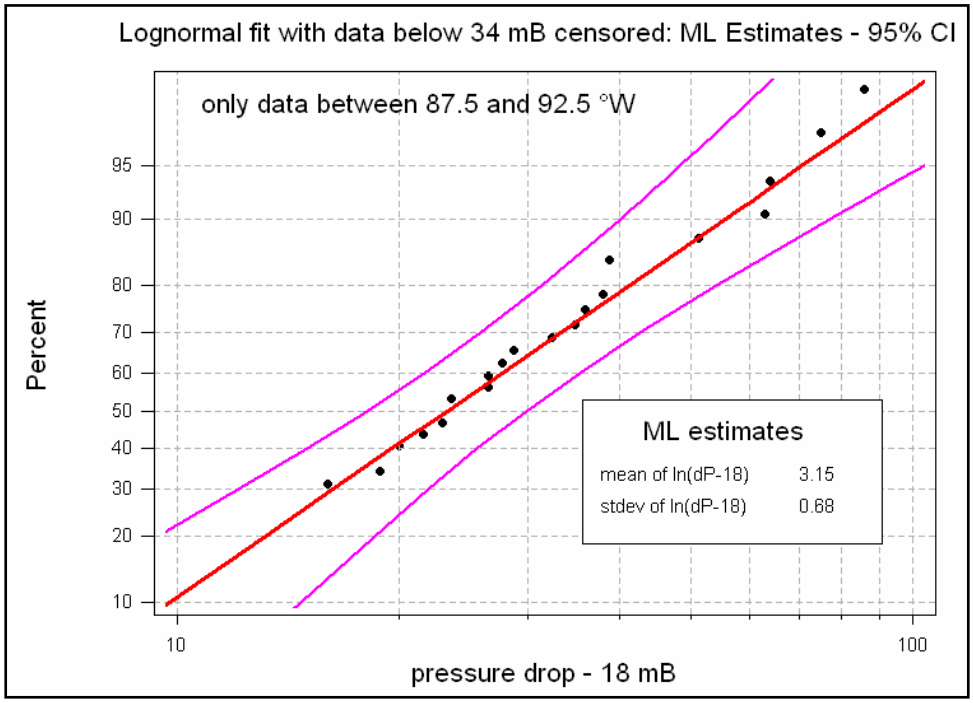

Figure 8-2. Lognormal Distribution of $(\Delta P - 18)$ Fitted to ΔP Values Above 34 mb in the Narrow Longitude Range

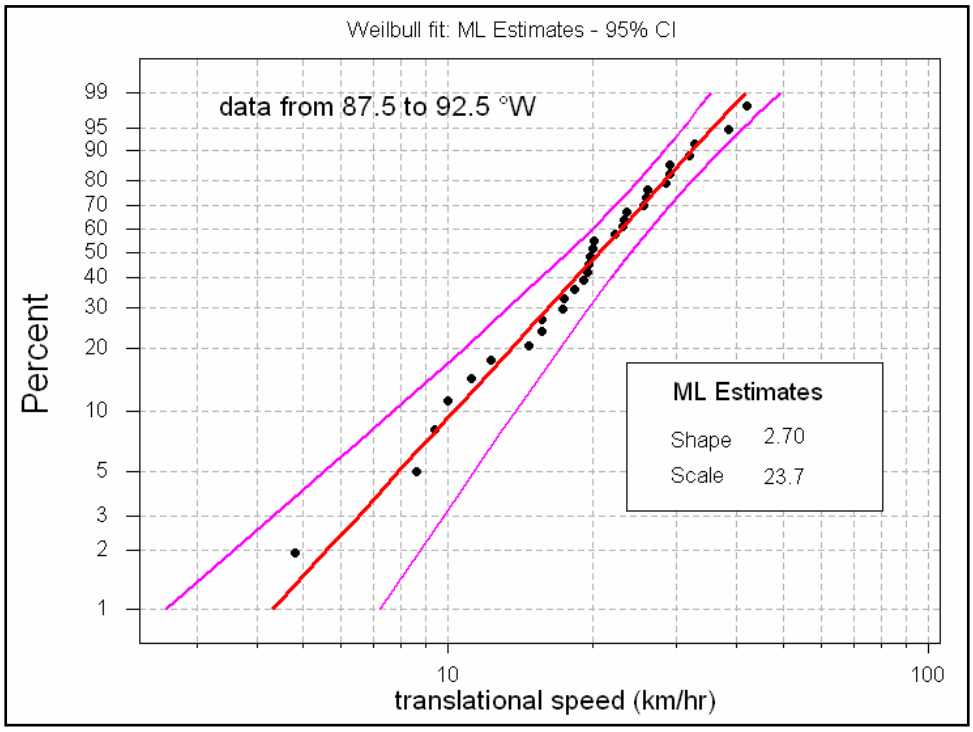

Figure 8-3. Weibull Fit to Storm Speed Data in the WL Data Set

Pre- and Post-Landfall Parameter Variation

The $\underline{\Theta}$ parameterization concerns exclusively the hurricane characteristics at landfall. One possibility, which has often been used in hurricane hazard analysis, is to assume straight paths and constant values of ΔP, $R_{\max}$, V and B prior to landfall; see for example Russell (1971), Batts et al. (1980), Georgiou et al. (1983), Neumann (1991), and Vickery and Twisdale (1995a). A more refined approach is used for the hurricane path and the pre-landfall variability of these parameters, as described in the following sections.

Pre-Landfall Parameter Variation. All tropical storms (not just hurricanes) after 1890 in the HURDAT record that made landfall within latitudes 85W and 95W are used to estimate the mean hurricane path for landfall angles θ around $-60^{\circ}, -30^{\circ}, 0, 30^{\circ}, 60^{\circ}$. Results are shown in Figure 8-4, where the dots represent average locations at 12 hour intervals relative to the time of landfall. These θ-dependent paths are used in all the hurricane analyses.

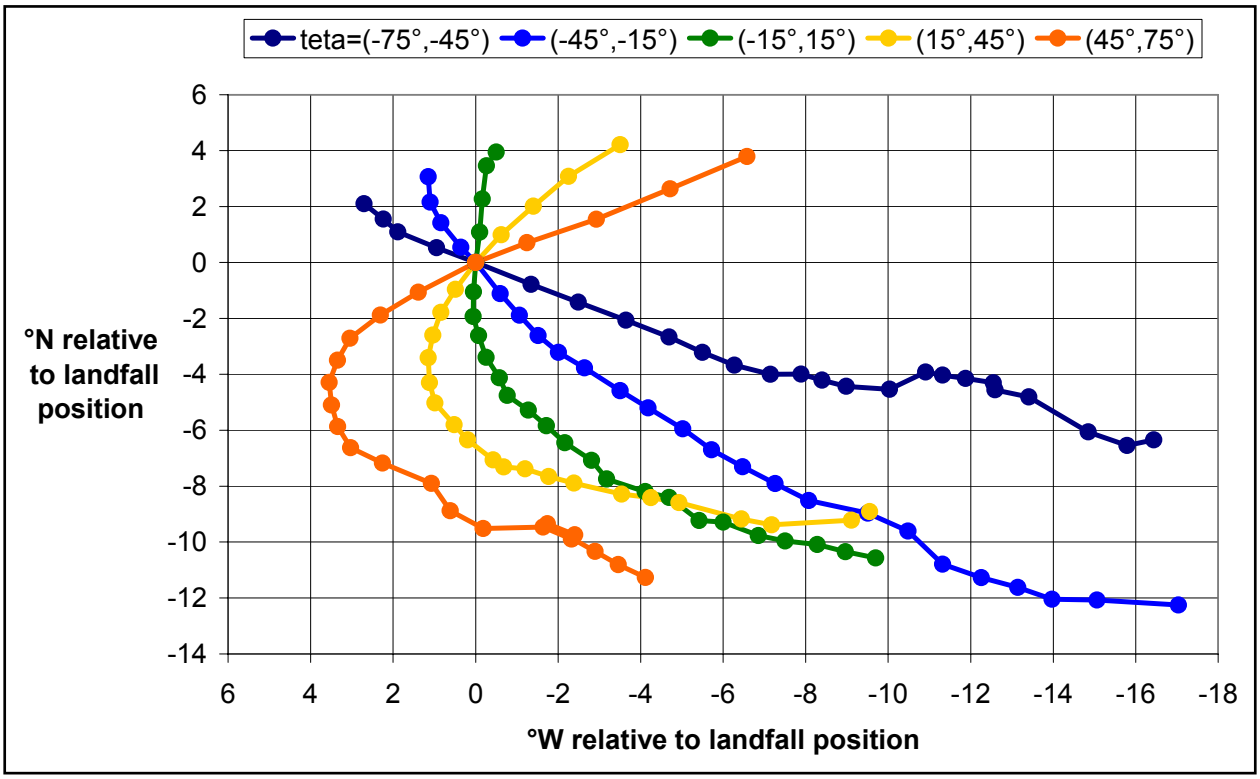

Figure 8-4. Mean Hurricane Path Depending on Landfall Angle θ

The temporal variation of ΔP and V is considered through the ratios

$$\Delta P_R(t) = \frac{\Delta P(t)}{\Delta P}$$
$$V_R(t) = \frac{V(t)}{V} \qquad (8\text{-}4)$$

where t is time before landfall and ΔP and V are the values at landfall (the values for t = 0). Dependence of $\Delta P_R(t)$ and $V_R(t)$ on the parameters $\underline{\Theta}$ at landfall has been investigated. While the statistics of $\Delta P_R(t)$ may be taken to be independent of $\underline{\Theta}$, $V_R(t)$ varies significantly with V (and to a negligible extent on the storm direction at landfall, θ). Since the ratios in Eq. 8-4 have significant temporal correlation, their uncertain evolution in time is represented by assuming perfect dependence. Under perfect dependence, the P-quantile values of $\Delta P_R(t)$ and $V_R(t)$ are connected at different times t to produce single time series, $\Delta P_{R,P}(t)$ and $V_{R,P}(t)$, for each probability P. Figure 8-5 shows empirical and smoothed estimates of $\Delta P_{R,P}(t)$ for P = 0.25, 0.5 and 0.75. Notice the tendency for ΔP to decrease during the 12 hours prior to landfall. This decrease is likely due to temperature gradients in the Gulf due to the Loop Current and its eddies and perhaps more importantly to the effect of land on the peripheral hurricane winds prior to landfall. In some cases (including hurricane Katrina), this intensity decay is rather pronounced, whereas in others (like hurricane Camille), it is not. The $\Delta P_R(t)$ profile for Katrina, which is shown in Figure 8-5 for comparison, lies within the inter-quartile range and is close to the upper 75% profile during the 18 hours prior to landfall.

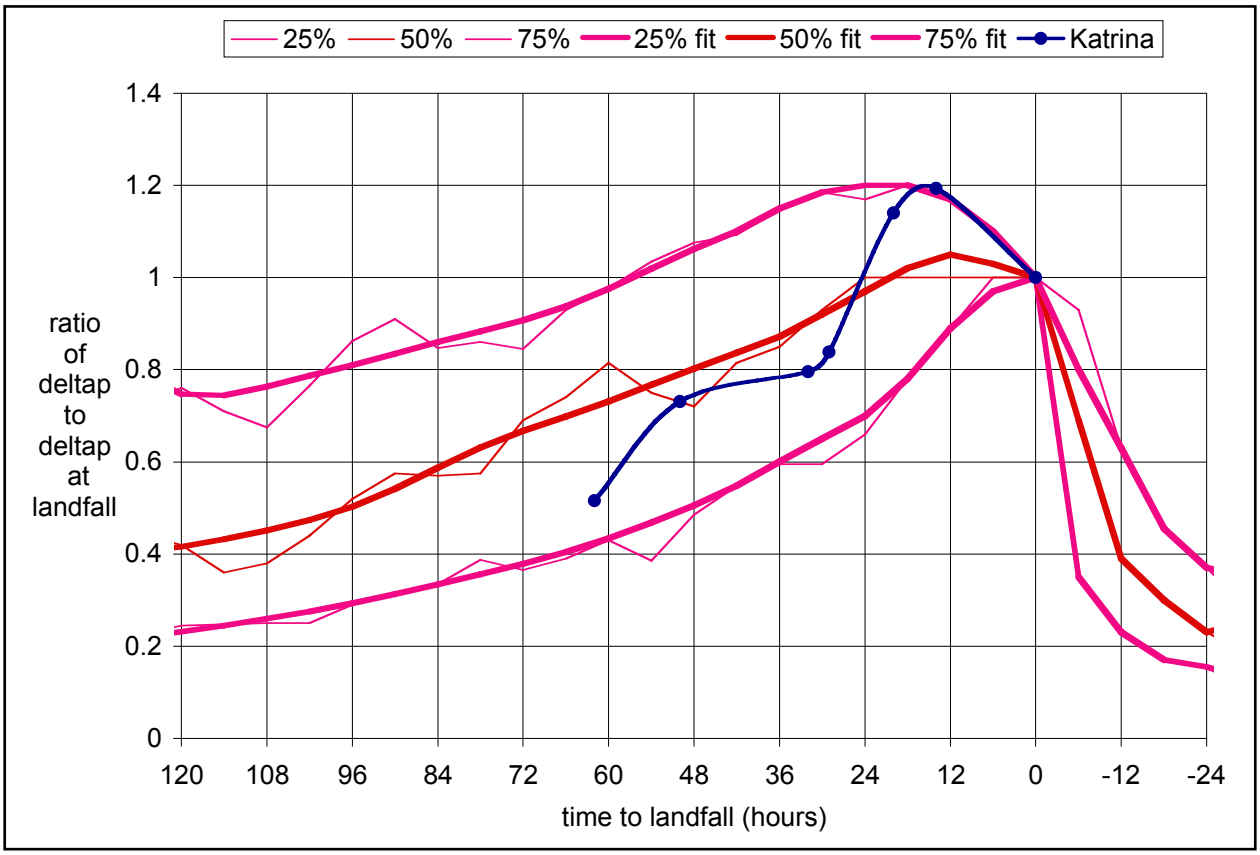

Figure 8-5. Pressure Deficit Ratios $\Delta P_{R,P}(t)$ for P = 0.25, 0.5 and 0.75

Figure 8-6 shows similar results for $V_{R,P}(t)$. Since $V_{R,P}(t)$ depends significantly on V at landfall, results are shown separately for $V < 15$ km/h, V between 15 and 25 km/h, and $V >$ 25 km/h (the empirical mean values of V within these ranges are close to the values of V used in the analysis. The temporal profiles of translational speed in Figure 8-6 reflect the fact that $V(t)$ is close to a stationary process. This is why, for large t, $V(t)$ looses memory of its value at landfall and $V_R(t)$ is small (large) for V large (small).

HURDAT does not include information on $R_{\max}$ and B. For $R_{\max}$, we use the model in Eq. 7 of Vickery et al. (2000), which gives

$$R_{\max}(t) \propto e^{-0.00005086\Delta P(t)^2 + 0.03949 Lat(t)} \tag{8-5}$$

as a first-order adjustment to the value at landfall using $\Delta P(t)$ and $Lat(t)$ along the track.

For B, Powell et al.'s (2005) model is used, which gives the dependence of $B(t)$ on $R_{\max}(t)$ and $Lat(t)$ as

$$B(t) = const. - 0.0109 Lat(t) - 0.00557\, R_{\max}(t) \tag{8-6}$$

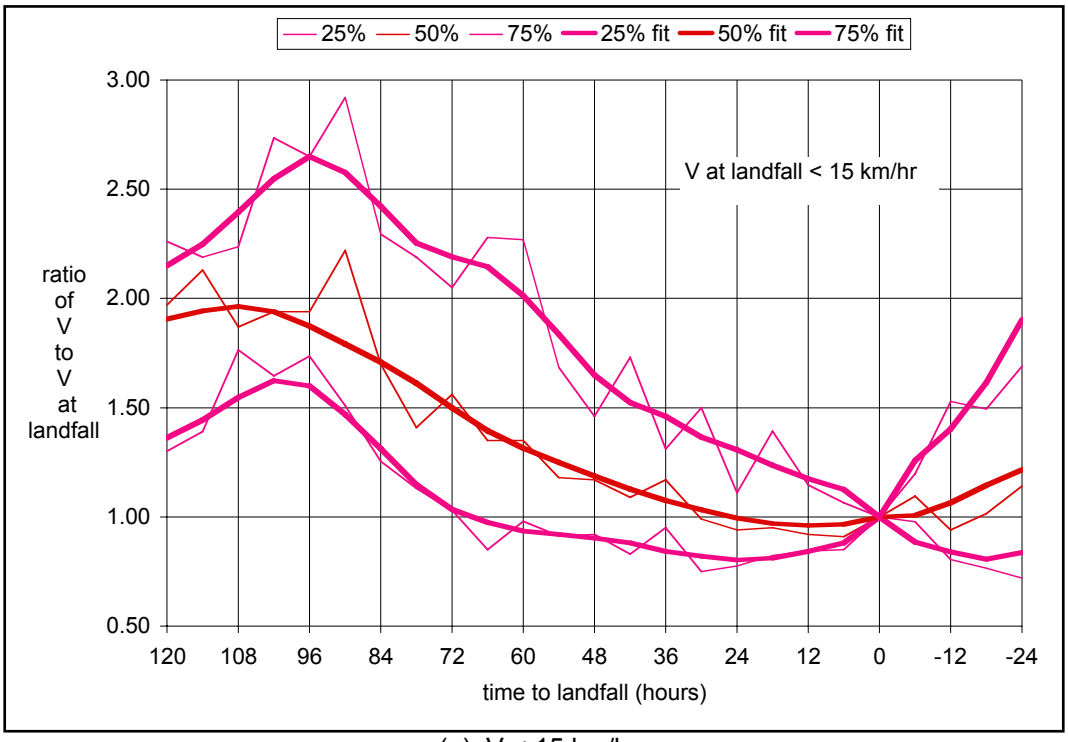

(a) V < 15 km/h

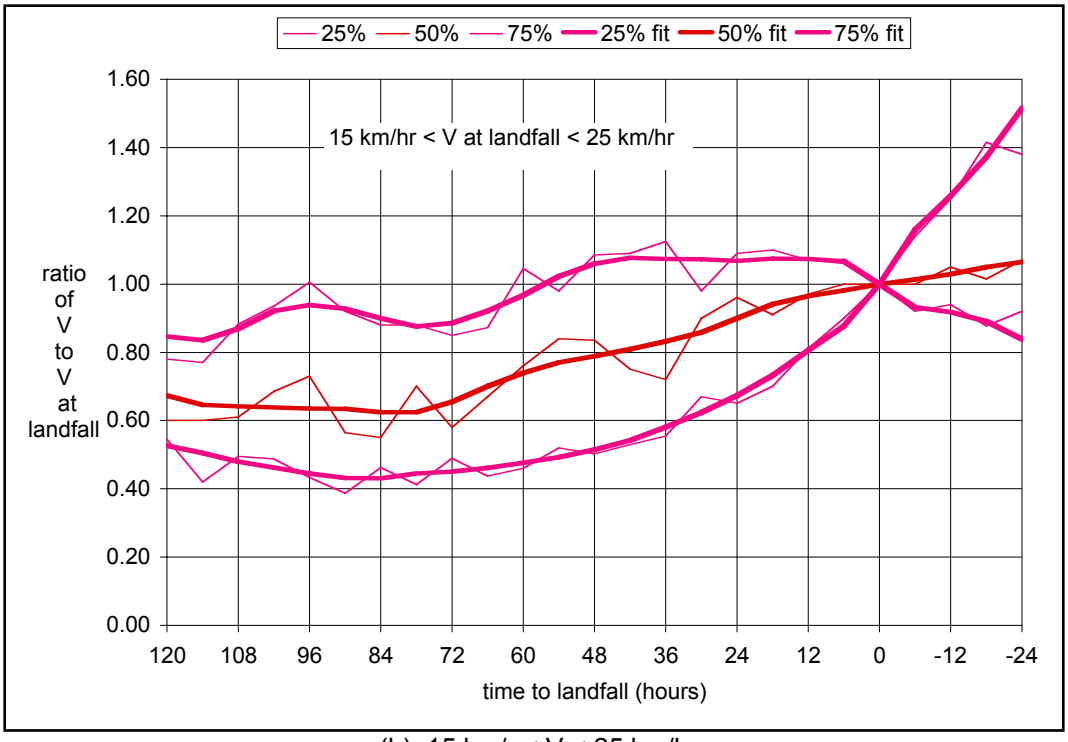

(b) 15 km/r < V < 25 km/h

Figure 8-6. Storm Speed Ratios $V_{R,P}(t)$ for P = 0.25, 0.5 and 0.75 and (a) V < 15 km/h, (b) V between 15 and 25 km/h, and (c) V > 25 km/h (Continued)

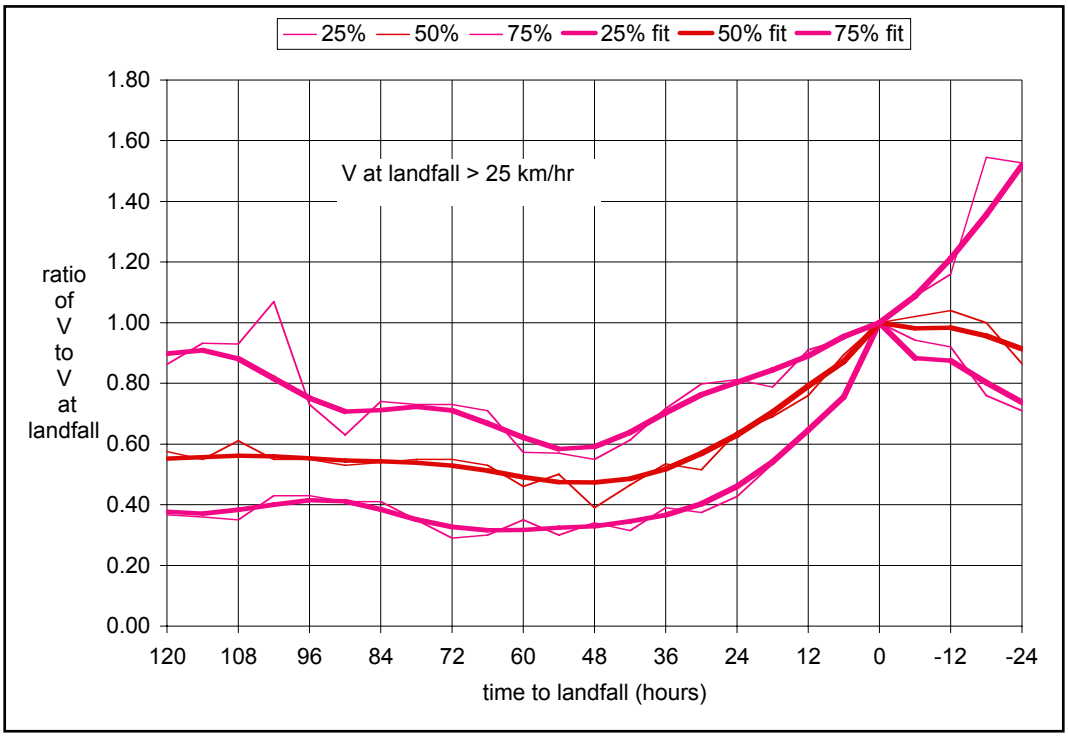

(c) *V > 25 km/h*

Figure 8-6. Concluded

The factor in Eq. 8-5 and the constant in Eq. 8-6 are adjusted to reproduce the values of $R_{\max}$ and B at landfall. Both equations give a mean-trend corrections along the track. No random temporal fluctuation of $R_{\max}$ or B is considered.

All of the analyses described below are performed using the mean tracks in Figure 8-4, the median ratios $\Delta P_{R,0.5}(t)$ and $V_{R,0.5}(t)$ in Figures 8-5 and 8-6, and the mean temporal evolutions of $R_{\max}$ and B in Eqs. 8-5 and 8-6. The ratios $\Delta P_{R,P}(t)$ and $V_{R,P}(t)$ for $P = 0.25$ and 0.75 in Figures 8-5 and 8-6 are used to assess uncertainty on the environmental loads due to variability in the pre-landfall values of ΔP and V.

Post-landfall Conditions. After landfall, several hurricane parameters undergo significant changes. For example, the pressure deficit ΔP decreases in an approximately exponential way and the radius of maximum winds $R_{\max}$ tends to increase. The only change that may have significant effect on surges and waves is the temporal decay of ΔP, which generally has the form

$$\Delta P(t) = \Delta P\, e^{-\alpha t} \tag{8-7}$$

where t is time after landfall, ΔP is pressure deficit at landfall, and α is a decay parameter. For t in hours and ΔP in mb, Vickery and Twisdale (1995b) found that for the Gulf of Mexico α has mean value $0.035 + 0.0005\,\Delta P$ and standard deviation 0.0355. These statistics are consistent with data in our narrower longitude range; see quantile plots in Figure 8-5 for $t < 0$. Since α is

not a sensitive parameter for waves and surges, we use this mean value expression in Eq. 8-7 and neglect the variability.

Parameter Discretization for Risk Analysis

Hurricane risk is evaluated by considering a large number of possible scenario hurricanes, each associated with one value of $\underline{\Theta}$. These scenario events are selected considering the joint density $f(\underline{\Theta})$ as well as the potential for induced damage.

For the parameters X and ΔP, which have a generally monotonic effect on the environmental loads, ranges have been that produce moderate to intense effects at the basins. Specifically, for the quantity $X\cos(\theta)$, which measures the minimum distance of the hurricane track from down-town New Orleans, the range [-130, +110] km is used. This choice is based on preliminary sensi-tivity runs, which indicate that hurricanes at greater distances from New Orleans do not dominate the risk. For the pressure deficit ΔP, we have used the range [41, 130] mb, where 41 mb is a representative value for Cat-2 hurricanes and 130 mb is well into the high Cat-5 range.

The effect of other parameters, in terms of sign and magnitude of which depends on location. We have generally varied them within their central 80% or 90% confidence intervals (i.e., the intervals that contain the value of the parameter with probability 0.8 or 0.9), obtained from the recurrence model. For parameters that depend significantly on other parameters, conditional rather than marginal ranges have been used.

The above ranges define a region in parameter space. A possible discretization of this region is given by all combinations of the parameter values listed in Table 8-1.

The parameters above the dashed line in Table 8-1 refer to conditions at landfall and those below the dashed line are for conditions before or after landfall. The first three values of ΔP in Table 8-1 are representative of hurricane Categories 2, 3 and 4 whereas the last three values represent various levels within Category 5. The values of V approximate the 5%, 25%, 50%, 75%, 95% Weibull quantiles in Figure 8-3. Finally notice that smooth $V_{R,0.5}(t)$ curves are shown in Figure 8-6 only for some ranges of V. Curves for specific values of V are obtained by first finding the average value of V for each range in Figure 8-3 (these average values are close to 8, 21, and 36 km/h) and then interpolating the curves for other values of V of interest.

Not all the 26,250 hurricane scenarios in Table 8-1 need be considered for risk assessment: some may be excluded because they are exceedingly rare and others because they are unlikely to cause significant losses. For example, hurricanes with small $R_{\max}$ and large $|X|$ do not pose a threat to the New Orleans region. Also, depending on the sensitivity of the loads L to each parameter, the number of parameter levels may be reduced. Conversely, if a better representation of a parameter or a more accurate decomposition of risk is required, then the number of levels may be increased. This is especially true for ΔP.

Table 8-1
Parameter Levels that May be Considered for Risk Analysis

Parameter	Levels for risk analysis
ΔP (mb)	41, 59, 80, 100, 115, 130
V (km/h)	8, 15, 21, 27, 36
$Xcos(\theta)$ (km)	-130, -90, -50, -10, 30, 70, 110
θ	-60, -30, 0, 30, 60
$R_{\max}$	10%, 50%, 90% quantiles from Eq. 8-2
B	5%, 25%, 50%, 75%, 95% quantiles from Eq. 8-3
----------	----------
$\Delta P_R(t)$	smooth $\Delta P_{R,0.5}(t)$ curve in Figure 8-5
$V_R(t)$	smooth $V_{R,0.5}(t)$ curves in Figure 8-6 depending on V
$R_{\max}(t)$	from $R_{\max}$, $\Delta P(t)$ and $Lat(t)$; see Eq. 8-5
$B(t)$	from B, $R_{\max}$ and $Lat(t)$; see Eq. 8-6
α	$0.035 + 0.0005\,\Delta P$
No. of cases	**26,250**

Assessment of Hurricane Loads $L(\underline{\Theta})$

Finding the environmental loads L for each parameter vector $\underline{\Theta}$ of interest is the most challenging task of hurricane hazard characterization. The following paragraphs describe how this is done for still water levels, waves, and rainfall intensity.

Still Water Levels and Waves. It is well known that surge and waves interact (surge affects waves and vice-versa). Therefore, these loads should be ideally assessed using a coupled formulation. Sophisticated coupled programs are currently being developed that reflect this coupling, but at the present time such programs are not at a stage that they can be routinely used.

An alternative is to follow an iterative approach, whereby the surge H(x,y,t) without waves are first calculated, the wave field W(x,y,t) estimated given the preliminary estimate of the surge, and finally the surge code is re-run considering the calculated wave field. While the treatment of waves has not been finalized yet, the plan is to use a simple wave parameterization scheme based on results obtained in previous detailed analyses. This parameterization approach should produce rather accurate results and greatly streamlines computations (Robert Dean, personal communication). Surges are calculated using the ADCIRC code (Luettich et al. 1992).

ADCIRC uses a triangular grid with spatially varying resolution, which for our application covers the entire Gulf of Mexico. The resolution increases in coastal areas, in particular near the Louisiana Coast. High-resolution grids may include millions of nodes and must be run with time steps on the order of 1 second to avoid numerical problems. Such dense grids produce accurate results and can adequately resolve topographic effects on horizontal scales of tens of meters along the coast.

Since it is not feasible to use such dense computational grids for all the parameter combinations in Table 8-1, a different strategy was adopted to avoid, running all cases by using computational grids at lower resolutions.

Reduction in the Number of ADCIRC Runs. Two conditions were taken advantage of reduce the number of runs: (1) If dependence of H on a parameter A is smooth, then H was calculated for a subset of levels of A and interpolation used for the other levels, and (2) If two parameters A and B do not interact (additively or multiplicatively), then the (additive or multiplicative) effect of varying one of them is the same irrespective of the level of the other parameter. In this case all combinations of A and B can be inferred for H for by varying each parameter while keeping the other parameter constant. Determination of whether either condition applies can be made using a low-resolution (LR) ADCIRC grid run with only a few thousand nodes ignoring the effect of waves.

These considerations reduce the number of needed ADCIRC runs from about 26,000 in Table 8-1 to about 1,000. However, even 1,000 hurricane scenarios are too many to be run with a high-density grid. The strategy selected is to run these cases with a medium-resolution (MR) grid with approximately 90,000 nodes and use the high-resolution (HR) grid for only about 40 cases. The HR runs are then used to calibrate the MR results.

The spatial pattern of surge and waves depends primarily on [$R_{\max}$, X, θ]. Since the effect of these parameters at a given geographic location is generally non-monotonic, interpolation involving these parameters would not produce accurate results. In addition, these parameters interact among themselves. Hence, all combinations of [$R_{\max}$, X, θ] in Table 8-1 must be run using the MR model. The use of only 3 levels of $R_{\max}$ in Table 8-1 reduces the computational effort in the MR runs.

The LR runs have shown that, for given [$R_{\max}$, X, θ], the water level H at each geographical location depends smoothly on ΔP, V, and B. Therefore a smaller number of levels of these parameters were considered and H calculated for the other levels through interpolation. This has led to the MR run plan in Table 8-2.

One may reduce the number of MR runs even further. From the LR runs, it was determined that the multiplicative effect of Holland's B on the surge depends mildly on ΔP and V. Therefore there is no need to run different values of B with each combination of ΔP and V. This produces the MR plan in Table 8-3, which comprises two sub-factorials of the levels in Table 8-2, with a total of only 1155 runs.

For the HR runs, the subset of 36 hurricanes in Table 8-3 is retained. In general, the levels in Table 8-4 have been chosen to maximize the accuracy of calibration of the MR results.

Table 8-2
Parameter Levels for Mid-Resolution Runs

Parameter	Levels for mid-resolution analysis
ΔP (mb)	41, 80, 115
V (km/h)	8, 21, 36
$Xcos(\theta)$ (km)	-130, -90, -50, -10, 30, 70, 110
θ	-60, -30, 0, 30, 60
$R_{\max}$	10%, 50%, 90% quantiles from Eq. 8-2
B	5%, 50%, 95% quantiles from Eq. 8-3
---	---
$\Delta P_R(t)$	smooth $\Delta P_{R,0.5}(t)$ curve in Figure 8-5
$V_R(t)$	smooth $V_{R,0.5}(t)$ curves in Figure 8-6 depending on V
$R_{\max}(t)$	from $R_{\max}$, $\Delta P(t)$ and $Lat(t)$; see Eq. 8-5
$B(t)$	from B, $R_{\max}$ and $Lat(t)$; see Eq. 8-6
α	$0.035 + 0.0005\,\Delta P$
No. of cases	**2835**

Table 8-3
Final Plan for the Mid-Resolution Runs

	Mid-resolution model runs	
Parameter	**Factorial 1**	**Factorial 2**
ΔP (mb)	41, 80, 115	80
V (km/h)	8, 21, 36	21
$Xcos(\theta)$ (km)	-130, -90, -50, -10, 30, 70, 110	-130, -90, -50, -10, 30, 70, 110
θ	-60, -30, 0, 30, 60	-60, -30, 0, 30, 60
$R_{\max}$	10%, 50%, 90% quantile from Eq. 8-2	10%, 50%, 90% quantile from Eq. 8-2
B	50% quantile from Eq. 8-3	5%, 95% quantiles from Eq. 8-3
---	---	---
$\Delta P_R(t)$	$\Delta P_{R,0.5}(t)$ from Figure 8-5	$\Delta P_{R,0.5}(t)$ from Figure 8-5
$V_R(t)$	$V_{R,0.5}(t)$ from Figure 8-6	$V_{R,0.5}(t)$ from Figure 8-6
$R_{\max}(t)$	from Eq. 8-5	from Eq. 8-5
$B(t)$	from Eq. 8-6	from Eq. 8-6
α	$0.035 + 0.0005\,\Delta P$	$0.035 + 0.0005\,\Delta P$
No. of runs	**945**	**210**
Total runs	**1155**	

Table 8-4
Factorial Plan for the High-Resolution Runs

Parameter	High-resolution model runs
ΔP (mb)	80, 115
V (km/h)	21
$Xcos(\theta)$ (km)	-90, -10, 70
θ	-60, 0, 60
$R_{\max}$	10%, 90% quantiles from Eq. 8-2
B	50% quantile from Eq. 8-3
----------	----------
$\Delta P_R(t)$	$\Delta P_{R,0.5}(t)$ from Figure 8-5
$V_R(t)$	$V_{R,0.5}(t)$ from Figure 8-6
$R_{\max}(t)$	from $R_{\max}$, $\Delta P(t)$ and $Lat(t)$; see Eq. 8-5
$B(t)$	from B, $R_{\max}$ and $Lat(t)$; see Eq. 8-6
α	$0.035 + 0.0005\,\Delta P$
No. of cases	**36**

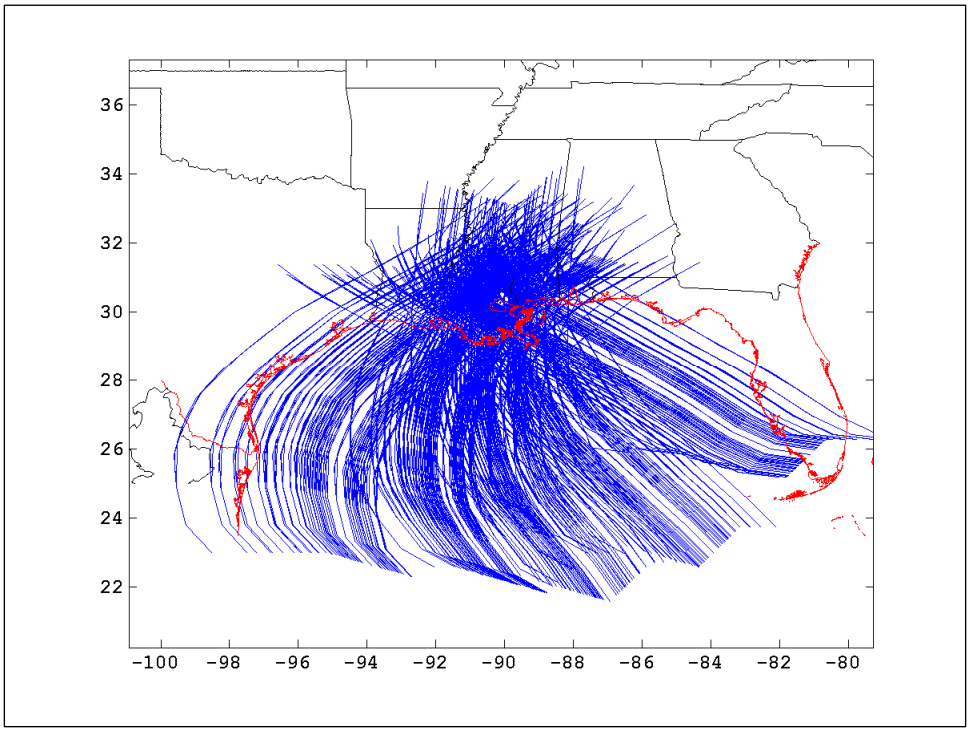

Figure 8-7. Storm tracks considered in the ADCIRC simulations

Calibration and Extension of the MR Results Using the HR Runs

For the 36 cases in Table 8-4, the water levels H and the wave characteristics W are directly extracted from the HR runs. For the remainder of the cases in Table 8-3, which are run only with the MR grid, corrections must be made to reflect the bias of that coarser discretization. The bias is site-specific, as it depends on the local geometry of the coast, the topography, and the different local land coverage of the MR and HR grids. The correction further depends on the hurricane parameters $\underline{\Theta}$. For example, the correction at a given location generally depends on landfall position X, direction θ, and possibly storm intensity ΔP. The approach that follows reflects these considerations.

Let Y be a generic response of interest, e.g., Y = water level or significant wave height. At each location of interest $k = (x_k, y_k)$ and for each of the 36 events in Table 8-4, we calculate $Y_{\max,MR,kj}$ and $Y_{\max,HR,kj}$, the maximum values of Y at k from the MR and HR runs, and the calibration factor

$$\gamma_{Y_{kj}} = \frac{Y_{\max,HR,kj}}{Y_{\max,MR,kj}} \tag{8-8}$$

If $Y_{\max,MR,kj}$ and $Y_{\max,HR,kj}$ fall below some minimum value, the ratio $\gamma_{Y_{kj}}$ is considered "undefined."

Next a distance d_{ij} between any pair of parameter vectors $(\underline{\Theta}_i, \underline{\Theta}_j)$ is defined where $\underline{\Theta}_i$ is the vector for MR case i in Table 8-3 and $\underline{\Theta}_j$ is the vector for HR case j in Table 8-4. The distance function should reflect the sensitivity of $\gamma_{Y_{kj}}$ in Eq. 8-8 to different parameters (if the loads are insensitive to a parameter, differences in that parameter level should be contributing little to d_{ij}).

Finally, the time history $Y_{MR,ki}(t)$ for hurricane i in Table 8-3 is corrected using a square-distance weighting scheme. The corrected values, $\hat{Y}_{ki}(t)$, are given by

$$\hat{Y}_{ki}(t) = \left(\frac{\sum_j \gamma_{Y_{kj}} / d_{ij}^2}{\sum_j 1 / d_{ij}^2} \right) Y_{MR,ki}(t) \tag{8-9}$$

where the two summations extend over the values of j for which $\gamma_{Y_{kj}}$ is defined.

The previous calibration procedure applies to locations k at which the MR grid produces realistic results. At locations where this is not so, for example along narrow canals where the MR values are not reliable or may not even exist (because the MR grid does not extend to those locations), HR results were used to fit regression relations in terms of values along the coast

where the MR solution is available and regressions were fitted to extrapolate the estimates from Eq. 8-9.

Rainfall Intensity

Rainfall is among the variables that affect the inundation of the basins. While rainfall is not of primary concern for the hurricane protection system, it is a contributor to the frequency of low-level flood losses. Hence it was decided that a relatively coarse model of hurricane-induced rainfall would suffice.

Prior to NASA's Tropical Rainfall Measuring Mission (TRMM) (Simpson et al. 1988), information on hurricane rainfall was scanty. The TRMM mission, which started in November 1997, produced vast amounts of rainfall estimates for tropical storms and hurricanes at a spatial scale of about 5 km in various tropical regions, including the Atlantic basin. These rainfall products have been analyzed statistically by Lonfat et al. (2004) and Chen et al. (2006). The model proposed below is based primarily on these two studies and on discussions with Dr. Shuyi Chen at the University of Miami.

Mean Rainfall Intensity. Hurricane rainfall intensity I (mm/h) varies with distance r from the hurricane center and azimuth β relative to the direction of motion. Moreover, the mean intensity field $m_I(r,\beta)$ varies with the central pressure deficit ΔP, the radius of maximum winds $R_{\max}$, the storm velocity V, and the vertical wind shear S (in the above quoted references, S is measured as the difference between the horizontal wind fields at the 200 and 850 hPa levels). Finally, rainfall intensity displays strong fluctuations at different scales around the mean value $m_I(r,\beta)$.

The azimuthal average of $m_I(r,\beta)$, $m_I(r)$, gives the symmetrical component of the mean rainfall field. This component has a maximum at a distance from the hurricane center close to $R_{\max}$ and decays in an approximately exponential way at larger distances. This decay is contributed by the approximately exponential decay of both the fraction of rainy area and the mean rainfall intensity at the rainy locations. The rate of exponential decay $m_I(r)$ is inversely proportional to the size of the hurricane; hence in good approximation it is inversely proportional to $R_{\max}$.

The value of $m_I(r)$ for $r = R_{\max}$ increases with increasing ΔP, approximately doubling from a Category 2 to a Category 4 to5 event. Considering the Category1-2 and Category3-5 results in Lonfat et al. (2004) as representative of the Cat1-2 boundary and of Cat4, respectively, assuming linear dependence of the mean rainfall intensity at $R_{\max}$ on Δp, and fitting an exponential decay with distance as mentioned above, the following is obtained

The rainfall accumulation within each of the 37 sub-basins for each of the storms in the basic simulation set (the 1080 storms of the ADCIRC storm surge simulation set MR1) was determined according to the procedure summarized in the following paragraphs. Note that the MR1 storm set is complete as far as the rainfall estimates are concerned. The other simulation sets (MR2 and HR) are used only to adjust storm surge estimates, and have no implications for rainfall.

The rainfall pattern within a storm was determined to be given by:

$$m_I(r) = \begin{cases} 1.14 + 0.12\Delta P, & for\ r \le R_{\max} \\ (1.14 + 0.12\Delta P)e^{-0.3\left(\frac{r - R_{\max}}{R_{\max}}\right)}, & for\ r > R_{\max} \end{cases} \quad (8\text{-}10)$$

in which m is the rainfall intensity in mm/hour and the central pressure deficit, ΔP, is in mb. R_{max} is the radius to maximum wind, and r is radial distance from the storm center. Additionally, the rainfall intensity is assumed to vary with azimuth around the eye. This is accounted for by an asymmetry factor of 1.5 which is applied to intensity on the right-hand side of the storm track.

Both the central pressure and the radius to maximum wind vary with time along a particular storm track. Furthermore, the storm tracks are curvilinear. Consequently, the determination of the rainfall accumulation in a particular sub-basin requires an integration of the expression given above over time, accounting at each time step for the instantaneous distance from the storm to the sub-basin, the corresponding instantaneous radius and pressure, and a determination of whether at that instant the sub-basin lies to the left or the right of the storm track. Note that as a storm proceeds through the area, a particular basin may be sometimes on the right and sometimes on the left of the same track.

It has been assumed that a sub-basin can be characterized by its location, given by the geographic coordinates of its centroid and its area. The rainfall volume accumulation within it has been approximated by the integral over time of the rainfall intensity at the centroid, multiplied by the sub-basin area. Spatial variation over a particular sub-basin has not been considered, and would not be supported by the accuracy to which the rainfall intensity is known. The adopted sub-basin locations and areas are shown in the appended table.

Integration of the rainfall was performed using the same tracks and time histories for pressure and radius as were used in the surge simulations. A one hour time step was adopted. The first task in the computation was to determine the storm's position along its track at each hour, and its associated pressure and radius at the same times. Given each of these hourly segments, the average radius and pressure over that segment were determined. Similarly, for each of the 37 sub-basins at each time step, the corresponding distances from the storm were computed and a left/right determination was made. The latter was based on the instantaneous projected storm track for each hourly track position. Distances were computed using the expression for great circle arcs on a sphere:

$$S = R_{earth} \cos^{-1}\left\{\sin\varphi_1 \sin\varphi_2 + \cos\varphi_1 \cos\varphi_2 \cos\left(\theta_1 - \theta_2\right)\right\} \quad (8\text{-}11)$$

in which φ and θ are latitude and longitude, and Earth's radius has been taken to be the quadratic mean value of 6372.8 km.

Finally, the rainfall contribution for each one-hour track segment was given directly by the expression for the intensity, m, converted to ft/hour (the multiplying time step was 1.0 hours). These were summed over the entire track for each sub-basin and multiplied by the basin area in sq ft to give the final volume estimates in cubic feet.

Table 8-5
Sub-basin Locations and Areas for Rainfall Analysis

	Centroid		Area	Area
Sub-Basin	Latitude	Longitude	Ft2	Mi2
New Orleans East				
NOE1	30 05 00.53478	89 52 50.29178	619571000.00	22.22
NOE2	30 02 57.81754	89 54 13.19397	249914743.99	8.96
NOE3	30 01 41.34316	89 55 25.51095	124110000.00	4.45
NOE4	30 00 27.81633	89 58 45.95704	108773000.00	3.90
NOE5	30 02 03.64004	89 58 38.84153	404196000.00	14.50
Orleans Main				
OM1	30 00 42.50491	90 03 44.89893	213793000.00	7.67
OM2	30 00 16.11471	90 06 13.60155	186831000.00	6.70
OM3	29 58 55.44943	90 02 52.69480	207859000.00	7.46
OM4	29 58 20.28696	90 08 27.45401	86934800.00	3.12
OM5	29 56 53.88112	90 05 57.65334	493096000.00	17.69
St. Bernard				
SB1	29 57 22.80173	89 59 30.65214	221286000.00	7.94
SB2	29 58 56.34666	89 58 27.24522	216951000.00	7.78
SB3	29 55 52.13899	89 55 29.91554	241570000.00	8.67
SB4	29 52 12.82452	89 50 52.01695	402609000.00	14.44
SB5	29 55 44.11473	89 51 55.45020	1052590000.00	37.76
Jefferson East				
JE1	29 57 40.75586	90 12 20.44431	339781000.00	12.19
JE2	30 00 00.20924	90 09 11.65984	250916000.00	9.00
JE3	30 00 30.03647	90 13 56.33463	652753000.00	23.41
Jefferson West				
JW1	29 55 59.04667	90 13 17.94346	465305000.00	16.69
JW2	29 53 36.19461	90 12 15.12590	437649000.00	15.70
JW3	29 51 41.38819	90 06 08.07269	655546000.00	23.51
JW4	29 53 06.66906	90 02 33.01369	547970000.00	19.66
St. Charles				
SC1	29 58 18.70696	90 20 34.99452	254190000.00	9.12
SC2	29 58 30.12714	90 21 50.74235	313332000.00	11.24
Plaquemines				
PL1	29 49 29.23208	89 58 23.27582	379283000.00	13.60
PL2 / PL 11	29 45 01.09738	90 01 19.41722	133960000.00	4.81
PL3	29 39 37.98101	89 58 46.13357	312305000.00	11.20
PL4	29 37 08.73123	89 52 29.71304	117303000.00	4.21
PL5	29 33 34.50015	89 45 57.68927	78203100.00	2.81
PL6	29 44 26.14917	89 59 38.16708	70836100.00	2.54
PL7	29 30 39.25862	89 43 52.38498	86598200.00	3.11
PL8	29 26 18.21557	89 38 02.65653	126026000.00	4.52
PL9	29 22 18.39493	89 34 33.90418	64024700.00	2.30
PL10	29 19 56.73243	89 26 53.45076	198180000.00	7.11
PL12	29 50 43.30476	90 00 27.04146	597345000.00	21.43
Orleans West Bank				
OW1	29 54 02.39070	89 56 16.33497	183015000.00	6.56
OW2	29 55 33.86860	90 00 54.13877	268024000.00	9.61

Uncertainty may be expressed by a lognormal random variable with mean value 1 and log standard deviation 0.69, which corresponds to an uncertainty factor of 2. This random factor should be applied to the entire mean rainfall time history. In reality, rainfall intensity inside a basin would display significant fluctuations in time and space, which locally could far exceed a factor of 2. However, the above random factor should adequately reflect uncertainty on the total precipitation in a basin during the passage of a hurricane.

Epistemic Uncertainty

Epistemic uncertainty (uncertainty due to limited information and knowledge) affects all aspects of the hazard characterization. While a thorough assessment of these uncertainties is beyond the scope of this project, a rough quantification of uncertainty on the hurricane rates $\lambda(\underline{\Theta})$ and the loads $L(\underline{\Theta})$ will be made.

General Considerations. The hurricane rates $\lambda(\underline{\Theta})$ are uncertain due to the limited historical sample size, possible errors in the assumed form of marginal and conditional distributions (especially in the tail regions), and the uncertain near-future hurricane activity due to fluctuations and trends associated with climate changes and multi-decadal cycles. A first-order assessment of uncertainty on $\lambda(\underline{\Theta})$ is based on the hurricane effects of global warming and shorter-term climatic fluctuations in the North Atlantic.

Causes of epistemic uncertainty on $L(\underline{\Theta})$ are hurricane model errors, for example the wind field idealization, the coefficient of friction with the water surface, the effects of waves on water level, etc., are estimated by hind casting historical events or by comparing results from different modeling assumptions.

Other epistemic uncertainties associated with the imperfect calibration of the MR model using the sparse HR results are by considering the variability of the calibration factors $\gamma_{Y_{kj}}$ in Eq. 8-8 in hurricane parameter space. Finally, there are interpolation errors when estimating water heights and waves for parameters $\underline{\Theta}$ not used in the MR plan.

Climatic Effects and Their Contribution to Epistemic Uncertainty

The potential effect of global warming on the frequency, size and intensity of tropical cyclones is a hotly debated issue in the technical literature; see Pielke et al. (2005), Emanuel (2005b), and Elsner (2005) for recent reviews. Theoretical analysis, numerical modeling and historical data analysis have all been used to study the effects of climate variations on various features of tropical cyclones. The main results on hurricane frequency and intensity are summarized below. What determines hurricane size is poorly understood; hence the possible dependence of $R_{\max}$ on global warming and other climatic factors is not considered.

Frequency of Tropical Cyclones. From an observational viewpoint, the frequency of tropical cyclones worldwide has remained remarkably constant during the past 100 years or more (Elsner and Kocher 2000; Webster et al. 2005; Emanuel 2005b). Since during this period the

planet has undergone global warming and cooling, it is concluded that climatic changes of this type and magnitude have small effects on the rate of tropical cyclones at the planetary scale.

On the other hand, significant fluctuations in tropical cyclone activity at decadal and multi-decadal scales have occurred in various parts of the world. For example, hurricane activity in the North Atlantic was low in the 1970s, 1980s, and early 1990s compared with the 1940s, 1950s and early 1960s or with the decade since 1995. Changes in hurricane frequency between active and quiescent periods have been by factors of 2 or more (Goldenberg et al. 2001). The current rate in the North Atlantic is about 50% higher than the historical average rate and will likely persist at least over the next 5 years (Elsner 2005). These fluctuations are due to well-known cycles like the El-Nino-Southern Oscillation (ENSO), which by increasing the wind shear dampens the rate and intensity of hurricanes, the tropical Atlantic sea-surface temperature (SST), with warmer temperatures usually producing higher hurricane rates, and the Atlantic multi-decadal oscillation (AMO), which is the difference in air pressure between Iceland and the Azores and is thought to affect mainly the hurricane tracks (Elsner 2005).

Intensity of Tropical Cyclones. The effect of global warming on tropical cyclone intensity is somewhat more controversial. It has been argued that an increase in sea surface temperature would make the atmosphere more thermodynamically unstable and increase the maximum potential intensity (PI) of hurricanes (Emanuel 1987; Lighthill et al. 1994; Henderson-Sellers et al. 1998). In turn, PI has been shown to be highly correlated with the average intensity of hurricanes (Emanuel 2000). Following this argument, increases in intensity under a warmer climate may be expected (Emanuel 2005a).

On the other hand, it may also be argued that an increase in sea surface temperature would increase the vertical wind shear, which tends to disrupt the symmetry of tropical cyclones and reduces their intensity.

Empirical evidence of higher hurricane intensity during the past 50 years, when the sea surface temperature has increased by about 0.2 degree centigrade, is weak (Landsea et al. 1999; Bister and Emanuel 2002; Free et al. 2004; Chan and Liu 2004). This is in agreement with findings based on global circulation models. For example, Knutson and Tuleya (2004) and Michaels et al. (2005) predict increases in wind speed of 5% or less by the year 2080. Therefore, while future variations in intensity due to global warming are considered possible, it is generally expected that such variations will be modest and overshadowed by the multi-decadal fluctuations.

Results that contrast with this general consensus are reported in Emanuel (2005a). Using data worldwide, Emanuel found that the energy released by hurricanes has increased by about 70% over the past 30 years and attributes the phenomenon to global warming. This phenomenon is contributed by an increase of 15% in the maximum wind speed and an increase of 60% in storm duration. These findings have been contested by other researchers and must be considered preliminary pending further validation.

Epistemic Uncertainty on Future Hurricane Climate. From the preceding discussion, uncertainty on the hurricane statistics in the Gulf of Mexico during the next 50-100 years is dominated by multi-decadal oscillations. Specifically, considering that the North Atlantic is now

experiencing a 50% higher-than normal activity and that this elevated activity may persist over a number of years and possibly decades, it is reasonable for the next 50-100 years to increase the average historical rate of hurricanes by 20% and allow for an additional 25% uncertainty factor around this corrected rate. The latter factor includes uncertainty on the historical rate due to the finite observation period (16%) as well as uncertainty on the future evolution of the hurricane frequency (judgmentally assessed).

Considering the general consensus and dissenting views on the effect of global warming on hurricane intensity, the historical mean pressure deficit is increased by 3% and an uncertainty factor of 5% is applied to the increased mean value. Since the effects of different factors on hurricane frequency and intensity are poorly correlated,, these components of epistemic uncertainty may be treated as independent.

Hurricane Waves

An approximate method was used for calculating waves and wave setup due to hurricane winds over the Gulf of Mexico. The quantification of deep water waves is based on a method published in the Shore Protection Manual[1] (1984). The wave setup is based on the physics governing wave setup, considers an average slope over the profile and employs the Dally et al (1985) wave breaking relationship over the full range from deep to shallow water.

Wave Characteristics

Deep Water Wave Conditions. The Shore Protection Manual (SPM) provided recommendations for calculating deep water wave characteristics in a hurricane. These methods included two equations, one for the maximum significant wave height and one for the associated wave period. In addition a graph was provided which represented the non-dimensional distribution of wave heights in a hurricane. Each of these is discussed below.

The wave characteristics (significant height and associated period) were presented in terms of the hurricane parameters in both English and metric systems. For purposes here, the equations below are presented for the English system. The parameters are:

Central pressure deficit: Δp in inches of mercury

Forward translational speed of hurricane: V_F in knots.

Radius to maximum winds: R in nautical miles.

Maximum sustained wind speed at 33 feet above the sea surface: U_R in knots

Coefficient depending on hurricane speed: α (dimensionless)

[1] The predecessor to the Coastal Engineering Manual of the U.S. Army Corps of Engineers.

Coriolis parameter: f (dimensionless)

where the Coriolis parameter, f, is given by

$$f = 0.524 \sin \phi \tag{8-12}$$

and ϕ is the latitude at the location of interest.

The equations for maximum significant wave height and associated period are:

$$H_{o,\max} = 16.5 e^{\frac{R\Delta p}{100}} \left[1 + \frac{0.208 \alpha V_F}{\sqrt{U_R}} \right] \tag{8-13}$$

and

$$T_s = 8.6 e^{\frac{R\Delta p}{200}} \left[1 + \frac{0.104 \alpha V_F}{\sqrt{U_R}} \right] \tag{8-14}$$

where

$$U_{\max} = 0.868 \left(73 \sqrt{\Delta p} - 0.575 R f \right) \tag{8-15}$$

The parameter, U_R, is expressed in terms of $U_{\max}$ as:

$$U_R = 0.865 U_{\max} + 0.5 V_F \tag{8-16}$$

The value of the parameter α is recommended as unity for slowly translating hurricanes and this value will be used here.

Figure 8-8 presents the relationship for non-dimensional significant wave height as a function of non-dimensional distances relative to the hurricane center.

As seen from Figure 8-8, the SPM model predicts waves which propagate in approximately the same direction as the local winds. For purposes here, wave height distributions are presented for two distances offshore and it is recommended that the applied distribution be prorated by the actual distance of the hurricane center from the shoreline. The two distributions are presented in Figure 8-8 along with the SPM distribution. The deviations from the SPM model are based on the recognition that waves diffract and disperse in advance of a hurricane. The two distributions are associated with distances of more than 4 radii from the shoreline and at the shoreline.

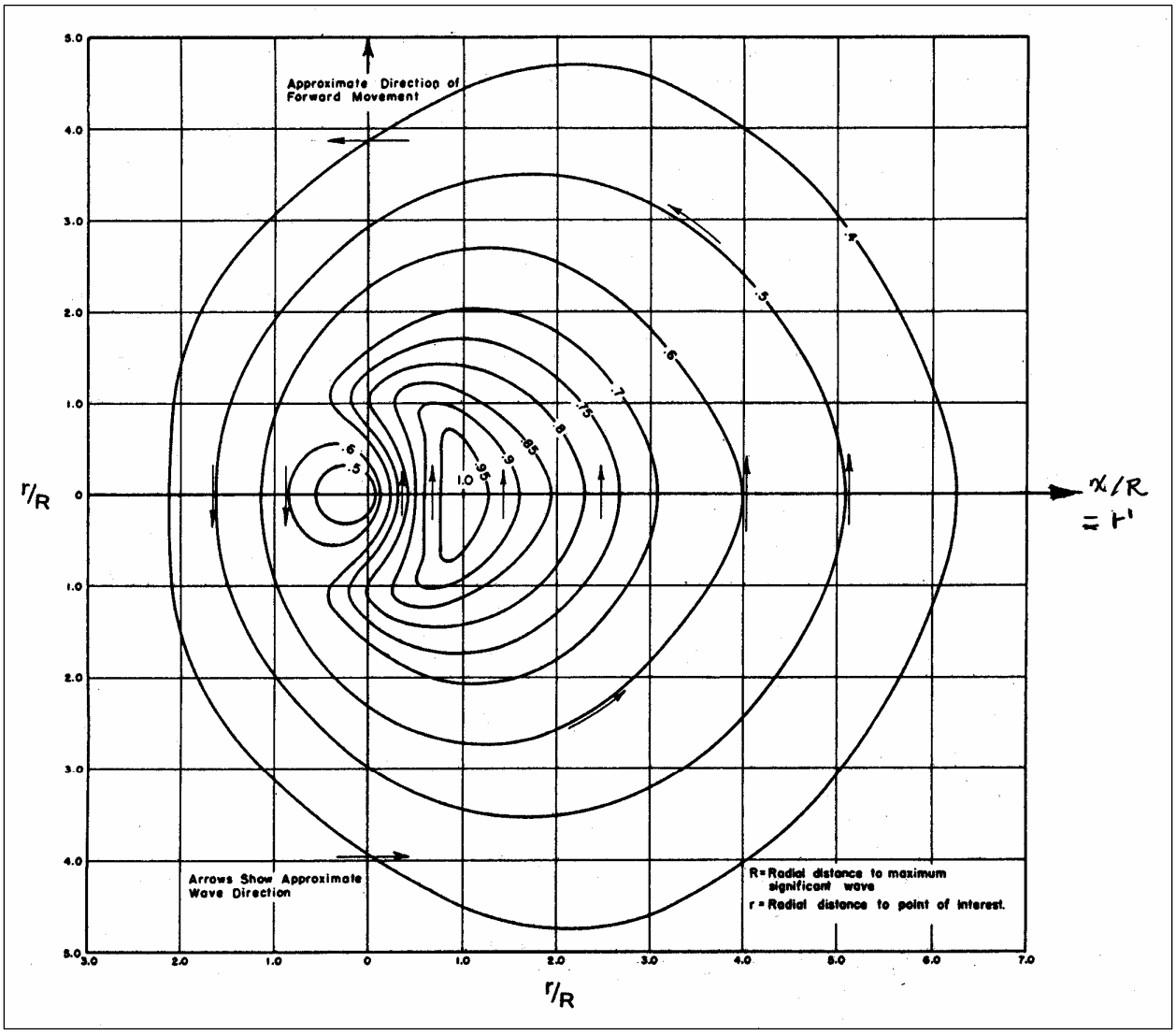

Figure 8-8. Shore Protection Manual Relationship for Wave Heights Relative to Their Maximum in a Hurricane

Specifically, the recommended relevant deep water wave heights at shore are:

For Hurricane Center More Than 4 Radii (R) From the Shoreline

$$H_o / H_{o,\max} = 0.40 + 0.20\cos^2\left[\frac{\pi}{2}\left(\frac{r'-2}{12}\right)\right], \text{-10< r'<14}$$

$$H_o / H_{o,\max} = 0.40, \text{ r'} < \text{-10, r'>14} \qquad \text{(8-17)}$$

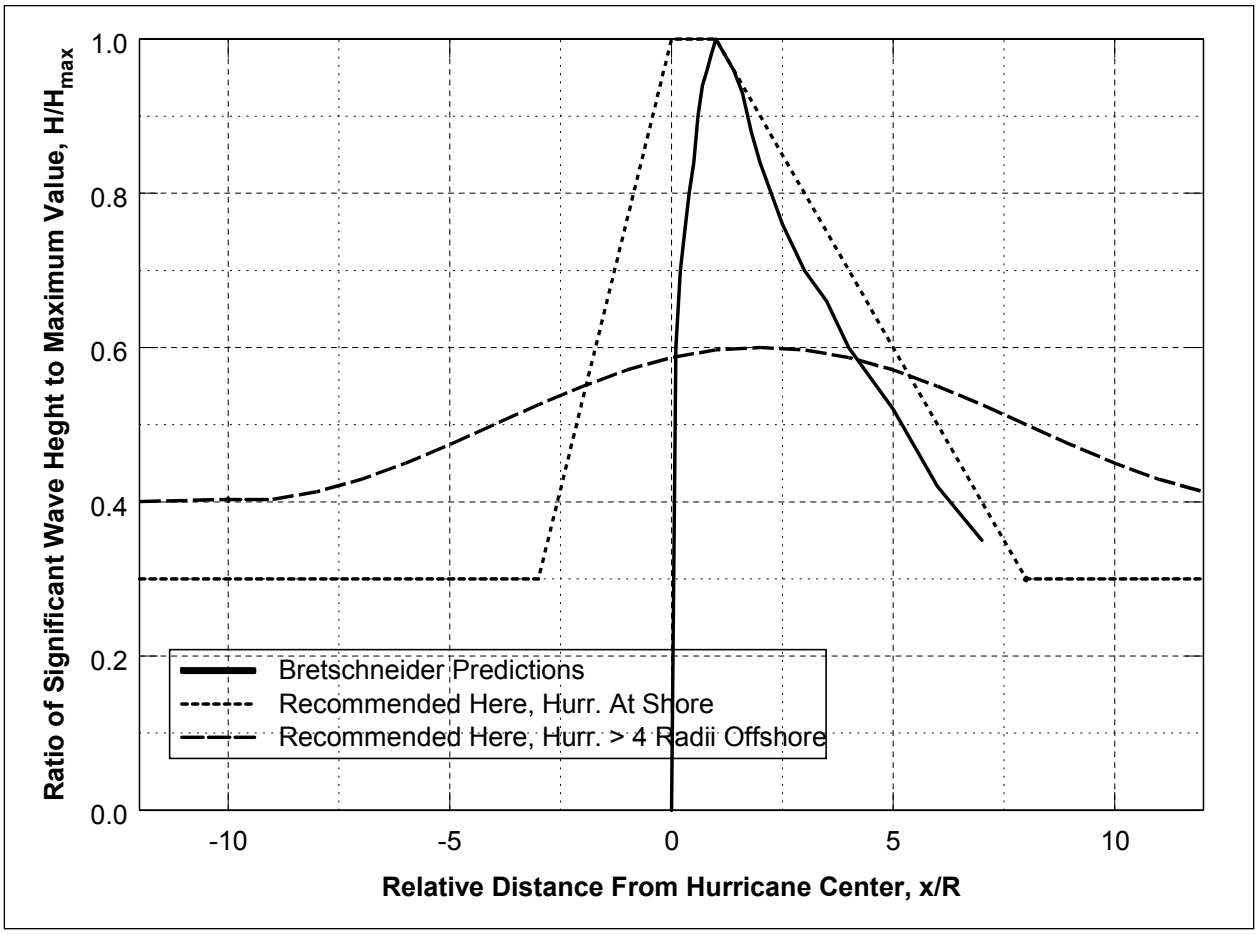

Figure 8-9. Recommended Relative Wave Height Along a Line Perpendicular to Hurricane Translation

For Hurricane Center at the Shoreline

$$
\begin{aligned}
H_o / H_{o,\max} &= 0.3, \quad r' < -3.0 \\
H_o / H_{o,\max} &= 0.3 + 0.233(r'+3), \quad -3.0 < r' < 0 \\
H_o / H_{o,\max} &= 1.0, \quad 0 < r' < 1.0 \\
H_o / H_{o,\max} &= 1.0 - 0.10(r'-1), \quad 1 < r' < 8 \\
H_o / H_{o,\max} &= 0.3, \quad r' > 6
\end{aligned}
\tag{8-18}
$$

and r’ = x/R.

With the maximum significant wave height and associated period known along a line perpendicular to the hurricane translation direction, the wave height at any location can be determined from the approximate graphical relationship in Figure 8-8 or Eqs. (8-17) and (8-18) which present local significant deep water wave height relative to the global maximum deep water significant wave height. The recommended wave period at all locations is that given by Eq. (9-3).

Breaking Wave Height and Water Depth. The non-dimensional breaking wave height and depth associated with the maximum local waves are based on the deep water wave steepness, H_o / L_o, where $L_o = 5.12T^2$. Figures 8-10 and 8-11 present these relationships which will be useful later in the case in which levees are present.

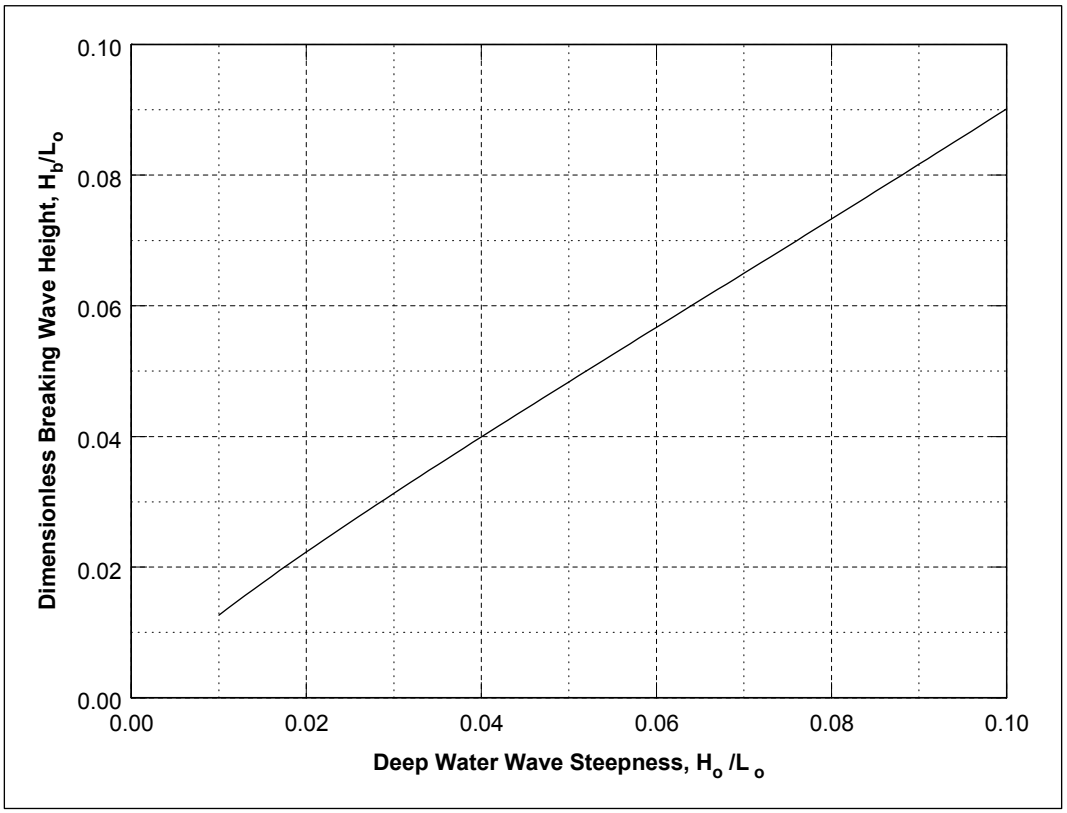

Figure 8-10. Dimensionless Breaking Wave Height versus Deep Water Wave Steepness

Wave Setup. Wave setup depends on local profile slope, wave breaking processes, etc. Methods have been developed to calculate the wave setup as a function of average slope and deep water wave steepness. These will be described in detail in a later document. For purposes here, simple guidelines are presented for calculating wave setup.

Minimum Wave Setup. A minimum wave setup of 1 foot is recommended at all locations.

Setup Along a Non-leveed Coastline. This category refers to cases where the nearshore and inland slopes are natural, i.e., on the order of 0.01 or less. The following equation is recommended for maximum wave setup, $\eta_{\max}$:

$$\eta_{\max} = 0.11 H_o \left[1.0 - 4.25 \left(\frac{H_o}{L_o} - 0.04 \right) \right] \tag{8-19}$$

where H_o and L_o are the local deep water wave conditions as described in Section 2.0.

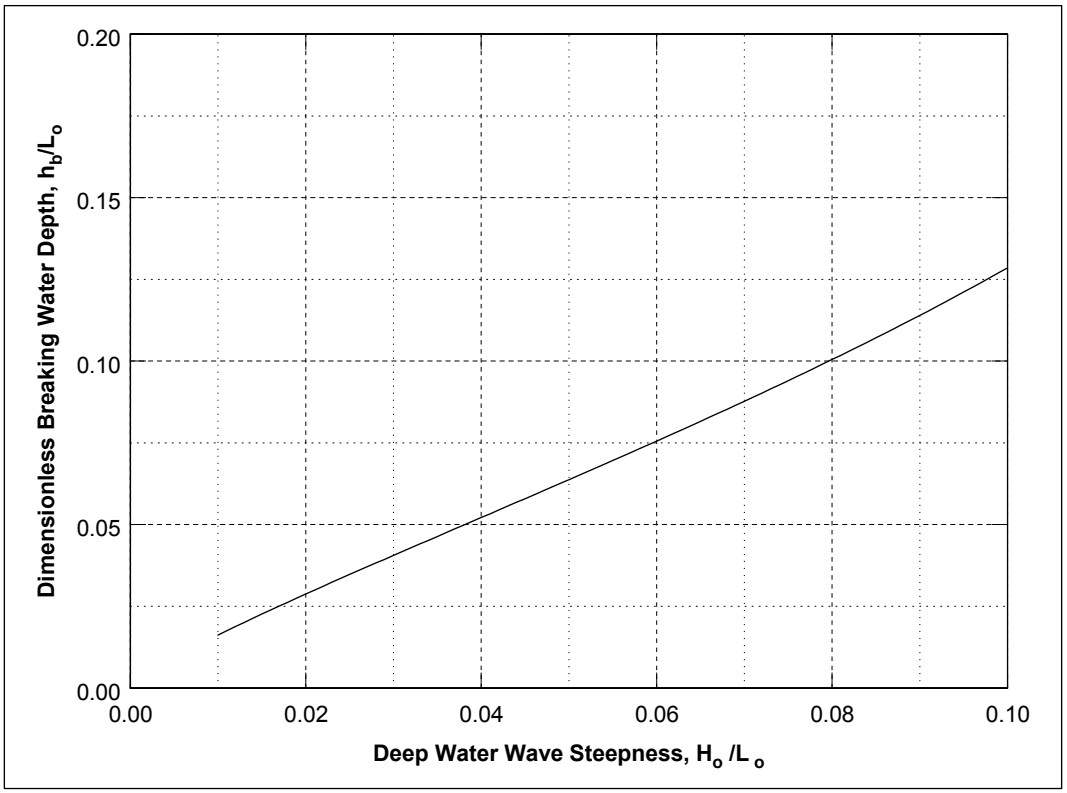

Figure 8-11. Dimensionless Breaking Water Depth versus Deep Water Wave Steepness.

Setup on Levees. Levee conditions are considered in two classes: (1) Non-overtopped, and (2) Overtopped. Recommendations are presented below for each class.

Non-overtopped Levees. A definition sketch of a non-overtopped levee is shown in Figure 8-12. The water depth including storm surge on the seaward side of the levee is denoted h_1. The recommended total wave setup is the wave setup η_1 that has occurred due to waves propagating to the depth h_1 and the additional wave setup on the levee, η_2 , i.e. $\eta_T = \eta_1 + \eta_2$. The wave setup at the depth, h_1 is determined with the use of Figure 8-11 which shows the percentage of the total setup which occurs seaward of a particular relative water depth. It is seen that most of the wave setup occurs in water depths relatively near to the breaking depth. This is a consequence of the Dally, et al breaking model on a very mild slope. This is the wave setup at the toe of the levee and should be added to the water depth which includes wind surge, etc. To determine the additional wave setup on the levee, we consider that the root mean square (rms) wave height at the levee toe is 0.3 times the total water depth and that the additional wave setup on the levee is 0.5 times the local rms wave height. Thus the additional wave setup on the levee, η_2 , is given by:

$$\eta_2 = 0.15(h_1 + \eta_1) \tag{8-20}$$

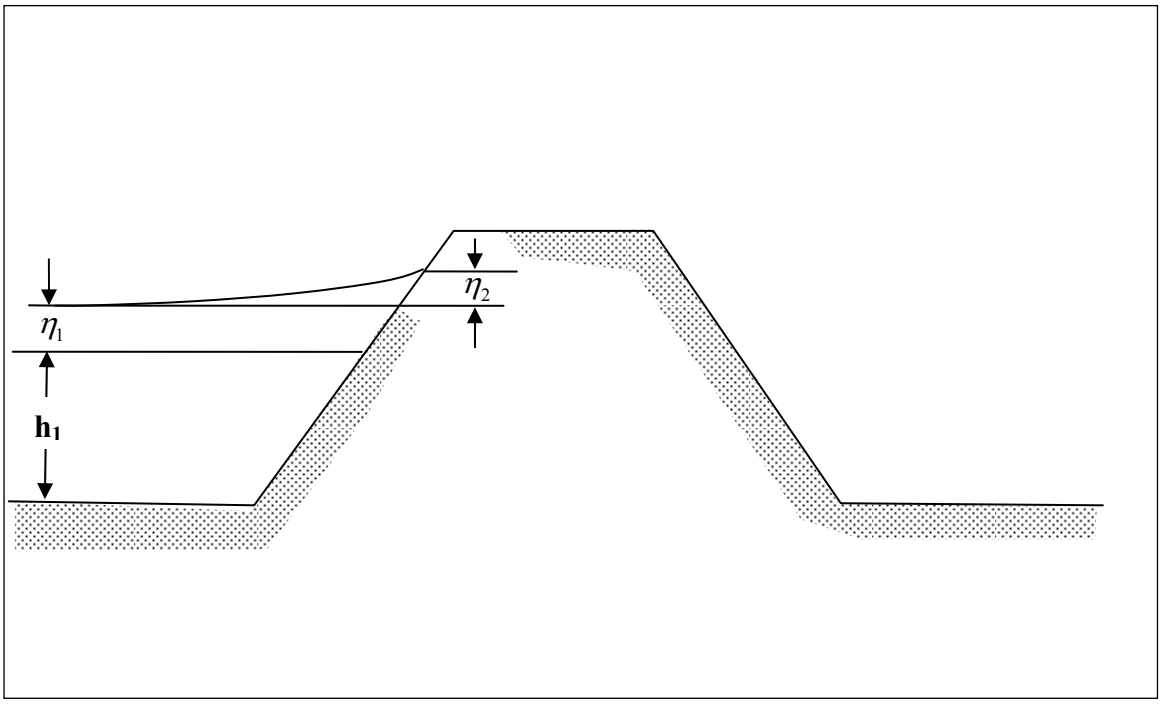

Figure 8-12. Definition Sketch for Non-Overtopped Levee

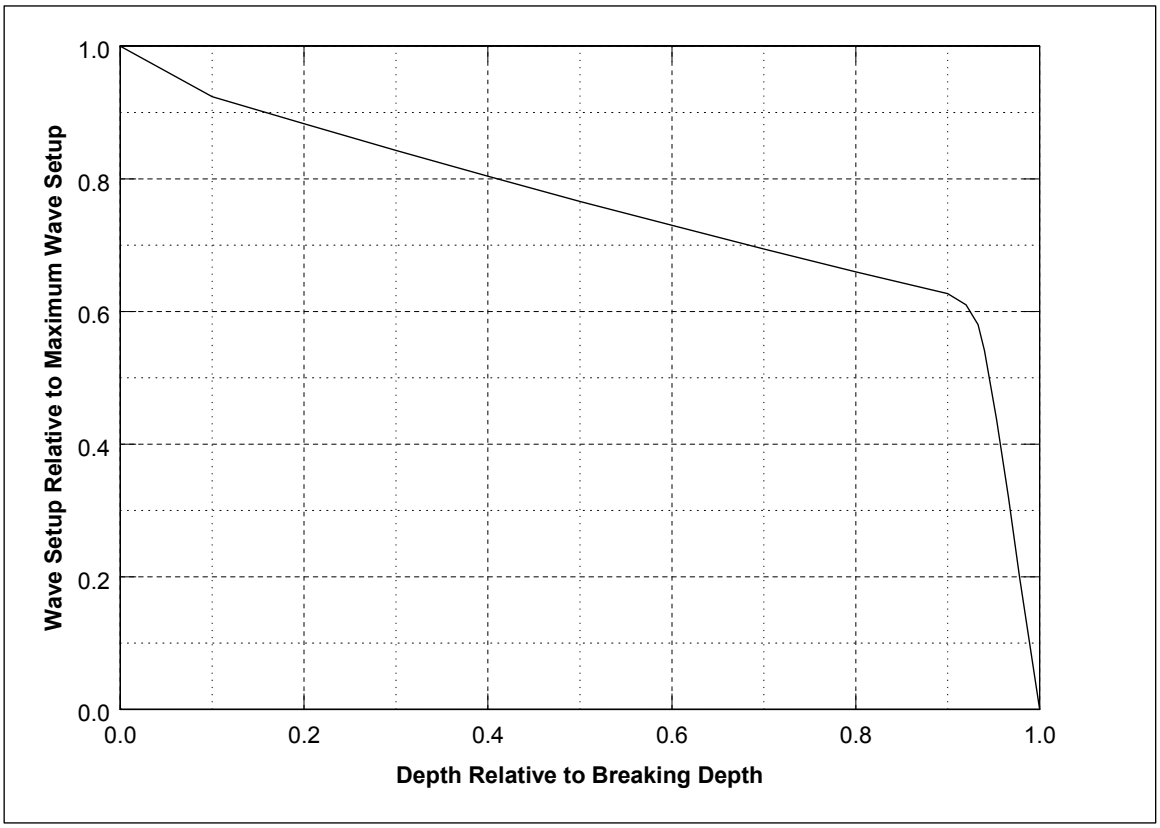

Figure 8-13. Proportion of Maximum Wave Setup that has Occurred versus a Proportion of the Breaking Depth

Overtopped Levees. For overtopped levees, the water depth (including calculated storm surge) on top of the levee is denoted h_2. The recommended additional wave setup η_2 for overtopped levees is

$$\eta_2 = 0.15(h_1 + \eta_1)\left[1 - \left(\frac{h_2}{h_1}\right)^2\right] \tag{8-21}$$

and, as before $\eta_T = \eta_1 + \eta_2$.

Examples Illustrating Application of the Methodology

Three examples will be presented illustrating application of the methodology. The hurricane parameters are presented in Table 8-6. For each of the cases, we will calculate the wave setup at a three locations: $x/R = r'$ = -1.5, 1.0, 4.0.

Table 8-6
Hurricane Characteristics Considered in Analysis

Case	Situation	Δp (in Hg)	R (n mi)	V_F (knots)	Hurricane Location Relative to Shoreline
1	Wave Setup on an Open Coast	2.5	40	12.0	At Shoreline
2	Wave Setup on a Non-Overtopped Levee	3.0	20	14.0	40 n mi Seaward
3	Wave Setup on an Overtopped Levee	3.0	20	14.0	40 n mi Seaward

Wave Setup on an Open Coast. For this case, the maximum significant deep water wave height and period are determined from Eqs. (9-1) and (9-2) as: $H_{o,\max}$ =56.8 ft and T_s = 16.1 sec.

For values of r' = -1.5, 1.0, and 4.0, the corresponding ratios of wave heights to the maximum are (Eq.(9-7)): $H_o / H_{o,\max}$ = 0.65, 1.0, and 0.70. Thus, the associated wave heights are: 36.9 ft, 56.8, and 39.8 ft, respectively. As noted, the appropriate period is determined from Eq. (9-3) and the deep water wave length, $L_o = 5.12T^2$ = 1327 ft.

The wave setup values at the three locations of interest are determined from Eq. (9-5) and are as shown in Table 8-7.

Table 8-7
Wave Characteristics and Setup at Three Locations for Case 1

Value of $r'(= x/R)$	H_o (ft)	η (ft)
-1.5	36.9	4.1
1.0	56.8	6.2
4.0	39.8	4.4

Wave Setup at a Non-Overtopped Levee. For this case, we consider that the water depth at the levee toe is 6 feet and that the levee is not overtopped. For the hurricane conditions, the wave height and period are: 38.8 ft and 13.3 sec. The deep water wave length, L_o=5.12 T^2 = 905.7 ft, H_o / L_o = 0.043. The breaking relative water depth is determined approximately from Figure 8-11 as h_b / L_o = 0.054. Thus the breaking depth is 48.9 ft. The ratio h_1 / h_b = 0.123 and from Figure 8-13, it is seen that approximately 92% of the maximum wave setup that would have occurred on an open coast has occurred at this water depth of 6 feet. Because the hurricane center is located at two times the radius to maximum winds from the shoreline, the wave height is determined as a prorated value of the two recommended relationships in Figure 8-9 and Equations (9-6) and (9-8). The ratios of wave height to maximum wave height for the three long shore distances relative to the center of the hurricane are: $H_o / H_{o,\max}$ = 0.61, 0.80, 0.64.

The total wave setup values if the levee were not present are shown in Column 3 of Table 8-8 and these values reduced by a factor of 0.92 are tabulated in Column 4. Finally, the wave setup as the waves propagate up on the levee is determined from Eq. (8-21) as 0.9 feet. The total wave setup at the levee is shown in Column 6 in Table 8-8 and is the sum of Columns 4 and 5.

Table 8-8
Wave Characteristics and Setup at Three Locations for Case 2

Value of $r'(= x / R)$	H_o (ft)	$\eta_{\max}$ (ft)	η_1 (ft)	η_2 (ft)	η_T (ft)
-1.5	23.5	2.7	2.5	1.3	3.8
1.0	31.0	3.5	3.2	1.4	4.6
4.0	25.0	2.9	2.7	1.3	4.0

Wave Setup at an Overtopped Levee. For this case, we consider that the water depth at the levee toe is 6 feet as in Case 2; however, the levee is overtopped and has a crest elevation of 4 feet relative to the adjacent ground. Because the hurricane conditions for Cases 2 and 3 are the same, the wave heights and periods are the same: 38.8 ft and 13.3 sec. The setup on the levee is reduced in accordance with Eq. (8-21) which reduces the additional setup values, η_2, as tabulated in Column 5 of Table 8-9. In this case, the overtopping only reduces the total wave setup by approximately 3%. The total wave setup values are presented in Column 6 of Table 8-9.

Table 8-9
Wave Characteristics and Setup at Three Locations for Case 3

Value of $r'(= x / R)$	H_o (ft)	$\eta_{\max}$ (ft)	η_1 (ft)	η_2 (ft)	η_T (ft)
-1.5	23.5	2.7	2.5	1.2	3.7
1.0	31.0	3.5	3.2	1.3	4.5
4.0	25.0	2.9	2.7	1.2	3.9

Summary. The methodology used to model waves is necessarily approximate due to the time and resources available, but does represent a first step toward the goal of accounting for

wave setup, a real process in storm surge. Mechanisms not accounted for here include the effects of vegetation and bottom friction which are known to reduce wave setup.

Determination of Hurricane Frequencies

Preliminary Comments

Each storm considered in the MR1 ADCIRC simulation set is envisioned to represent all possible storms with similar values of radius, central pressure, and so forth. Accordingly, a rate of occurrence is assigned to each storm, representing the total rate of occurrence of all similar storms.

The controlling factors are the overall density of storms in space and time – λ_0 – and the fractional occurrence rates of each of a storm's several defining parameters. These are the central pressure deficit, ΔP, the radius to maximum winds, R_{max}, the forward translation speed of the storm, V, the shoreline crossing angle, θ, and the crossing location, X. The fractional occurrence rates for the parameters are derived from the cumulative probability distribution functions for each, by dividing the CDF into segments centered on each selected parameter value.

For example, crossing angles of -60, -30, 0, 30, and 60 degrees clockwise from north were selected for simulation. The fraction of all storms represented by the discrete value 30, say, is equal to the total probability mass for all angles between 15 and 45 degrees. This is simply the difference between the angle-CDF values at 15 and 45 degrees. This is the approach used for angle, forward speed, radius, and central pressure, although some adjustment of the pressure probabilities are needed, as discussed below. The radius to maximum winds is handled in a different manner. Each factor is discussed below.

Storm Density

The storm density, λ_0, is the most important factor, giving the total rate at which storms occur within the study region both in space and time. In the present application, λ_0 was determined to be 5.7E-04 storms per year per km of longitude. Note that this corresponds to hurricanes only; that is, the rate for all storms, including weaker tropical storms, is greater, but the weaker storms are not included in our analysis.

Storm Crossing Point, X

Storms with a given radius were simulated on a set of tracks displaced to both the left and right of the study area. Imagine a set of straight and parallel tracks (for simplicity – the tracks used in this study were actually curvilinear) crossing the coast at an angle θ. In order to ensure adequate resolution in the surge estimates, tracks were spaced one radius apart (measured perpendicular to the track direction). Consequently, two adjacent tracks cross the shoreline at points separated by $R_{max}/\cos\theta$. Each track is intended to represent all possible tracks in the interval extending halfway on both the left and the right to the next adjacent track, which is also an interval equal to $R_{max}/\cos\theta$. It is found that the storm crossing point is approximately

uniformly distributed, so that within this interval $\lambda_0 R_{max}/\cos\theta$ storms are expected to occur per year (with the given angle and radius).

Track Angle

As shown in herein, track angle at the time of landfall was found to be approximately normally distributed with a mean of -5.4 degrees (direction of travel measured clockwise from north) and a standard deviation of 34.9 degrees. The simulated storm set included angles of -60, -30, 0, 30, and 60 degrees. Dividing the probability mass into discrete pieces bounded by the midpoints between these values (and by the lower and upper limits of 0 and 1), the following probability assignments are obtained:

Angle, θ	Probability
-60	0.128
-30	0.264
0	0.329
30	0.205
60	0.074

Note that the assigned probabilities add to 1.0.

Forward Speed

Forward speed at landfall (in km/hr) was determined to have a Weibull distribution with a shape factor of 2.70 and a scale factor of 23.7. Three landfall forward speeds were simulated: 8, 21, and 36 km/hr. Assigning all speeds from 0 to 14.5 km/hr to the discrete value, 8, all speeds from 14.5 to 28.5 km/hr to the discrete choice 21, and all values above 28.5 to 36 km/hr, gives the following probability assignments:

Speed, V	Probability
8	0.233
21	0.574
36	0.193

Central Pressure Deficit

The distribution of central pressure depression (in mb) was found to be approximately log-normal in the shifted parameter ΔP-18 mb. The mean of the natural logarithm of this parameter was found to be 3.15 with a standard deviation of 0.68. The pressure deficits selected for simulation were 41, 80, and 115 mb.

In determining probabilities in this instance, however, there is a special consideration that has to be made. In this analysis, the storm density, λ_0, is the density of storms stronger than 34mb. Consequently, weaker storms should not be included in the probability assignment, and the probability mass assigned to 41mb is chosen to include all pressures between 34 mb and 60.5 mb, the midpoint between 41 and 80 mb. When the assignments are made, the result is as shown in the second column of the following table:

ΔP	Probability (all storms)	Probability (adjusted)
41	0.521	0.734
80	0.153	0.216
115	0.036	0.050

Note that the probabilities in the second column do not add to 1.0 since the 29% of all storms which are weaker than 34 mb are not included. Consequently, it is necessary to scale these values to achieve the proper total, as shown in the third column. This adjustment maintains consistency with the definition of λ_0; that is, about 73% of all the storms contained in the density λ_0 have pressure deficits less than 60.5 mb.

Radius to Maximum Winds

Storm radius (in km) has been taken to depend upon central pressure in this study, in accordance with the following expression

$$\ln(R_{\max}) = 3.962 - 0.00567\Delta P + \varepsilon_R \tag{8-22}$$

in which the pressure deficit is in mb and ε_R is a normally distributed variable with mean 0 and standard deviation 0.313. The storm simulation set includes radii at the 10%, 50%, and 90% levels for each of the three central pressures. With these choices, and following the same procedures as already illustrated, the following storm radii and probability assignments are obtained:

Radius; ΔP = 41mb	Radius; ΔP = 80mb	Radius; ΔP = 115mb	Probability
10% level: 27.9	22.4	18.3	0.282
50% level: 41.6	33.4	27.4	0.478
90% level: 62.2	49.9	40.9	0.240

Holland's B Factor

The MR1 simulation set involves only the mean value of B, so that the probability of B is always set to 1.0. The simulations in MR2 investigate the dependence on B, conditional on R_{max}, using values at the 5%, 50%, and 95% quantiles.

Assignment of Frequencies

With the foregoing determinations of storm density and fractional occurrence rates for each discrete parameter value, the total frequency (perhaps rate of occurrence would be a better term) is computed from

$$F = (\lambda_0 R_{\max} / \cos\theta) P(\Delta P) P(R_{\max}) P(V) P(\theta) \quad (8\text{-}23)$$

in which *P(Q)* is the probability mass assigned to the discrete parameter value *Q*. Although these probabilities are multiplied, the conditional dependence of *R* on *ΔP* has been accounted for, as discussed above.

Sample Storm Frequencies

Table 8-10 shows a sample of the hurricane frequencies determined using the above procedures.

Table 8-10
ADCIRC Hurricane Runs Frequency

CaseID	Frequency	XRate	P(pressure)	P(radius)	P(Speed)	P(theta)
mr1_track_00211	0.00020	0.0318	0.734	0.282	0.233	0.128
mr1_track_00212	0.00023	0.0184	0.734	0.282	0.233	0.264
mr1_track_00213	0.00025	0.0159	0.734	0.282	0.233	0.329
mr1_track_00214	0.00018	0.0184	0.734	0.282	0.233	0.205
mr1_track_00215	0.00011	0.0318	0.734	0.282	0.233	0.074
mr1_track_00216	0.00020	0.0318	0.734	0.282	0.233	0.128
mr1_track_00217	0.00023	0.0184	0.734	0.282	0.233	0.264
mr1_track_00218	0.00025	0.0159	0.734	0.282	0.233	0.329
mr1_track_00219	0.00018	0.0184	0.734	0.282	0.233	0.205
mr1_track_00220	0.00011	0.0318	0.734	0.282	0.233	0.074
mr1_track_00221	0.00020	0.0318	0.734	0.282	0.233	0.128
mr1_track_00222	0.00023	0.0184	0.734	0.282	0.233	0.264
mr1_track_00223	0.00025	0.0159	0.734	0.282	0.233	0.329
mr1_track_00224	0.00018	0.0184	0.734	0.282	0.233	0.205
mr1_track_00225	0.00011	0.0318	0.734	0.282	0.233	0.074
mr1_track_00226	0.00020	0.0318	0.734	0.282	0.233	0.128
mr1_track_00227	0.00023	0.0184	0.734	0.282	0.233	0.264
mr1_track_00228	0.00025	0.0159	0.734	0.282	0.233	0.329
mr1_track_00229	0.00018	0.0184	0.734	0.282	0.233	0.205
mr1_track_00230	0.00011	0.0318	0.734	0.282	0.233	0.074
mr1_track_00231	0.00020	0.0318	0.734	0.282	0.233	0.128
mr1_track_00232	0.00023	0.0184	0.734	0.282	0.233	0.264
mr1_track_00233	0.00025	0.0159	0.734	0.282	0.233	0.329
mr1_track_00234	0.00018	0.0184	0.734	0.282	0.233	0.205
mr1_track_00235	0.00011	0.0318	0.734	0.282	0.233	0.074
mr1_track_00236	0.00020	0.0318	0.734	0.282	0.233	0.128

Appendix 9
Risk Methodology

Risk Analysis Methodology

Overview

The following sections describe the overall risk analysis methodology of the hurricane protection system. Sections that follow discuss individual parts of the analysis as they relate to the overall risk analysis methodology. The basic elements of the risk analysis methodology are illustrated in Figure 9-1. The analysis is represented in terms of a series of modules which interface to provide a risk model for the New Orleans HPS.

Contributing Factors and Their Relationships

The development of a risk analysis model was facilitated by the preparation of an influence diagram. The process of creating an influence diagram helped establish a basic understanding of the elements of the hurricane protection system and their relationship to the overall system performance during a hurricane event and the analysis of consequences and risks.

Figure 9-2 shows the influence diagram for the hurricane protection system and the analysis of consequences. There are four parts to the influence diagram:

- Value nodes (rounded-corner box)
- Chance nodes (circular areas)
- Decision nodes (square-corner boxes)
- Factors and dependencies in the form of arrows.

The influence diagram shown in Figure 9-2 was used to develop an event (or probability) tree for the hurricane protection system. Figure 9-3 shows an initial probability tree derived from the influence diagram in Figure 9-2. The top events across the tree identify the random events whose state following the occurrence of the hurricane could contribute to flooding in a protected area. The tree begins with the initiating event, a hurricane that generates a storm surge, winds and rainfall in the region.

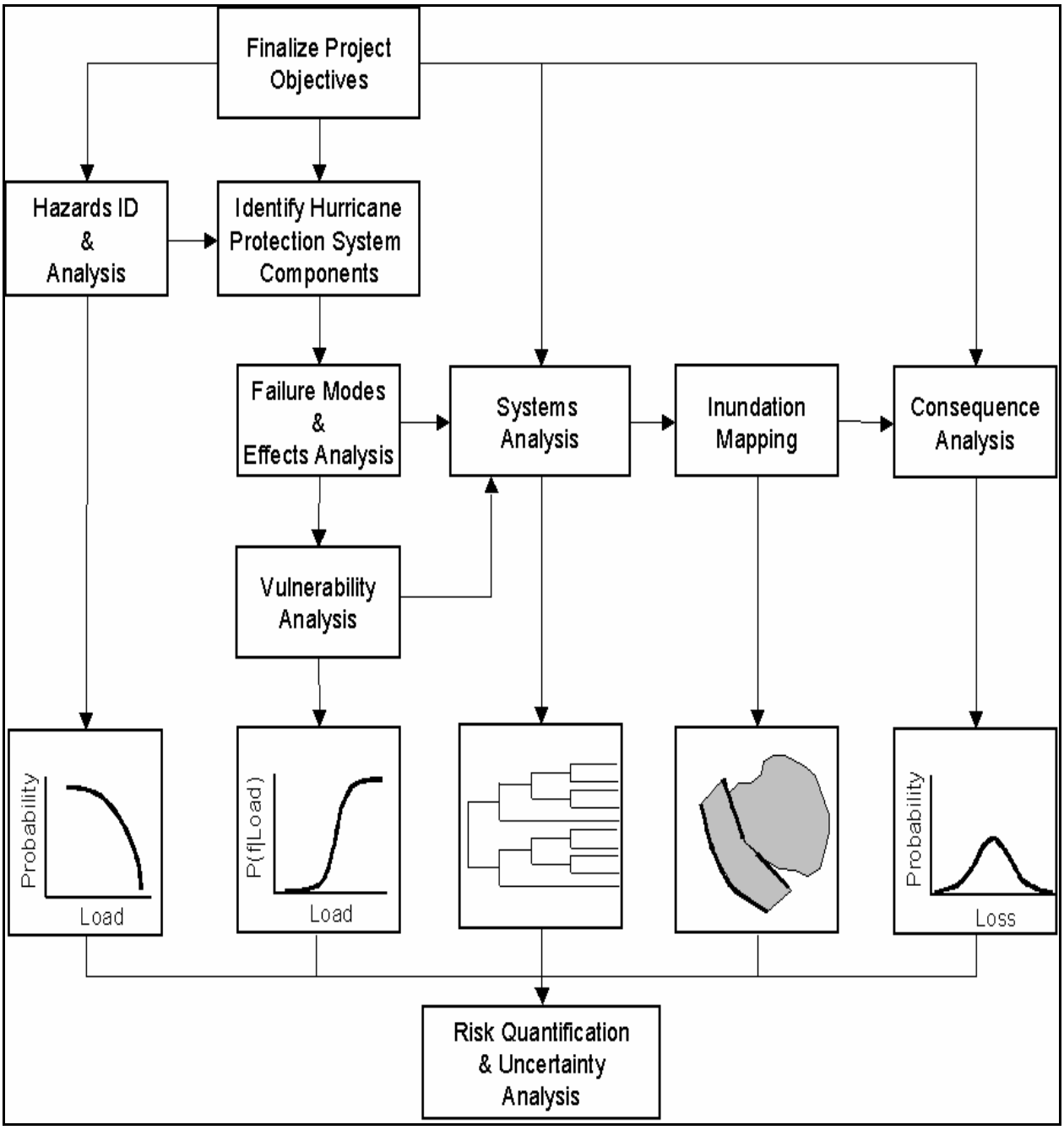

Figure 9-1. Risk Analysis Logic Diagram

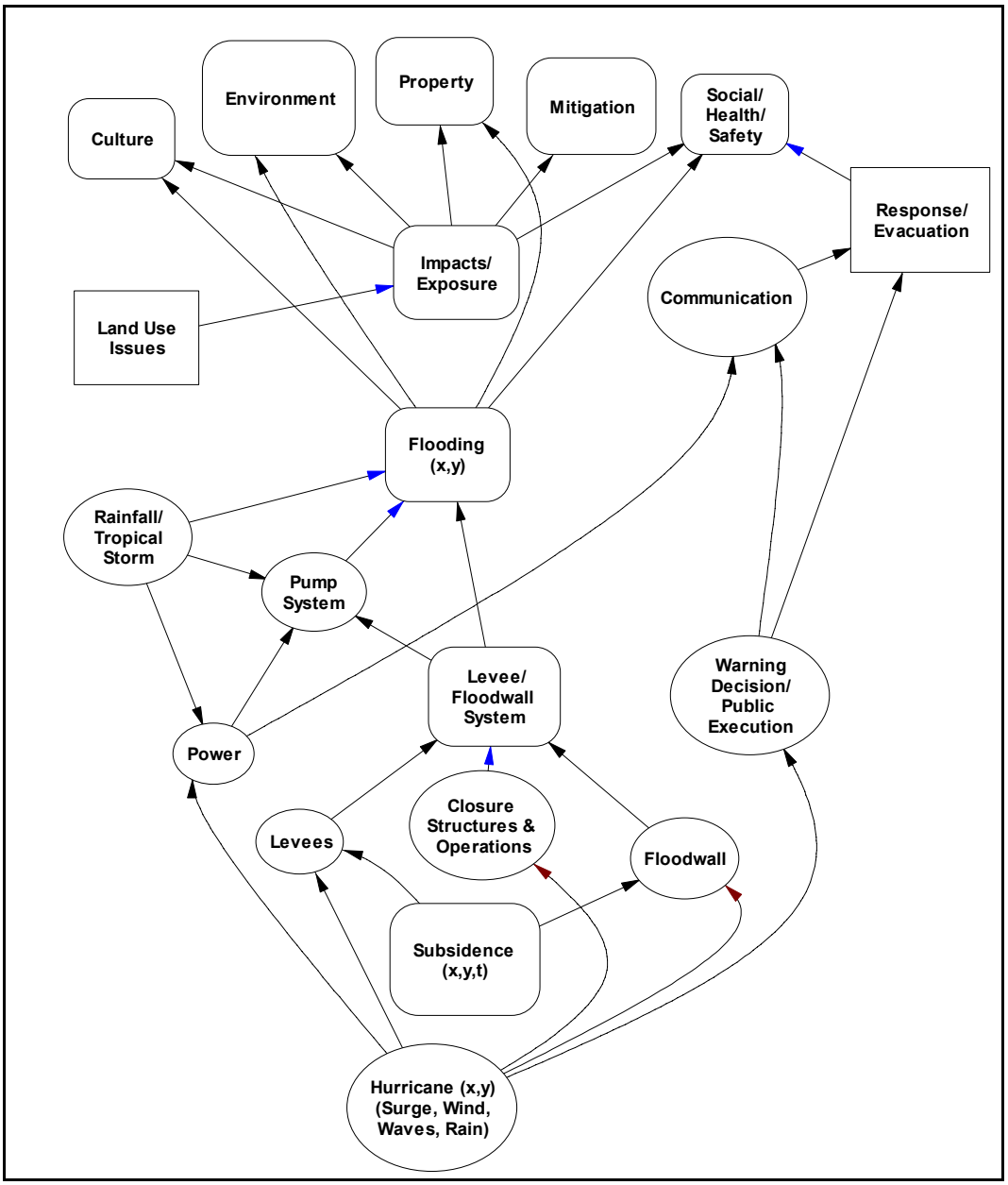

Figure 9-2. Influence Diagrams for Risk Analysis

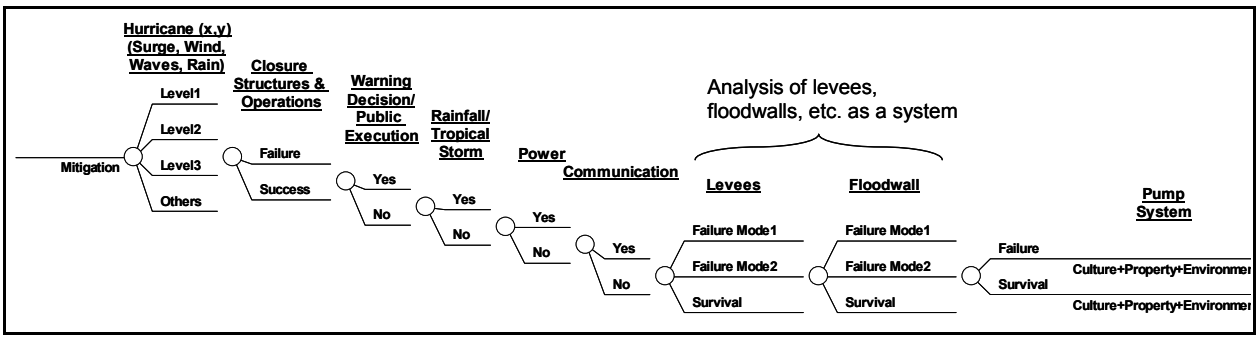

Figure 9-3. Probability Tree for the Hurricane Protection System

Hurricane Protection System

The hurricane protection system (HPS) for the New Orleans metropolitan area is provided in Figure 1. The HPS has been discretized for the reliability and risk analysis tasks as schematically shown in Figure 9-4. A complete definition of the system is provided in subsequent sections. The system consists of basins, sub-basins and reaches. The definition of these basins, sub-basins and reaches are based on the following considerations:

- Local jurisdiction,
- Floodwall type and cross section,
- Levee type and cross section,
- Engineering parameters defining structural performance,
- Soil strength parameters,
- Foundations parameters, and

Surge and wave levels.

Reaches (*R*) of each basin are uniquely identified using sequential numbers illustrated in the Figure 9-4. Figure 9-4 also shows the approximate locations of pumping stations for the purpose of illustration.

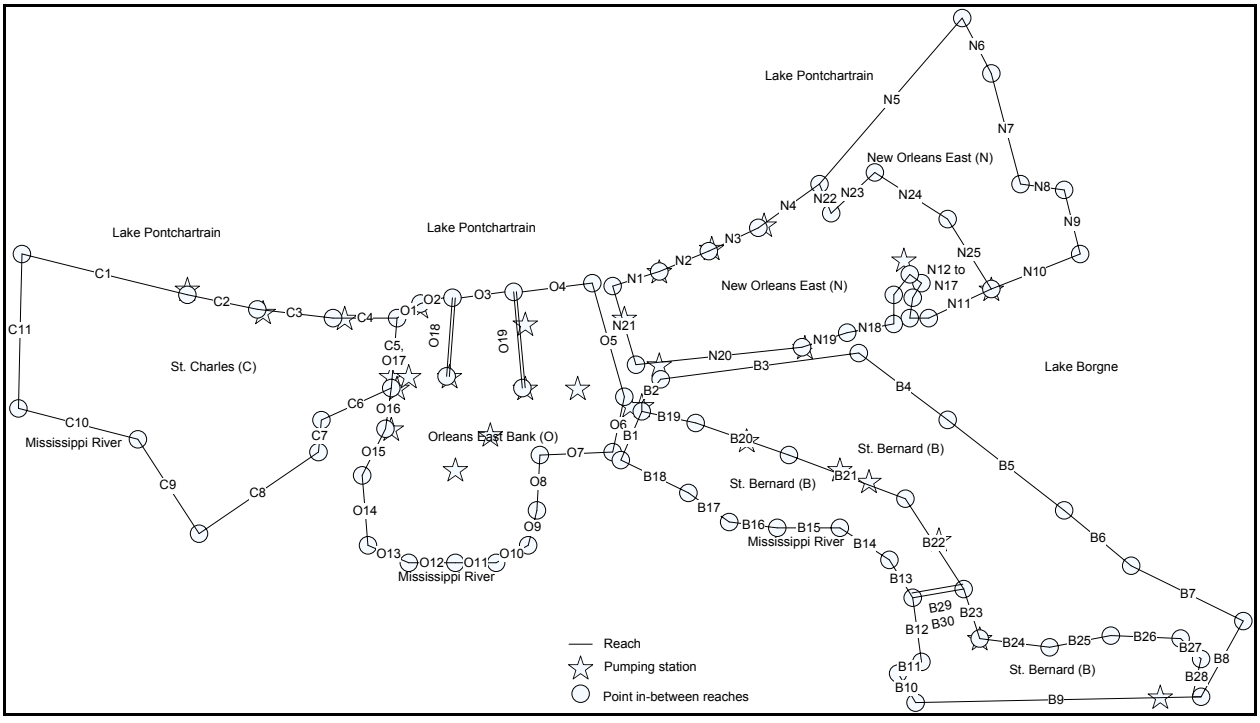

Figure 9-4. Hurricane Protection System Defined by Basins and Reaches

Probabilistic Risk Model

Risk associated with the hurricane protection system is quantified through a regional hurricane rate (λ) and the probability $P(C > c)$ with which a consequence measure C exceeds different levels c. The loss exceedance probability per event is evaluated as

$$P(C > c) = \sum_i \sum_j P(h_i) P(S_j \mid h_i) P(C > c \mid h_i, S_j) \tag{9-1}$$

An annual loss exceedance rate can be estimated as follows

$$\lambda(C > c) = \sum_i \sum_j \lambda P(h_i) P(S_j \mid h_i) \times P(C > c \mid h_i, S_j) \tag{9-2}$$

where $P(h_i)$ is the probability of hurricane events of type i, $P(S_j|h_i)$ is the probability that the system is left in state j from the occurrence of h_i, and $P(C > c \mid h_i, S_j)$ is the probability that the consequence C exceeds level c under (h_i, S_j). Summation is over all hurricane types i and all system states j in a suitable discretization. Simulation studies of hurricanes for risk analysis require the use of representative combinations of hurricane parameters and their respective probabilities. The outcome of this process is a set of hurricane simulation cases and their respective conditional rates $\lambda P(h_i)$.

Evaluation of the regional hurricane rate λ and the probability $P(h_i)$, the conditional probabilities $P(S_j \mid h_i)$, and the conditional probabilities $P(C > c \mid h_i, S_j)$ is the main objective of the hurricane model, the system model, and the consequence model, respectively. The probability $P(S_j \mid h_i)$ should cover the states of the components of the HPS, such as closure structure and operations, precipitation levels, electric power availability, failures modes of levees and floodwalls, and pumping station reliability. To assess the state of the HPS given a hurricane event requires an evaluation of the reliability of individual structures, systems and components (e.g., levees, floodwalls, pump systems) when they are exposed to the loads and effects of the hurricane (e.g., the peak surge, wave action) and the relationship of these elements to the overall function of the system to prevent flooding in protected areas.

If point estimates of consequences (i.e., $(c \mid h_i, S_j)$) are available instead of $P(C > c \mid h_i, S_j)$, order statistics can be used to construct the exceedance probability $P(C > c \mid h_i, S_j)$ as provided in Appendix 7.

The hurricane loss provided by Eq. 9-1 can be used to compute a cumulative distribution function (CDF) $F_S(s)$ as $1\text{-}P(C > c)$. The CDF of the accumulated damage (loss) during a non-random time interval $[0, t]$ is given by

$$F(s;\ \ t, \lambda) = \sum_{n=0}^{\infty} e^{-\lambda t} \frac{(\lambda t)^n}{n!} F_S^{(n)}(s) \tag{9-3}$$

where $F_S(^n)(s)$ is the n-fold convolution of FS(s).

where $F_S^{(n)}(s)$ is the n-fold convolution of $F_S(s)$ that produces the CDF of the sum of n loss variables. Equation 9-3 can be generalized to consider non-identical and correlated losses with CDFs of $F_{Si}(s)$, i=1,2, …, n, requiring the development of conditional distributions. Equation 9-3 is not used in this study.

Event Tree

The probability tree of Figure 9-4 can be simplified to determine the rate of flooding levels and displaying the results as inundation contours within the basins. The processes of transforming inundation to consequences is simplified by grouping communication, warning decision and public execution into an *exposure factor* parameter applied to lives and property at risk, and grouping power and pumping availability into one event. The resulting event tree appropriately branched out is shown in Figure 9-5. The events of the tree are defined in Table 9-1.

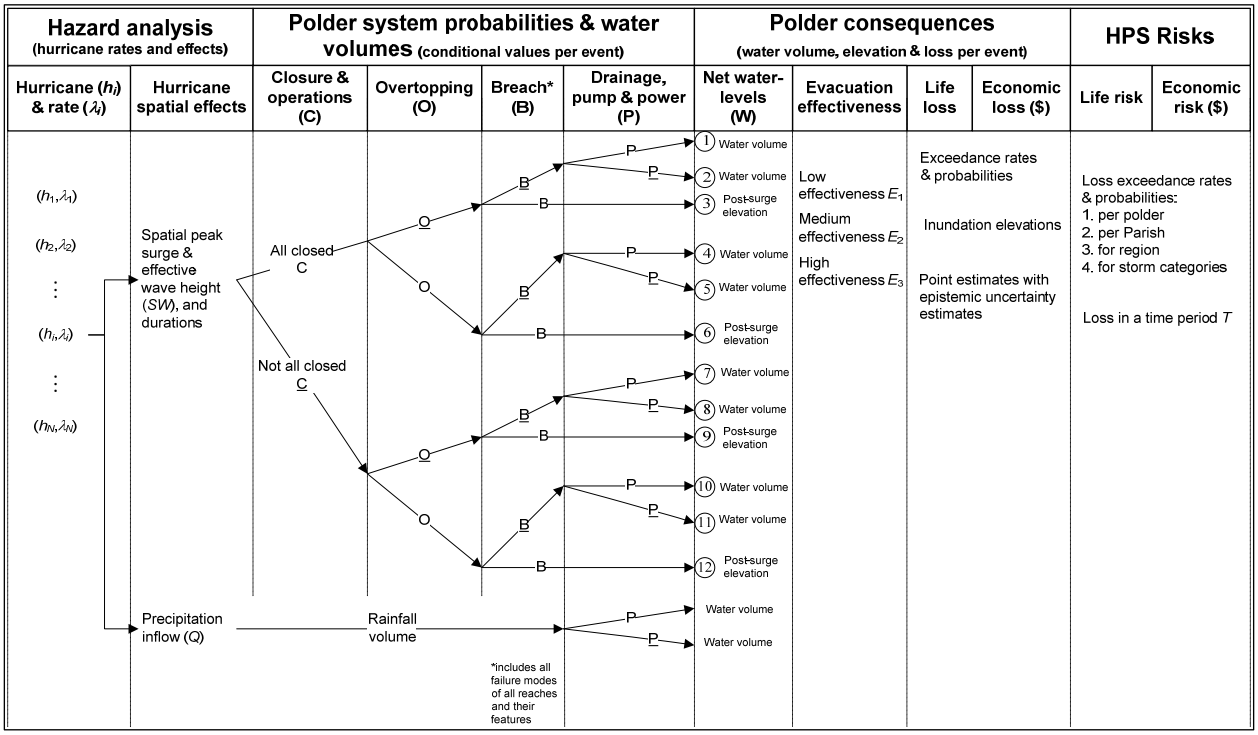

Figure 9-5. Event Tree for Quantifying Risk. Underlined events (i.e., $\underline{C}$, $\underline{P}$, $\underline{O}$, and $\underline{B}$) are the complements of the respective events (i.e., C, P, O, and B)

Table 9-1
Summary of the Event Tree Top Events

Top Event	Description
Hurricane initiating event	The hurricane initiating event is mapping of the peak flood surge with waves in the study area with a hurricane rate λ. This event can be denoted, hi(x,y), and has a probability of occurrence, P(hi(x,y)) and a rate of occurrence of λP(hi(x,y)).
Closure structure and operations (C)	This event models whether the hurricane protection system closures, i.e., gates, have been sealed prior to the hurricane. This event depends on a number of factors as illustrated in the influence diagram. The closure structures are treated in groups in terms of probability of being closed in preparation for the arrival of a hurricane. This vent can be used to account for variations in local practices and effectiveness relating to closures and their operations.
Precipitation inflow (Q)	This event corresponds to the rainfall that occurs during a hurricane event. The precipitation inflow per subbasin is treated as a random variable.
Drainage, pumping and power (P)	This event models the availability of power (normal) power for the pump systems. This event is modeled in the event tree to represent a common mode of failure for the pump systems, and is included in developing a model for drainage and pumping efficiency or lack thereof including backflow through pumps. The event also models the availability of the pump system and its ability to handle a particular floodwater volume. This event is treated in aggregate with drainage effectiveness and power reliability including backflow through pumps.
Overtopping (O)	This event models the failure of the enclosure/protection system due to overtopping, given that failure has not occurred by some other (non-overtopping) failure mode. If failure (breach) does not occur, some flooding due to overtopping could result.
Breach (B)	This event models the failure of the enclosure/protection system (e.g., levees/floodwalls, closures) during the hurricane, exclusive of overtopping failures). This event includes all other failures and it models all 'independent' levee/floodwall sections. This event is treated using conditional probabilities as provided in Figure 9-5.

Risk Quantification

Functional Modeling and Computational Considerations. The HPS has the primary function of keeping water away from protected areas, however water also enters the system during rainfall events and from groundwater. The protected areas of the HPS are sub-divided into basins and sub-basins. This partitioning is based on the internal drainage and pumping system within each Basin. Figure 9-4 illustrates the New Orleans East basin and the two sub-basins for illustration purposes. Basins and sub-basins are divided into sections, or reaches, that have similar cross-sections, material strength parameters and foundation conditions. For each reach, the following items are defined:

1. start and end stations
2. reach length
3. protection height
4. basin and sub-basin membership designation
5. point features within the reach, such as drainage structures, closures and transitions
6. for closures, their total width, bottom elevation, and probability of being closed during a hurricane based on current practices

The quantification of risk associated with a hurricane protection system requires quantifying its performance or lack thereof. A measure of the lack of performance is the amount of water that is expected to reach the protected areas for a particular hurricane, i.e., a given hurricane run. The water enters protected areas as a result of one or more of the following two cases:

1. non-breach events producing overtopping water volume, water volume entering through closures (i.e., gates) that are left open, precipitation, and potential backflow from pumping stations
2. breach events leading to water elevations in protected areas

The risk quantification framework has, therefore, the objective of obtaining estimates of water volumes and elevations according to these cases.

The event tree presented in Figure 9-5 shows the two quantities of interest in the net water levels (*W*) column resulting from overtopping, precipitation, open closures, i.e., gates, and backflow from pumping stations in non-breach cases, and the post-surge elevation that would result in cases of breach. The branches of the rainfall volume are added to all the other branches for a particular hurricane. The figure shows a total of twelve branches that are constructed per hurricane. These branches are numbered sequentially as shown in the figure for the purpose of identification and reference in subsequent sections. These sections describe the computations needed to quantify risk. They are presenting in a manner that correspond to the events shown in Figure 9-5, and were implemented in a spreadsheet to perform the computations. The sections that follow provide the background information and basis behind the approaches used for these computations.

Definition of Basins, Subbasins, Reaches and Features. The hurricane protection system is divided into basins, subbasins, and reaches including their features. Table 9-2 illustrates the information structure needed for this definition for selected reaches. The definition includes the following basins with their respective numeric identification:

1. Orleans West Bank (OW)
2. New Orleans East (NOE)
3. Orleans (OM)
4. St. Bernard (SB)
5. Jefferson East (JE)
6. Jefferson West (JW)
7. Plaquemines Area (PL)
8. St. Charles (ST)

For each reach, the following information is required:

- Reach numeric identification that can be associated with a unique station in hurricane simulation
- Reach length (ft)
- The reach crest elevation (ft)
- Reach type of either a levee (L) or a floodwall (W)

Table 9-2
Definition of Reaches

Reach	Length (ft)	Elevation (ft)	Design Water Elevation (ft)	Reach Type	Reach Weir Coefficient	Polder Reference	Subpolder Reference
1	5.000E+03	4.000E+00	1.000E+00	L	2.6	NOE	NOE1
2	5.000E+03	4.000E+00	1.000E+00	W	3.0	NOE	NOE1
3	5.000E+03	4.000E+00	1.000E+00	L	2.6	NOE	NOE2
4	5.000E+03	4.000E+00	1.000E+00	W	3.0	NOE	NOE2
5	5.000E+03	4.000E+00	1.000E+00	L	2.6	NOE	NOE3
6	5.000E+03	4.000E+00	1.000E+00	W	3.0	NOE	NOE3
7	5.000E+03	4.000E+00	1.000E+00	L	2.6	NOE	NOE4
8	5.000E+03	4.000E+00	1.000E+00	W	3.0	NOE	NOE4
9	5.000E+03	4.000E+00	1.000E+00	L	2.6	NOE	NOE5
10	5.000E+03	4.000E+00	1.000E+00	W	3.0	NOE	NOE5

- Reach weir coefficient needed to compute overtopping water volume of either 2.6 for a levee or 3.0 for a floodwall (in units of ft and sec)
- Basin reference that define the location of the reach in reference to the basin breakdown
- Subbasin reference that define the location of the reach in reference to the subbasin breakdown

Table 9-3 illustrates the definitions of features within each reach for selected reaches. For each feature, the following information is required:

- Feature number for unique identification
- Type of features of drainage structure (D), or closures (i.e., gate G), or transition structure (T)
- Reach reference that define the location of the feature in reference to the features
- A reference value for correlated gates for assigning the same probability of closure
- Length (ft) of water inflow within open gates
- Bottom elevation (ft) of gates
- Probability of not closing gates

Sources of Information – The Risk Team collected data from design documents, construction drawings and studies conducted by other IPET teams to develop detailed descriptions of the basins. Maps were assembled from aerial photos and information was overlayed in GIS files that included: lat/long data, geotechnical profiles and boring logs, crest elevations, stationing used to define reaches and the locations of critical features such as closure gates and pump stations. The information on these maps was confirmed by field surveys of the entire system by members of the risk team who traveled every mile of the system. Photos, GPS coordinates and notes were taken during these surveys to document each feature and reach used in the risk model. In addition to the maps, data was compiled for use in the reliability analyses and the risk model. This process has resulted in a comprehensive description of the HPS. The basin descriptions are provided in Appendices 2 thru 7.

Table 9-3
Definition of Features with Respective Reaches

Feature Number	Type	Reach	Correlated Features	Length (ft)	Bottom Elevation (ft)	Not-Closed Probability
1	G	1	1	5.000E+01	0	1.000E-01
2	G	1	1	5.000E+01	0	1.000E-01
3	G	2	3	6.667E+01	0	2.000E-02
4	G	2	3	6.667E+01	0	5.000E-01
5	G	2	3	6.667E+01	0	5.000E-01
6	D	1				
7	T	1				
8	G	3	8	1.250E+02	0	2.300E-01
10	D	3				
11	T	3				
12	G	7	12	1.500E+02	0	4.000E-02
13	D	7				
14	T	7				5.000E-03
15	G	14	15	7.500E+01	0	7.500E-02

Reach Descriptions – The HPS perimeter is discretized into reaches that define sections that have similar physical and engineering characteristics. Initially the reaches were defined using the beginning and ending stations shown in the design memoranda (DM). The stations were then adjusted based on examinations of the subsurface material information to form reaches that were expected to have similar performance (reliability).

Elevations of Crests – The elevations of the tops of walls and levees, adjusted to the current datum, of the entire New Orleans area HPS were developed for use in the suite of hurricane simulations and the risk assessment model calculations of water volumes from overtopping and breaching. Various sources elevations of segments of the HPS existed, some adjusted to current datum, but most were not. The 1 ft. and 15 ft. lidar on the IPET repository been adjusted to current datum and gave about a 99% coverage of the HPS system. These gave good values for portions of the HPS that had clear levees and numerous hard surveys were available for short portions of the walls, some of which been adjusted.

Using the 1 ft lidar where it was available, cross section profiles were cut approximately every 200-500 ft along the entire HPS. Where the 1 ft lidar was not available, the 15 ft lidar was used. For the levees, these elevations were compared to the current expected values obtained from various MVN records, Taskforce Guardian and any available hard survey information for verification. The location of walls, drainage structures, closures, and gaps were known from the sites visits and documented with photos and notes for the entire HPS. Some walls had adjusted hard survey info available but for most walls, it was necessary to go back to the lidar data and examine the areas by drawing numerous profiles, searching for patterns of "good hits" on wall tops and to determine the elevations of the surrounding soil. Then using the photos and notes obtained from the site visits, estimates of the wall elevations were made. This same process was used for transition regions. A final comparison to the elevations used in the ADCIRC grid developed by the Storm Team was made for consistency.

Hurricane Hazard Analysis. The hurricane hazard analysis method parameterizes hurricanes using a vector $\underline{\theta}$ of characteristics at landfall (central pressure drop, radius of maximum

wind, etc.). From the values of $\underline{\theta}$ for historic events, the recurrence rate density $\lambda(\underline{\theta}) = \lambda f(\underline{\theta})$ is estimated where λ is the rate of hurricane events in a neighborhood of the region of interest and $f(\underline{\theta})$ is the joint probability density function of $\underline{\theta}$ in that neighborhood. The possible combinations of winds, surges and waves (M) would be computationally demanding if every combination was run through the ADCIRC models. To reduce the number of runs of M, a response surface approach can be used. In this approach a relatively small number m of vectors $\underline{\theta}_i$ are selected and M is used to calculate the corresponding surge and wave levels at the sites of interest. Then a response surface model is fitted to each response variable (surge or wave level at a specific site) in terms of $\underline{\theta}$. Finally, a refined discretization $\{\underline{\theta}_i\}$ of parameter space is used with the response surface as a proxy model in place of M to represent the hurricane hazard. The outcomes of these computations are combined surge and effective wave values at particular locations of interest along the hurricane protection system, e.g., representative values at the reaches. These values are denoted as h_i in Figure 9-5.

The water elevation required by risk model as a loading is taken as the surge elevation plus wave setup if waves are present, called the surge/wave elevation. Surge only, therefore, need not to be considered as a separate loading condition.

Hurricane rate modeling and prediction methods are then used to compute the corresponding exceedance rates to h_i values, and are denoted as λ_i in Figure 9-5. Also, the water elevation in a basin after a breach is termed the post-surge elevation. This post-surge elevation in a basin could be higher than the applicable lake or river water level.

The epistemic uncertainties in both the surge/wave elevation and the rates are considered as discussed separately in a subsequent section. Figure 9-6 shows for the purpose of illustration surge water elevation as a function of time, i.e., hydrographs, at stations defining the hurricane protection system for one storm. The hurricane rates can be also obtained and used to construct a peak elevation exceedance curve for a station as shown in Figure 9-7. Table 9-4 illustrates information and results related to hurricane simulations that include:

- Hurricane run numeric identification
- Hurricane rates
- National Hurricane Center Category designation
- Reach overtopping volume mean and standard deviation with computational models provided in subsequent sections

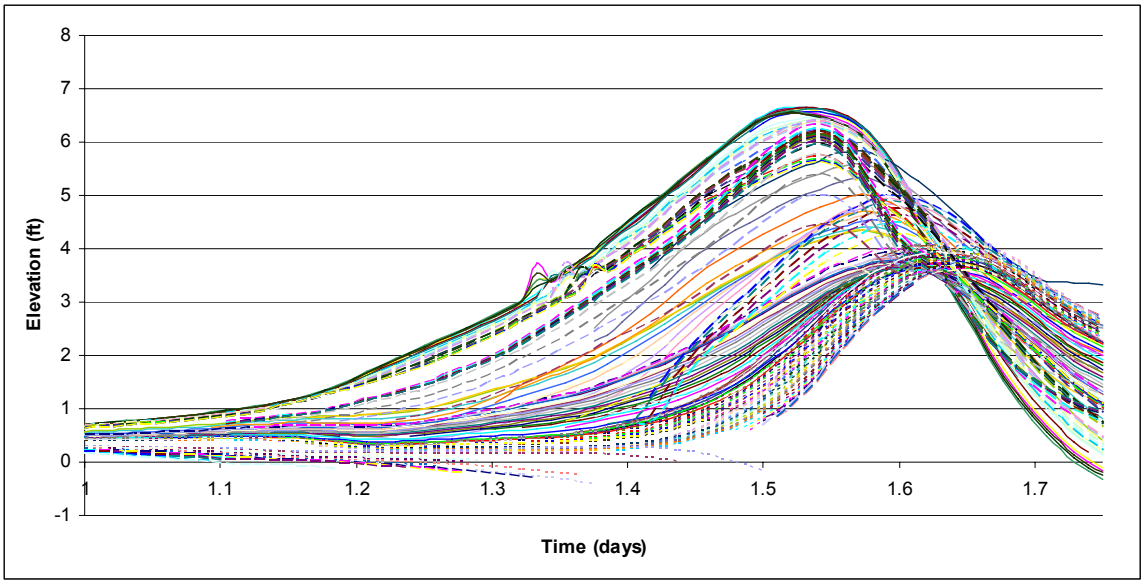

Figure 9-6. Hydrographs at Stations Defining the Hurricane Protection System for a Storm

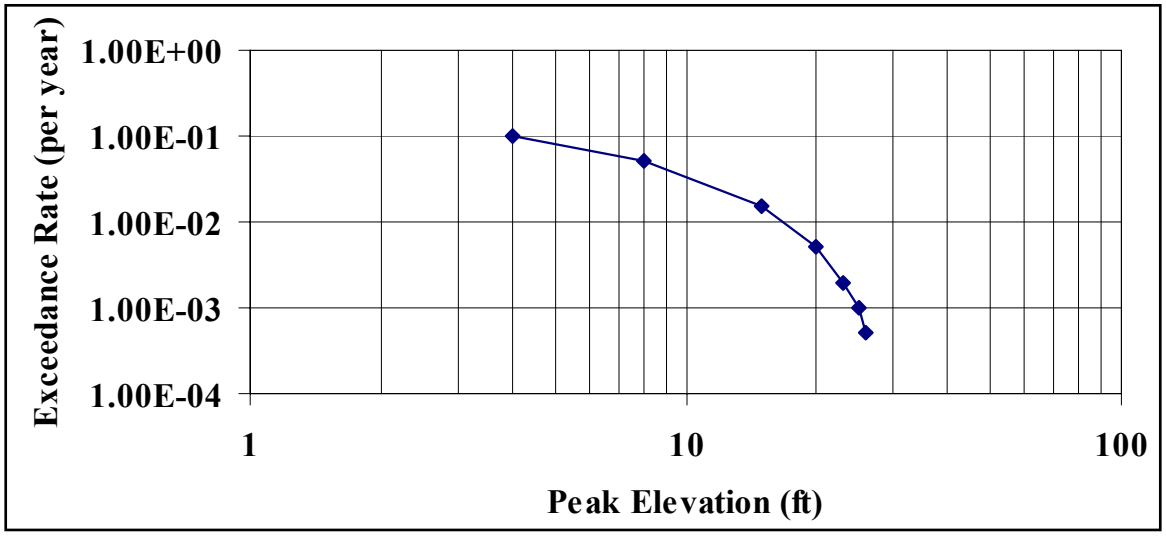

Figure 9.7. Surge and wave Exceedance Curve Corresponding to a Station

Table 9-4
Hurricane Runs, Rates, Category, and Reach Overtopping Volume Results

Run	Rate (Events/Yr)	Category	OW1-M	OW1-S	OW2-M	OW2-S	NOE1-M	NOE1-S
			Mean (ft^3)	StD (ft^3)	Mean (ft^3)	StD (ft^3)	Mean (ft^3)	StD (ft^3)
1	1.000E-01	I	0.000E+00	0.000E+00	0.000E+00	0.000E+00	8.276E+03	1.655E+03
2	5.000E-02	III	0.000E+00	0.000E+00	0.000E+00	0.000E+00	1.655E+04	3.310E+03
3	1.000E-02	IV	0.000E+00	0.000E+00	0.000E+00	0.000E+00	3.310E+04	6.621E+03
4	7.500E-02	III	0.000E+00	0.000E+00	0.000E+00	0.000E+00	1.655E+04	3.310E+03
5	2.000E-02	II	0.000E+00	0.000E+00	0.000E+00	0.000E+00	3.310E+04	6.621E+03
6	2.000E-01	I	0.000E+00	0.000E+00	0.000E+00	0.000E+00	8.276E+03	1.655E+03
7	5.000E-03	IV	0.000E+00	0.000E+00	0.000E+00	0.000E+00	3.310E+04	6.621E+03
8	9.000E-02	II	0.000E+00	0.000E+00	0.000E+00	0.000E+00	1.655E+04	3.310E+03
9	1.500E-01	I	0.000E+00	0.000E+00	0.000E+00	0.000E+00	8.276E+03	1.655E+03

Overtopping Flow Rate and Volume Models, and Probabilities.

Deterministic Models. The overtopping rate can be computed using the rectangular weir formulae (Daugherty et al. 1985). The overtopping water flow requires the elevation H and width L. If the water is assumed to be the ideal liquid, it can be shown using the energy conservation law that the flow rate Q (L3/T) is given by the following equation:

$$Q = \frac{2}{3}(2g)^{1/2} LH^{3/2} \tag{9-4}$$

where g is the acceleration of gravity. The actual flow over the weir is known to be less than ideal (Daugherty et al. 1985) because the effective flow area is considerably smaller than the product LH.

The model can be enhanced further for engineering applications by replacing the term $\frac{2}{3}(2g)^{1/2}$ in Eq. 9-4 by an empirical coefficient, known as the weir coefficient C_w, so that Eq. 9-4 takes on the following form:

$$Q = C_W LH^{3/2} \tag{9-5}$$

where

$$C_W = \begin{cases} 3.33 & \textit{if } L \textit{ and } H \textit{ are given in English units} \\ 1.84 & \textit{if } L \textit{ and } H \textit{ are given in SI units} \end{cases} \tag{9-6}$$

Note that the Cw for the ideal fluid case is $\frac{2}{3}(2g)^{1/2}$ which is equal to 2.95 m/s2. This coefficient is assumed to have a coefficient of variation (COV) of 0.2. This coefficient takes a value of 3.0, 2.6, and 2.0 for floodwalls, levees, and gates, respectively, with a coefficient of variation of 0.2 in English units (L and H in feet).

For the application considered, the mean volume of the overtopping (OT) water μ_V for a given reach can be calculated as

$$\mu_V = C_w L \int_{over\ t\ where\ h_s > H_r} \left(X_s h_s(t) - H_r\right)^{3/2} dt \tag{9-7}$$

where a surge hydrograph is represented by $h_s(t)$ as illustrated in Figure 9-8; H_r is the reach height; L is the reach length; C_w is the weir coefficient with a coefficient of variation of 0.2, and a mean $\mu(C_w)$ of 3.0, 2.6, and 2.0 for floodwalls, levees, and gates, respectively; X_s is an aleatory uncertainty random factor with a lognormal distribution (0.20 log standard deviation and a median of 1.0), which means that we have to apply the lognormal distribution with the following parameters:

$$\mu = \mathrm{E}(\ln(x)) = 0, \text{ and } \sigma((\ln(x)) = 0.2 \tag{9-8}$$

The resulting volume is the conditional mean volume *given* overtopping. The computations account for X_s by numerically using a step size of Δx_{si} and n steps as follows:

$$\mu_{Vi} = \mu_{C_w} L \int_0^{\infty} \left(x_{si} h_s(t) - H_r\right)^{3/2} dt \tag{9-9}$$

where the probability $P(\Delta x_{si})$ can be computed based on the density function f_{X_s} as follows:

$$P(\Delta x_{si}) = \int_{\Delta x_{si}} f_{X_s}(x_s) dx_s \tag{9-10}$$

such that

$$\sum_{i=1}^{n} P(\Delta x_{si}) = \sum_{i=1}^{n} \int_{\Delta x_{si}} f_{X_s}(x_s) dx_s = 1 \tag{9-11}$$

For each hurricane, the event tree is evaluated n times, and the branch probabilities for these evaluations are multiplied by the respective $P(\Delta x_{si})$ according to Eq. 9-11. The impact of this step is that the number of branches produces is multiplied by n. The variance of the water volume for each case is computed based on the coefficient of variation (δ) of the weir coefficient as follows:

$$\sigma_{Vi}^2 = (\mu_{Vi} \delta_{Cw})^2 \tag{9-12}$$

where μ_{Vi} is provided by Eq. 9-9, and the coefficient of variation (δ) of the weir coefficient is taken as 0.2.

Wave setup is included in the hydrograph for each hurricane as discussed in a subsequent section. The uncertainty in the wave setup can be added in the same manner by making X_s in Eq. 9-7 to become the product of two lognormal random variables, the aleatory uncertainty random factor with a lognormal distribution (0.20 log standard deviation and a median of 1.0), and the wave setup factor with a lognormal distribution (0.15 log standard deviation and any median of interest).

Uncertainty Analysis. This section uses Monte Carlo simulation and nonlinear curve fitting based on least squares to propagate uncertainty in the weir equation. The uncertainty analysis of the overtopping flow rate can be assessed using Monte Carlo simulation based on a normally distributed epistemic uncertainty of the H_s at a reach for a particular hurricane run. Using Eq. 9-5, the overtopping rate for a unit width (i.e., $L = 1$) is

$$q = 3.33 H^{3/2} \tag{9-13}$$

where $H = H_s - H_r$ with the constraint that $H_s > H_r$. A truncated distribution resulting from such a formulation requires the use of Monte Carlo simulation. The simulation was performed using 100 cycles for mean H values incremented from -6 to 10 ft using an increment of 0.01 ft, and standard deviation (S) values of 0, 1, and 2 ft as shown in Figure 9-8. Figure 9-9 shows the differential increase in flow rate due to the standard deviation of water Head. Regression analysis was performed to obtain the mean and standard deviation of the conditional overtopping rate as follows:

$$\bar{q} = \left(\overline{H} + 10\right)^{3.87577} \exp\left(0.01916 S_H - 6.92066\right) \tag{9-14a}$$

$$S_q^2 = 80.65\left(\overline{H} + 10\right) + 165.67 S_H^2 - 1344.26 \quad if \geq 0; \quad otherwise \quad S_q^2 = 0 \tag{9-14b}$$

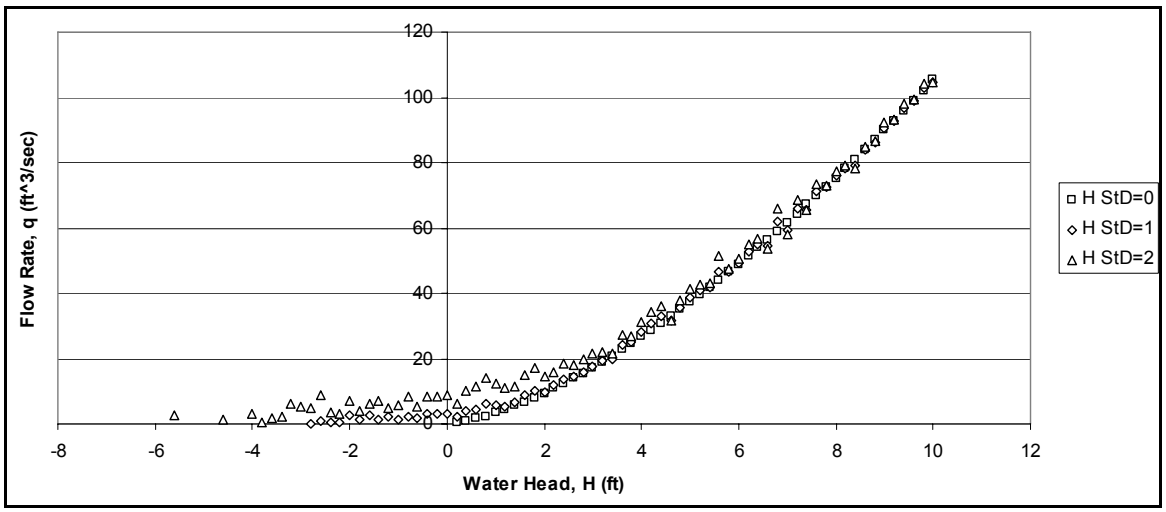

Figure 9-8. Simulated Flow Rate

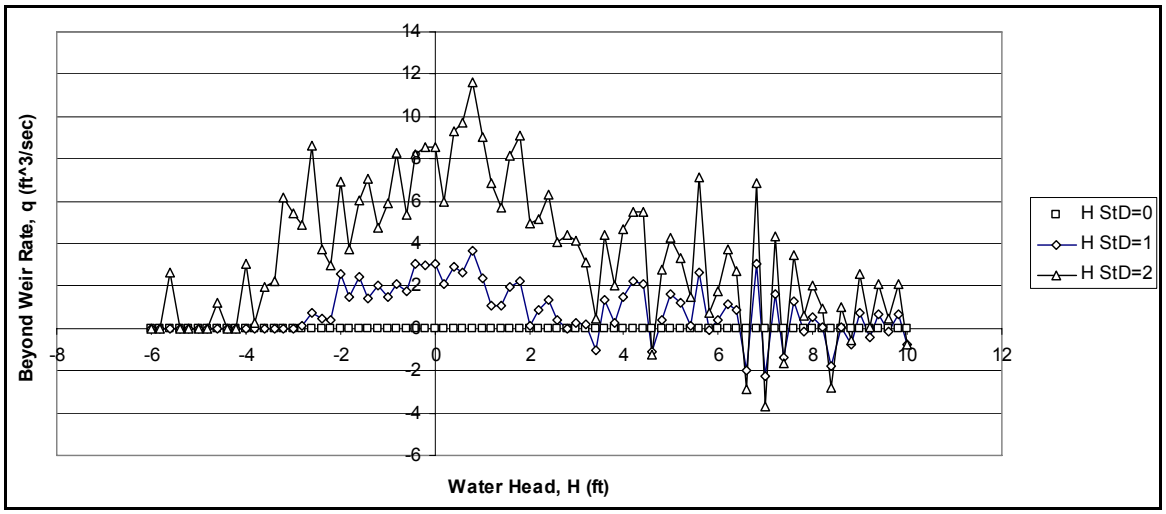

Figure 9-9. Differential Increase in Flow Rate Due to Standard Deviation of Water Head

The respective multiple correlation coefficients are 0.996 and 0.870. The coefficient of variation of the flow rate ($COV(q)$) can be computed as $COV(q) = S_q / \bar{q}$. Equations 14a and 14b can be adjusted to account for various weir coefficients, such as 2.6 for levees and 3.0 for floodwalls. Similar models can be used for flow through open closures.

Equations 9-14a and 9-14b can be used to compute water volume moments in the case of random water elevation, which at least assumes that it is applicable for $S_H > 0$. Physically, Eq. 9-14a shows that water overtopping is possible even when $H_s < H_p$, i.e., when the water elevation is negative.

Failure and Overtopping Probability. Failure probabilities including overtopping probability can be computed based on a performance function as commonly used in structural reliability assessment (see for example Ayyub 2003; Ayyub and McCuen 2003) as given by

$$Z = R - L \tag{9-15}$$

where Z = performance function, R = strength (resistance) and L = loading in the structure. In this case the resistance is provided by the hurricane protection elevation, and the loading is provided by the surge/wave elevation. The non-performance probability can be computed as

$$P = \text{Prob}\ (g < 0) \tag{9-16}$$

The reliability index for normally distributed random variables is

$$\beta = \frac{\mu_R - \mu_L}{\sqrt{\sigma_R^2 + \sigma_L^2}} \tag{9-17}$$

where μ_R = mean value of strength R, μ_L = mean value of the load effect L, σ_R = standard deviation of strength R, and σ_R = standard deviation of the load effect L.

The reliability index for lognormally distributed random variables is

$$\beta = \frac{\ln\left(\frac{\mu_R}{\mu_L}\sqrt{\frac{\delta_L^2 + 1}{\delta_R^2 + 1}}\right) - \mu_L}{\sqrt{\ln\left(\left(\delta_R^2 + 1\right)\left(\delta_L^2 + 1\right)\right)}} \tag{9-18}$$

where d = coefficient of variation. Equation 9-18 is used in this study. The relationship between the reliability index β and the probability of failure is given by

$$P_f = 1 - \Phi(\beta) \tag{9-19}$$

where $\Phi(\beta)$ = cumulative probability distribution function of the standard normal distribution. Additional information on reliability assessment methods including non-normal and correlated random variables is provided by Ayyub (2003), and Ayyub and McCuen (2003).

The cumulative distribution function (CDF) of the total water volume contained in a subbasin of n reaches can be computed as follows:

$$F_V = \sum_{i=1}^{n} p_i F_{V_i} \tag{9-20}$$

where p_i = a overtopping probability, and F = CDF. The overtopping probability can be treated as a binary variable and Eq. 9-20 is still valid. For the case of point estimates of flooding per reach, computations can be based on order statistics as provided in Appendix 7. Once the total volume is obtained from all overtopping and breach cases, the net volume (as a random variable) needed for consequence analysis can be computed by adding water volume from rainfall, and the effect of pumping that includes backflow. The pumping volume and backflow are considered as a multiplier called the pumping factor.

Illustrations. As was stated previously, Table 9-4 provides typical results for a reach. Several hypothetical reaches were used to construct overtopping results that were aggregated by subbasins as illustrated in Table 9-5. In this example, the basin is assumed to contain one or more subbasins. The overtopping results for this subbasin include the overtopping volume based on an overtopping condition, i.e., V|O. The overtopping (O) probability, i.e., P(O), can be computed using system reliability concepts as

$$P(O) = 1 - \prod_{i=1}^{m} (1 - P_i(O)) \tag{9-21}$$

where $P_i(O)$ is the probability of overtopping of reach i in a subbasin with m reaches.

Water Volumes from Other Features of the Protection System. The hurricane protection system includes other features that could allow water volume to enter the protected areas during a hurricane. These features include:

1. closure structures, i.e., gates, that are left open or failed to close
2. localized changes in levee or floodwall elevations that create a transition in the HPS

These features are identified within each reach and assigned to subbasins in case of nonperformance. For the closure structures case, the water volume resulting from failure of the closure structure for a given hurricane can be computed based on respective gate closing failure probabilities, width of the closure structure, elevation of the bottom of the structure, and Eqs. 9-9 and 9-12. The water volume associated with the localized changes in levee or floodwall elevations requires identification of the changes in elevation and the lengths over which the elevation varies. Table 9-5 shows a tabulated structure for computing volumes associated with features.

Table 9-5
A Tabulated Structure for Water Volumes for Sub basins and Basins

Subpolder Number	Overtopping Volume (V|OT)		Precipitation Rainfall Volume		Closures Water Volume		Breach Volume Elevation		Breach Volume Volume	
	Mean (ft^3)	StD (ft^3)	Mean (ft^3)	StD (ft^3)	Mean (ft^3)	StD (ft^3)	Mean (ft)	StD (ft)	Mean (ft^3)	StD (ft^3)
OW1	0.000E+00	0.000E+00	0.000E+00	0.000E+00	0.000E+00	0.000E+00	1.187E+00	5.937E-02	1.743E+08	4.571E+06
OW2	0.000E+00	0.000E+00	0.000E+00	0.000E+00	0.000E+00	0.000E+00	1.187E+00	5.937E-02	4.858E+08	9.056E+06
NOE1	0.000E+00	0.000E+00	1.655E+04	3.310E+03	4.724E+02	7.162E+01	1.187E+00	5.937E-02	4.461E+08	3.157E+07
NOE2	0.000E+00	0.000E+00	3.775E+06	7.551E+05	4.977E+02	9.954E+01	1.187E+00	5.937E-02	1.109E+09	1.355E+07
NOE3	0.000E+00	0.000E+00	2.703E+06	5.406E+05	0.000E+00	0.000E+00	1.187E+00	5.937E-02	3.059E+08	5.171E+06
NOE4	0.000E+00	0.000E+00	1.550E+01	3.100E+00	5.972E+02	1.194E+02	1.187E+00	5.937E-02	8.688E+07	2.631E+06
NOE5	0.000E+00	0.000E+00	9.367E+07	1.873E+07	0.000E+00	0.000E+00	1.187E+00	5.937E-02	2.463E+09	2.281E+07
OM1	0.000E+00	0.000E+00	0.000E+00	0.000E+00	0.000E+00	0.000E+00	1.187E+00	5.937E-02	7.075E+08	9.807E+06
OM2	0.000E+00	0.000E+00	0.000E+00	0.000E+00	0.000E+00	0.000E+00	1.187E+00	5.937E-02	6.399E+08	8.787E+06
OM3	0.000E+00	0.000E+00	0.000E+00	0.000E+00	0.000E+00	0.000E+00	1.187E+00	5.937E-02	2.480E+08	6.962E+06
OM4	0.000E+00	0.000E+00	0.000E+00	0.000E+00	0.000E+00	0.000E+00	1.187E+00	5.937E-02	7.016E+07	2.248E+06
OM5	0.000E+00	0.000E+00	0.000E+00	0.000E+00	0.000E+00	0.000E+00	1.187E+00	5.937E-02	4.371E+08	1.257E+07
SB1	0.000E+00	0.000E+00	0.000E+00	0.000E+00	0.000E+00	0.000E+00	1.187E+00	5.937E-02	1.753E+08	5.671E+06
SB2	0.000E+00	0.000E+00	0.000E+00	0.000E+00	0.000E+00	0.000E+00	1.187E+00	5.937E-02	1.367E+06	4.737E+04
SB3	0.000E+00	0.000E+00	0.000E+00	0.000E+00	0.000E+00	0.000E+00	1.187E+00	5.937E-02	1.491E+08	4.839E+06
SB4	0.000E+00	0.000E+00	0.000E+00	0.000E+00	0.000E+00	0.000E+00	1.187E+00	5.937E-02	1.581E+07	2.990E+06

Breach Elevation and Volume Models.

Three Cases of Breach Failure Within Reaches. The risk quantification can be effectively performed by examining three cases of breach failure that correspond to branches presented in the event tree of Figure 9-5. The three cases are:

1. breach given overtopping
2. breach given no overtopping
3. breach due to feature (closure gate, pump house, etc.) failures

The computations of breach failure probability for these cases can be performed using Eqs. 9-15 to 9-19. The first case of breach given overtopping is primarily driven by erosion resulting from overtopping water flow. Fragility curves for these cases were developed as described in the reliability methodology section.

Breach Parameters. The inundation mapping of the risk analysis is based on determining the volume of water entering a basin due to levee/floodwall overtopping and/or breaching, open gates and rainfall. The breaching scenarios require knowledge of the breach size, depth and surge hydrograph at the breach in order to determine basin inflows. The Katrina experience was reviewed to identify basic characteristics of the major breaches in order to develop general rules to use in the risk model for breach size.

One critical characteristic that determines the volume of water flowing through a breach is the duration of time that the breach is open. Katrina proved that the breaches could not be repaired in time to have an effect on the level of water achieved inside the basins. Therefore the duration that the breach is open will have no effect on inflow volumes and water elevations.

IPET studies indicate that the Katrina induced London Ave. and 17th St. canal breaches occurred before the water level in the canals reached the top of wall and appear to have been the result of a foundation or design failure. Therefore, this would be a breach given no overtopping scenario in the risk analysis. The high water marks (HWM) experienced during Katrina inside

the Orleans basin where the canal breaches occurred and the length of time that surge elevations exceeded lake levels in the canals were examined. Experienced HWM during Katrina in the basins were very close (within about 1') to the peak surges in the canals. For example, it appears that the London Avenue South breach occurred when the canal water level was at about 7 to 8 feet, or 3' or so below the top of wall. The peak surge in the area was about 10-11 feet and HWM is also about 10'. The hydrographs experienced in those areas show that the time that the surge elevation exceeded the failure elevation was on the order of several hours. It appears that this was sufficient time for the water elevations inside the basin to closely follow the surge levels. The inverts of the canal breaches were well below the normal lake level so water flowed back into the lake after the surge passed. Based on this it would seem appropriate to use the peak surge level as the water elevation achieved inside the basin when a catastrophic breach (full levee height) occurs during a non-overtopping event.

Therefore for a breach that occurs without overtopping, the following assumptions are used in the risk model:

- All breaches would be considered to be a result of a structural or foundation failure and would be catastrophic (full depth of levee or floodwall).
- The breach depth would extend below lake or river level.
- The maximum interior water levels caused by the breach would be the same as the maximum surge level experienced adjacent to the breach.

For the case of a breach during an overtopping event, a reliability model for overtopping erosion is under development. The erosion model for levees is expected to show different breach inverts based on the amount of overtopping from surge or waves and the type of soil in the levee. In the case where the breach invert is higher than lake or river level, the depth and length of the breach, the duration of time that the surge exceeds the breach invert and the weir coefficient through the breach is required to calculate inflow volumes. The breach widths for the levees and floodwalls could also be expected to be similar to that experienced during Katrina. Breach widths at the major canal breaches varied (450 to 1000+ feet) but were all on the order of several hundred feet. At the industrial canal (IHNC) where overtopping did occur, the two Lower Ninth Ward breaches were similar in width to the other canals where overtopping did not occur, and the depth of the breaches were below the normal canal water levels so water also flowed back through these breaches when the surge passed. Based on these observations, using the peak surge level as the maximum water elevation achieved inside the basin would be appropriate when a catastrophic breach (full levee height) occurs during an overtopping event.

For the case of a less than catastrophic breach given overtopping, it will be necessary to calculate the basin inflow volume over the reach from overtopping in the same manner as for the non-breaching case and add an amount that would account for the flow through the breach. Breach parameters for width and height must be available in order to determine inflows. The risk model does not consider breaches that are less than catastrophic. This refinement should be added once an erosion model is available. The risk model instead considers the mean depth of overtopping required to cause a full breach and estimates the uncertainty in that value. This method provides a conservative estimate of basin inflows by assuming the breach width, depth and weir coefficient and then calculating the inflow volume in the same way that the open-gate inflow volume is calculated. Some suggested overtopping values are shown in the table below.

Therefore for a breach that occurs during an overtopping event, the following assumptions are used in the risk model:

- Breaches would be as a result of an erosion failure due to surge and/or waves.
- All breach depths are assumed to be full levee height however the depth of overtopping required to cause a breach is dependent upon soil properties. Assumed values are shown in the table below.

Levee/Wall Material	Overtopping Depth (ft) for Full Breach	
	Mean	Std Dev
Clay	6'	2'
Sand/Clay	4'	2'
Hydraulic Fill	2'	2'

- Durations of overtopping should come from the surge hydrographs.
- The interior water levels in the basin would be the same as the surge level for the Full depth levee breach.

Basin Reliability Analysis. Failure modes, performance functions, basic random variables, and computational procedures of failure probability are provided in the reliability analysis section. The failure probabilities of n failure modes for all reaches in a basin are denoted as $p1$, $p2$, …, p_n. The breach failure probability for a basin (P_B) can be computed as (assuming that the reach failures are statistically independent events),

$$P_B(Polder) = 1 - \prod_{i=1}^{n} (1 - p_i) \tag{9-22}$$

Equation 9-22 can be used for the cases of probability of breach given overtopping, the probability of breach given non-overtopping, and the probability of breach of features.

Water Elevation and Volume. The surge hydrograph produced by a hurricane is used to compute the water volume entering a basin during levee overtopping or breaching, and the maximum water elevation (H_{ps}) within the Basin. In the case of levee overtopping, H_{ps} within a basin is based on a water volume computed using the duration of overtopping. If a breach occurs and the invert of the breach is below the final elevation of the adjacent body of water, H_{ps} is the elevation of that body of water. If the breach invert is above the final elevation of the adjacent body of water, H_{ps} is based on a water volume entering the basin computed using the duration that the surge is above the breach invert. The topography of the Basin, and the drainage and pumping models are used to construct such a relationship. An example of this relationship was provided in the 2000 unwatering plan of the greater metropolitan area of New Orleans, LA prepared the District which has figures that relate stage elevation to storage. Figure 9-10 shows such a stage-storage plot for the New Orleans East (Citrus). Regression analysis was used to illustrate fitting a model for this plot. The resulting model with a multiple correlation coefficient of 0.998 is

$$V = 1.8690 \times 10^7 (E + 7.5)^2 + 2.9492 \times 10^8 (E + 7.5) \tag{9-23}$$

Figure 9-10. Stage-Storage Relationship of New Orleans (Citrus)

where V = storage volume (ft3), E = stage elevation (ft), and E domain of -7.5 to 15 ft. Such relationships can be developed. For example, relationships for New Orleans East Basin are shown in Figure 9-11 for the sub-basins shown in Figure 9-12. For the purposes of the risk model, rather than using fitted curves, stage-storage relationship were numerically evaluated and tabulated in increments of 1 ft of elevation and linear interpolation was used.

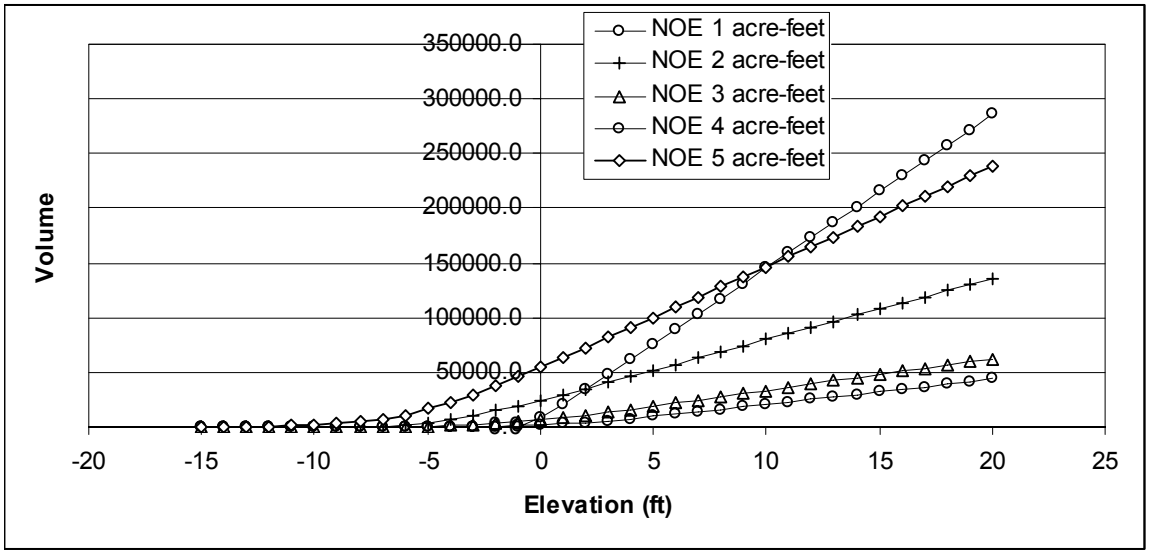

Figure 9-11. Stage-Storage Relationships of Sub-basins and Basin New Orleans East

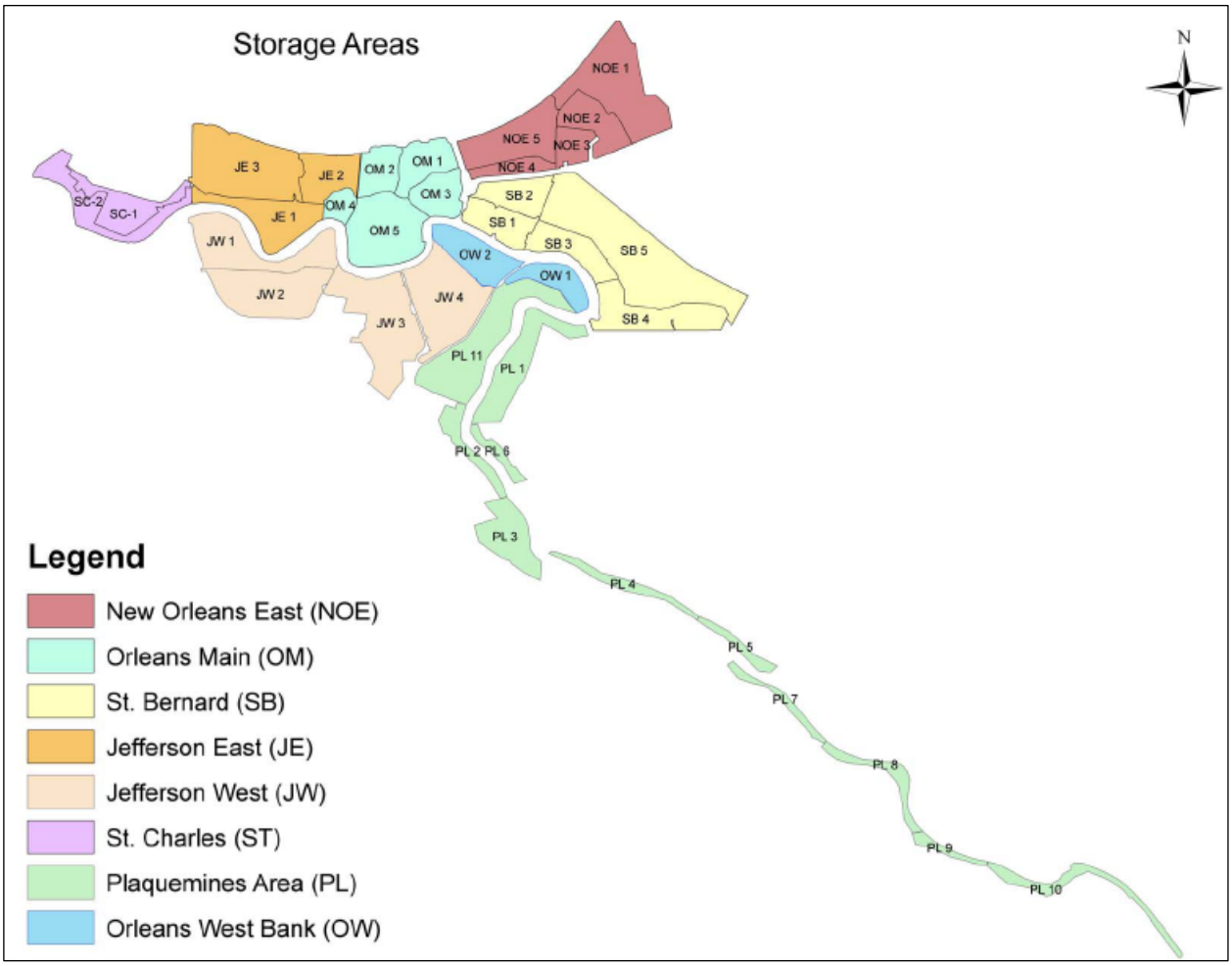

Figure 9-12. Definition of Sub basin for Stage-Storage Relationships

The computations of water elevations in subbasins after allowing for interflow among the subbasins at the connections, i.e., interfaces, becomes complicated when a basin has two or more sub-basins in which flooding is controlled by separate pumping and drainage systems. The cases of two to five subbasins are discussed herein. For the two sub-basin case, the computations of the final volumes can be used as a basic case to iteratively determine water volumes and elevations for the cases of more than two subbasins. For the following specified parameters:

V_1 inflow volume to subbasin 1

V_2 inflow volume to subbasin 2

E_1 inflow elevation in subbasin 1 ($E_1 > E_2$), where $E_1 = SV_1(V_1)$

E_2 inflow elevation in subbasin 2 ($E_1 > E_2$),where $E_2 = SV_2(V_2)$

C_{E12} water elevation capacity at the connection between subbasins 1 and 2

C_{V12} capacity of sub-basin 1 for water flowing from subbasin 1 to subbasin 2 defined by the elevation E_{12} at the connection between subbasin 1 and subbasin 2, where $C_{V12} = SV_1(C_{E12})$

C_{V21} capacity of sub-basin 2 for water flowing from subbasin 2 to subbasin 1 defined by the elevation E_{12} at the connection between subbasin 1 and subbasin 2, where $C_{V21} = SV_2(C_{E12})$

SV stage-storage relationship to compute the elevation (*E*) as a function of volume (*V*), i.e., *E*=*SV*(*V*), for subbasin 1, subbasin 2, and combined subbasins 1 and 2

SE stage-storage relationship to compute the volume (*V*) as a function of elevation (*E*), i.e., *V*=*SE*(*E*), for subbasin 1, subbasin 2, and combined subbasins 1 and 2

The following parameters can be computed using the logic presented in Table 9-6:

E_{1f} final water elevation in subbasin 1

E_{2f} final water elevation in subbasin 2

V_{1f} final water volume in subbasin 1

V_{2f} final water volume in subbasin 2

V_{12f} final water volume for combined subbasins 1 and 2

For each storm, the subbasins are sorted such that $E_1 > E_2 > ... > E_5$. Also, the following volumes can be computed:

$$\text{Cumulative inflow volume } (CV) = V_1 + V_2$$

$$\text{Cumulative volume capacity } (CC) = C_{12} + C_{21}$$

$$\text{Final cumulative water volume } (CV_f) = V_{1f} + V_{2f}$$

The logic presented in Table 9-6 is used to model the interflow among the subbasins, and to obtain the respective final volumes and elevations. The interflow logic in Table 9-6 is implemented as a function called interflow with the following input and output parameters:

Input:

E_1 and E_2 such that $E_1 > E_2$
V_1 and V_2
C_{E12}
SV_1
SV_2
SV_{12}

Table 9-6
Two-Sub basin Interflow Model

Case	Conditions	Volume	Elevation
1.	$E_1 < C_{E12}$ and $E_2 < C_{E21}$	$V_{1f} = V_1$ and $V_{2f} = V_2$	$E_{1f} = E_1$ $E_{2f} = E_2$
2.	$E_1 \geq C_{E12}$ and $E_2 \geq C_{E21}$	$V_{12f} = V_1 + V_2 = CV$	$E_{12f} = SV_{12}(V_{12f})$
3.	$E_1 > C_{E12}$ and $E_2 < C_{E12}$:		
3.1	$SV(CV) \geq C_{E12}$	$V_{12f} = V_1 + V_2 = CV$	$E_{12f} = SV_{12}(V_{12f})$
3.2	$SV(CV) < C_{E12}$	$\Delta V_1 = V_1 - C_{12}$ $V_{1f} = C_{12}$ $V_{2f} = V_2 + \Delta V_1$	$E_{1f} = E_1$ $E_{2f} = SV_2(V_{2f})$

Output:

E_{1f}
E_{2f}

A MATLAB function can be constructed with the following call statement:

$[E_{1f}, E_{2f}]$ = interflow($E_1, E_2, V_1, V_2, C_{E12}, SV_1\ SV_2, SV_{12}$)

The resulting final cumulative water volume (CV_f) must equal the cumulative inflow volume (CV).

Subbasins. For the case of three subbasins, the final elevations can be computed by implementing the pseudo code of a for-loop as defined below with C_{Eij} = -9999 indicating that subbasins *i* and *j* are not connected.

```
while error > 0.05
  E1i = E1
  E2i = E2
  E3i = E3
  for i=1:2
    for j=(i+1):3
      if C_Eij==-9999, break, end
      [E_if , E_jf ] = interflow(E_i , E_j , V_i , V_j , C_Eij , SV_i SV_j , SV_ij )
      E_i = E_if
      E_j = E_jf
```

```
    end
  end
  error1=abs(E1i-E1 )/abs(E1i)
  error2=abs(E2i-E2)/abs(E2i)
  error3=abs(E3i-E3)/abs(E3i)
  error=(error1+error2+error3)/3
end
```

For the case of four subbasins, the final elevations can be computed by implementing the pseudo code of a for-loop as defined below with C_{Eij} = -9999 indicating that subbasins *i* and *j* are not connected.

```
while error > 0.05
  E1i = E1
  E2i = E2
  E3i = E3
  E4i = E4
  for i=1:3
    for j=(i+1):4
      if CEij==-9999, break, end
      [Eif , Ejf ] = interflow(Ei , Ej , Vi , Vj , CEij , SVi SVj , SVij )
      Ei =Eif
      Ej =Ejf
    end
  end
  error1=abs(E1i-E1 )/abs(E1i)
  error2=abs(E2i-E2)/abs(E2i)
  error3=abs(E3i-E3)/abs(E3i)
  error4=abs(E4i-E4)/abs(E4i)
  error=(error1+error2+error3+error4)/4
end
```

For the case of five subbasins, the final elevations can be computed by implementing the pseudo code of a for-loop as defined below with C_{Eij} = -9999 indicating that subbasins *i* and *j* are not connected.

```
while error > 0.05
  E1i = E1
  E2i = E2
  E3i = E3
  E4i = E4
```

```
  E5i = E5
  for i=1:4
    for j=(i+1):5
      if C_Eij==-9999, break, end
      [E_if , E_jf ] = interflow(E_i , E_j , V_i , V_j , C_Eij , SV_i SV_j , SV_ij )
      E_i = E_if
      E_j = E_jf
    end
  end
  error1=abs(E1i- E_1 )/abs(E1i)
  error2=abs(E2i- E_2 )/abs(E2i)
  error3=abs(E3i- E_3 )/abs(E3i)
  error4=abs(E4i- E_4 )/abs(E4i)
  error5=abs(E5i- E_5 )/abs(E5i)
  error=(error1+error2+error3+error4+error5)/5
end
```

Event Tree Branch Probabilities. The event tree of Figure 9-5 consists of 12 branches per hurricane. This section develops and summarizes the probabilities for these branches.

The event tree includes the following primary independent subbasin-level events:

C is the event that *all gates* within a subbasin are closed

P is the event that *all pumps* in the subbasin work

B is the event that at least one reach (or one of its features) in a subbasin is breached

Thus there are eight scenarios as follows: $\{C, P, B\}$, $\{C, P, \underline{B}\}$, $\{C, \underline{P}, B\}$, $\{C, \underline{P}, \underline{B}\}$, $\{\underline{C}, P, B\}$, $\{\underline{C}, P, \underline{B}\}$, $\{\underline{C}, \underline{P}, B\}$, and $\{\underline{C}, \underline{P}, \underline{B}\}$. Since the total probability has to equal 1, the expression for total probability for all combinations of scenarios is:

$$\begin{aligned} &P(C)P(P)P(B) + P(C)P(P)P(\underline{B}) + P(C)P(\underline{P})P(B) + P(C)P(\underline{P})P(\underline{B}) + \\ &P(\underline{C})P(P)P(B) + P(\underline{C})P(P)P(\underline{B}) + P(\underline{C})P(\underline{P})P(B) + P(\underline{C})P(\underline{P})P(\underline{B}) = 1 \end{aligned} \quad (9\text{-}24)$$

Since $P(\underline{X}) = 1 - P(X)$ where X is any event, Eq. 9-24 can be rewritten as:

$$\begin{aligned} &P(C)P(P)\left(1 - P(\underline{B})\right) + P(C)P(P)P(\underline{B}) + P(C)\left(1 - P(P)\right)\left(1 - P(\underline{B})\right) + \\ &P(C)\left(1 - P(P)\right)P(\underline{B}) + \left(1 - P(C)\right)P(P)\left(1 - P(\underline{B})\right) + \left(1 - P(C)\right)P(P)P(\underline{B}) + \\ &\left(1 - P(C)\right)\left(1 - P(P)\right)\left(1 - P(\underline{B})\right) + \left(1 - P(C)\right)\left(1 - P(P)\right)P(\underline{B}) = 1 \end{aligned} \quad (9\text{-}25)$$

The event $\underline{B}$ is realized where none of the failure events leading to breach occur. The failure events *i* corresponding to breaches of reaches (*R*), drainage structures (*D*) and transitions (*T*). Thus, the $P(\underline{B})$ can be expressed as:

$$P(\underline{B}) = \prod_i \left(\left(1 - P_i\left(B \mid O\right)\right) P_i\left(O\right) + \left(1 - P_i(B \mid \underline{O})\right)\left(1 - P_i(O)\right) \right) \tag{9-26}$$

where O is the event that overtopping occurs at reach i. Note in Eq. 9-26 that i represents a breach failure in reach (R), drainage structure failure (D), or transition erosion failure (T). The probability of at least one breach failure $P(B)$ in a basin can then be determined as:

$$P(B) = 1 - \prod_i \left(\left(1 - P_i\left(B \mid O\right)\right) P_i(O) + \left(1 - P_i(B \mid \underline{O})\right)\left(1 - P_i(O)\right) \right) \tag{9-27}$$

Defining O as the event that overtopping occurs at one or more reaches in the Basin, $P(O)$ can be determined as:

$$P(O) = 1 - \prod_i P_i(\underline{O}) = 1 - \prod_i \left(1 - P_i(O)\right) \tag{9-28}$$

$P(\underline{B})$ can be expressed as:

$$P(\underline{B}) = P(\underline{B} \mid O)P(O) + P(\underline{B} \mid \underline{O})\left(1 - P(O)\right) \tag{9-29}$$

Since $\underline{O}$ is the event that overtopping does not occur anywhere in the Basin, P($\underline{B}|\underline{O}$) can be determined from Eq. 9-26 as:

$$P(\underline{B} \mid \underline{O}) = \prod_i \left(1 - P_i(B \mid \underline{O})\right) \tag{9-30}$$

Since the event $\underline{B}|O$ denotes at least one reach overtops, $P(\underline{B}|O)$ can be determined from Eqs. 29 and 30 as:

$$P(\underline{B} \mid O) = \frac{\prod_i \left(\left(1 - P_i\left(B \mid O\right)\right) P_i\left(O\right) + \left(1 - P_i(B \mid \underline{O})\right) P_i(\underline{O}) \right) - \prod_i \left(1 - P(B \mid \underline{O})\right)\left(1 - P(O)\right)}{P(O)} \tag{9-31}$$

With Eqs. 30 and 31 and their complements, Eq. 9-26 can be rewritten as:

$$\begin{aligned}
&P(C)P(P)\left(1 - P(\underline{B} \mid O)\right)P(O) + P(C)P(P)\left(1 - P(\underline{B} \mid \underline{O})\right)\left(1 - P(O)\right) + \\
&P(C)P(P)P(\underline{B} \mid O)P(O) + P(C)P(P)P(\underline{B} \mid \underline{O})\left(1 - P(O)\right) + \\
&P(C)\left(1 - P(P)\right)\left(1 - P(\underline{B} \mid O)\right)P(O) + P(C)\left(1 - P(P)\right)\left(1 - P(\underline{B} \mid \underline{O})\right)\left(1 - P(O)\right) + \\
&P(C)\left(1 - P(P)\right)P(\underline{B} \mid O)P(O) + P(C)\left(1 - P(P)\right)P(\underline{B} \mid \underline{O})\left(1 - P(O)\right) + \\
&\left(1 - P(C)\right)P(P)\left(1 - P(\underline{B} \mid O)\right)P(O) + \left(1 - P(C)\right)P(P)\left(1 - P(\underline{B} \mid \underline{O})\right)\left(1 - P(O)\right) + \\
&\left(1 - P(C)\right)P(P)P(\underline{B} \mid O)P(O) + \left(1 - P(C)\right)P(P)P(\underline{B} \mid \underline{O})\left(1 - P(O)\right) + \\
&\left(1 - P(C)\right)\left(1 - P(P)\right)\left(1 - P(\underline{B} \mid O)\right)P(O) + \left(1 - P(C)\right)\left(1 - P(P)\right)\left(1 - P(\underline{B} \mid \underline{O})\right)\left(1 - P(O)\right) + \\
&\left(1 - P(C)\right)\left(1 - P(P)\right)P(\underline{B} \mid O)P(O) + \left(1 - P(C)\right)\left(1 - P(P)\right)P(\underline{B} \mid \underline{O})\left(1 - P(O)\right) = 1
\end{aligned} \tag{9-32}$$

Note that Eq. 9-32 now has 16 scenarios as opposed to the original 8 scenarios provided in Eq. 9-26. Generally, if breach occurs, it does not matter whether the gates are open or pumps are working since the breach is expected to overwhelm the system. Thus, Eq. 9-32 can be reduced to 10 scenarios as follows:

$$\begin{aligned}
&\left(1-P(\underline{B}\,|\,O)\right)P(O)+\left(1-P(\underline{B}\,|\,\underline{O})\right)\left(1-P(O)\right)+\\
&P(C)P(P)P(\underline{B}\,|\,O)P(O)+P(C)P(P)P(\underline{B}\,|\,\underline{O})\left(1-P(O)\right)+\\
&P(C)\left(1-P(P)\right)P(\underline{B}\,|\,O)P(O)+P(C)\left(1-P(P)\right)P(\underline{B}\,|\,\underline{O})\left(1-P(O)\right)+\\
&\left(1-P(C)\right)P(P)P(\underline{B}\,|\,O)P(O)+\left(1-P(C)\right)P(P)P(\underline{B}\,|\,\underline{O})\left(1-P(O)\right)+\\
&\left(1-P(C)\right)\left(1-P(P)\right)P(\underline{B}\,|\,O)P(O)+\left(1-P(C)\right)\left(1-P(P)\right)P(\underline{B}\,|\,\underline{O})\left(1-P(O)\right)=1
\end{aligned} \tag{9-33}$$

In Eq. 9-32, the first two terms represent the breach scenarios, whereas the latter eight terms are non-breach scenarios.

The probability of all gates being closed, $P(C)$ is given as:

$$P(C)=\prod_{i}\left(1-P_i(\underline{C})\right) \tag{9-34}$$

Equations 9-26 to 9-34 are used to construct Table 9-7 that summarizes the expanded expressions for the probability of each branch in the event tree of Figure 9-5. Table 9-8 summarizes the respective procedures for water volume and elevation computation. It should be noted that the water volume associated with the branches involving *not-all-gates closed* requires a procedure to account for all possible combinations of not-all-gates closed. Let i be the index denoting a unique scenario among the set of 2^n scenarios of gate open/closed combinations (n = number of uncorrelated gates). The mean water volume (μ) for use in the not-all-gates closed branches is:

$$\mu_{\underline{C}}=\frac{\sum_{i=1}^{2^n}p_i\mu_{\underline{C}i}}{\left(1-p_C\right)} \tag{9-35}$$

where p_C is the probability of all gates closed, $\mu_{\underline{C}i}$ the mean volume associated with not-closing gates according to the i^{th} scenario, and p_i the multinomial probability of the i^{th} scenario. The volume variance for use in the not-all-gates closed branches is:

$$\sigma^2_{\underline{C}}=\frac{\sum_{i=1}^{2^n}p_i^2\sigma^2_{\underline{C}i}}{\left(1-p_C\right)^2} \tag{9-36}$$

where $\sigma^2_{\underline{C}i}$ the volume variance associated with not-closing gates according to the i^{th} scenario.

Table 9-7
A Computational Summary for Branches of the Event Tree of Figure 9-5 for a Hurricane and a Basin

Branch	Branch Probability (See Figure 9-5)
1. Non-Breach	$P(C)P(P)P(\underline{B}\cap\underline{O}) = P(C)P(P)\left(\prod_i (1-P_i(B\mid\underline{O}))P_i(\underline{O})\right)$
2. Non-Breach	$P(C)P(\underline{P})P(\underline{B}\cap\underline{O}) = P(C)P(\underline{P})\left(\prod_i (1-P_i(B\mid\underline{O}))P_i(\underline{O})\right)$
3. Breach	$P(C)P(B\cap\underline{O}) = P(C)\left(1-\left(\prod_i (1-P_i(B\mid\underline{O}))P_i(\underline{O})\right)\right)$
4. Non-Breach	$P(C)P(P)P(\underline{B}\cap O) = P(C)P(P)\left(P(\underline{B})-P(\underline{B}\cap\underline{O})\right) =$ $P(C)P(P)\left(\prod_i ((1-P_i(B\mid O))P_i(O)+(1-P_i(B\mid\underline{O}))P_i(\underline{O}))-\prod_i (1-P_i(B\mid\underline{O}))P_i(\underline{O})\right)$
5. Non-Breach	$P(C)P(\underline{P})P(\underline{B}\cap O) = P(C)P(P)\left(P(\underline{B})-P(\underline{B}\cap\underline{O})\right) =$ $P(C)P(\underline{P})\left(\prod_i ((1-P_i(B\mid O))P_i(O)+(1-P_i(B\mid\underline{O}))P_i(\underline{O}))-\prod_i (1-P_i(B\mid\underline{O}))P_i(\underline{O})\right)$
6. Breach	$P(C)P(B\cap O) = P(C)\left(1-P(\underline{B})-P(\underline{B}\cap\underline{O})\right) =$ $P(C)\left(1-\prod_i ((1-P_i(B\mid O))P_i(O)+(1-P_i(B\mid\underline{O}))P_i(\underline{O}))-\prod_i (1-P_i(B\mid\underline{O}))P_i(\underline{O})\right)$
7. Non-Breach	$(1-P(C))P(P)P(\underline{B}\cap\underline{O}) = (1-P(C))P(P)\left(\prod_i (1-P_i(B\mid\underline{O}))P_i(\underline{O})\right)$
8. Non-Breach	$(1-P(C))P(\underline{P})P(\underline{B}\cap\underline{O}) = (1-P(C))P(\underline{P})\left(\prod_i (1-P_i(B\mid\underline{O}))P_i(\underline{O})\right)$
9. Breach	$(1-P(C))P(B\cap\underline{O}) = (1-P(C))\left(1-\left(\prod_i (1-P_i(B\mid\underline{O}))P_i(\underline{O})\right)\right)$
10. Non-Breach	$(1-P(C))P(P)P(\underline{B}\cap O) = P(C)P(P)\left(P(\underline{B})-P(\underline{B}\cap\underline{O})\right) =$ $(1-P(C))P(P)\left(\prod_i ((1-P_i(B\mid O))P_i(O)+(1-P_i(B\mid\underline{O}))P_i(\underline{O}))-\prod_i (1-P_i(B\mid\underline{O}))P_i(\underline{O})\right)$
11. Non-Breach	$(1-P(C))P(\underline{P})P(\underline{B}\cap O) = P(C)P(P)\left(P(\underline{B})-P(\underline{B}\cap\underline{O})\right) =$ $(1-P(C))P(\underline{P})\left(\prod_i ((1-P_i(B\mid O))P_i(O)+(1-P_i(B\mid\underline{O}))P_i(\underline{O}))-\prod_i (1-P_i(B\mid\underline{O}))P_i(\underline{O})\right)$
12. Breach	$(1-P(C))P(B\cap O) = P(C)\left(1-P(\underline{B})-P(\underline{B}\cap\underline{O})\right) =$ $(1-P(C))\left(1-\prod_i ((1-P_i(B\mid O))P_i(O)+(1-P_i(B\mid\underline{O}))P_i(\underline{O}))-\prod_i (1-P_i(B\mid\underline{O}))P_i(\underline{O})\right)$
Combined Branches 3 and 9	$\left(P(C)+P(\underline{C})\right)\left(P(P)+P(\underline{P})\right)(B\cap\underline{O}) = 1-\left(\prod_i (1-P_i(B\mid\underline{O}))P_i(\underline{O})\right)$
Combined Branches 6 and 12	$\left(P(C)+P(\underline{C})\right)\left(P(P)+P(\underline{P})\right)\left(1-P(\underline{B})-P(\underline{B}\cap\underline{O})\right) =$ $1-\prod_i ((1-P_i(B\mid O))P_i(O)+(1-P_i(B\mid\underline{O}))P_i(\underline{O}))-\prod_i (1-P_i(B\mid\underline{O}))P_i(\underline{O})$

Table 9-8
A Computational Summary for the Water Volumes Associated with the Branches of the Event Tree of Figure 9-5 for a Hurricane and a Basin

Branch	Branch Water Volume (See Figure 9-5)
1. Non-Breach	Use precipitation volume, and apply pumping factor
2. Non-Breach	Use precipitation volume without pumping
3. Breach	Use post-surge breach water elevation, no pumping
4. Non-Breach	Use overtopping and precipitation volume, apply pumping factor
5. Non-Breach	Use overtopping and precipitation volume without pumping
6. Breach	Use post-surge breach water elevation, no pumping
7. Non-Breach	Use precipitation and not-all-closed-closure volume apply pumping factor
8. Non-Breach	Use precipitation and not-all-closed-closure volume without pumping
9. Breach	Use post-surge breach water elevation, no pumping
10. Non-Breach	Use overtopping, precipitation and not-all-closed-closure volume apply pumping factor
11. Non-Breach	Use overtopping, precipitation and not-all-closed-closure volume without pumping
12. Breach	Use post-surge breach water elevation, no pumping

The sub basin interflow analysis as previously described (see Table 9-6) is performed subsequent to Table 9-8 procedures. Uncertainty propagation from the volume (V) moments (μ_V and σ_V^2) to elevation (E) moments (μ_E and σ_E^2) using the tabulated stage-storage relationship for a sub basin can be based on linear interpolation. Linear interpolation is used to define this relationship since the increment size of 1 ft for tabulation has been selected relatively small for this purpose. This linear relationship can be expressed as

$$E = a + bV \tag{9-37}$$

where a and b are model coefficient that are determined from interpolation. The moments of E can be computed as

$$\mu_E = a + b\mu_V \tag{9-38}$$

and

$$\sigma_E^2 = b^2\sigma_V^2 \tag{9-39}$$

The uncertainty propagation Eqs. 9-38 and 9-39 should be used after performing the interflow analysis with the applicable final stage-storage relationships.

Risk Profile by Water Elevation. The results produced so far can be summarized by subbasin, and for all storms and the branches of the event tree in the form of water elevation (mean and variance) and occurrence rate. These results can be used to evaluate elevation-exceedance rate for a subbasin at selected e values according to Eq. 9-40 as follows:

$$\lambda(E > e) = \sum_{All\ storms\ \&\ branches} \lambda P(h)P(S \mid h)P(E > e \mid h, S) \tag{9-40}$$

Monetary and Life Loss Risk Profiles. Monetary and life losses were estimated and results were provided as elevation-loss curves per subbasins. Figure 9-13 provides example results for selected subbasins. Using results from Eq. 9-40 and elevation-loss curves per subbasin, loss-exceedance curves can be easily developed.

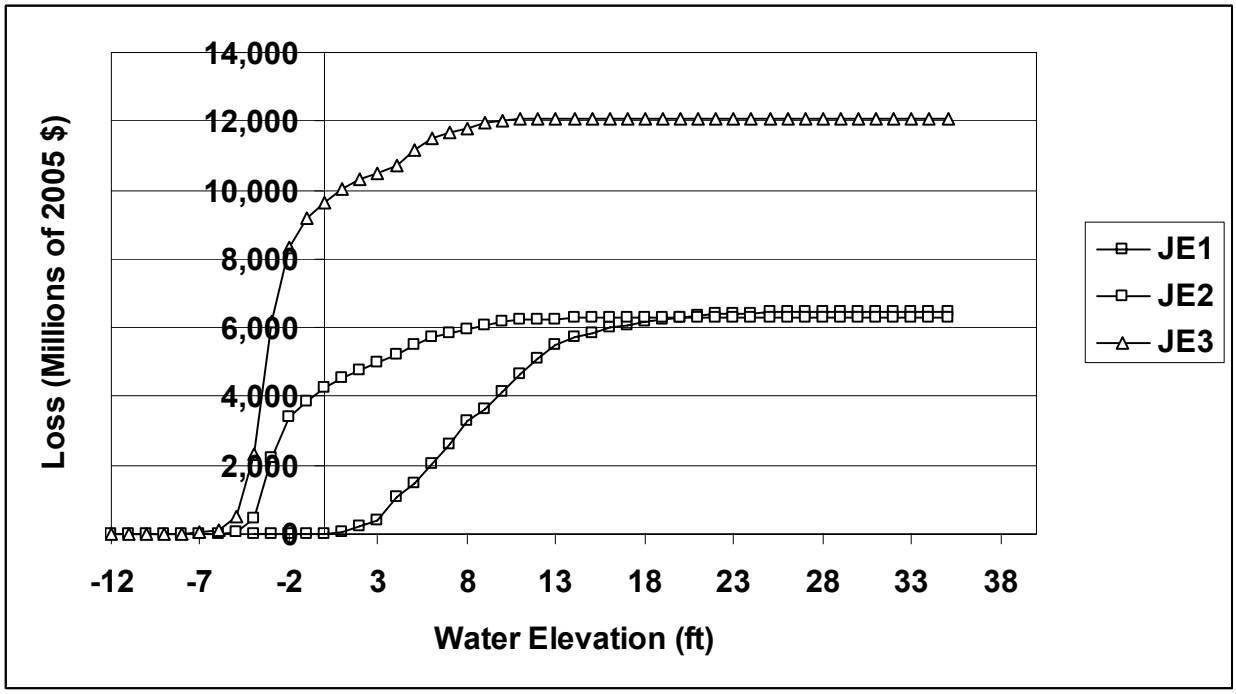

Figure 9-13. Elevation-Loss Curves for Jefferson East (JE) Subbasins

Risk Profile by Basins, Storm Categories, and for the region. The risk profiles for basins and storm categories can be evaluated by performing the corresponding aggregation similar to what is done for the sub-basins, and results can be displayed using similar curves to the ones provided in Figure 9-14. The risk profile for the region can only be expressed in the direct and indirect consequence scales (monetary and life losses). This risk profile for the region requires evaluating per storm all combinations of all the branches for all the basins with dependency modeling. The number of combination per storm is n^m, where n = number of basins and m = the number of branches in the event tree. For example, with $n = 8$, and $m = 10$, the number of combinations per storm is 1,073,741,824 combinations. Dependency among the basins has not been examined and therefore not understood. Without the appropriate representation of dependency among the basins, any regional risk profile would have some value although limited.

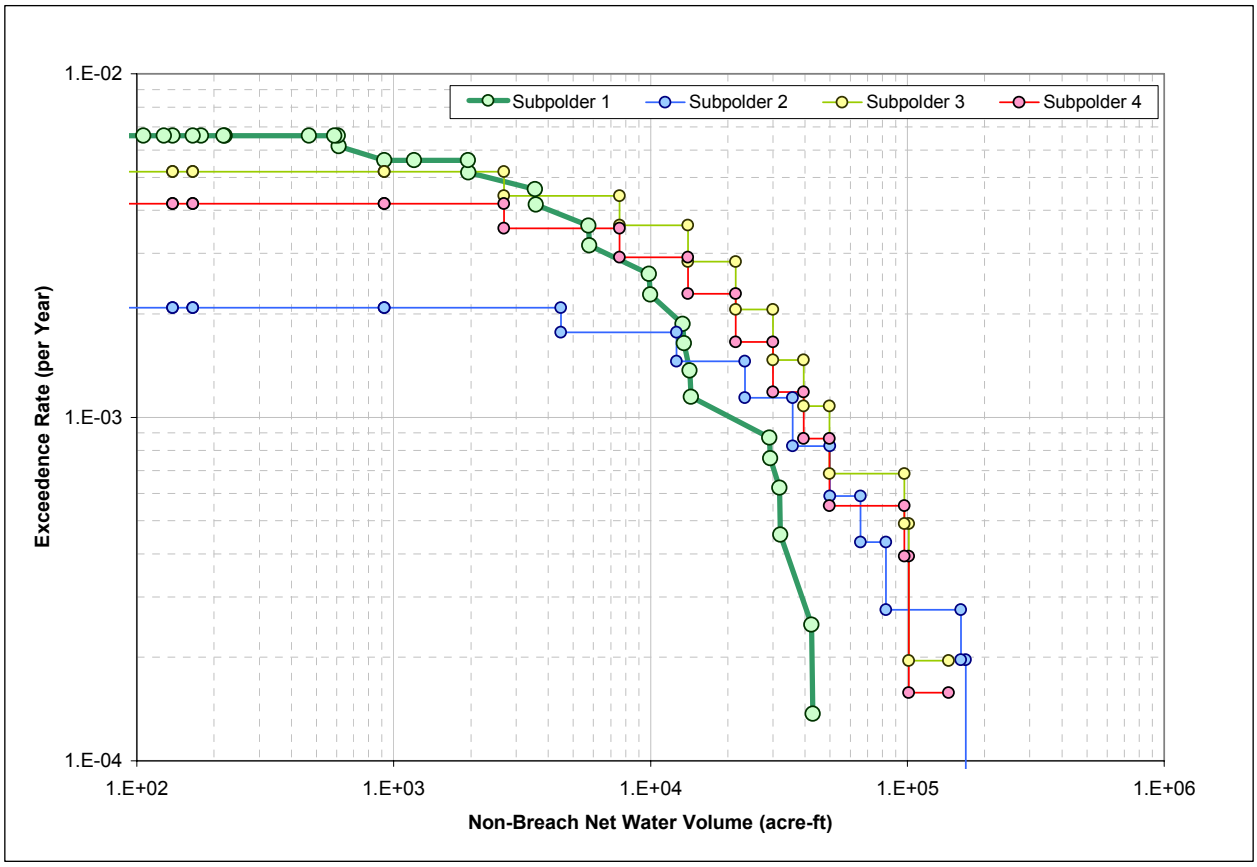

Figure 9-14. Overtopping Risk Profile for Subbasin

Appendix 10
Reliability Modeling

Reliability Analysis

Reliability analysis is that part of the risk study that leads to an evaluation of the conditional probability of failure (i.e., reliability) of structures, systems, and components when they are exposed to the loads of a hurricane. The reliability analysis had three steps:

1. Specify the structures, components, and systems constituting the hurricane protection system (HPS) for each drainage basin.
2. Define failure and identify failure modes and limit states for each structure, system and component.
3. Assign conditional probabilities to HPS failure states for given water elevations caused by hurricane conditions.

Two conditions were analyzed for the reliability of levees, flood walls, and pumping stations: pre-Katrina and post-reconstruction and repair as projected for June 2006.

Appendices B through G contain an inventory of the structures, systems, and components in each drainage basin that were considered in the risk analysis. Subsystems and components of the HPS are shown in Table 10-1.

Approach

The reliability of the hurricane protection system under potential water elevations due to surge and waves was quantified using structural and geotechnical reliability models integrated within a larger system description of each drainage basin. The reliability models for the HPS components were developed based on design and construction information, and on the results of the Performance Team and the Pump Stations Team studies. Reliability models were developed and evaluated to determine dominant, or most likely, failure modes for each reach defined in a drainage basin.

Table 10-1
Components in the Hurricane Protection System.

1	Levees	a. Embankment section (Reaches were defined on the basis of physical discontinuities - geometric, physical, soils, and construction characteristics) b. Foundation
2	Floodwalls	a. Wall structure b. Joints within a wall section c. Transitions (joints and interfaces to other components) d. Wall-embankment interface e. Wall foundation
3	Closures	a. Closure support structure b. Closure structures - logs, gate, or other c. Position – open or closed
4	Pump Systems	a. Pump and motors b. Power – grid availability c. Emergency power (diesel generator) d. Diesel fuel availability e. Pump house structure f. Operators – present or evacuated g. Intakes – open or closed

The reliability models included uncertainties in structural material properties, geotechnical engineering properties, subsurface soil profile conditions, and engineering performance models of levees, floodwalls, and transition points. Uncertainties due to spatial and temporal variation, and due to limited knowledge are tracked separately in the analysis, providing a best estimate of the frequency of failure under given loads, along with a measure of the uncertainty in that frequency.

The HPS was comprised of levees, flood walls, levees with floodwalls on top, and various points of transition or localized facilities such as pumping stations, drainage works, pipes penetrating the HPS, and gates. Each drainage basin perimeter was divided into segments, referred to as reaches, which were deemed to be homogeneous in three respects: structural cross-section, elevations in the cross section, and geotechnical cross-section. For example, 30 such reaches were identified for the New Orleans East (NOE) drainage basin.

Geometric and engineering material properties were identified for each reach and summarized in data tables. Structural cross-sections were initially identified by review of as-built drawings, aerial photographs, and GIS overlays; and were subsequently confirmed in on-site reconnaissance. Elevations were assessed in the same reconnaissance, supplemented by LIDAR and field surveys provided to the Risk Team. Geotechnical cross-sections and corresponding soil engineering properties were derived from original USACE General Design Memoranda (GDM) for the respective project areas of each drainage basin, supplemented by site characterization data collected post-Katrina at levee and flood wall failure sites (cone penetrometer and laboratory measurements on undisturbed samples).

Engineering performance models and calculations were adapted from the GDM's. Engineering parameter and model uncertainties were propagated through those calculations to obtain approximate fragility curves as a function of water height for components of the HPS. These results were calibrated against the analyses of the Performance Team, which applied more sophisticated analysis techniques to similar structural and geotechnical profiles in the vicinity of failures. Failure modes identified by the Performance Team were incorporated into the reliability analyses as those results became available.

Reliability assessments were performed for individual reaches of the HPS for given water elevations. This resulted in fragility curves for each reach by mode of failure. A fragility curve gives the probability of failure, conditional upon an event (water elevation in this study), at which a limiting failure state is exceeded.

Reliability assessments for each reach and component of the drainage basin perimeter were combined in the HPS risk model. The risk model used the water elevations from the hurricane hazard and the HPS fragilities to calculate probability of volume and duration of flooding within each drainage basin. The system risk model is structured around an event-tree description of the occurrence of hurricane events, corresponding water and wave heights, and the resulting response of the HPS. The risk model separately tracks natural variations and knowledge uncertainties from both the hurricane hazard and the structural and geotechnical response, to give a best estimate of frequency and duration of flooding, along with measures of uncertainty in those frequencies.

Definition of failure

Failures that lead to breach of the drainage basin perimeters were associated with four principal failure modes: (1) levee or levee foundation failure, (2) floodwall or floodwall foundation failure, (3) levee or floodwall erosion caused by overtopping, and (4) failure modes associated with point features such as transitions, junctions, and closures. The Performance Team found no failures in the HPS which originated in structural failure of the I-wall or T-wall components. All documented failures at I-wall and T-wall locations were geotechnical in nature, with structural damage resulting from the geotechnical failures.

Each reach within the drainage basin perimeter was analyzed and tracked separately, so that the number of failed reaches and their location around the drainage basin perimeter was known for each repetition of the HPS risk model.

The pumping system may have had a mitigating effect on the water elevation of each drainage basin. If the capacity of the pumping system was exceeded by the inflow volume from a single breach then the number and location of the breaches may not matter and the pumping system can be ignored in the risk analysis. If, however, the inflow volume is within the capacity of the pumping system to remove, then the probability that the pumps are operating must also be calculated.1

The Risk Team has relied on other IPET Teams to clarify technical issues. Technical input from other Teams helped the Risk Team determine the level of detail with which failure states need to be represented.

Hurricane Protection System

The HPS for each drainage basin has four components: (1) levees, (2) I-walls (which may be atop levees), (3) T-walls (which may be atop levees), and (4) transitions and closures. The

[1] Data for evaluating the effect of pump station operation on basin water elevations was not available for the HPS risk analysis.

reliability analysis examined the performance of the each of component, separately and in combination.

The following structures in the HPS were not independently evaluated for their failure modes: (1) concrete aprons associated with some I-walls, and (2) sheetpiles with a short (3 to 4 ft.) concrete cap. Either could be addressed with failure modes developed for I-walls, but were not included in the present study.

The following failure modes or contributing factors were not considered in the reliability analysis:

1. Internal erosion (piping) of levees due to seepage; note, this is in contrast to high pore pressures in sand strata, which was considered, as in the vicinity of the London Avenue Canal or the northern end of the IHNC. Internal erosion may be reconsidered in later studies.
2. The effects of maintenance on the HPS capacity over time. Improper maintenance or neglect can lead to reduced capacity of the levees in particular; gates and other moving components also require maintenance. Trees, landscaping, and pools were observed on protected embankments after Hurricane Katrina, indicating a lack of code enforcement and maintenance of the levees. However, there was insufficient information to include maintenance considerations.
3. Impact by a barge, floating debris, or other large object on the floodwalls or levees.
4. Failure of 3-bulb water stops between I-wall sections.

Component Performance

For each component, a performance level was defined such that its occurrence corresponded to a failure to perform an intended function. The critical components within the HPS, as stated above, are the levees, I-walls, T-walls, and transitions and closures. These components can fail in a variety of modes. For each mode of failure a limit state was defined, which, if it were to occur would result in a failure to keep water out of the drainage basin.

Engineering models of the mechanics of component performance are limited in their ability to explicitly model a failure state. As a result, an analysis is usually carried out for incipient failure by examining the limits of stability. If this state is equaled or exceeded, the structure or component is expected to fail to perform as intended. Incipient failure models were usually similar to design calculations, and in many cases were adapted from the GDM's.

For the purpose of evaluating the performance of the levees and floodwalls, *failure* was defined as complete breaching, which allowed water to enter the drainage basin. This failure occurred in two ways: (1) loss of levee or wall stability when the strength of the levee or wall and its foundation was insufficient to withstand the forces placed upon the structure for a given water elevation below the top of the wall or levee (no overtopping); or (2) overtopping caused the protected side of the levee or wall to erode substantially and result in a wall or levee breach, which allowed water to flow freely into the drainage basin.

System Failure

Depending on the performance of individual components in the HPS, various outcomes may result. For purpose of evaluating the performance of the HPS, the outcome of most interest is whether a protected area was flooded or not.

The HPS was assumed to fail if flooding occurred in a protected area, beyond that expected from rainfall and runoff which can be handled by pumping. Given this definition, a failure of the HPS occurred even if the components making up the system did not fail, for example, if levees or walls were overtopped but not breached.

Flooding can occur as a result of chains of events occurring individually or in combination. Among these are:

1. Levee or floodwall breaching.
2. Inflow into an area due to levee or flood wall overtopping that does not result in breeching, and which exceeds the capacity of the pumping system.
3. Inflow to an area that occurs as a result of rainfall.
4. Inflow to an area that occurs when the capacity of the pump system is exceeded as a result of backflow through pump houses.

Flooding that occurs as a result of rainfall or transient overtopping in most cases will not be as consequential and may be mitigated by the pumping system.

Uncertainties

There are two types of uncertainties. Aleatory uncertainties are those associated with natural variability, presumed to reflect an inherent randomness of natural processes, manifesting as variability over time for phenomena that take place at a single location (temporal variability), or variability over space for phenomena at that take place at different locations but at a single time (spatial variability), or as variability over both time and space. Epistemic uncertainties are those associated with lack of knowledge or information about events and processes, or lack of understanding of physical laws that limits our ability to model the real world.

Aleatory and epistemic uncertainty affect the outcomes of a reliability analysis in different ways. Aleatory uncertainty manifests as variations, or frequencies of occurrence, over space or time. Epistemic uncertainties manifest as statistical error and systematic biases in probability estimates, and may introduce correlations among aleatory frequencies.

Four categories of uncertainty were included in the reliability analysis:

1. Geological and geotechnical uncertainties, involving the spatial distribution of soils and soil properties within and beneath the HPS.
2. Structural uncertainties, involving the performance of man-made systems such as levees, floodwalls, and point features such as drainage pipes; and the engineering modeling of that performance, including geotechnical performance modeling.

3. Erosion uncertainties, involving the performance of levees and fills around floodwalls during overtopping, and at points of transition between levees and floodwall, in some cases leading to loss of grade or loss of structural support, and consequently to breaching.
4. Mechanical equipment uncertainties, including gates, pumps, and other operating systems, and human operator factors affecting the performance of mechanical equipment.

The reliability analysis takes water elevations from hurricane loading conditions as given, and calculates conditional probabilities of failure for specifically stated water elevations. Thus, hurricane effects, wind loads, water heights, and other factors of the loading conditions are not considered to be uncertainties in the reliability modeling. Uncertainties in water elevations from hurricane conditions are convoluted with the results of the reliability analysis in the systems risk model to generate marginal (i.e., unconditional) probabilities.

Geological profile

The stratigraphy of the New Orleans area is Pleistocene and Holocene in age. Observed levee and floodwall failures during Katrina principally involved shallow Holocene aged sediments. Generally, sediments constituting the New Orleans area are less than 7,000 years old (Holocene). Formation of the present day New Orleans began with the rise in global sea level, beginning about 12,000 to 15,000 years before present.

A typical profile for much of the New Orleans HPS shows a layer of fill at the top, underlain by organic clays ('marsh'), in turn underlain by lacustrine (distributary) plastic clays, in turn underlain by stiffer Pleistocene clays. Figure 10-1 shows the profile under the New Orleans East (NOE) Lakefront Levee which is typical of this profile.

As sea level rise slowed, five short-lived delta complexes evolved across the Louisiana coast by depositing Mississippi River sediments through branching distributary channels. These channels transported and deposited fluvial sediments along the margin of the delta and built into shallow coastal water. Distributary channels from one of these, the St. Bernard delta, are responsible for filling the shallow Gulf waters in the greater New Orleans area (Frazier 1967). On top of these distributary clays grew Cypress swamps which would eventually become the marsh formations. On top of these came fills, mostly clayey, on which the present levees and floodwalls were constructed.

The spatial variability of this typical section has to do with variations in thickness of the various strata, and interbedding of sand or silt lenses and other local conditions. In some places, for example, the marsh can be thicker than average, as for example in the vicinity of the 17th Street Canal failures.

Equally important to the performance of levees in Orleans East Bank (OEB) and NOE is the Pine Island Beach deposit, a buried, barrier island or beach dating to ca. 5,000 years before present (see Figure 10-2). This feature extends northeast along the southern shore of Lake Pontchartrain, adjacent to and north of the Metairie and Gentilly ridges, former natural levees of

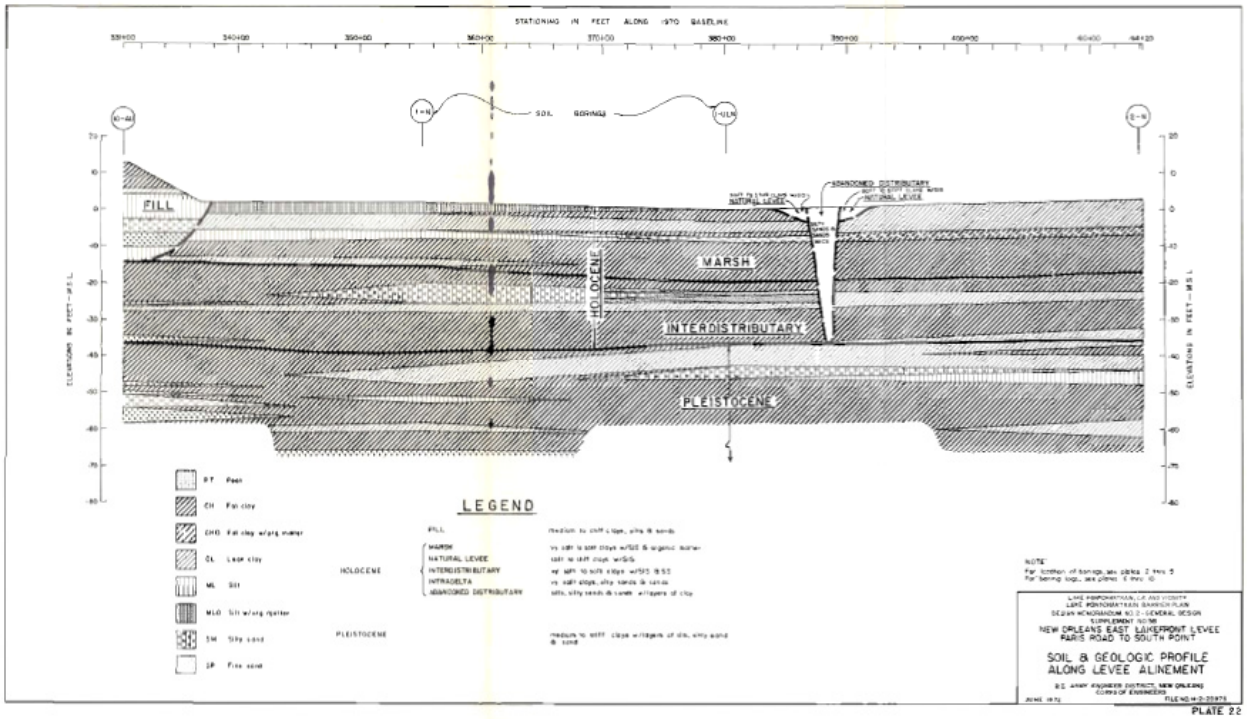

Figure 10-1. Typical geological profile, NOE lakefront section (USACE 1972).

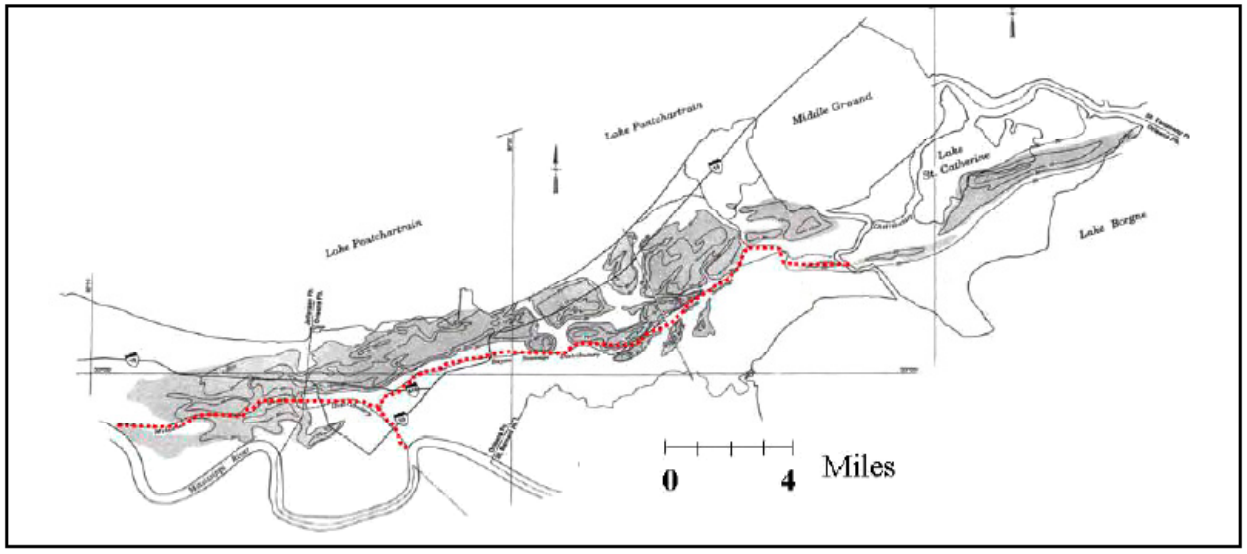

Figure 10-2. Pine Island (buried) beach ridge, and locations of the canal breaches (after Saucier 1994). The 17th Street breach is located behind the axis of the beach ridge while the London Canal breaches are located on the axis of the ridge. Bayou Metairie is identified in red and forms the Bayou Sauvage distributary course.

the Mississippi. Sea level was 10 to 15 ft lower than the current level when the beach ridge formed. Consequently, foundation soils beneath OEB and NOE are affected by this buried sand which provides a high permeability channel for pore pressures. Under the London Avenue Canal and the northern end of the IHNC, the sand rises close to the present ground surface.

Soil engineering properties

The principal uncertainty contributing to probability of failure of the levee and I-wall sections in the reliability analysis is soil engineering properties, specifically undrained shear strength, *Su*. Uncertainties in soil engineering properties are presumed to have two main components: (1) data scatter caused by actual variation of soil properties in space and by random measurement errors, and (2) systematic errors caused by limited numbers of measurements (i.e., statistical estimation error), and by measurement bias (see Figure 10-3).

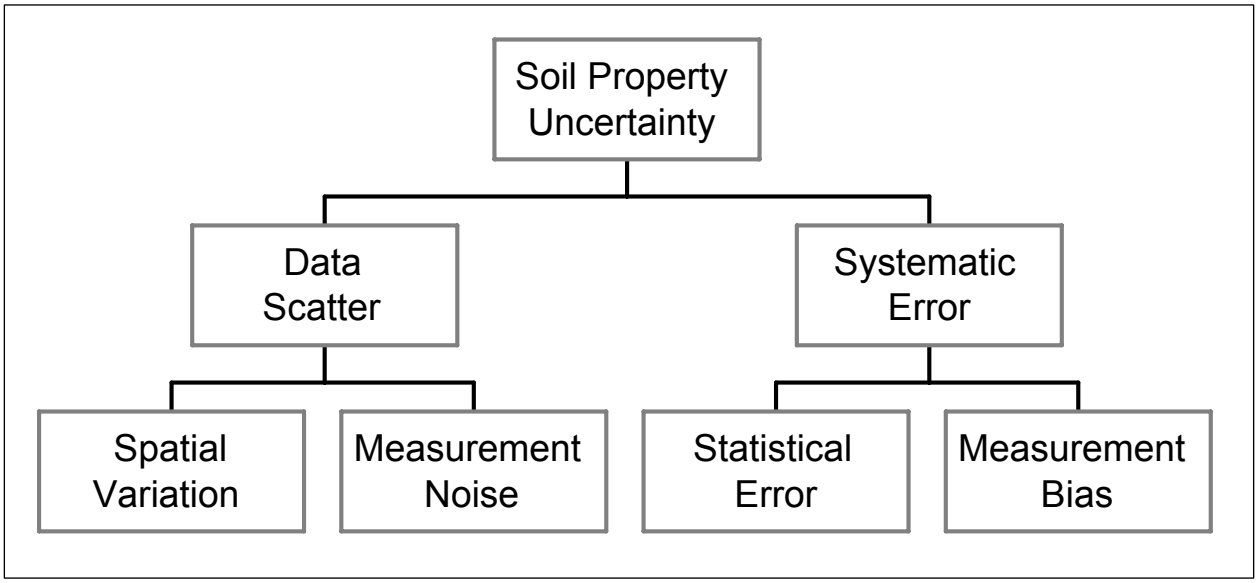

Figure 10-3. Sources of soil property uncertainty in geotechnical reliability model.

The variance in soil properties is a composition of these four terms,

$$Var(Su) = Var(x) + Var(e) + Var(m) + Var(b)$$

in which *Var(·)* is variance, *Su* is the soil property as input to the analysis (in this case, undrained strength), *x* is the soil property *in situ*, *e* is measurement error (noise), *m* is the spatial mean of the soil property (which has some error due to the statistical fluctuations of small sample sizes), and *b* is a model bias or calibration term caused by systematic errors in measuring soil engineering properties.

The NOE drainage basin is used here to describe the reliability analysis approach. Analyses of the other drainage basins are similar. The soil profile underlying NOE consists typically of clayey fill overlying 'marsh' (OH, CH), in turn overlying 'distributary clays' (CH), as shown in Figure 10-2. Critical sections in the GDMs and failures observed during Katrina occur in these uppermost strata. The engineering properties of deeper, stronger strata of the Pleistocene formations were not statistically characterized.

Measured Q-test results reported in the GDMs of NOE are shown as histograms in Figure 10-5. Second-moment statistical properties of these data are shown in Table 10-2. Test values larger than750 PCF were assumed to be local effects and removed from the statistics to the right in the table. These moments were used in subsequent calculations.

The spatial pattern of soil variability is characterized by autocovariance functions. These describe the covariance of soil properties as a function of separation distance. Soils whose properties vary erratically from spot to spot display little spatial covariance, while soils whose properties vary with more waviness display more spatial covariance.

The autocovariance function of a soil property z is defined as, $C_z(\delta) = E[z(i), z(i+\delta)]$, in which E[·] is expectation, *z(i)* is the soil property at some location *i*, and *z(i+δ)* is the property at another location at distance δ from the first. The autocorrelation function is found by normalizing the autocovariance by the variance, $R_z(\delta) = E[z(i), z(i+\delta)]Var^{-1}(z)$. The autocovariance distance is indexed as that separation distance at which $R_z(\delta) = e^{-1}$. This is a representative or characteristic length of the spatial correlation.

The autocovariance function can only be estimated for distances at least as great as the minimum spacing among observations, that is the minimum boring spacing in the present case. The minimum boring spacings in NOE are on the order of many hundred feet, with some spacings between adjacent borings as much as several thousand feet. To supplement the information in the GDMs, post-Katrina borings made in the vicinity of the 17th Street and London Avenue breaches were used to estimate autocovariance functions, and correspondingly the magnitude of measurement noise and the autocorrelation distance.

Statistical estimates of the autocovariance were made using the ESRI Geostatistical Analyst®, an application running in ArcMap®. Results for the undrained strength (Q-tests) of London Avenue the Distributary Clay clays are shown in Figure 10-4. Analyses for Marsh and Fill show similar patterns.

Soil strength is measured destructively, therefore replicate measurements cannot be used to estimate the magnitude of random measurement error. However, the spatial covariance structure provides an indirect way to make the estimate. Assuming that the measurement z of soil property x is corrupted by a zero-mean error e that is independent from one measurement to the another and independent of the value x, the measurement can be expressed as $z = x + e$. The autocovariance function of z is the summation of the autocovariance functions of x and of e: $C(z) = C(x) + C(e)$. But, the autocovariance function of e is a spike at the origin and zero otherwise. Thus, the difference between the intersection of the observed autocovariance function of z extrapolated back to the origin, and the total variance Var(z), provides an estimate of the variance of the error, Var(e).

The conclusions drawn from these autocovariance analyses were: (1) the measurement noise (or fine-scale variation) in the Q-test data is roughly 3/4 the total variance of the data (suggesting the COVs in the top row of Table 10-3; (2)the representative autocovariance distance in the

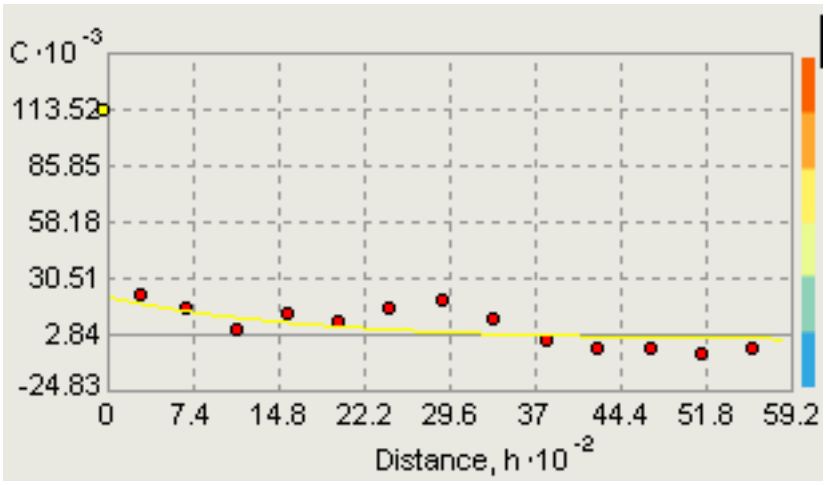

Elevation +5 to 0 feet

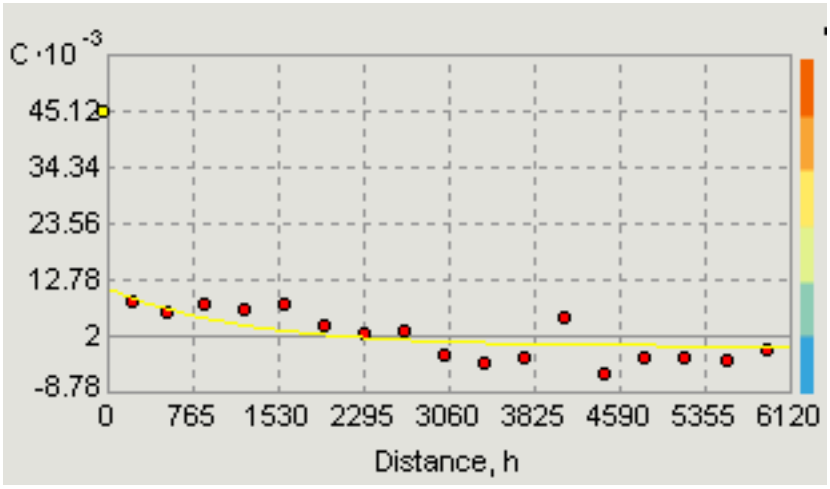

Elevation 0 to -10 feet

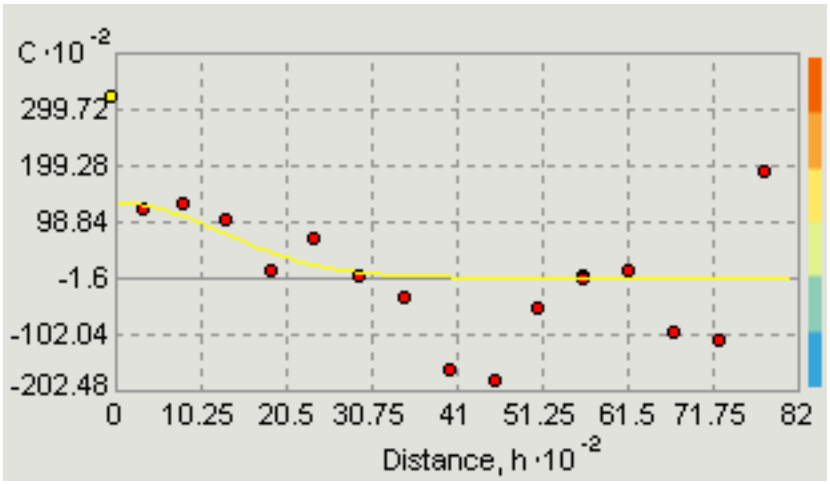

Elevation 10 to 20 feet

Figure 10-4. Estimated autocovariance function for CH soils in 17th Street Canal area post-Katrina borings, undrained strength (PCF) from Q tests

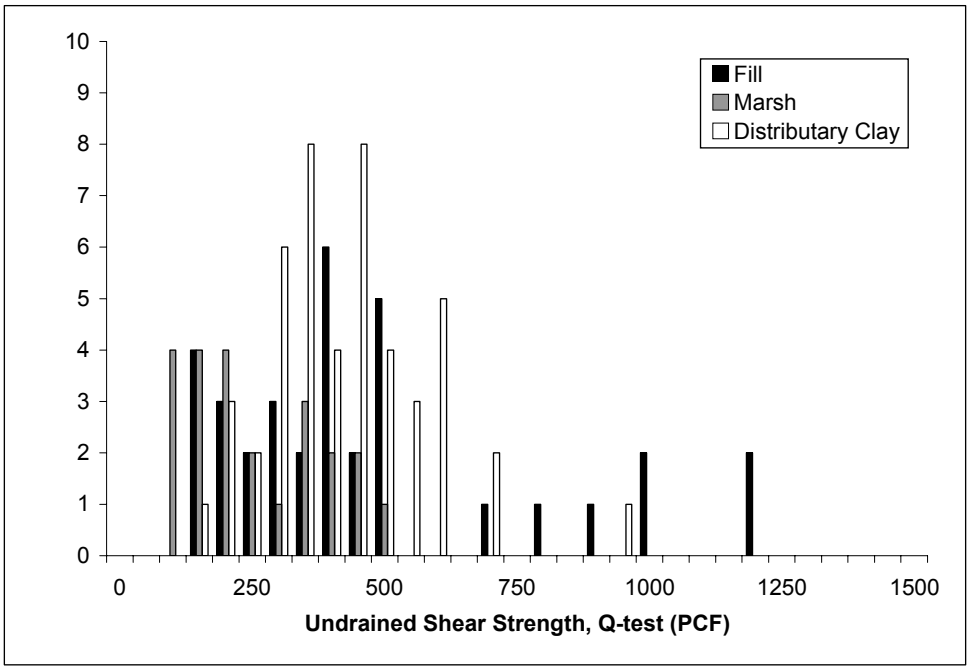

Figure 10-5. Histograms of undrained strength data (Q-tests), NOE General Design Memoranda: (black) Fill, (gray) Marsh, (white) Distributary Clay

Table10-2
Statistics of Undrained Strength Data (Q-tests), NOE General Design Memoranda. COV is the coefficient of variation, or standard deviation divided by the mean

	All data			Data less than 750PCF		
	Fill	**Marsh**	**D. Clay**	**Fill**	**Marsh**	**D. Clay**
Mean (PCF)	452	405	238	333	392	238
Std Dev (PCF)	297	154	124	142	132	124
COV (data scatter)	0.66	0.38	0.52	0.43	0.34	0.52

Table 10-3
Estimates of Component Uncertainties to Soil Engineering Property Model

	Fill	**Marsh**	**D. Clay**
Spatial COV	0.20	0.17	0.25
Number of measurements	48	21	23
Statistical error in mean	0.06	0.07	0.11
Model bias	0.1	0.1	0.1

horizontal direction is on the order of 1,000 feet; (3) the representative autocovariance distance in the vertical direction is assumed to be on the order of 1/100 of the horizontal distance, or about 10 feet, although there are too few Q-test data in individual borings to statistically estimate this value.

Statistical estimation error in the mean soil property is approximated from the standard error.[2] The variance of the error is approximated as $Var(m) \approx Var(x)/n$, in which m is the mean soil property, x is the spatial variation component of data scatter, and n is the number of measurements (Table 10-3).Model bias was calculated based on a comparison of the detailed modeling results of the Performance Team compared to the more simple general method of planes used in the GDMs. On average, the GDMs calculated factors of safety that were approximately 10% lower than more precise model analysis, varying from about 7% to about 18%.

Fragility curves

Fragility curves summarize the probability of components reaching their respective limit states (i.e., failure), conditioned on levels of water elevation from hurricane conditions. For example, the fragility curve of Figure 10-6 schematically represents the probability of failure by deep-sliding instability of a levee section as a function of water height. Design basis water elevation indicates the probability of failure at the design water level (i.e., 3 ft from the top of the levee).

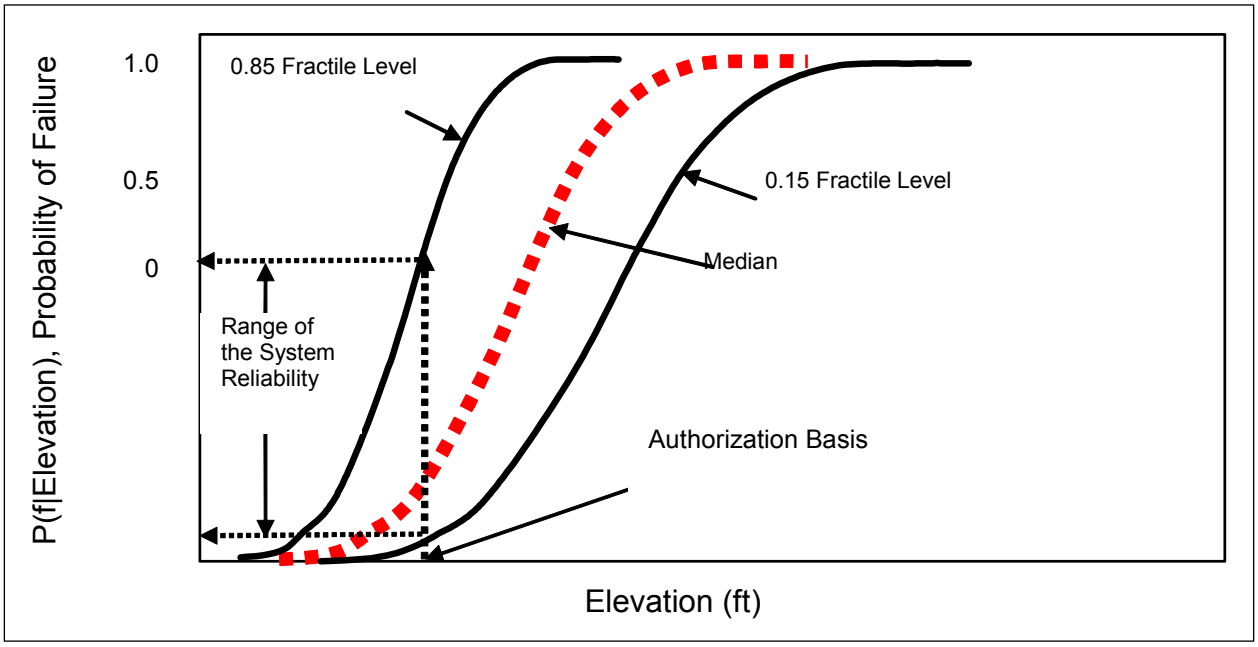

Figure 10-6. Schematic fragility curve

Fragility curves for levees and floodwalls were calculated for two conditions: (1) global stability without overtopping, for which reliability was calculated at two water elevations, design elevation and top of levee, and a smooth curve approximated to lower water elevation at sea level; and (2) overtopping with subsequent erosion, for which reliability was estimated from empirical experience during Katrina at four water elevations of overtopping: ½ foot, 1 foot, 2 feet, and 3 feet above the top of levee or flood wall.

[2] Although the standard error is a sampling distribution concept, it is approximately the *a posteriori* standard deviation in a Bayesian sense.

Once the fragility curves for each component failure mode was determined, they were input to the HPS risk model, which is based on event tree analysis. For each sequence in the event tree, a 'sequence' fragility curve is determined by evaluating the event tree logic at each successive water elevation level. Once each sequence of events has been evaluated, the composite or total fragility for system failure can be determined for each system performance state of interest (e.g., no flooding has occurred in any area protected by the HPS, or flooding occurred as a result of levee or floodwall failure, or flooding occurred as a result of overtopping) by simply summing the fragility curves for the sequence of events for the same state.

Reliability assessments were performed for individual reaches of approximately homogeneous structural type, elevation, geotechnical conditions, and water elevations. This resulted in fragility curves for each reach by mode of failure. Such fragility curves represented the aleatory (i.e., random) uncertainties from one hurricane to another. These fragility curves were offset to include epistemic uncertainties.

Levee fragility, no overtopping

Engineering performance models were adapted from the GDM for the respective reaches of levee. Engineering parameter and model uncertainties were propagated through those calculations using a first-order second-moment approximation to obtain approximate fragility curves as a function of water height. The geotechnical models used in the GDMs were calibrated against the analysis work of the Performance Team which used more refined calculations.

The reliability analysis was based on limiting equilibrium calculations of factor of safety against instability. For levees, the analysis was based on GDM calculations of factor of safety against wedge instability (Figure 10-7). The calculations were based on undrained (ϕ=0) failure conditions. Undrained strengths of soils underlying the levees and walls are based on Q-test (unconsolidated -undrained) results.

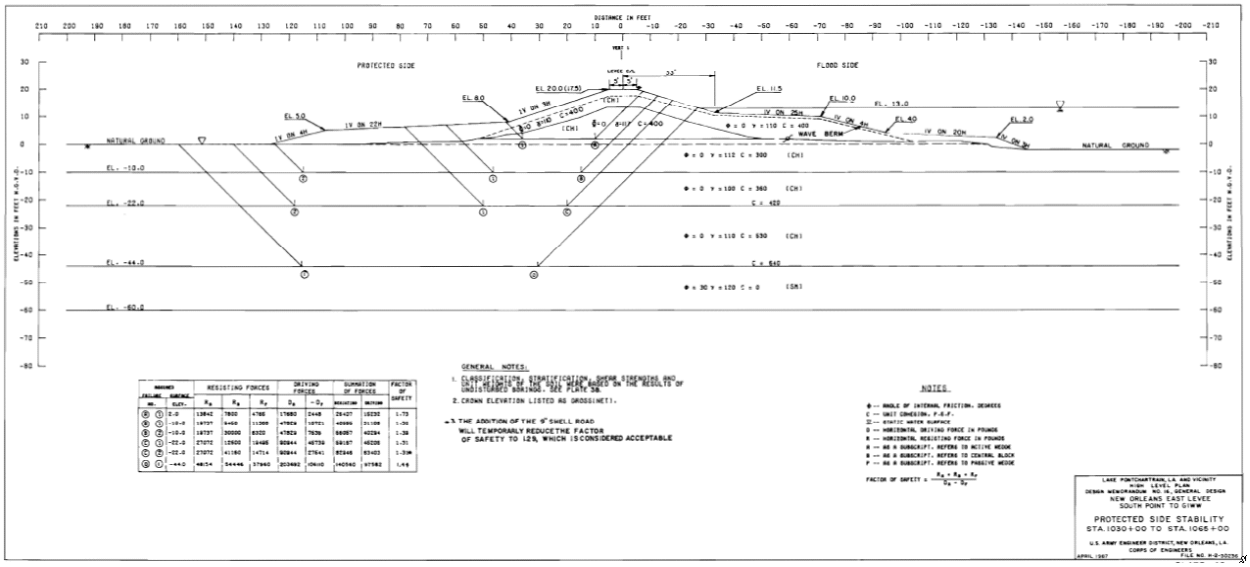

Figure 10-7. Typical wedge stability analysis of levee section from GDM (USACE 1972)

Best estimate calculations were based on average (mean) soil properties, adjusted from calculations in the GDMs, which used factored average soil properties. That is, the calculation of factor of safety in the GDMs was not based on mean observed undrained strengths, but factored strengths, using a reduction factor of 1.2 to 1.3. These were corrected for the reliability analysis to yield a mean factor of safety.

Uncertainties in undrained shear strength were propagated through the GDM calculations to estimate a coefficient of variation in the calculated factor of safety. The factor of safety was assumed to be Normally distributed, and a fragility curve was approximated through a limited number (typically two) of calculation points.

Soil property uncertainty in the form of coefficients of variation for undrained soil strengths underlying the levees and walls was propagated through the limiting equilibrium wedge stability calculations to obtain coefficients of variation on factors of safety, shown in Table 10-4. In most cases, the stability analyses were linear functions of undrained soil strength so that the coefficient of variation of the factor of safety was the same as the coefficient of variation of the input soil strengths. The mean factor of safety was taken as that calculated in the GDMs, adjusted for factored strengths.

Table 10-4
Uncertainty Analysis for Example Levee Reach in NOE

Water level	Design basis	¾ design basis	Top of levee
Mean FS	1.3	2	1.2
Spatial COV	0.17	0.17	0.17
Spatial average reduction factor	0.8	0.8	0.8
Systematic COV	0.07	0.07	0.07
Total COV	0.15	0.15	0. 15
Reliability Index, β	2.2	6	1.7
Pf for specific 1000 ft reach	0.014	0	0.045
Increase in Pf per 1000 feet reach	2%	0.0	5%

Fragility curves summarize the conditional probability of levee or wall failure as a function of water elevation. Calculations were made for a three specific water elevations: typically design water level, some level lower than design (i.e. sea level), and at the top of the levee or wall.

For a given water elevation, uncertainty in the realized factor of safety against sliding depends principally on the average soil strength, *Su*, across the area of the failure surface. This average strength varies from cross-section to cross-section because the soil properties themselves vary from spot to spot (Figure 10-8). The variability in the average soil strength is less than the variability in the point-to-point properties because, to some extent, the highs and lows of the soil strength balance against each other over the failure surface. The larger the failure surface relative to the autocorrelation of the soil properties, the greater the variance reduction from the local averages. Vanmarcke (1977) has shown that the variance of the spatial average for a unit-width plain strain cross section decreases approximately in proportion to (L/r_L), for $L>r_L$, in which L is the cross-sectional length of the failure surface, and r_L is an equivalent autocovariance distance

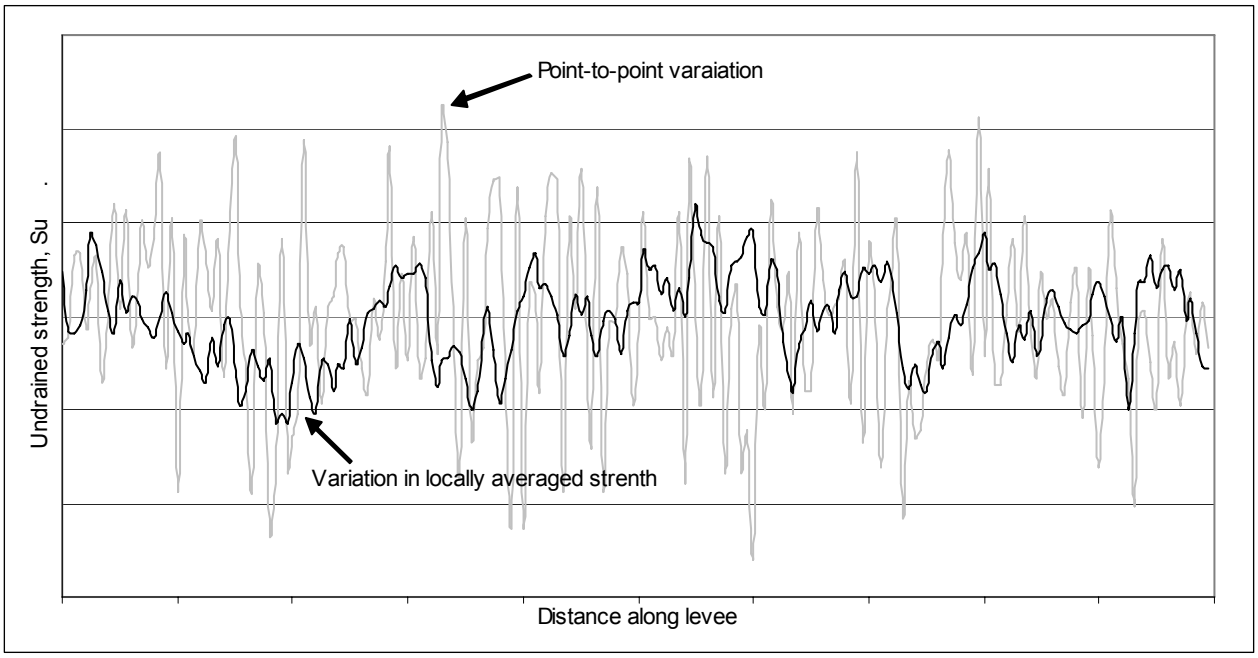

Figure 10-8. Point variation in undrained strength and variation among locally averaged strength

of the soil properties across the failure surface weighted for the relative proportion of horizontal and vertical segments of the surface. For the wedge failure modes this is approximately the vertical autocovariance distance. The variance across the full failure surface of width *b* along the axis of the levee is further reduced by averaging in the horizontal direction by an additional factor (b/r_H), for $b>r_H$, in which r_H is the horizontal autocovariance distance. At the same time that the variance of the average strength on the failure surface is reduced by the averaging process, so, too, the autocovariance function of this averaged process stretches out from that of the point-to-point variation.

For a failure length of approximately 1000 feet along the levee axis and 30 feet deep, with horizontal and vertical autocovariance distances of 1000 feet and 10 feet, respectively, the corresponding variance reduction factors are approximately 0.75 for averaging over the cross-sectional length *L,* and between 0.73 and 0.85 for averaging over the failure length *b*, assuming either an Exponential or squared-exponential (Gaussian) autocovariance. The corresponding reduction to the COV of soil strength based on averaging over the failure plane is the root of the product of these two factors, or between 0.74 and 0.8.

The Reliability Index for the specific levee reach of length *b* is the number of standard deviations separating the mean condition from the limiting state,

$$\beta_b = \frac{E[FS]-1}{Var(FS)} = \frac{E[FS]-1}{\Omega_{FS} E[FS]}$$

in which *E[FS]* is the mean factor of safety, *Var(FS)* is the variance, and Ω_{FS} is the COV.

For a long levee, the chance of at least one failure is equivalent to the chance that the variations of the mean soil strength across the failure surface shown schematically in Figure 10- drop below that required for stability at least once along the length. Vanmarcke (1977) has shown that this can be determined by considering the first crossings of a random process. The approximation to the probability of at least one failure as provided by Vanmarcke (1977) was used in the calculations. A typical fragility curve for one reach is shown in Figure 10-9.

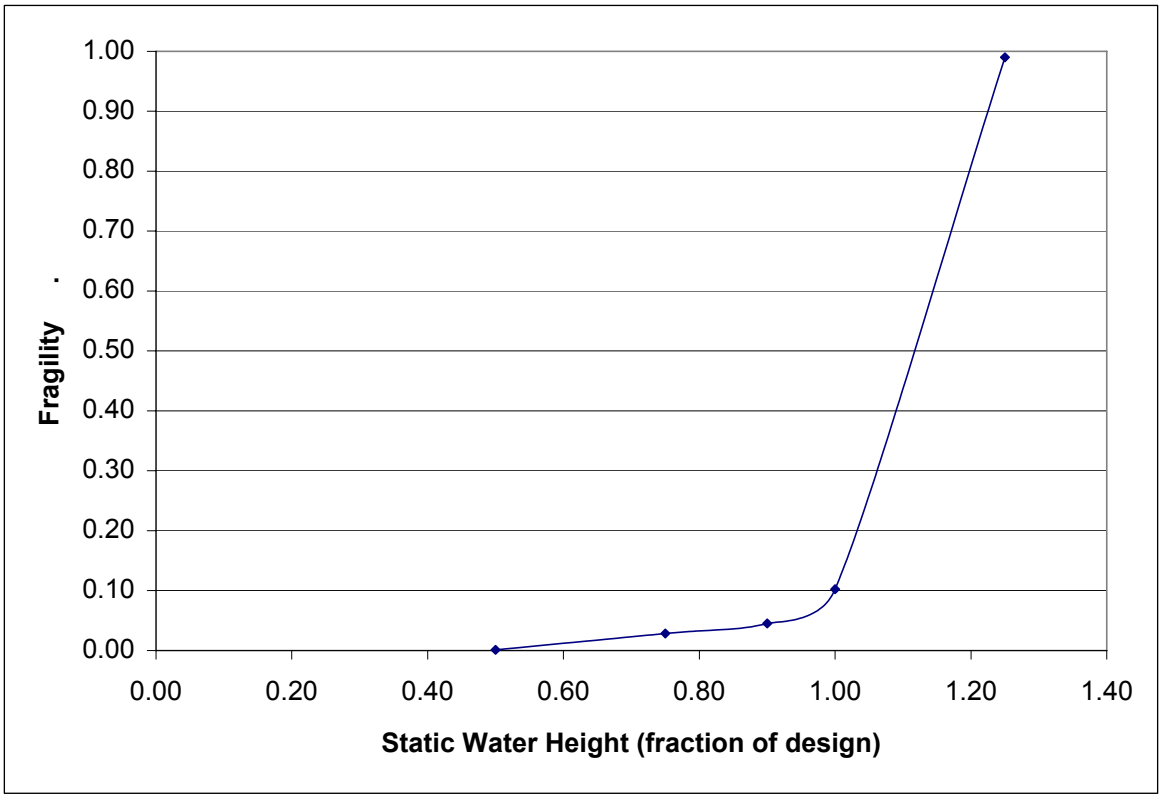

Figure 10-9. Fragility curve for Reach NOE15, New Orleans East Back Levee, combined aleatory and epistemic uncertainties.

The calculations above, based on limiting equilibrium of wedges, were calibrated to the Performance Team's circular arc and finite element analyses to correct for model bias.

The shear resistance of the soils was reduced as seepage occurs until the flood-induced loads exceed the soil shear capacity. A failure along the wedge lines of least resistance (or factor of safety) due to excess pore pressure led to a shear failure in the soil. Reliability calculations were based on the probability that shear capacity of the saturated soils was exceeded by the loads on the levee for a given water elevation.

I-Wall fragility, no overtopping

The reliability analysis for I-walls was similarly based on limiting equilibrium calculations of factor of safety against instability. For I-walls, the analysis is based on the Performance Team's mechanism of cracks developing in the soil immediately behind the wall and sheetpile, allowing

hydrostatic pressure on the sheetpile. The equilibrium of a soil wedge to the protected side of the wall (Figure 10-10) was calculated for this condition. The calculations were based on undrained ($\phi = 0$) failure conditions. Undrained strengths of soils underlying the levees and walls were based on "Q-test" results. The design consideration of balancing forces and moments on the sheet pile to determine depth of penetration was considered immaterial to the reliability analysis of the wall sections.

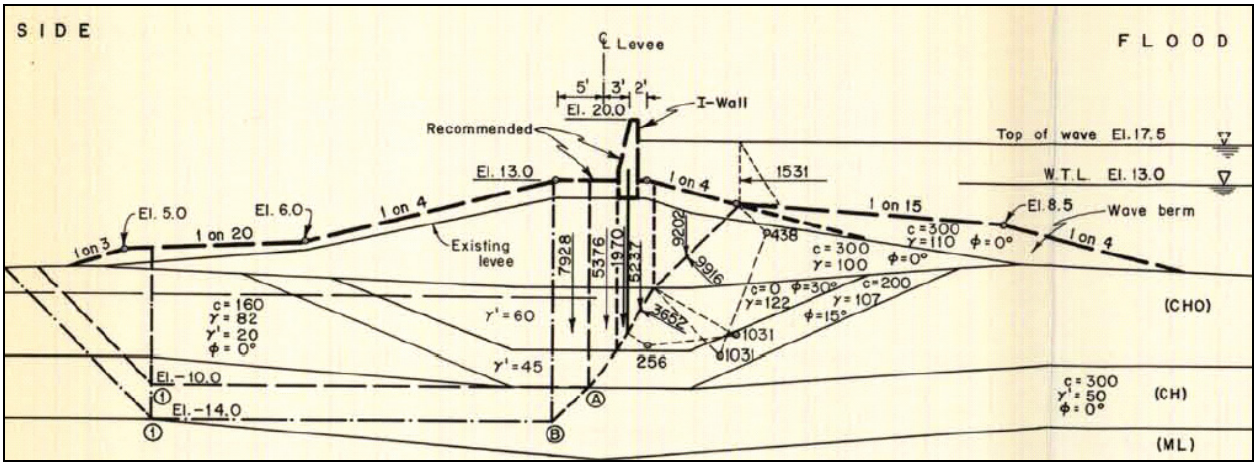

Figure 10-10. Sheet pile failure by deep wedge instability

Based on the results of the Performance Team's analyses, it was assumed that cracking initiated at 5 feet of water elevation on an I-wall. Thus, for water elevations lower than 5 feet, the factor of safety was that calculated in the GDMs. But at 5 feet, when a crack formed in the soil, the factor of safety underwent a step change to a forward (protected side) wedge failure.

If soil separations developed in front of the sheetpile or the levee, the condition resulted in increased hydrostatic forces on the flood side of the I-wall and the levee. If the separation was of sufficient depth, the hydrostatic forces on the wall may exceed the shear strength of the supporting soil and cause failure along wedge lines of least resistance behind the sheetpile. Reliability calculations were based on the probability that shear resistance of a wedge was exceeded by the loads on the levee and floodwall for a given hurricane.

Levee and I-Wall fragility, with overtopping

Reliability calculations were based on the probability of overtopping causing erosion of the protected side of a levee that led to a breach. Two approaches were considered: The first approach considered flow velocities over the levee. The second approach considered water elevation, which is estimated by the storm surge modeling, as an indirect parameter of flow velocity.

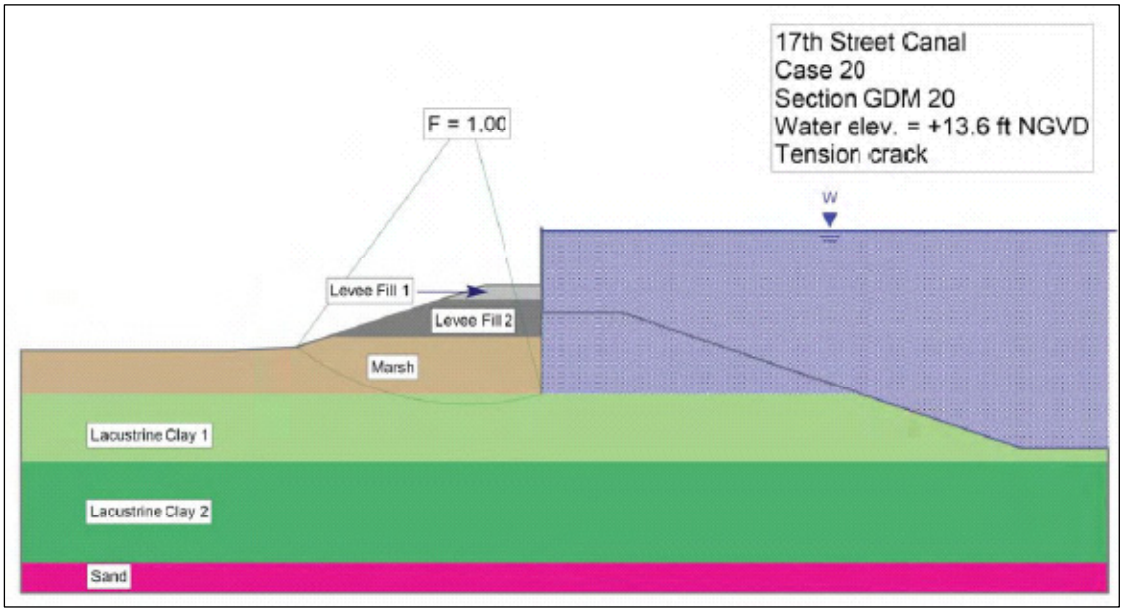

Figure 10-11. Failure Mode B4a. Failure by rotation of I-wall, reducing I-wall elevation

Based on the Performance Team's results, the probability of erosion breaching was considered to be negligible for floodwall sections, and related to the presence of significant depth of hydraulic fill for levee sections. The fragility curve for levee sections was assumed to be that of the static failure analysis (above) up to the point of overtopping, and then a step function to Pf = 1.0 for those sections with significant depths of hydraulic fill. For levee sections without significant hydraulic fill, the fragility curve remained flat at the top of wall fragility for overtopping.

Figure 10-12 shows fragility curves developed for reaches defined in the Jefferson drainage basin. The fragilities values were developed as described in the preceding sections for conditions of no overtopping (water elevations up to the top of the wall or levee) and overtopping.

Transitions and Point Structures

A number of HPS breaches were observed at transitions between HPS components. These breaches were typically at levee to I-wall, levee to T-wall or I-wall to T-wall transitions. Many of the HPS breaches were at point structures such as gates (road and railroad), pump stations, or around drainage control structures. These transitions indicate a weak link in the HPS due to the differing stiffness of the components which permit them to become areas of significant erosion during a hurricane event.

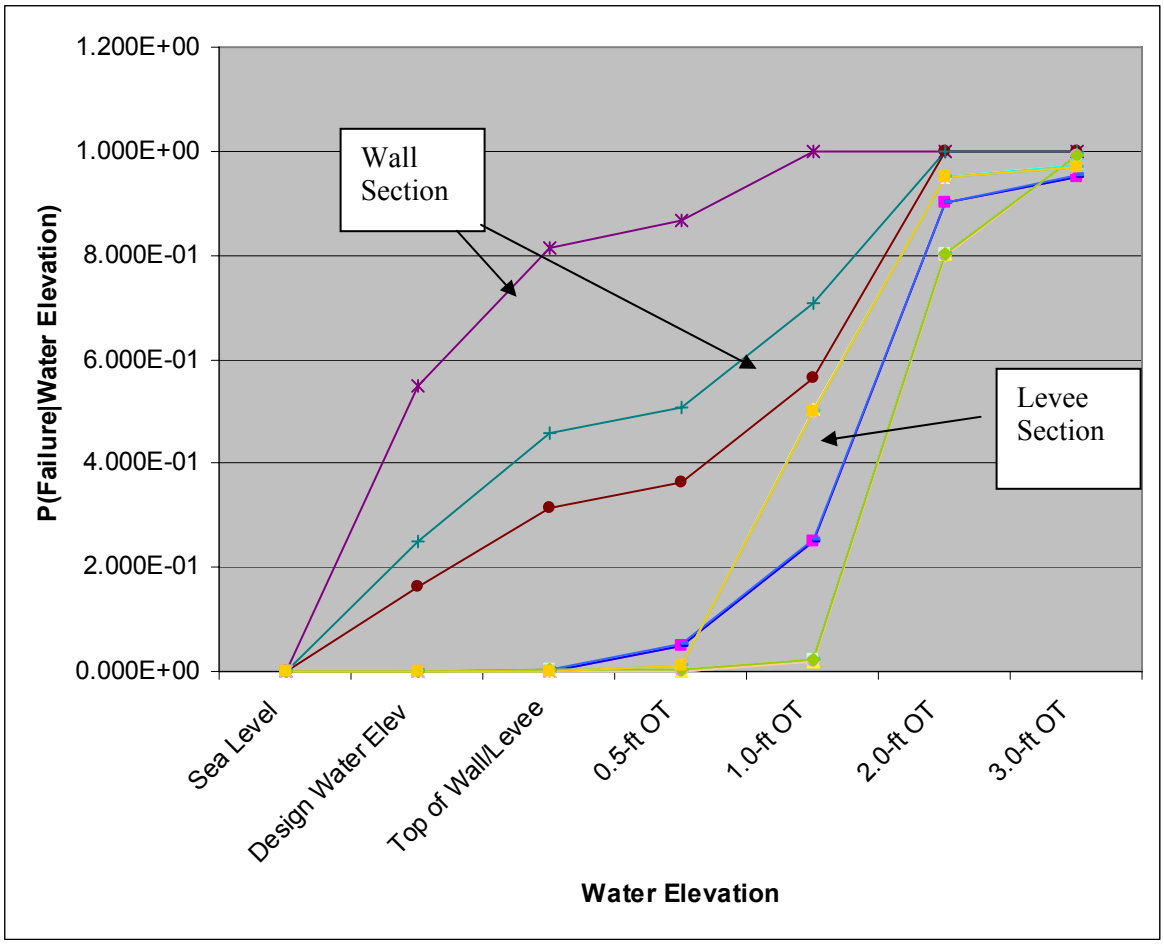

Figure 10-12. Fragilities for levees and walls in the Jefferson drainage basin

Many of these transitions zones failed use a "wrap-in" levee section to a more rigid wall structure. Instead, the levee sections sloped quickly away from the transition to expose the I- or T-wall. The steep slopes permitted a concentrated zone for the erosion of the levee that eventually exposed the I-wall or T-wall structure to additional loading and continued eroding. This dynamic process could lead to instability and collapse or damage to end sections of the wall. An example of a levee transition for a gate section on the east bank of the INHC is shown in Figure 10-13 below.

The failure modes for these transitions zones are complex and dynamic. The failure modes use the qualitative erosion parameters developed by the Performance Team as the basis for change in the stability of components at the transition zones. That is, the fragility of the transitions was taken to be similar to that of overtopped levee sections, and to depend on the combination of height of overtopping water and the presence of hydraulic fill enlargement to the levee section. Reliability for point structures (gates, control structures, pump stations) was taken as a point probability of failure for design loading.

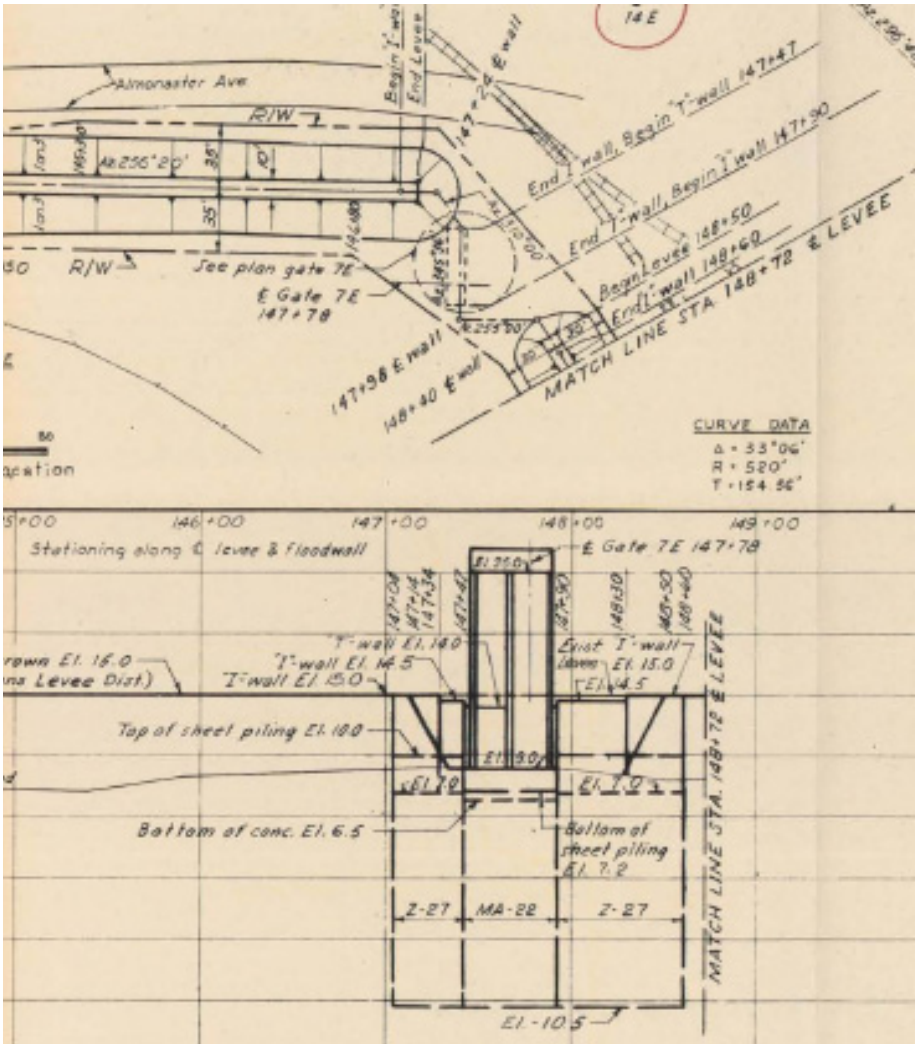

Figure 10-13. Example of Transition Zone for East Bank of INHC

Failure Mode 1–Scour and erosion caused point structure (i.e. drainage pipe) instability. A levee breach may occur due to loss of the I- or T-walls at a point structure and scour could create instability and collapse of the structure, resulting in a breached area.

Failure Mode 2–Breach occurs at the water stop between the I-wall and T-wall panel junction. This failure mode may be caused by differential displacement between panels and may develop tensile and shear forces in the water stop and panels. This may be due to levee erosion on the flood side or different rotation point between panels, or to lateral displacement of the levee from a foundation shear failure. This failure mode was not explicitly included in the risk calculations.

Failure Mode 3–Breach at the levee and I-wall transition. This failure mode occurs due to levee erosion on the protected side, where the erosion starts at the end of the levee transition and progresses back toward the I-wall, until the I-wall rotates toward the protected side. This was treated as Failure Mode 1.

Pumping Stations

The adverse performance of mechanical, electrical, and human elements of the HPS, such as pumps, the availability of power, and the closure of gates, is treated as random point (i.e., aleatory) events with discrete probabilities of failure based on the statistical record during Katrina and on information provided by other IPET teams.

The pumping stations are critical HPS system components because they maintain the flood levels on the protected side. Unfortunately, many of the pumping stations during Katrina reached and exceeded their pumping capacity shortly into the storm. Their reliability during Katrina was not exceedingly high as the stations primarily failed due to rising waters at the plants, a lack of external or backup power source, or were shut down due to inefficient pumping. These systems are designed to handle specific level of rainfall and are easily overwhelmed when the levees are overtopped by a hurricane event. The following failure modes were possible for the pumping stations: no commercial power, back up generator failed, mechanical fuel unavailable, pumps not functioning at time of incident, mechanical failure of components, operator unavailability, debris blocking intakes, or reversed or back flow through outfall pipes

The reliability of the pumping stations was included in the risk model as point sources. The reliability is based on data collected by the Pumping Team, performance data maintained by Task Force Hope, and information from the dewatering plan for New Orleans developed by the New Orleans District. The fragility curves for each pumping stations will be limited to a specific elevation or volume of water within the drainage basin. These fragility curves will vary for each pumping station and will reflect the interior drainage areas and back flow potential as determined by the Interior Drainage Team.

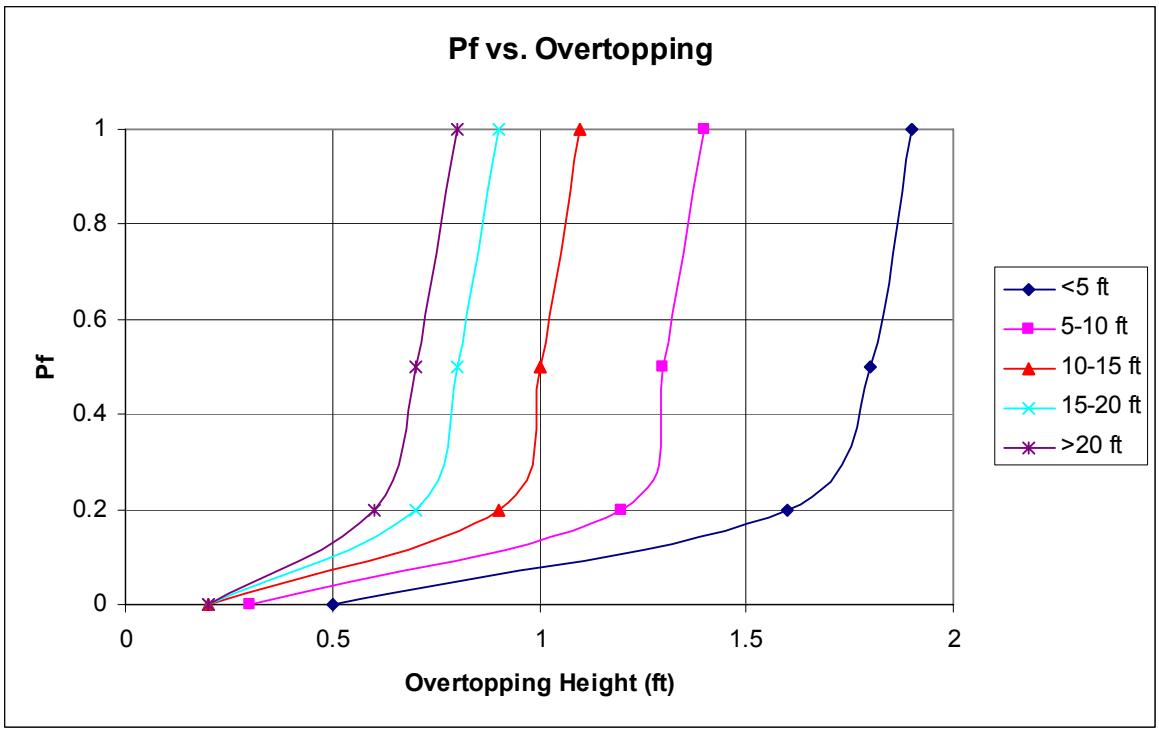

Figure 10-14.

Table 10-5				
	Height of Water Above Top of Levee (ft)			
Height of Levee (Top to Toe)	**Pf = 0.0**	**Pf = 0.2**	**Pf = 0.5**	**Pf = 1.00**
levee height < 5 feet (inclusive)	0.5	1.6	1.8	1.9
5 < levee height < 10 (inclusive)	0.3	1.2	1.3	1.4
10 < levee height < 15 (inclusive)	0.2	0.9	1.0	1.1
15 < levee height < 20 (inclusive)	0.2	0.7	0.8	0.9
levee height > 20 feet	0.2	0.6	0.7	0.8

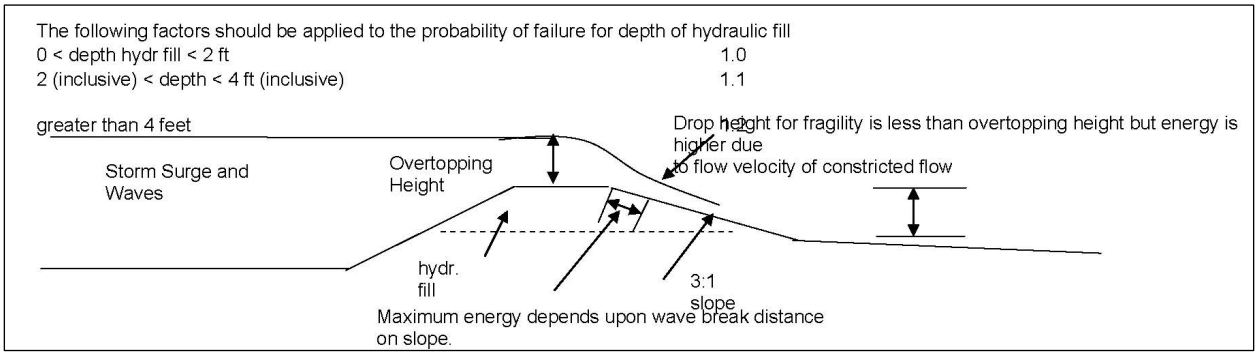

Figure 10-15.

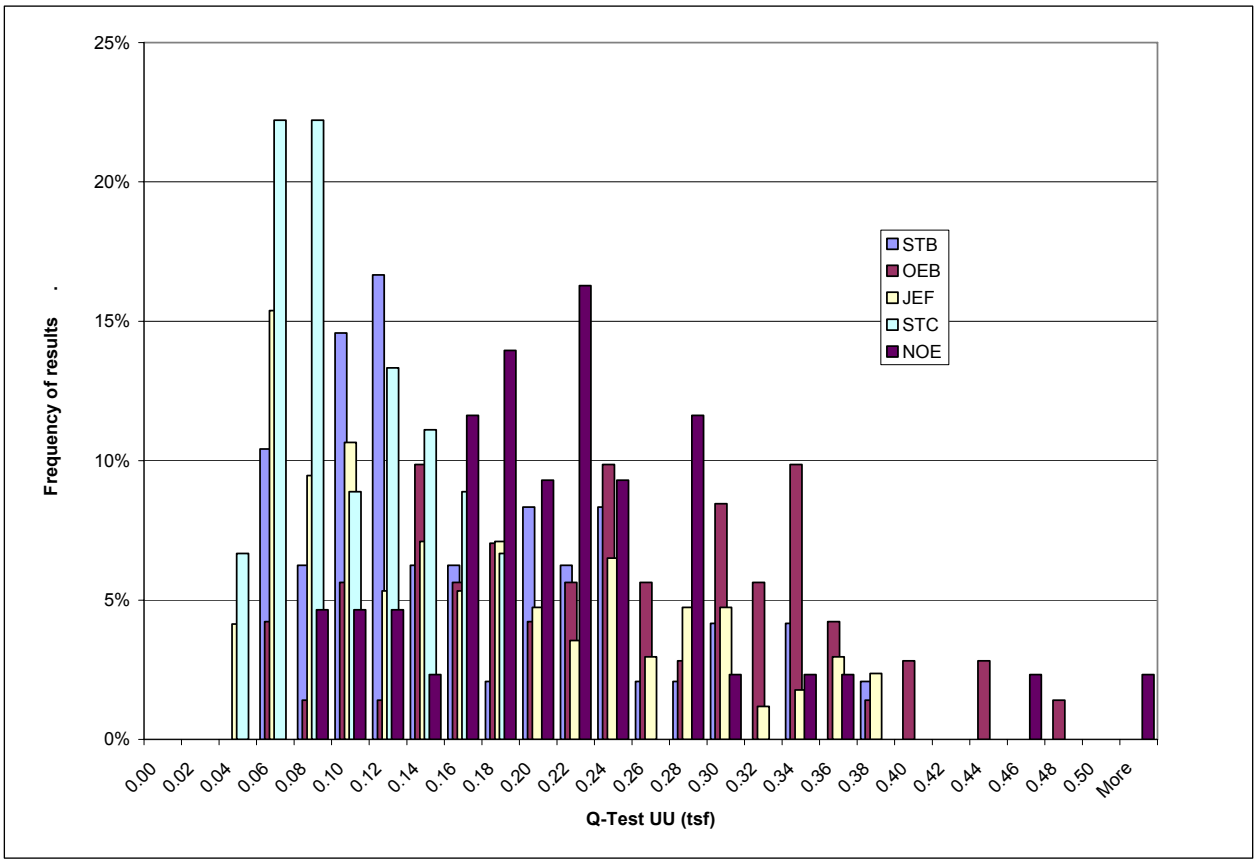

Figure 10-16.

Table 10-6

Parish	Mean Su (TSF)	Point COV	Point COV less noise	Spatial reduction	COV Averaged	N	Depth of data	Bound for outliers	Std Dev in mean
OEB	0.24	0.43	0.22	0.70	0.15	71	0 to -40	0.4	0.05
STB	0.16	0.53	0.27	0.70	0.19	64	0 to -40	0.4	0.07
NOE	0.22	0.58	0.29	0.70	0.20	43	0 to -40	0.4	0.09
STC	0.09	0.41	0.21	0.70	0.14	45	0 to -40	0.4	0.06
JEF	0.16	0.62	0.31	0.70	0.22	169	0 to -40	0.4	0.05

Appendix 11
Uncertainty Analysis

Introduction

The consequence vs. exceedance-frequency curves resulting from this risk analysis represent best estimates of risk. More formally, they describe either the mean or median estimate of the frequency of water levels, economic costs, or lives lost (Figure 11-1). Typically, they describe the median. The mean is the average over possible uncertainties in the risk estimate, while the median is the 50th percentile.

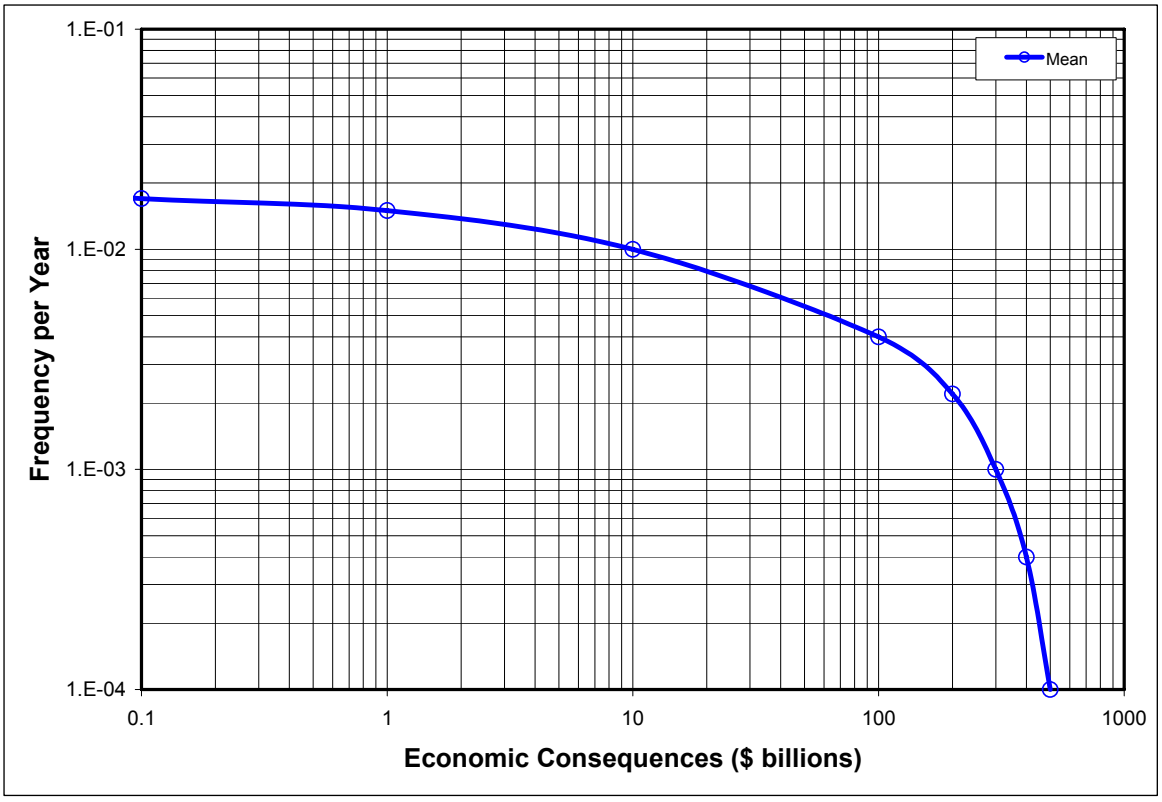

Figure 11-1. Illustration of Typical Risk Analysis Results for Economic Consequences. The best-estimate curve (here, the mean curve) shows the frequency with which events leading to the corresponding economic consequence occur per year.

There is uncertainty in the risk estimates because the models, parameter values, and assumptions entering the risk analysis may themselves contain uncertainty. For example, atmospheric or engineering performance models may be imperfect characterizations of reality, parameter values needed for those models may have to be estimated from limited numbers of data, and simplifying assumptions may be needed to make a calculation feasible. This Appendix discusses the types of uncertainty in the calculated risk assessments, how those uncertainties arise, and the magnitude of aggregate uncertainty.

Types of Uncertainty in Risk Estimates

Two distinct types of uncertainty affect the estimation of the frequency of future events and corresponding consequences. The first is those uncertainties assumed to be caused by inherent randomness in nature. Natural processes such as rainfall, surge elevations, and soil properties vary in either time or space or both. These variations are usually modeled as if they arise from a naturally random process. Many scientists would say that such temporally or spatially variable natural phenomena are not, in fact, random, but follow deterministic laws of physics. Nevertheless, it is both convenient and traditional practice to model them as if they were random. These events are predicted by their chance of occurring within some interval of time or some region of space (e.g., much like the chance of 'heads' in a coin flip). This source of uncertainty is known as *aleatory uncertainty*, after the Latin word for gambler or dice thrower (Hacking 1975).

The second type of uncertainty is that associated with our lack of knowledge or information. For example, the ability to determine the likelihood of an event (i.e., its rate of occurrence) requires that certain data be available. Depending on the volume of data that is available, the accuracy of the estimate of the rate of occurrence will vary. If limited data are available, the estimated rate may be quite uncertain (i.e., statistical confidence intervals on parameter estimates will be large). A second type of knowledge uncertainty is attributed to our lack of understanding about physical processes that must be modeled (e.g., the meteorological processes that generate hurricane events). Often scientists and engineers have interpretations of existing data and models of physical processes of interest that often competing in the sense they lead to different results, while at the same time are consistent with observations. In these instances expert evaluations are often required to assess the current state of knowledge and to quantitatively evaluate the level of uncertainty. These sources of uncertainty are referred to as *epistemic uncertainties*, after the Greek word for knowledge.

The distinction between what is aleatory and what is epistemic uncertainty is a modeling decision, and can sometimes seem arbitrary. For example, the distinction depends on the models that are used in a particular analysis. In addition, the estimates of the relative proportion of total uncertainty that is attributable to aleatory vs. epistemic sources can change in time as models or understand change. Nonetheless, making a distinction between the sources of uncertainty in logical manner helps insure that all uncertainties are quantified and those that can be reduced with additional data or knowledge are identified.

Wen et al (2003) illustrate the choice involved in separating aleatory from epistemic uncertainty using the example of a pseudo-random number generator:

To better understand this point, we draw an analogy between nature and a [pseudo-]random number generator (RNG). The RNG is an entirely deterministic algorithm, the outcome of which has relative frequency properties that can be described by a probability distribution. Both the deterministic algorithm and the long-term distribution of the outcomes give correct representations of the RNG, but at different levels of detail. The deterministic mechanism is a more fundamental description of the RNG and can be used to predict the exact value of future observations (if one knows the current state of the generator, i.e. the value of the "seed"), whereas the long-term distribution gives only an ensemble property of the sequence.

Like the outcomes of an RNG, atmospheric storms and geological formations originate in fundamentally deterministic ways, and the grand laws of physics that control these phenomena are more or less understood. But the behavior of atmospheric storms and geological formations depend on many detailed factors that either are not well known or are not practical to measure. Thus, statistical models are invoked to represent them.

In principle, aleatory uncertainty is irreducible, because it reflects the inherent randomness of nature. More information can better characterize the level of variation, but it cannot reduce it. In contract, epistemic uncertainties are reducible with the collection of additional data or the development of improved models.

Figure 11-2 shows an example of how epistemic uncertainty manifests in the results of the hurricane protection system (HPS) risk analysis. Shown is the probability density function on the estimated frequency of HPS failure (where failure is used here as inundation in one or more protected areas). The frequency of failure reflects aleatory uncertainty; the uncertainty in the estimate of the frequency of failure is an aggregation of the epistemic uncertainties. These are due to estimation errors in the frequency and magnitude of hurricane storm surge and in the estimate of the reliability of the protective structures, systems, and components that comprise the HPS.

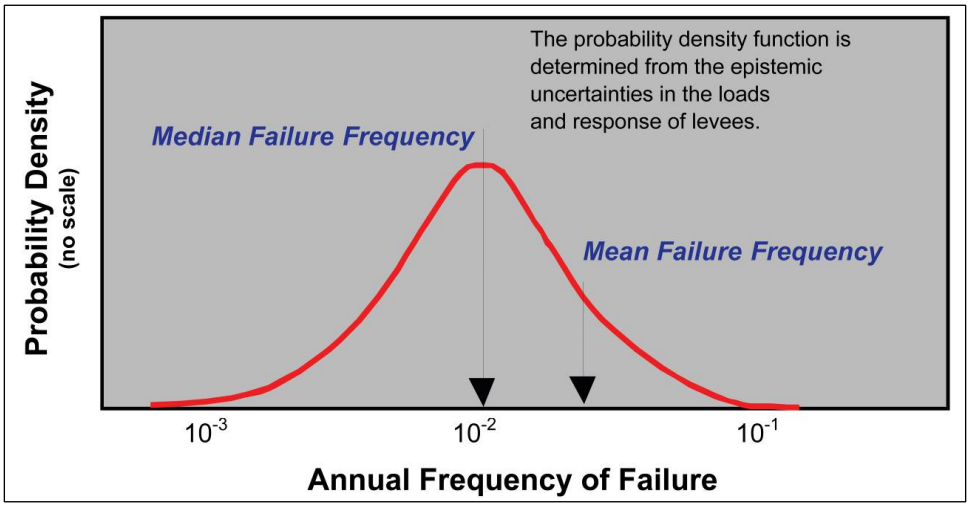

Figure 11-2. Illustration of the Uncertainty in the Estimate of the Frequency HPS Failure due to Hurricane Events. Aleatory uncertainties contribute to the “best estimate” of failure frequency, described either by the mean or median. In the HPS risk assessment, best estimate curves are medians. Epistemic uncertainty contributes a distribution of probability about the best estimate, represented here by a probability density function. Fractiles of this probability density function manifest as banding curves in Figure 11-4.

The effectiveness of the HPS is also dependent upon how well the operational elements of the system perform. Elements such as road closure structures, gate operations and pumping plants that require human operation and proper installation during a flood fight can dramatically impact flood levels. These uncertainties are treated as aleatory in the current risk analysis, that is, they were presumed to be random processes with give (but possibly unknown) probabilities.

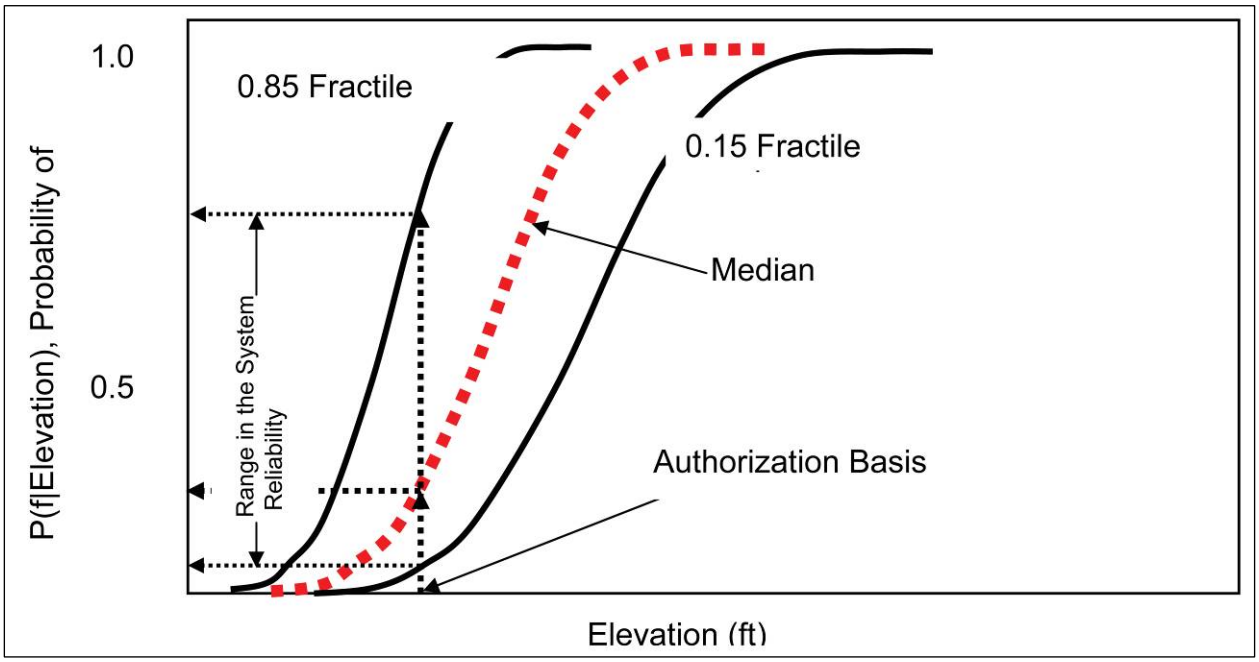

Figure 11-3. Illustration of the Fragility for the HPS Including Modeling Uncertainty and the Effect at the Authorization Basis. The dotted curve reflects the median or best estimate of risk. The 0.15-factile fragility curve is that representing the upper 0.15 probability of Figure 11-2, while the 0.85-fractile curve that that representing the lower 0.15 probability of Figure 11-2.

Figure 11-3 shows the fragility for the HPS including uncertainty and its effect on the estimate of the reliability at the design basis water height. The epistemic uncertainties in each part of the analysis lead to uncertainty in the final risk results. Propagating the uncertainties of the individual parts of the analysis through to the final result, produces a probability distribution on the frequency of exceedance of consequence metrics (e.g., economic consequences). This result is shown in Figure 11-4.

The principal uncertainties in the probability side of the HPS risk assessment derive from

- hurricane recurrence,
- water loads resulting from a given hurricane,
- amounts of rain falling directly into protected basins,
- structural and geotechnical responses of the HPS to loadings, and
- floodwater depth within protected basins affected by drainage and pumping.

The principal uncertainties in the consequence side of the HPS risk assessment derive from

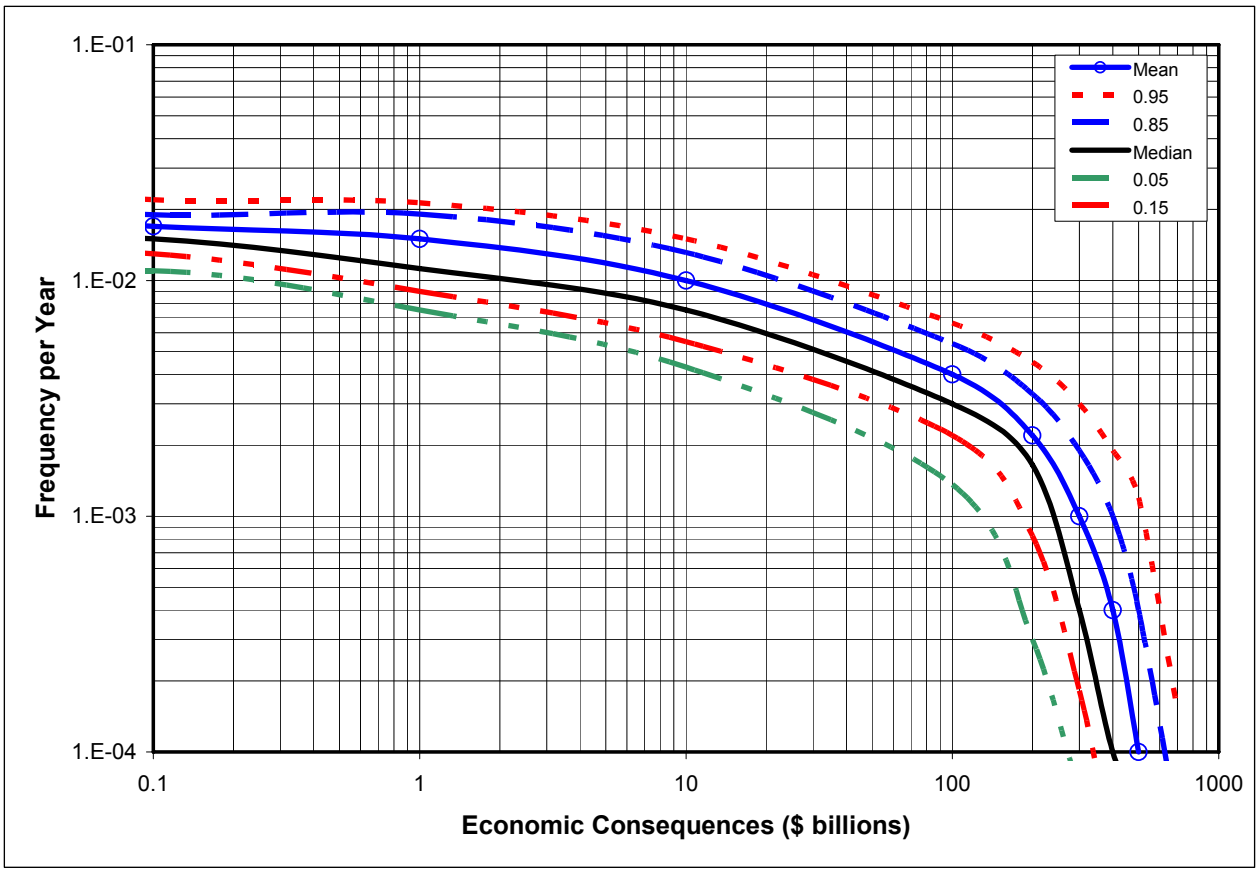

Figure 11-4. Illustration of Typical Risk Analysis Results for Economic Consequences Including Uncertainty. Solid line in middle shows the median estimate of risk, comprising aleatory components of the risk assessment. The surrounding curves show probability levels of the uncertainty in the risk estimate, comprising epistemic uncertainty.

- economic consequences resulting from flooding, and
- loss of life estimation.

These uncertainties are briefly summarized in the remainder of this appendix.

Uncertainty in Hurricane Recurrence Rates

Epistemic uncertainty on the rate density $\lambda(\underline{\Theta})$, in which λ is rate and $\underline{\Theta}$ is the set (vector) of parameters defining the hurricane, comes from two principal sources: (A) uncertainty in hurricane rates during historic times, due to parameterization errors, noise in data sets, and parameter uncertainty caused by the limited historical record; and (B) uncertainty in future climatic conditions and their effects on hurricane rates, which in turn depends on the time period considered.

Much of the discussion in the literature focuses on the frequency and mean intensity of future hurricanes. These two quantities were treated as independent in the present analysis, as they generally depend on different factors. Assuming lognormal distributions, the rate density

accounting for epistemic uncertainty on the hurricane pressure depression, $\lambda_e(\Delta P)$ may be written as

$$\lambda_e(\Delta P) = \frac{\varepsilon_{e1}}{\varepsilon_{e2}} \hat{\lambda}(\frac{\Delta P}{\varepsilon_{e2}}) \tag{11-1}$$

where $\hat{\lambda}(\Delta P)$ is the current best estimate of the true rate and ε_{e1} and ε_{e2} are independent log-normal epistemic variables associated with the frequency and intensity of hurricanes, respectively. The variable $\ln(\varepsilon_{e1})$ might have mean value 0 and standard deviation 0.22, whereas $\ln(\varepsilon_{e2})$ might have mean value 0.03 and standard deviation 0.05.

Source (A) of epistemic uncertainty can be assessed statistically. For example, the overall rate of events estimated from the historic record has a standard error of about 18%. One can account for this uncertainty by multiplying the right hand side of Equation 11-1 by a lognormal random variable ε_{e3} such that $\ln(\varepsilon_{e3})$ has mean value 0 and standard deviation 0.17. This is equivalent to changing the standard deviation of $\ln(\varepsilon_{e1})$ in Equation 11-1 to $\sqrt{(0.22)^2 + (0.17)^2} = 0.28$. Similarly, one can include statistical uncertainty on the mean value of ΔP by increasing the standard deviation of $\ln(\varepsilon_{e2})$.

Other parameters of $\lambda(\underline{\Theta})$, are treated in a similar manner. However, some of these hurricane characteristics are less critical to hurricane risk and in some cases, *e.g.,* concerning the hurricane radius $R_{\max}$, original data are not immediately available.

Aleatory uncertainty refers to random statistical fluctuations. In the case of $\lambda(\underline{\Theta})$, these include high-frequency temporal fluctuations (e.g. decadal oscillations in the rate and characteristics of North Atlantic hurricanes due to cyclic atmospheric circulation patterns). However, the preent interest was in the average rate over relatively long time periods, for which these short-duration cycles have little effect. Hence aleatory uncertainty on $\lambda(\underline{\Theta})$ was neglected.

Uncertainty in Water Loads

Let $H(\underline{x},t \mid \underline{\Theta})$ be the surge time history at location $\underline{x}$ due to a hurricane with parameters $\underline{\Theta}$. In general, epistemic uncertainty on *H* for different $(\underline{x},t,\underline{\Theta})$ is highly correlated. This is especially true for locations and times when *H* is large, which are the conditions of interest for hurricane risk. Hence, in a simple representation of epistemic uncertainty the present analysis assumes perfect dependence. Further assuming a lognormal distribution, $H_e(\underline{x},t \mid \underline{\Theta})$ is expressed as

$$H_e(\underline{x},t \mid \underline{\Theta}) = \eta_e \hat{H}(\underline{x},t \mid \underline{\Theta}) \tag{11-2}$$

where $\hat{H}(\underline{x},t \mid \underline{\Theta})$ is the best estimate and $\ln(\eta_e)$ is a normal random variable with mean value 0 and a given standard deviation, say 0.10.

Hurricanes with identical $\underline{\Theta}$ parameters do not produce identical surges. The reason is that $\underline{\Theta}$ gives only a partial characterization of a hurricane and for example does not completely describe the pre-landfall variation of hurricane properties, does not deterministically control the wind field, and so on. The storm-to-storm variability of the surge time history $H(\underline{x},t \mid \underline{\Theta})$ for given $\underline{\Theta}$ corresponds to aleatory uncertainty. Aleatory variables may be considered independent from event to event.

The variability of *H* due to pre-landfall conditions can be estimated by running hypothetical events with different pre-landfall parameters, whereas variability due to randomness of the wind field under $\underline{\Theta}$ is more difficult to evaluate. A representation of aleatory uncertainty may involve a random factor η_{a1} on the surge height $H(\underline{x},t \mid \underline{\Theta})$ and a random factor η_{a2} that scales the time axis to capture the effect of slower or faster storms in their approach to landfall. However, given the storm speed at landfall *V*, the effect of η_{a2} on the risk should be small relative to η_{a1} and a simplified representation of aleatory uncertainty involves only random variability in surge height. A model that includes both epistemic and aleatory uncertainty has the form

$$H(\underline{x},t \mid \underline{\Theta}) = \eta_a \eta_e \hat{H}(\underline{x},t \mid \underline{\Theta}) \tag{11-3}$$

in which $\ln(\eta_a)$ is a normal random variable with mean value 0 and a given standard deviation.

Equation 11-3 says that the surge height might be systematically over- or under-estimated by a factor and the variability of *H* among storms with the same parameters is similar. Note that a fundamental difference between the random variables in Equation 11-3 is that η_a varies independently from storm to storm, whereas η_e is constant for all storms.

A related variable is significant wave height, *HS*. Qualitatively, the considerations on *HS* are similar to those on *H*. In fact, as a first approximation, one may consider the value of *HS* when *H* is high to be deterministically proportional to *H*,

$$HS(\underline{x},t \mid \underline{\Theta}) = c\,H(\underline{x},t \mid \underline{\Theta}) \tag{11-4}$$

in which c is a constant. Then, the aleatory and epistemic uncertainties on *HS* are directly related to the same uncertainties on *H*.**4.**

For rainfall in the sub-drainage basins, let $I(j,t \mid \underline{\Theta})$ (mm/hr) be the rainfall intensity time history averaged over sub-polder *j* due to a hurricane with parameters $\underline{\Theta}$. The risk assessment is not interested in the detailed temporal fluctuations of this spatially averaged rainfall intensity, but in a suitably low-passed version, smoothed also in time. The place to start is the mean value of $I(j,t \mid \underline{\Theta})$, $m_I(j,t \mid \underline{\Theta})$. This mean value function can be estimated by the procedure described in the methodology report on hurricane hazard.

In analogy with surge height *H*, a simple representation of epistemic uncertainty might involve a single random factor δ_e for all polders, sub-polders, times and values of $\underline{\Theta}$. Hence,

$$I_e(j,t \mid \underline{\Theta}) = \delta_e\, m_I(j,t \mid \underline{\Theta}) \tag{11-5}$$

where $\ln(\delta_e)$ is a normal random variable with mean value 0 and standard deviation that I judgmentally estimate at 0.20.

As explained in the main body of this report, aleatory uncertainty on spatially and temporally averaged rainfall is very large. This uncertainty may be expressed by a lognormal random variable, δ_a, with independent values for different storms but the same value for all *j* and *t*. Hence

$$I(j,t \mid \underline{\Theta}) = \delta_a \delta_e m_I(j,t \mid \underline{\Theta}) \tag{11-6}$$

The distribution of $\ln(\delta_a)$ is normal, with some mean value and some standard deviation. Again note a fundamental difference between the variables δ_a and δ_e in Equation 11-6: δ_a varies independently from hurricane to hurricane, whereas δ_e is the same for all hurricanes.

Uncertainty in Response

The response of a levee and floodwall to hurricane loading is a fragility curve – or set of curves – expressing probability of failure as a function of water height on the levee or wall. Water height in this analysis is taken as given. The uncertainties in the fragility curve depend on uncertainties in the geological profile, load-deformation-breach models, and soil engineering properties.

The soil profile underlying New Orleans consists typically of clayey fill overlying 'marsh' (OH, CH), in turn overlying 'distributary clays' (CH), as shown in Figure 11-6. In Orleans East Bank and New Orleans East, the Pine Island Sand formation also appears in geological profiles and may affect engineering performance of levees and floodwalls. Critical sections in the General Design Memoranda (GDM) and failures observed during Katrina occur in these uppermost strata. The engineering properties of deeper, stronger strata are not statistically characterized.

Measured Q-test results reported in the Gym's and other geotechnical property data were analyzed statistically to obtain second-moment statistical properties of these data (*i.e.,* means, variances, and covariances). Test values larger than certain values were assumed to be local effects or outliers and removed from the statistics.

The spatial pattern of soil variability was characterized by autocovariance functions. These describe the covariance of soil properties as a function of separation distance. Soils whose properties vary erratically from spot to spot display little spatial covariance, while soils whose properties vary with more waviness display more spatial covariance. The autocovariance function of a soil property *z* is defined as, $C_z(\delta) = E[z(i), z(i+\delta)]$, in which E[·] is expectation, *z(i)* is the soil property at some location *i*, and *z(i+δ)* is the property at another location at distance δ from the first. The autocorrelation function is found by normalizing the autocovariance by the variance, $R_z(\delta) = E[z(i), z(i+\delta)]Var^{-1}(z)$. The autocovariance distance is indexed as that separation distance at which $R_z(\delta) = e^{-1}$. This is a representative or characteristic length of the spatial correlation.

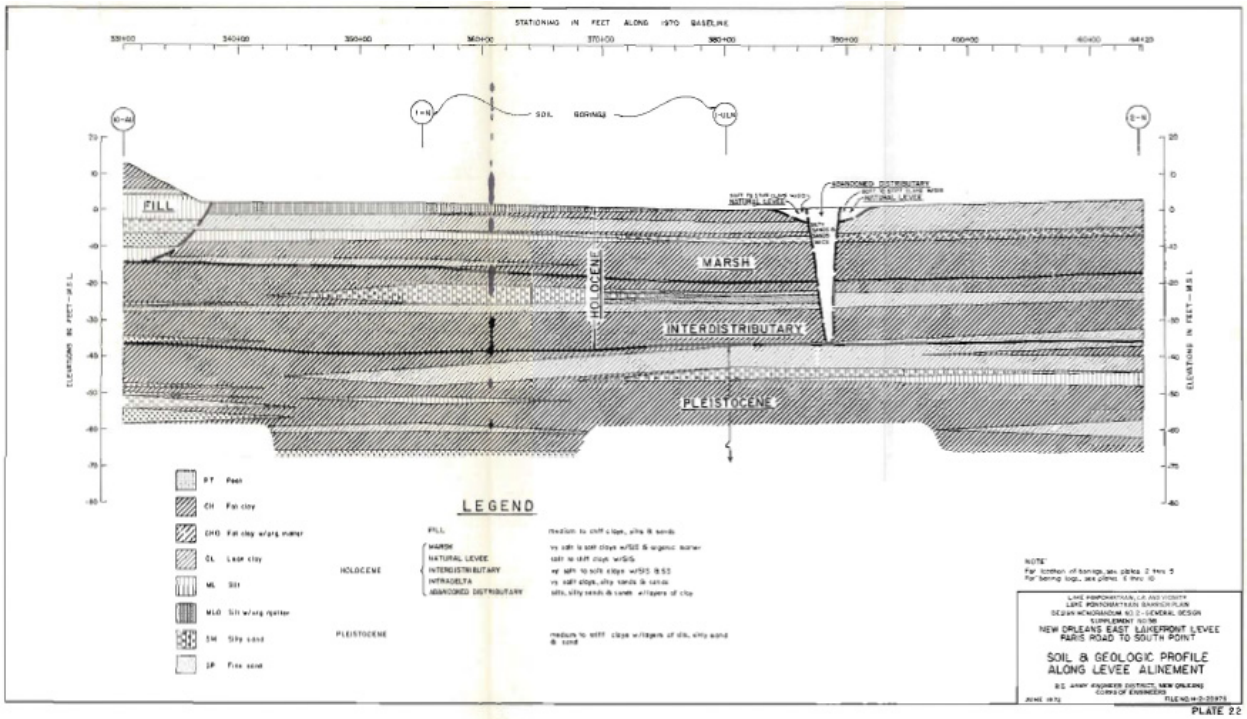

Figure 11-5. Typical geological profile, NOE lakefront section

The principal uncertainty leading to probability of failure of the levee and I-wall sections analyzed is that of soil engineering properties, specifically undrained strength, *Su*. Uncertainties in soil engineering properties are presumed to have two main components: (1) data scatter caused by actual variation of soil properties in space, and by random measurement errors; and (2) systematic errors caused by limited numbers of measurements (*i.e.,* statistical estimation error), and by model error (Figure 11-6).

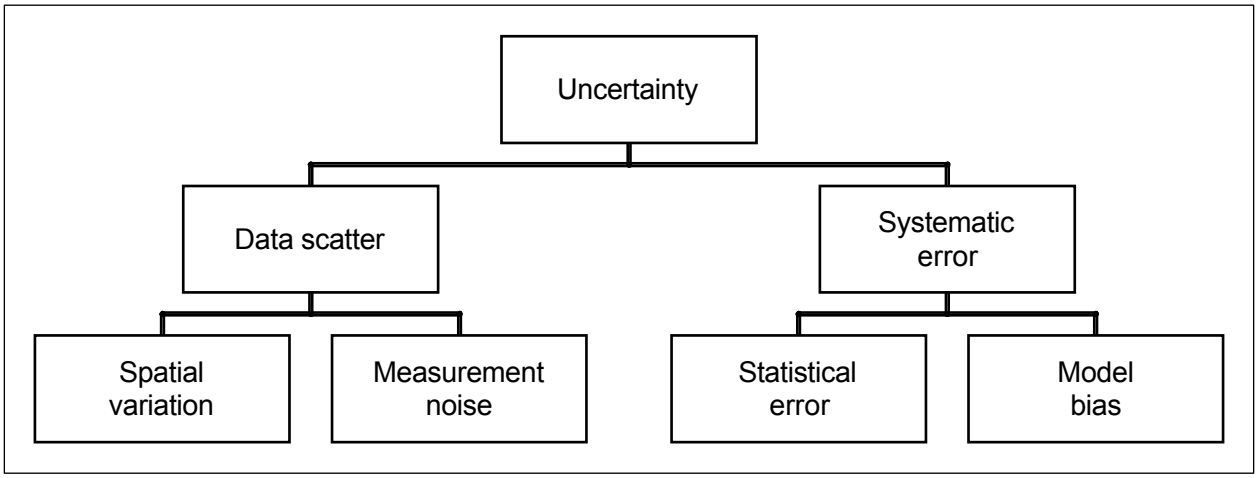

Figure 11-6. Sources of uncertainty in geotechnical reliability model

The variance of the uncertainty in a soil property entering the reliability analysis is a composition of these four terms,

$$Var(Su) = Var(x) + Var(e) + Var(m) + Var(b) \quad (11\text{-}7)$$

in which *Var(·)* is variance, *Su* is the soil property (in this case, undrained strength), *x* is the soil property *in situ*, *e* is measurement error (noise), *m* is the spatial mean of the soil property (which has some error due to the statistical fluctuations of small sample sizes), and *b* is a model bias or calibration term caused by systematic errors in measuring soil engineering properties.

The autocovariance function can only be estimated for distances at least as great as the minimum spacing among observations, that is the minimum boring spacing in the present case. The minimum boring spacings in NOE are on the order of many hundred feet, with some spacings between adjacent borings as much as several thousand feet. To supplement the information in the GDM's, post-Katrina borings made in the vicinity of the 17th Street and London Avenue breaches were used to estimate autocovariance functions, and correspondingly the magnitude of measurement noise and the autocorrelation distance. Statistical estimates of the autocovariance were made using the ESRI *Geostatistical Analyst*®, an application running in ArcMap®. Results for the undrained strength (Q-tests) of London Avenue the Distributary Clay clays are shown in the main report.

Soil strength is measured destructively, therefore replicate measurements cannot be used to estimate the magnitude of random measurement error. However, the spatial covariance structure provides an indirect way to make the estimate. Assuming that the measurement *z* of soil property *x* is corrupted by a zero-mean error *e* that is independent from one measurement to the another and independent of the value *x*, the measurement can be expressed as $z=x+e$. The autocovariance function of *z* is the summation of the autocovariance functions of *x* and of *e*: $C(z)=C(x)+C(e)$. But, the autocovariance function of *e* is a spike at the origin and zero otherwise. Thus, the difference between the intersection of the observed autocovariance function of *z* extrapolated back to the origin, and the total variance Var(*z*), provides an estimate of the variance of the error, Var(*e*).

The conclusions drawn from these autocovariance analyses were: (A) the measurement noise (or fine-scale variation) in the Q-test data is roughly 3/4 the total variance of the data (suggesting the COV's in the top row of Table 10-3); (B) the representative or autocovariance distance in the horizontal direction is on the order of 500 to 1000 feet; and (C) the representative autocovariance distance in the vertical direction is assumed to be on the order of 1/100 of the horizontal distance, or about 10 feet, although there are too few Q-test data in individual borings to statistically estimate this value.

Statistical estimation error in the mean soil property was approximated from the standard error. Although the standard error is a sampling distribution concept, it is approximately the *a posteriori* standard deviation in a Bayesian sense for Normal sampling. The variance of the error is approximated as $Var(m) \approx Var(x)/n$, in which *m* is the mean soil property, *x* is the spatial variation component of data scatter, and *n* is the number of measurements.

Model error was approximated by comparing the method-of-planes calculations and other models to more detailed and precise analysis carried out by Team 7 on failed levee or I-wall sections. These more precise analyses were performed using finite element analysis and circular arch limiting equilibrium stability analyses.

Uncertainty in the Depth of Flooding

Depth of flooding was based on the difference between a water surface elevation and the first floor elevation. The first floor elevation is based on the ground elevation plus the foundation height or, First Floor Elevation = Ground Elevation + Foundation Height.

Therefore, several things contribute to the error in depth of water above the first floor. The accuracy of spot elevation for each point in the census block contributes some error. Each pixel in the raster image of the digital elevation map (DEM) has a ground elevation. The DEM used is that developed by IPET using the latest LIDAR. For the purposes of the analysis of uncertainty an accuracy of 90% within ±1-foot was assumed. Assuming that the error in ground elevation is normally distributed, the error in ground elevation has a mean of zero and a variance of 0.37. This represents a fundamental error that is common to all spot elevations.

A second source of error in ground elevation arises from representing the elevation in a census block by a single value. Because a census block represents a spatial area, the ground elevation is variable across the block. However, the ground elevation must be represented by a single value. For each census block, the mean, minimum, and maximum ground elevation is calculated from the spot elevations extracted from the DEM. This represents an additive error to the underlying ground elevation errors. Ideally, estimates of error in damages could be computed at the census block level using the elevation variability because each census block can have a different range of spot ground elevations. Given the time available, this approach was not feasible. Instead a single average standard deviation was approximated to represent the variability of ground elevation across each census block. The range of spot elevations across each census block was assumed to represent a 99.5% confidence interval or approximately six standard deviations. Equation 11-8 represents the computation of the approximate standard deviation of ground elevation across each census block.

$$CBi_{,\max} - CBi_{,\min} / 6 \sim SD_i \tag{11-8}$$

These were averaged to develop a single approximate standard deviation for the variability of ground elevation by,

$$\frac{\sum_{i}^{N} (CBi, \max - CBi, \min) / 6}{N} \sim \text{the average standard deviation} \tag{11-9}$$

For the approximate 20,000 census blocks in the five parishes, this value computed using (63) is 0.82 feet or variance of 0.67.

From the above, the ground elevation for each census block was represented by a normal distribution with the mean equal to the mean computed from the spot elevations and a standard deviation equal to 1.02 feet.

As noted above, the depth of flooding is the difference between the water stage and the first floor elevation, where the first floor elevation is equal to the ground elevation plus the founda-

tion height. The uncertainty in the foundation height adds an additional error in the estimate of flood depth. Estimates of foundation height were based on previous Corps of Engineers surveys. Two types of foundations are common in the study area: pier and slab on grade. In the computation of damage, these heights and the proportion of structures with each foundation type were used to proportion the census block value of damageable property. However, this uncertainty and its contribution to the uncertainty in flood losses are not quantified. Therefore, the uncertainty in damage is underestimated.

Uncertainty in Consequences

The stage-damage estimates were developed for a range of flood elevations for 27 basins and sub-basins. The highest resolution of measurement of damageable property was the census block. Within each census block, estimates of the number and value of damageable property for residential, commercial, industrial, public and vehicles were developed. These values were combined with depth-percent damage for each of the occupancy categories to estimate economic losses at each level of flooding within the basin. There are several issues within this calculation that contribute to uncertainty in estimated damage at each stage.

The approach to estimating damages is at a higher level of aggregation than typically used by the Corps in evaluating a flood damage reduction project. Traditionally, Corps economists inventory all structures in the study area. This inventory includes information on the type of structure, its construction and its use. Each of these is important in selecting the appropriate damage function to apply to predict damages from different levels of flooding. Estimates of the depreciated replacement value for each structure are developed using tools such as Marshall & Swift Residential Estimator. The first floor elevation of each structure is measured using surveyors, topographic maps, or other methods. Using all of this information economists develop stage-damage relationships for a range of flood stages. These are aggregated damages from the individual structure damage for each flood stage evaluated. Each of the measurements that are part of this analysis introduces some error. For instance, the method of measuring the spot elevation of each first floor has an error based on the method. The Corps has developed tools and methods to quantify these errors and to combine them in a statistically valid way for this detailed method.

In the case of the IPET study, this detailed evaluation starting at the individual structure level was not feasible. Instead, the analysis started at the census block. This means that structures and values were aggregated to that level of resolution. Additionally, depths were representative for the entire census block. The basic approach to identifying and quantifying uncertainties is described below.

In traditional Corps of Engineers flood damage analysis, the depth of flooding provides the quantity to lookup a percentage of value damaged from depth-damage relationships. There are different relationships or curves depending on the type of structure, its construction, and its use. In addition to mean values, confidence intervals around the mean percent damage are established. These error bands typically are established by statistical means based on data and the method for estimating damage. Incorporating this uncertainty was not feasible with the IPET schedule and the nonlinear depth-damage functions. Therefore, this uncertainty and its contri-

bution to the uncertainty in flood losses were not quantified. Therefore, the uncertainty in damage is underestimated.

A final uncertainty that contributes to the uncertainty in flood damage is the value of the damageable property. As noted earlier, flood damages estimated by the Corps of Engineers are based on depreciated replacement values. The New Orleans District of the Corps of Engineers has conducted several flood damage reduction studies requiring quantification of the uncertainty in structure values. In general they have relied on commercially available estimating software such as that developed by Marshall & Swift. Based on these previous studies, estimates of the standard deviation of the value, as a percentage of the mean value, were developed. These percentages are shown in Table 11-1. New Orleans District Standard Deviations of Structure Value as Percentage of the Mean Value.

Table 11-1
New Orleans District Standard Deviations of Structure Value as Percentage of the Mean Value

Structure Type	Standard Deviation as % of Mean
Mobile Home	11.4
Residential	11.4
Multi-Family	11.6
Commercial	11.6
Public	11.6
Warehouse	11.6

The damage at each flood stage is the damage in a category at a stage summed across all census blocks in a basin. That is mean damage at a stage is the sum of the mean of damage at that stage in each census block. The variance of each damage quantity is the squared product of value and the corresponding values, e.g., from Table 11-2. Assuming that the uncertainty in damage at a stage is independent across the census blocks in a basin, the variance of the total damage at a stage is the sum of the variances. In equation form, the variance in damage in a census block is

$$V[X_i] = (a X_i)^2 \quad (11\text{-}10)$$

where X_i is the damage in the i^{th} census block at a stage and n is the value from Table11-2. Therefore, the variance in the sum of the damage in a basin at a stage is

$$V[X1+ X2+ \ldots+ Xn] = \Sigma V(Xi) = \Sigma (a Xi) 2 = a2 \Sigma Xi 2 \quad (11\text{-}11)$$

The foregoing describes two types of uncertainty. One type is the uncertainty in the depth of water resulting from each flood stage. The second type is uncertainty in the dollar damage. The first type is effectively the uncertainty in the stage at which damages begin or the zero damage stage. The uncertainty is represented a shifting in the entire stage-damage relationship by the amount of the error corresponding to the desired confidence. For a 90% confidence interval, this

means shifting the stage-damage curve up by approximately 2 feet, for the upper limit, and shifting it down approximately 2 feet for the lower limit.

Table11-2
Uncertainty in Damage for Given Subbasin as a Function of Water Height

Water Elevation	Basin Name	5%	Mean	95%
-4	JE1	0	0	0
-3	JE1	0	0	1
-2	JE1	0	0	10
-1	JE1	0	1	51
0	JE1	0	9	231
1	JE1	1	49	437
2	JE1	8	218	1,154
3	JE1	46	420	1,560
4	JE1	206	1,093	2,133
5	JE1	404	1,490	2,715
6	JE1	1,032	2,049	3,389
7	JE1	1,420	2,617	3,749
8	JE1	1,965	3,277	4,279
9	JE1	2,519	3,632	4,767

The results of the calculation in standard deviation in damages described above was used to develop a confidence interval for damage at each stage. This incorporates the second type of uncertainty.

Ideally, the uncertainties would be conjoined during the damage computation process. However, as noted above this was not possible. Therefore, the 90% confidence interval is approximated by shifting the 5% lower limit stage-damage up by 2 feet and shifting the 95% upper limit down by 2 feet. Therefore, the confidence interval is only an approximation.

With respect to loss of life, Team 10 worked in close collaboration with Team 9 (Consequences) to obtain estimate of life loss as a function of maximum inundation elevation in the 27 sub-basins that constitute the New Orleans HPS. The estimates of life loss were developed as probability distributions rather than single-value or point estimates. The probability distributions for life loss represent various types of uncertainties in the estimates.

A Monte Carlo Uncertainty Model, was developed to take the vertically re-distributed estimates of population in three flood lethality zones from the LIFESim model runs and estimate: a) the immediate loss of life using fatality rate probability distributions accounting for evacuation effectiveness as a random variable that varied from according to a triangular probability distribution (65%, 80%, 95%); and b) delayed fatalities amongst those who survived the initial inundation but were not rescued, where the rescue effectiveness was accounted for a random variable that varied from according to a uniform probability distribution between 99.5% and

100% in the Safe Flood Lethality Zone and between 95% and 100% in the Compromised and Chance Flood Lethality Zones.

Various limitations in this approach and some potential future improvements are described in the report by Abt Associates, Inc. (2006). The distributions of life-loss estimates for each sub-basin currently combine aleatory uncertainty associated with the fatality rates in each Flood Lethality Zone and epistemic uncertainties associated with evacuation and rescue effectiveness. It is desired to treat the epistemic and aleatory uncertainties separately in future work.

References

Hacking, I. (1975). *The Emergence of Probability*. Cambridge, Cambridge University Press.

Wen, Y. K., B. R. Ellingwood, et al. (2003). "Uncertainty Modeling in Earthquake Engineering," MAE Center Project, Report FD-2.

Appendix 12
Consequences

Overview

One of the primary outputs of the risk and reliability modeling of Risk Team are estimates of the probability distributions of life loss and direct physical damage relating to the performance of the Hurricane Protection System (HPS) in the Greater New Orleans area. The risk was estimated for the following two scenarios:

1) Pre-Katrina (August 28, 2005)

2) Conditions projected for the 2006 Hurricane Season (June 1, 2006).

Risk Team worked in close collaboration with Consequence Team to obtain estimates of life loss and property loss as a function of maximum inundation elevation in the 27 subbasins that comprise the following ten basins of the New Orleans HPS:

East Bank

1) New Orleans Metro - Orleans East Bank

2) New Orleans East

3) St. Bernard Parish

4) Jefferson Parish

5) St. Charles Parish

6) Plaquemines

West Bank

1) Cataouatche

2) Westwego to Harvey Canal

3) Harvey Canal to Algiers Canal

4) Algiers Canal to Hero Canal

The numbers of subbasins that are contained within portions of the following Parishes are indicated in parentheses: Jefferson (7), Orleans (12), Plaquemines (1), Saint Bernard (5), and Saint Charles (2) Parishes (See Figure 12-1).

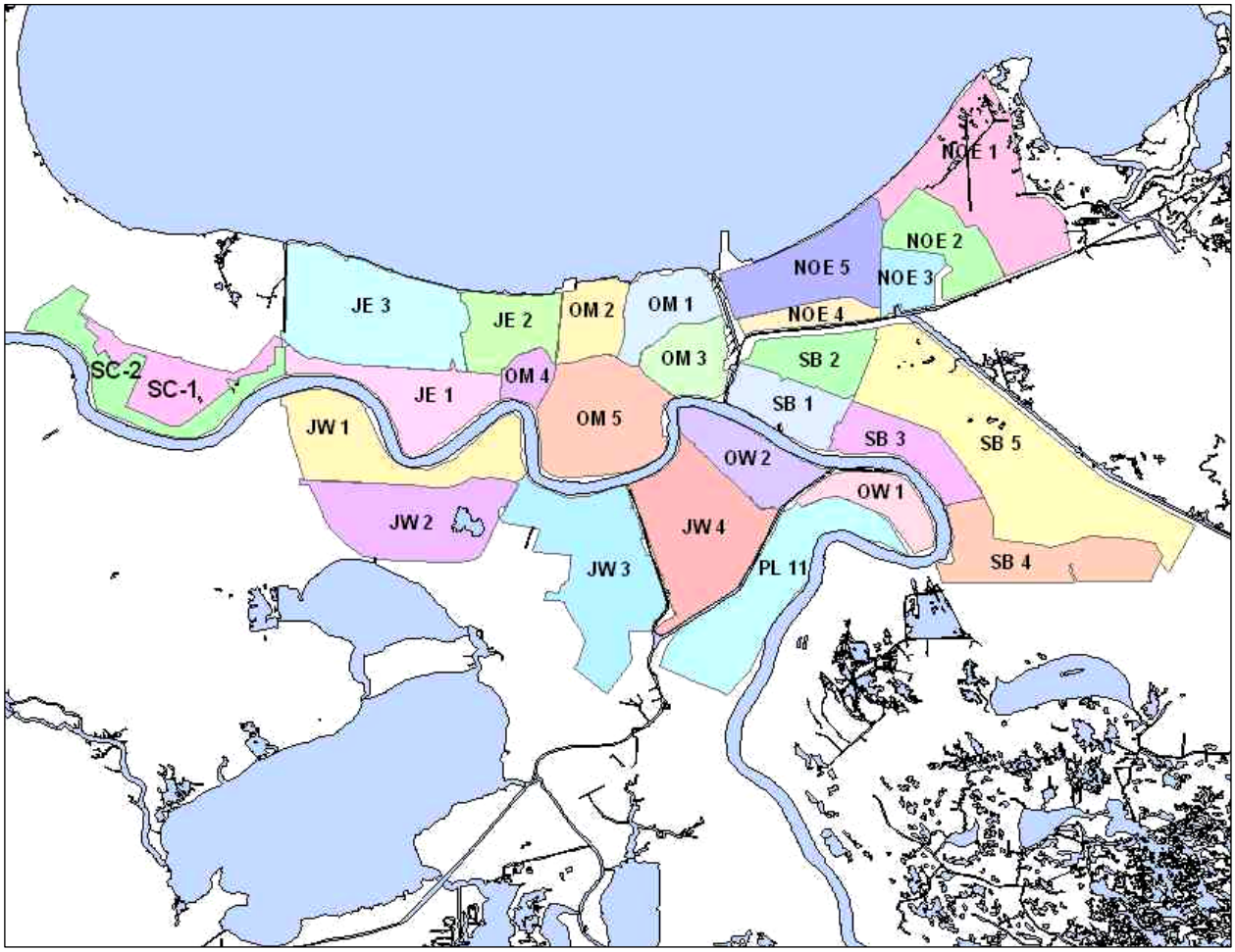

Figure 12-1. Subbasin map

The Risk Model was run for more than 1,100 different hurricane realizations that represent a wide range of hurricane events with different severities, directions, points of landfall, etc. For each of these hurricane realizations, the Risk Model represented the performance of the HPS and estimated the probability that inundation would result from insufficient internal drainage, overtopping of the levees without breaching, and levee breaching. The resulting estimates of maximum inundation depths were used as a basis for interpolation of life loss and property loss estimates using the relationships that were provided by Consequence Team. Estimates were made for each of the 27 subbasins and for the Pre-Katrina and June 1, 2006 scenarios. Thus it was necessary that the life loss and property loss estimates covered a range of elevations

associated with a range of hurricane events that could impact New Orleans from minor inundation to Elevation 36 above sea level.

The estimates of life loss were developed as probability distributions and the estimates of property loss were developed as best estimates with an associated 90% confidence interval rather than single-value or point estimates. The probability distributions for life loss and confidence intervals for property losses represent various types of uncertainties in the estimates, which are described below.

Life Loss Estimation

Life loss was estimated by Consequence Team using two computer models as follows:

- LIFESim Modeling System3 developed to: a)to estimate how the population in the flooded subbasins would redistribute vertically in relation to the depth of inundation; and b) to classify population into one of three flood lethality zones, which are defined in the LIFESim model and by McClelland and Bowles (2002), and an additional sub-zone for people who would be expected to be able to walk away from the inundation area following inundation. Thus LIFESim was run without evacuation.

- A Monte Carlo Uncertainty Model, which was developed to take the vertically re-distributed estimates of population in the three flood lethality zones from LIFESim and estimate: a) the immediate loss of life using fatality rate probability distributions from LIFESim and McClelland (2000) accounting for evacuation effectiveness as a random variable that varied from according to a triangular probability distribution (65%, 80%, 95%); and b) delayed fatalities amongst those who survived the initial inundation but were not rescued, where the rescue effectiveness was accounted for a random variable that varied from according to a uniform probability distribution between 99.5% and 100% in the Safe Flood Lethality Zone and between 95% and 100% in the Compromised and Chance Flood Lethality Zones.

The entire process is described in a report by Abt Associates, Inc. (2006) and involved the following steps:

1) Calibration of LIFESim to the Hurricane Katrina event.

2) Use of LIFESim and the Monte Carlo Uncertainty Model to estimate immediate and delayed life loss associated with the entire range of maximum inundation levels given the population and housing stock that existed prior to Hurricane Katrina.

3) Use of LIFESim and the Monte Carlo Uncertainty Model to estimate immediate and delayed life loss associated with the entire range of maximum inundation levels given the population and housing stock that are expected to exist in June 1, 2006.

---

3 Institute for Dam Safety Risk Management at Utah State University (Aboelata and Bowles 2005) LIFESim includes a simulation module for warning and evacuation, which was not used in this study.

Various limitations in this approach and some potential future improvements are described in the report by Abt Associates, Inc. (2006). The distributions of life-loss estimates for each subbasin currently combine aleatory uncertainty associated with the fatality rates in each Flood Lethality Zone and epistemic uncertainties associated with evacuation and rescue effectivenesses. It is desired to treat the epistemic and aleatory uncertainties separately in future work.

Direct Economic Loss Estimation

The objective of the direct economic damage analysis was to develop potential stage-damage curves that might represent the flood damage potential as of June 1, 2006. This required accounting for the severity of the Katrina damage and the amount of property loss recovery since Katrina. In some areas flooded by Katrina, where water depths were low, recovery has been almost complete. In other areas, where water depths were high, little recovery or reinvestment has taken place. It is extremely difficult and at the peril of the analyst to make general estimates the amount of recovery. None the less, some guidance exists in terms of what others have assumed about recovery. The analysis conducted followed the basic parameters provided in the RAND Gulf States Policy Institute published a report titled "The Repopulation of New Orleans after Hurricane Katrina." (2006) In developing estimates of repopulation over time, the authors relied on the depth of flooding as the basic determinant of the rate of population recovery. Table 12-1 shows the recovery rates by depth assumed in the RAND report. The use of these values resulted in an estimate of the March 2006 population of New Orleans of approximately 155,000 people. This is within the range of other estimates.

The June 2006 estimate of potential stage-property damage started with these assumptions. However, the range of depths of flooding was expanded to include more depth of flooding categories while preserving the basic concept.

Table12-1
Estimated Repopulation Rates for New Orlenas

Period	Depth of Flooding	Repopulation Rate (%)
December 2005	No flooding	65
	<2 feet	20
	2–4 feet	5
	>4 feet	1
March 2006	No flooding	100
	<2 feet	35
	2–4 feet	15
	>4 feet	5
September 2006	No flooding	110
	<2 feet	75
	2–4 feet	25
	>4 feet	10

Source: RAND (2006), "The Repopulation of New Orleans after Hurricane Katrina."

Table 12-1 shows the depth categories and damage recovery rates assumed in developing the June 2006 stage-damage. A RAND category of <2 foot was subdivided into two categories: <1 foot and 1 to 2 feet. Additionally, the >4 feet category was subdivided into three categories: 4 to 6 feet; 6 to 8 feet; and >8 feet. These categories are consistent with those used in social, cultural and historic analysis of the impacts of Katrina the post-Katrina recovery. However, the values of recovery rates are to some degree arbitrary and other rates may be justified. For the estimate of the post Katrina stage-damage functions shown in this section, these rates are used.

Approach

The post-Katrina stage-damage tables and curves were estimated by the same subbasin definitions as the pre-Katrina values. Additionally, the estimation started with the same census block approach. The Katrina depth grid was used to estimate the depth of flooding for each census block. These depths were then used to select the census blocks that incurred damages within each of the categories shown in Table 12-2. For instance, within the Orleans Metro 5 subbasin, 1,535 census blocks had flooding of 1 foot or less while a total of 4,400 census blocks were flooded. Table 12-3 shows the complete estimate of the number of the census blocks flooded by Katrina by depth category.

Table 12-2
Number of Census Blocks within Each Subbasin Flooded by Katrina by Depth Category

Subbasin Name	Count Of Census Blocks within Katrina Flood Depth Category					
	0-1 feet	1 to 2 feet	2 to 4 feet	4 to 6 feet	6 to 8 feet	> 8 feet
JE2	5	6	8	1	1	1
NOE2	1	2	2	10	19	7
NOE3	7	8	12	8	59	7
NOE4	18	3	0	0	0	0
NOE5	27	31	156	173	371	99
OM1	37	37	107	126	163	361
OM2	24	24	46	56	121	321
OM3	301	136	387	358	219	61
OM4	63	51	72	50	9	1
OM5	1535	346	871	957	640	35
SB1	31	25	91	153	200	375
SB3	62	32	49	117	173	44
SB4	5	37	62	50	13	0

From these selected census blocks, damages at each stage were aggregated to the subbasin level for each of the recovery category. This calculation determined the amount of the Katrina damage within each depth category. This was repeated for each of the Katrina flood depth categories.

For each resulting subbasin stage-damage, the recovery factors from Table 12-1 were applied. The recovered potential damage value was then aggregated at each stage. This provides an estimate of the June 2006 potential property damage at each stage for all property damaged estimated to have occurred from Katrina: the Katrina recovery. The last step in the process was to adjust the potential pre-Katrina stage-damages by first subtracting the Katrina damage at each stage and then adding the potential recovered damage at each stage. This was necessary because the Katrina stage was not high enough to damage all the property in a subbasin, at least for some subbasins.

Therefore, for some property, recovery from flooding was not necessary so it contributed its full damage potential to the post-Katrina, June 2006, stage-damage. Table 12-3 provides the recovered damage, the pre-Katrina damage potential and the June 2006 damage potential by stage for all subbasins flooded by Katrina. Stage-damage for all other subbasins retain the pre-Katrina stage-damages. All stages are in NAVD88 (2004.65).

Table 12-3
Stage-Damage for All Subbasins

Subbasin Name	Water Elevation	Katrina Damage Recovery June 2006	Pre-Katrina Stage-Damage	Post-Katrina Stage-Damage June 2006
JE2	-12	0.0	0.0	0.0
JE2	-11	0.0	0.0	0.0
JE2	-10	0.0	0.0	0.0
JE2	-9	0.0	0.9	0.9
JE2	-8	0.0	1.0	1.0
JE2	-7	0.0	2.4	2.4
JE2	-6	0.0	8.1	8.1
JE2	-5	0.0	52.0	52.0
JE2	-4	0.0	470.7	470.7
JE2	-3	0.0	2,190.3	2,190.3
JE2	-2	0.0	3,394.0	3,394.0
JE2	-1	0.0	3,857.5	3,857.5
JE2	0	0.0	4,228.2	4,228.2
JE2	1	0.4	4,506.3	4,504.7
JE2	2	1.4	4,752.0	4,747.6
JE2	3	3.8	4,994.2	4,985.7
JE2	4	17.0	5,237.5	5,224.7
JE2	5	27.0	5,499.4	5,485.1
JE2	6	28.2	5,736.9	5,722.4
JE2	7	28.8	5,864.8	5,850.0
JE2	8	29.2	5,943.8	5,928.9
JE2	9	29.5	6,079.7	6,064.5
JE2	10	29.7	6,175.8	6,160.3
JE2	11	30.1	6,215.7	6,199.9
JE2	12	31.0	6,243.1	6,227.0
JE2	13	32.0	6,262.7	6,246.4
JE2	14	32.5	6,277.7	6,261.2
JE2	15	32.6	6,286.6	6,269.9
JE2	16	33.0	6,292.0	6,275.2
JE2	17	33.6	6,295.9	6,279.0
JE2	18	33.7	6,298.8	6,281.9
JE2	19	33.7	6,300.2	6,283.3
JE2	20	33.7	6,300.6	6,283.7
JE2	21	33.7	6,300.7	6,283.8
JE2	22	33.7	6,300.7	6,283.9
JE2	23	33.7	6,300.7	6,283.9
JE2	24	33.7	6,300.7	6,283.9

Subbasin Name	Water Elevation	Katrina Damage Recovery June 2006	Pre-Katrina Stage-Damage	Post-Katrina Stage-Damage June 2006
NOE1	-3	0.0	0.0	0.0
NOE1	-2	0.0	0.0	0.0
NOE1	-1	0.0	0.0	0.0
NOE1	0	0.0	0.1	0.0
NOE1	1	0.1	6.0	0.1
NOE1	2	0.1	8.0	0.1
NOE1	3	0.1	9.1	0.1
NOE1	4	0.1	10.5	0.1
NOE1	5	0.1	10.9	0.1
NOE1	6	0.1	10.9	0.1
NOE1	7	0.1	10.9	0.1
NOE1	8	0.1	11.3	0.1
NOE1	9	0.1	11.7	0.1
NOE1	10	0.1	12.0	0.1
NOE1	11	0.1	12.1	0.1
NOE1	12	0.1	12.1	0.1
NOE1	13	0.1	12.3	0.1
NOE1	14	0.1	12.4	0.1
NOE1	15	0.1	12.4	0.1
NOE1	16	0.1	12.4	0.1
NOE1	17	0.1	12.4	0.1
NOE1	18	0.1	12.4	0.1
NOE1	19	0.1	12.4	0.1
NOE1	20	0.1	12.4	0.1
NOE1	21	0.1	12.4	0.1
NOE1	22	0.1	12.4	0.1
NOE1	23	0.1	12.4	0.1
NOE1	24	0.1	12.4	0.1

Subbasin Name	Water Elevation	Katrina Damage Recovery June 2006	Pre-Katrina Stage-Damage	Post-Katrina Stage-Damage June 2006
NOE2	-8	0.0	0.0	0.0
NOE2	-7	0.0	0.0	0.0
NOE2	-6	0.0	0.0	0.0
NOE2	-5	0.0	0.5	0.0
NOE2	-4	0.0	19.3	0.0
NOE2	-3	0.0	29.0	0.0
NOE2	-2	0.7	98.3	0.7
NOE2	-1	0.9	114.5	0.9
NOE2	0	0.9	116.3	0.9
NOE2	1	1.0	120.6	1.0
NOE2	2	1.0	123.3	1.0
NOE2	3	1.1	124.1	1.1
NOE2	4	1.1	126.1	1.1
NOE2	5	1.1	127.6	1.1
NOE2	6	1.1	134.5	1.1
NOE2	7	1.2	138.6	1.2
NOE2	8	1.2	139.8	1.2
NOE2	9	1.2	140.8	1.2
NOE2	10	1.2	142.0	1.2
NOE2	11	1.2	142.5	1.2
NOE2	12	1.2	142.5	1.2
NOE2	13	1.2	142.6	1.2
NOE2	14	1.2	142.6	1.2
NOE2	15	1.2	142.7	1.2
NOE2	16	1.2	142.7	1.2
NOE2	17	1.2	142.7	1.2
NOE2	18	1.2	142.7	1.2
NOE2	19	1.2	142.7	1.2
NOE2	20	1.2	142.7	1.2
NOE2	21	1.2	142.7	1.2
NOE2	22	1.2	142.7	1.2
NOE2	23	1.2	142.7	1.2
NOE2	24	1.2	142.7	1.2

Subbasin Name	Water Elevation	Katrina Damage Recovery June 2006	Pre-Katrina Stage-Damage	Post-Katrina Stage-Damage June 2006
NOE3	-6	0.0	0.0	0.0
NOE3	-5	0.0	0.3	0.0
NOE3	-4	0.0	8.0	0.0
NOE3	-3	0.1	39.6	0.1
NOE3	-2	1.6	189.0	1.6
NOE3	-1	3.6	365.8	3.6
NOE3	0	4.5	399.8	4.5
NOE3	1	5.6	416.2	5.6
NOE3	2	22.3	510.1	22.3
NOE3	3	25.0	528.7	25.0
NOE3	4	31.5	563.7	31.5
NOE3	5	33.3	577.3	33.3
NOE3	6	33.8	594.1	33.8
NOE3	7	34.4	618.7	34.4
NOE3	8	35.2	629.6	35.2
NOE3	9	35.9	636.6	35.9
NOE3	10	37.6	649.1	37.6
NOE3	11	40.3	666.7	40.3
NOE3	12	40.4	668.4	40.4
NOE3	13	40.9	671.0	40.9
NOE3	14	42.2	677.1	42.2
NOE3	15	42.5	678.8	42.5
NOE3	16	42.8	680.2	42.8
NOE3	17	42.8	680.3	42.8
NOE3	18	42.8	680.3	42.8
NOE3	19	42.8	680.3	42.8
NOE3	20	42.8	680.3	42.8
NOE3	21	42.8	680.3	42.8
NOE3	22	42.8	680.3	42.8
NOE3	23	42.8	680.3	42.8
NOE3	24	42.8	680.3	42.8
NOE3	25	42.8	680.3	42.8

Subbasin Name	Water Elevation	Katrina Damage Recovery June 2006	Pre-Katrina Stage-Damage	Post-Katrina Stage-Damage June 2006
NOE4	-1	0.0	0.0	0.0
NOE4	0	0.1	0.1	0.1
NOE4	1	12.7	24.9	12.7
NOE4	2	19.4	32.6	19.4
NOE4	3	20.7	34.6	20.7
NOE4	4	33.9	49.1	33.9
NOE4	5	38.7	54.3	38.7
NOE4	6	40.0	55.7	40.0
NOE4	7	40.7	56.6	40.7
NOE4	8	41.2	57.4	41.2
NOE4	9	41.7	58.0	41.7
NOE4	10	42.9	59.5	42.9
NOE4	11	43.3	60.1	43.3
NOE4	12	43.7	60.5	43.7
NOE4	13	44.4	61.9	44.4
NOE4	14	45.1	62.9	45.1
NOE4	15	45.6	63.6	45.6
NOE4	16	47.4	65.4	47.4
NOE4	17	47.7	65.8	47.7
NOE4	18	47.9	65.9	47.9
NOE4	19	47.9	66.0	47.9
NOE4	20	47.9	66.0	47.9
NOE4	21	47.9	66.0	47.9
NOE4	22	47.9	66.0	47.9
NOE4	23	47.9	66.0	47.9
NOE4	24	47.9	66.0	47.9

Subbasin Name	Water Elevation	Katrina Damage Recovery June 2006	Pre-Katrina Stage-Damage	Post-Katrina Stage-Damage June 2006
NOE5	-12	0.0	0.0	0.0
NOE5	-11	0.0	0.1	0.0
NOE5	-10	0.0	1.2	0.0
NOE5	-9	0.0	5.2	0.0
NOE5	-8	0.0	42.7	0.0
NOE5	-7	0.5	241.5	1.8
NOE5	-6	6.2	962.3	9.9
NOE5	-5	20.9	2,316.5	25.4
NOE5	-4	37.9	3,083.4	42.5
NOE5	-3	58.8	3,484.4	63.4
NOE5	-2	141.8	4,121.0	146.5
NOE5	-1	220.6	4,560.7	225.3
NOE5	0	320.3	4,940.0	325.0
NOE5	1	354.5	5,066.5	359.3
NOE5	2	372.9	5,183.0	378.0
NOE5	3	462.6	5,430.1	467.7
NOE5	4	503.2	5,594.9	508.4
NOE5	5	512.7	5,674.0	517.9
NOE5	6	524.7	5,778.1	529.9
NOE5	7	535.6	5,878.2	540.8
NOE5	8	548.8	5,945.3	553.9
NOE5	9	558.6	5,974.5	563.8
NOE5	10	564.1	5,993.7	569.3
NOE5	11	570.5	6,007.4	575.7
NOE5	12	579.4	6,021.6	584.6
NOE5	13	581.9	6,025.7	587.1
NOE5	14	583.8	6,028.0	589.0
NOE5	15	590.0	6,034.6	595.2
NOE5	16	592.0	6,036.7	597.1
NOE5	17	592.6	6,037.3	597.7
NOE5	18	592.7	6,037.5	597.9
NOE5	19	592.7	6,037.5	597.9
NOE5	20	592.7	6,037.5	597.9
NOE5	21	592.7	6,037.5	597.9
NOE5	22	592.7	6,037.5	597.9
NOE5	23	592.7	6,037.5	597.9
NOE5	24	592.7	6,037.5	597.9

Subbasin Name	Water Elevation	Katrina Damage Recovery June 2006	Pre-Katrina Stage-Damage	Post-Katrina Stage-Damage June 2006
OM1	-12	0.0	0.0	0.0
OM1	-11	0.0	0.0	0.0
OM1	-10	0.0	0.0	0.0
OM1	-9	0.0	0.0	0.0
OM1	-8	0.0	0.0	0.0
OM1	-7	0.0	8.4	0.0
OM1	-6	0.0	102.8	0.0
OM1	-5	0.0	401.7	0.0
OM1	-4	0.0	782.6	0.0
OM1	-3	0.7	1,008.1	0.7
OM1	-2	3.3	1,269.7	3.3
OM1	-1	9.3	1,531.3	9.3
OM1	0	16.7	1,713.2	16.7
OM1	1	29.1	1,864.2	29.1
OM1	2	51.5	2,012.0	51.5
OM1	3	89.3	2,208.9	89.3
OM1	4	131.2	2,339.4	131.2
OM1	5	188.1	2,458.6	188.1
OM1	6	221.6	2,526.4	221.6
OM1	7	234.9	2,574.8	234.9
OM1	8	238.7	2,603.0	238.7
OM1	9	242.1	2,625.3	242.1
OM1	10	245.8	2,650.3	245.8
OM1	11	251.1	2,675.0	251.1
OM1	12	255.4	2,689.4	255.4
OM1	13	261.0	2,702.4	261.0
OM1	14	268.7	2,717.7	268.7
OM1	15	272.8	2,725.8	272.8
OM1	16	276.2	2,731.7	276.2
OM1	17	279.5	2,737.6	279.5
OM1	18	280.3	2,738.9	280.3
OM1	19	280.9	2,739.7	280.9
OM1	20	281.1	2,739.9	281.1
OM1	21	281.1	2,739.9	281.1
OM1	22	281.1	2,739.9	281.1
OM1	23	281.1	2,739.9	281.1
OM1	24	281.1	2,739.9	281.1

Subbasin Name	Water Elevation	Katrina Damage Recovery June 2006	Pre-Katrina Stage-Damage	Post-Katrina Stage-Damage June 2006
OM2	-11	0.0	0.0	0.0
OM2	-10	0.0	0.0	0.0
OM2	-9	0.0	0.0	0.0
OM2	-8	0.0	0.0	0.0
OM2	-7	0.0	2.0	0.0
OM2	-6	0.0	69.9	0.0
OM2	-5	0.0	347.6	0.0
OM2	-4	0.0	677.1	0.0
OM2	-3	0.2	884.1	0.2
OM2	-2	1.1	1,040.1	1.8
OM2	-1	2.6	1,196.3	4.1
OM2	0	4.4	1,260.9	6.9
OM2	1	12.4	1,376.7	26.7
OM2	2	29.9	1,482.4	44.3
OM2	3	49.4	1,573.3	64.0
OM2	4	88.4	1,685.3	103.2
OM2	5	127.7	1,763.0	142.9
OM2	6	173.2	1,835.0	188.5
OM2	7	176.0	1,858.6	191.5
OM2	8	179.0	1,877.2	194.5
OM2	9	181.9	1,893.8	197.9
OM2	10	184.6	1,909.8	201.1
OM2	11	186.9	1,922.1	203.6
OM2	12	191.0	1,930.7	207.6
OM2	13	195.9	1,938.9	212.8
OM2	14	201.1	1,945.5	218.0
OM2	15	203.6	1,948.6	220.5
OM2	16	204.3	1,949.5	221.2
OM2	17	204.6	1,950.0	221.5
OM2	18	205.5	1,950.9	222.4
OM2	19	205.6	1,951.1	222.5
OM2	20	205.7	1,951.1	222.6
OM2	21	205.7	1,951.1	222.6
OM2	22	205.7	1,951.1	222.6
OM2	23	205.7	1,951.1	222.6
OM2	24	205.7	1,951.1	222.6

Subbasin Name	Water Elevation	Katrina Damage Recovery June 2006	Pre-Katrina Stage-Damage	Post-Katrina Stage-Damage June 2006
OM3	-10	0.0	0.0	0.0
OM3	-9	0.0	0.0	0.0
OM3	-8	0.0	0.0	0.0
OM3	-7	0.0	0.0	0.0
OM3	-6	0.0	0.8	0.0
OM3	-5	0.0	8.7	0.0
OM3	-4	0.0	29.8	0.0
OM3	-3	0.1	65.9	0.1
OM3	-2	1.1	154.4	1.1
OM3	-1	4.7	376.1	4.7
OM3	0	16.0	661.8	16.0
OM3	1	40.5	1,030.8	40.5
OM3	2	87.0	1,364.6	87.0
OM3	3	166.7	1,708.7	166.7
OM3	4	287.9	2,030.1	287.9
OM3	5	456.3	2,281.0	456.3
OM3	6	582.1	2,436.6	582.1
OM3	7	691.5	2,581.6	691.5
OM3	8	774.4	2,696.6	774.4
OM3	9	832.9	2,793.1	832.9
OM3	10	866.2	2,859.7	866.2
OM3	11	887.7	2,910.0	887.7
OM3	12	903.5	2,952.5	903.5
OM3	13	919.7	2,984.3	919.7
OM3	14	936.8	3,010.0	936.8
OM3	15	950.5	3,029.5	950.5
OM3	16	963.0	3,045.5	963.0
OM3	17	976.3	3,060.7	976.3
OM3	18	984.1	3,069.1	984.1
OM3	19	987.9	3,073.2	987.9
OM3	20	990.3	3,075.8	990.3
OM3	21	991.5	3,077.0	991.5
OM3	22	991.8	3,077.3	991.8
OM3	23	992.1	3,077.7	992.1
OM3	24	992.2	3,077.7	992.2
OM3	25	992.2	3,077.7	992.2

Subbasin Name	Water Elevation	Katrina Damage Recovery June 2006	Pre-Katrina Stage-Damage	Post-Katrina Stage-Damage June 2006
OM4	-6	0.0	0.0	0.0
OM4	-5	0.0	2.9	0.0
OM4	-4	0.0	5.8	0.0
OM4	-3	0.1	8.8	0.1
OM4	-2	0.7	27.7	0.7
OM4	-1	1.8	68.5	1.8
OM4	0	7.2	142.1	7.2
OM4	1	13.7	219.1	13.7
OM4	2	28.6	308.1	28.6
OM4	3	59.1	420.5	59.1
OM4	4	158.1	618.1	158.1
OM4	5	288.4	790.4	288.4
OM4	6	366.2	880.0	366.3
OM4	7	429.5	954.5	430.0
OM4	8	448.0	982.0	449.4
OM4	9	468.7	1,013.4	470.1
OM4	10	478.5	1,034.5	480.0
OM4	11	489.4	1,055.3	490.9
OM4	12	499.2	1,075.7	500.7
OM4	13	512.6	1,096.4	514.2
OM4	14	524.2	1,110.8	525.7
OM4	15	530.3	1,119.4	531.8
OM4	16	538.3	1,131.1	539.9
OM4	17	545.5	1,139.5	547.2
OM4	18	551.1	1,145.6	552.7
OM4	19	556.3	1,151.2	557.9
OM4	20	558.5	1,153.5	560.1
OM4	21	559.9	1,155.0	561.6
OM4	22	560.2	1,155.3	561.9
OM4	23	560.5	1,155.6	562.1
OM4	24	560.5	1,155.6	562.2

Subbasin Name	Water Elevation	Katrina Damage Recovery June 2006	Pre-Katrina Stage-Damage	Post-Katrina Stage-Damage June 2006
OM5	-9	0.0	0.0	0.0
OM5	-8	0.0	0.0	0.0
OM5	-7	0.0	0.0	0.0
OM5	-6	0.0	0.7	0.0
OM5	-5	0.0	0.8	0.0
OM5	-4	0.1	6.8	0.1
OM5	-3	0.4	37.9	0.4
OM5	-2	2.3	200.5	2.3
OM5	-1	10.6	785.0	10.6
OM5	0	34.8	1,483.2	34.8
OM5	1	79.3	2,167.0	79.3
OM5	2	177.1	2,859.8	177.1
OM5	3	358.5	3,721.4	358.5
OM5	4	827.4	4,837.3	827.4
OM5	5	1,296.7	5,522.0	1,296.7
OM5	6	1,701.3	6,034.1	1,701.3
OM5	7	2,387.0	6,834.7	2,387.0
OM5	8	2,966.8	7,538.2	2,966.8
OM5	9	3,415.2	8,112.3	3,415.2
OM5	10	3,758.4	8,574.3	3,758.4
OM5	11	4,012.9	8,920.2	4,012.9
OM5	12	4,303.0	9,305.7	4,303.0
OM5	13	4,449.5	9,511.7	4,449.5
OM5	14	4,572.3	9,679.7	4,572.3
OM5	15	4,675.5	9,846.8	4,675.5
OM5	16	4,800.2	10,031.8	4,800.2
OM5	17	4,897.0	10,144.1	4,897.0
OM5	18	5,003.6	10,260.3	5,003.6
OM5	19	5,092.2	10,353.9	5,092.2
OM5	20	5,137.0	10,401.1	5,137.0
OM5	21	5,170.6	10,436.4	5,170.6
OM5	22	5,191.1	10,457.9	5,191.1
OM5	23	5,220.1	10,488.4	5,220.1
OM5	24	5,242.9	10,512.5	5,242.9
OM5	25	5,247.9	10,517.8	5,247.9
OM5	26	5,250.0	10,520.0	5,250.0
OM5	27	5,250.5	10,520.5	5,250.5
OM5	28	5,250.6	10,520.6	5,250.6
OM5	29	5,250.6	10,520.6	5,250.6
OM5	30	5,250.6	10,520.6	5,250.6
OM5	31	5,250.6	10,520.6	5,250.6
OM5	32	5,250.6	10,520.6	5,250.6
SB1	-5	0.0	0.0	0.0

Subbasin Name	Water Elevation	Katrina Damage Recovery June 2006	Pre-Katrina Stage-Damage	Post-Katrina Stage-Damage June 2006
SB1	-4	0.0	0.3	0.0
SB1	-3	0.0	8.7	0.0
SB1	-2	0.0	53.7	0.0
SB1	-1	0.0	196.4	0.0
SB1	0	0.0	476.7	0.3
SB1	1	1.0	876.7	4.7
SB1	2	2.8	1,262.7	8.3
SB1	3	5.9	1,496.9	11.5
SB1	4	11.6	1,722.8	17.3
SB1	5	26.9	1,983.3	32.6
SB1	6	47.3	2,159.9	53.1
SB1	7	72.4	2,306.0	78.2
SB1	8	93.1	2,403.4	98.9
SB1	9	109.9	2,480.3	116.1
SB1	10	118.5	2,542.2	124.8
SB1	11	122.8	2,582.0	129.2
SB1	12	127.0	2,617.0	133.5
SB1	13	131.7	2,650.5	138.2
SB1	14	135.0	2,676.6	141.4
SB1	15	137.7	2,694.2	144.2
SB1	16	140.6	2,707.6	147.1
SB1	17	142.8	2,717.6	149.3
SB1	18	144.5	2,725.5	150.9
SB1	19	145.7	2,729.7	152.2
SB1	20	146.3	2,731.4	152.8
SB1	21	146.9	2,732.3	153.3
SB1	22	147.3	2,732.8	153.7
SB1	23	147.7	2,733.3	154.2
SB1	24	147.8	2,733.3	154.2
SB1	25	147.8	2,733.4	154.3
SB1	26	148.0	2,733.5	154.4

Subbasin Name	Water Elevation	Katrina Damage Recovery June 2006	Pre-Katrina Stage-Damage	Post-Katrina Stage-Damage June 2006
SB3	-5	0.0	0.0	0.0
SB3	-4	0.0	0.0	0.0
SB3	-3	0.0	0.1	0.0
SB3	-2	0.0	0.3	0.0
SB3	-1	0.0	3.7	0.0
SB3	0	0.0	70.6	0.0
SB3	1	0.3	217.6	0.3
SB3	2	3.5	633.5	3.7
SB3	3	10.2	1,149.7	10.4
SB3	4	23.3	1,524.6	23.5
SB3	5	33.2	1,723.6	33.4
SB3	6	44.0	1,836.2	44.2
SB3	7	63.3	1,938.8	63.5
SB3	8	117.2	2,077.3	117.4
SB3	9	185.0	2,190.4	185.2
SB3	10	239.0	2,298.0	239.2
SB3	11	270.7	2,393.5	270.9
SB3	12	285.9	2,455.8	286.1
SB3	13	294.1	2,490.8	294.3
SB3	14	297.7	2,509.6	297.9
SB3	15	301.2	2,524.3	301.4
SB3	16	306.6	2,540.0	306.9
SB3	17	314.4	2,554.3	314.6
SB3	18	320.3	2,563.1	320.5
SB3	19	323.7	2,568.0	323.9
SB3	20	327.1	2,573.5	327.3
SB3	21	329.5	2,576.7	329.7
SB3	22	331.0	2,578.6	331.2
SB3	23	332.3	2,580.0	332.6
SB3	24	332.7	2,580.4	333.0
SB3	25	332.9	2,580.6	333.1

Subbasin Name	Water Elevation	Katrina Damage Recovery June 2006	Pre-Katrina Stage-Damage	Post-Katrina Stage-Damage June 2006
SB4	1	0.0	0.0	0.0
SB4	2	0.0	0.4	0.0
SB4	3	0.1	7.3	0.1
SB4	4	1.3	32.7	1.3
SB4	5	6.4	89.7	6.4
SB4	6	21.7	190.2	21.7
SB4	7	48.0	295.3	48.0
SB4	8	81.1	387.5	81.1
SB4	9	100.6	438.6	100.6
SB4	10	106.5	465.4	106.5
SB4	11	112.5	491.2	112.5
SB4	12	113.9	497.1	113.9
SB4	13	114.8	503.4	114.8
SB4	14	116.6	515.7	116.6
SB4	15	119.1	527.7	119.1
SB4	16	122.5	537.8	122.5
SB4	17	124.8	544.7	124.8
SB4	18	126.0	549.4	126.0
SB4	19	126.7	552.6	126.7
SB4	20	127.2	553.7	127.2
SB4	21	127.5	554.3	127.5
SB4	22	127.5	554.5	127.5
SB4	23	127.6	554.5	127.6
SB4	24	127.6	554.5	127.6
SB4	25	127.6	554.5	127.6
SB4	26	127.6	554.5	127.6
SB4	27	127.6	554.5	127.6
SB4	28	127.6	554.5	127.6
SB4	29	127.6	554.5	127.6
SB4	30	127.6	554.5	127.6
SB4	31	127.6	554.5	127.6
SB4	32	127.6	554.5	127.6
SB4	33	127.6	554.5	127.6
SB4	34	127.6	554.5	127.6
SB4	35	127.6	554.5	127.6
SB4	36	127.6	554.5	127.6

References

Kevin McCarthy, D.J. Peterson, Narayan Sastry, and Michael Pollard. (2006) "The Repopulation of New Orleans after Hurricane Katrina." RAND Gulf States Policy Institute. RAND URL: http://www.rand.org/

Aboelata, M. and D.S. Bowles. 2005. LIFESim: A Model for Estimating Dam Failure Life Loss. Draft report to the Institute for Water Resources, US Army Corps of Engineers by the Institute for Dam Safety Risk Management, Utah State University, Logan, Utah

Aboelata, M., D.S. Bowles, and D.M. McClelland. 2003. 'Life-loss Estimation for Floods including Dam Failure.' GIS Model for Estimating Dam Failure Life Loss. In Y.Y. Haimes and D.A. Moser, (eds.), American Society of Civil Engineers.

Aboelata, M., D.S. Bowles, and D.M. McClelland. 2004a. 'A Model for Estimating Dam Failure Life Loss.' ANCOLD Bulletin 127:43-62. August.

Aboelata, M., D.S. Bowles, and A. Chen. 2004b. 'Transportation model for evacuation in estimating dam failure life loss.' Proceedings of the Australian National Committee on Large Dams Conference, Melbourne, Victoria, Australia.

Abt Associates, Inc. 2006. Estimating Loss of Life from Hurricane-Related Flooding in the Greater New Orleans Area. Loss-of-Life Modeling Report. Prepared for U.S. Army Corps of Engineers, Institute for Water Resources, Alexandria, VA

McClelland, D.M. 2000. Personal Communication of Updated Probability Distributions for Fatality Rates for Each Flood Zone. November 30.

McClelland, D. M. 2002. "A team approach to improving dam-safety emergency action plans, flood maps, and emergency response plans using life-loss risk assessment." EAP 2002: International Workshop for Emergency Preparedness at Dams, sponsored by FERC and ASDSO.

McClelland, D.M. and Bowles, D.S. 2002. 'Estimating Life Loss for Dam Safety Risk Assessment - a Review and New Approach.' Institute for Water Resources, U.S. Army Corps of Engineers, Alexandria, VA.

Appendix 13
Risk Analysis Results

Volume VIII outlines the procedures and methodologies used in the risk studies. The results of the risk analysis are undergoing review and validation and will be published subsequent to a full peer review.

Appendix 14
Flood Risk Analysis for Tropical Storm Environments (FoRTE)

The Flood Risk Analysis for Tropical Storm Environments (FoRTE) is a prototype computer program that was developed by BMA Engineering, Inc. for the IPET project to evaluate the elevation and loss exceedance rates of a hurricane protection system for a region, and to summarize these risk profiles to inform decisions. The underlying risk model used for performing the computations in FoRTE is described in Appendix J.

The FoRTE prototype was implemented in Microsoft Excel 2003 with visual basic program modules. Figure 14-1 shows the control tab of FoRTE with instructions.

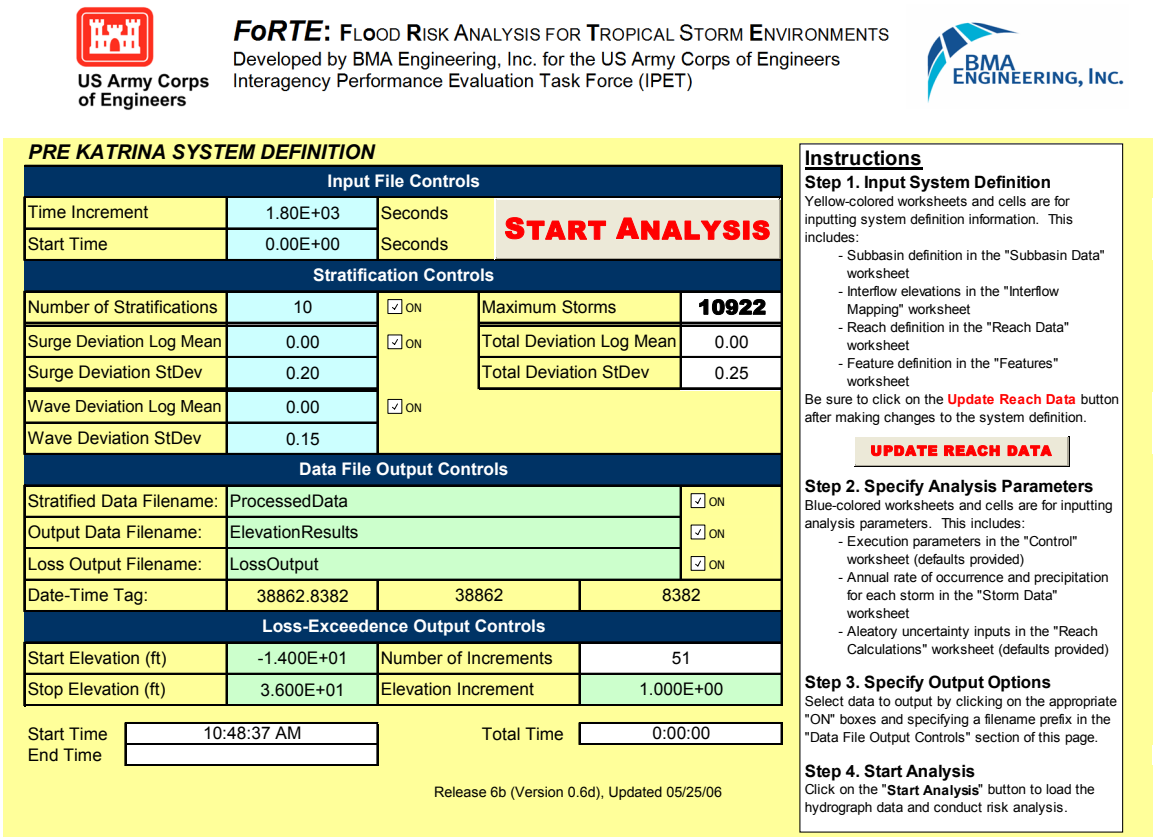

Figure 14-1. Flood Risk Analysis for Tropical Storm Environments (FoRTE)